Reflector Technology Development and System Design for Concentrating Solar Power (CSP) Technologies

Final Report

Approved for Public Release

Issued: March 6, 2012

Project Title: Reflector Technology Development and System Design for CSP Technologies

Covering Period: March 1, 2008 – December 30, 2011

Date of Report: January 31, 2011

Recipient: DOE – Golden Field Office

Award Number: DE-FC36-08GO18028

Working Partners: CSP Services (DLR), Sandia National Laboratories (SNL), National Renewable Energy Laboratory (NREL)

Cost-Sharing Partners: Alcoa Inc. and DOE – Golden Field Office

Contacts:

Adam Schaut
Alcoa Project Manager
Phone: 724-337-2669
Fax: 724-558-9036
adam.schaut@alcoa.com

Christine Retarides
Alcoa Contract Manager
Phone: 724-337-3720
Fax: 724-337-4849
christine.retarides@alcoa.com

DOE Project Team: DOE Field Contracting Officer - Andrea Lucero
DOE Field Project Officer - Brad Ring
Senior Project Engineer – Suzanne Atkinson

Contents

Figures

Tables

Acknowledgements

The following individuals are acknowledged for the contribution to the success of the "Reflector Technology Development and System Design for Concentrating Solar Power (CSP) Technologies" program:

Alcoa	NREL	DOE	Sandia
S. Kelly	K. Gawlik	S. Baca (Atkinson)	T. Mancini
M. Kiley	A. Gray	B. Ring	G. Kolb
C. Retarides	C. Kennedy		
D. Serafin	A. Lewandowski		
A. Schaut	M. Mehos		
D. Smith	J. Netter		
P. Smith	K. Stynes		
R. Speer	T. Wendelin		
D.J. Spinella			

1.0 Executive Summary

Alcoa began this program in March of 2008 with the goal of developing and validating an advanced CSP trough design to lower the levelized cost of energy (LCOE) as compared to existing glass based, space-frame trough technology. In addition to showing a pathway to a significant LCOE reduction, Alcoa also desired to create US jobs to support the emerging CSP industry.

Alcoa's objective during Phase I: "Concept Feasibility" was to provide the DOE with a design approach that demonstrates significant overall system cost savings without sacrificing performance. Phase I consisted of two major tasks; reflector surface development and system concept development. Two specific reflective surface technologies were investigated, silver metallized lamination, and thin film deposition both applied on an aluminum substrate. Alcoa prepared samples; performed test validation internally; and provided samples to the NREL for full-spectrum reflectivity measurements. The final objective was to report reflectivity at t = 0 and the latest durability results as of the completion of Phase 1. The target criteria for reflectance and durability were as follows: (1) initial (t = 0), hemispherical reflectance >93%, (2) initial spectral reflectance >90% for 25-mrad reading and >87% for 7-mrad reading, and (3) predicted 20 year durability of less than 5% optical performance drop.

While the results of the reflective development activities were promising, Alcoa was unable to down-select on a reflective technology that met the target criteria. Given the progress and potential of both silver film and thin film technologies, Alcoa continued reflector surface development activities in Phase II.

The Phase I concept development activities began with acquiring baseline CSP system information from both CSP Services and the DOE. This information was used as the basis to develop conceptual designs through ideation sessions. The concepts were evaluated based on estimated cost and high-level structural performance. The target criteria for the concept development was to achieve a solar field cost savings of 25%-50% thereby meeting or exceeding the DOE solar field cost savings target of $350/m^2.

After evaluating various structural design approaches, Alcoa down-selected to a monocoque, dubbed 'Wing Box', design that utilizes the reflective surface as a structural, load carrying member. The cost and performance potential of the Wing Box concept was developed via initial finite element analysis (FEA) and cost modeling. The structural members were sized through material utilization modeling when subjected to representative loading conditions including wind loading. Cost modeling was utilized to refine potential manufacturing techniques that could be employed to manufacture the structural members.

Alcoa concluded that an aluminum intensive collector design can achieve significant cost savings without sacrificing performance. Based on the cost saving potential of this Concept Feasibility study, Alcoa recommended further validation of this CSP approach through the execution of Phase II: Design and Prototype Development.

Alcoa's Phase II objective was to provide the DOE with a validated CSP trough design that demonstrates significant overall system cost savings without sacrificing performance.

Phase II consisted of three major tasks; Detail System Design, Prototype Build, and System Validation. Additionally, the reflector surface development that began in Phase I was continued in Phase II. After further development work, Alcoa was unable to develop a reflective technology that demonstrated significant performance or cost benefits compared to commercially available CSP reflective products. After considering other commercially available reflective surfaces, Alcoa selected Alanod's MIRO-SUN© product for use on the full scale prototype. Although MIRO-SUN© has a lower specular reflectivity compared to other options, its durability in terms of handling, cleaning, and long-term reflectivity was deemed the most important attribute to successfully validate Alcoa's advanced trough architecture.

To validate the performance of the Wing Box trough, a 6 meter aperture by 14 meter long prototype trough was built. For ease of shipping to and assembly at NREL's test facility, the prototype was fabricated in two half modules and joined along the centerline to create the Wing Box trough. The trough components were designed to achieve high precision of the reflective surface while leveraging high volume manufacturing and assembly techniques.

Extensive testing of the trough prototype was performed at Alcoa and NREL's SIMTA facilities. Tests included complete component and assembly part tolerance verification, through coordinate measuring equipment and laser trackers, that were compared to Geometric Dimensioning and Tolerancing (GD&T) simulations; static load testing and wind load testing that were compared to analytical FEA models; extensive V-SHOT testing to calculate the trough's intercept factor; and optical efficiency testing on NREL's two-axis tracker.

The test results indicated that the Wing Box architecture could achieve high intercept factors (>99% average) without any adjustment after the final assembly. The optical efficiency results of approximately 75% (average), with a MIRO-SUN© reflector, also confirmed the high geometric accuracy of the Wing Box design. The results of the tolerance simulations and wind load tests were utilized to optimize the performance and cost savings of the trough architecture in Phase III of the program.

Based on the validation results and production cost modeling efforts, Alcoa validated that an aluminum-intensive, Wing Box trough design could significantly reduce the installed costs for solar field thereby reducing the LCOE.

The purpose of Phase III of the program was to establish a detailed manufacturing and commercialization plan for the Wing Box trough technology. Given the need to further validate the technology through a system's level validation prior to commercialization, this detailed plan was deemed premature. Per the existing SOPO, Alcoa updated the Wing Box design to incorporate the Phase II learning's, and a high-level manufacturing and commercialization plans were developed. Additionally during Phase III, Alcoa established a development partner for completing the systems validation via a test loop program. Due to corporate strategy changes by the development partner, the test loop program was eventually terminated.

As a result, Alcoa made the internal decision not to pursue a test loop program under the existing DOE program, and to conclude Phase III of the program. Alcoa plans to remain active in the CSP market as there is a significant potential for future growth of both aluminum and Alcoa sales within this market.

2.0 Project Objective

Alcoa's overall project objective is to develop, prototype, and validate through testing an aluminum-intensive trough (supporting structure and reflector) that provides superior (lower) total life cycle cost of energy compared to current baseline troughs. This will be achieved by employing a system solution approach that focuses on the design and optimization of the supporting structure and state-of-the-art reflector coating technology.

The objective of Phase I, Concept Feasibility, was to provide the DOE with a system design approach to demonstrate significant overall system cost savings for the solar field without sacrificing performance.

During Phase II, Design and Prototype Development, Alcoa performed a detailed design and analysis of the Phase I conceptual design and built and tested a prototype to validate its performance. The objective of Phase II, Design and Prototype Development, was to provide the DOE with a design that demonstrates significant overall system cost savings without sacrificing performance. Alcoa was to develop, using a systems approach, a utility scale parabolic solar thermal trough that takes advantage of structurally integrated metallic mirrors to provide a means for reducing the levelized cost of electricity produced by the solar plant.

During Phase III, Commercialization Planning, Alcoa optimized the trough design based upon the Phase II results, and outlined the manufacturing and commercialization plan to bring the technology to market.

The original Statement of Project Objectives (SOPO) is shown in Appendix A. It provides detailed information regarding the original objective of the individual tasks. A breakdown of the task by Phases is listed below.

Phase I: Technical Feasibility Study

Task 1.1: Reflector Surface Optimization

Task 1.2: System Ideation
Task 1.3: Down-Select Preliminary Concepts
Task 1.4: Develop Phase II Plan
Task 1.5: Phase 1 Prep & Review with DOE

Phase II: Design and Prototype Development
Task 2.1: Detail System Design
Task 2.2: Internal Critical Design Review
Task 2.3: Prototype Build
Task 2.4: System Validation
Task 2.5: Develop Phase III Plan
Task 2.6: Phase II Prep & Review with DOE

Phase III: Field Validation Plan
Task 3.1: Update Design to Incorporate Phase II Lessons Learned
Task 3.2: Finalize Pre-Production Build Plan
Task 3.3: Finalize Pre-Production Field Validation Plan
Task 3.4: Internal Critical Design Review
Task 3.5: Final Reporting
Task 3.6: Phase III Review with DOE

3.0 Background

Current baseline solar trough troughs differ in supporting systems (e.g., aluminum spaceframe vs. steel torque-box), but both predominantly use parabolic silver-metalized glass mirrors that present numerous disadvantages including fragility, weight, and cost. Based on specular reflectivity, cost, and durability, there are only a few commercially available parabolic trough reflector technologies with the potential to displace the incumbent silvered glass mirror.

Development of an aluminum-intensive trough will address current technology and cost gaps by focusing on system design optimization including various reflector technologies. A decrease in total cost is achievable through a holistic design approach that integrates innovative design, process, and product technologies to create an optimized design for the supporting structure without sacrificing performance and stiffness. Desired specular reflectance is attainable by employing reflectivity management, metallization, and surface protection technologies to optimize the performance and durability of an aluminum reflector surface. A properly designed aluminum trough that exhibits a superior and long-term performance-to-cost ratio will create a lower levelized cost of energy. Due to existing U.S.-based mass assembly and production capabilities, it also will positively impact the U.S. manufacturing base.

4.0 Phase I Results

The following section provides a detailed account of the Phase I tasks as defined in the original Statement of Project Objectives (SOPO). This detailed account highlights the approach for each task as well as the subsequent results.

Task 1.1: Reflector Surface Optimization

The objective of the reflector development portion of Phase I was to develop an aluminum sheet based reflector that, when used in designing a parabolic solar trough, at least meets the reflectance, durability and cost criteria of existing systems. From a surface reflectivity target standpoint, key initial (t = 0) hemispherical reflectance was >93% and initial (t = 0) spectral reflectance was >90% for 25-mrad reading and >87% for 7-mrad reading. Key accelerated performance screening testing included QUV/A-Bulb per ASTM G53 and Salt Spray per ASTM B117, which were intended to predict 10 year durability.

The results of a high-level engineering study performed prior to this DOE Phase I program highlighted the requirement to meet these minimum performance requirements. Specifically, it was determined that the cost advantages of employing a system design approach are quickly negated in the absence of the reflector performance requirements defined above. Additionally, to achieve desired cost reductions, it was determined that the reflector technology would need to be manufactured in a coil form as coil production of commercial materials is typically the most cost effective manufacturing process.

Two separate technologies were included in the Phase I reflector development activity:

(1) Metalized silver film that is laminated onto an aluminum sheet substrate, and

(2) Thin film stack deposited directly onto a level coated aluminum sheet substrate

1.1.1 Silver Film Technology and Results

A cross section of the silver film prototype is shown in Figure 1:

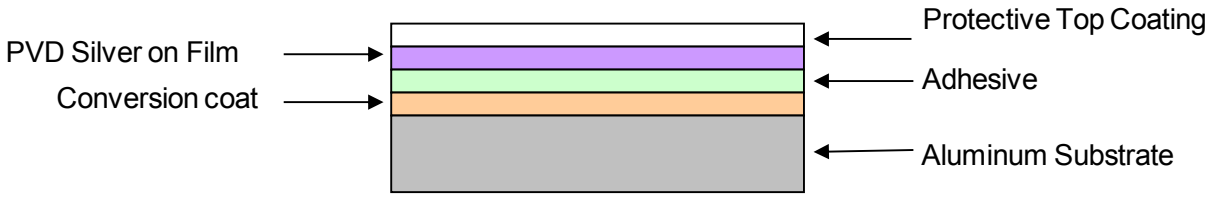

Figure 1: Cross Section of Silver Film Technology Option

There are several steps involved in the fabrication of the silver film technology product. The first step is the metallization of a carrier film. After laminating the metalized film to the aluminum substrate, the carrier film is on the outside of the "stack" and exposed to the environment. Therefore, key attributes of this carrier film are optical clarity, UV-light stability, and moisture barrier properties. Under Phase I, four specific film types were evaluated:

1. UV-stabilized polyethylene terephthalate (PET),
2. Ethylene Tetrafluoroethylene (ETFE),
3. Melinex® D733,
4. Teflon®.

The metallization process is done via Physical Vapor Deposition (PVD). Plasma cleaning is first performed to prepare the carrier film surface for the PVD coatings. To enhance adhesion and to provide some protection of the reflective silver layer, a thin 50 to 100 nm layer metal oxide is deposited next. The reflective silver layer is next deposited at approximately 100 nm, and a metal protective layer is deposited last.

Next, the silver film is laminated to the metal substrate. For film development purposes, the lamination of the metalized films were batch laminated under nip pressure using double back adhesive tape. In continuous coil production, one acceptable adhesive option previously used to laminate silver film to aluminum is M805 polypropylene.

Finally, an optional protective top coat may be applied. Ideally, once the metalized film is laminated to the aluminum sheet substrate, it will possess adequate durability characteristics for use in concentrated solar panel applications. For added protection against UV-light and moisture, a polysilazane-based coating system has been successfully tested.

The procedure described above was used to manufacture silver film samples with the four films defined above. Samples were successfully manufactured with the exception of the Teflon film sample. During the metallization process, the Teflon film exhibited objectionable shrinkage, and it was not worthy of further testing. The remaining samples were evaluated by measuring the initial optical properties and by performing accelerated testing. These tests were performed at both the Alcoa Technical Center (ATC) as well as the National Renewable Energy Laboratory (NREL). The test equipment at ATC is not specifically designed for measuring of CSP applications; however, the results were used as initial guidance and feedback while the NREL results could be generated.

Table 1 below contains the optical results from the four films. Note that the Total Reflectance data was generated at the Alcoa Technical Center using a Technidyne Corporation Total Hemispherical Reflectometer Model TR-2, and the specular reflectance was measured by NREL at 7- and 25-mrad cone angle with a Device and Services (D&S) Field Portable Specular Reflectometer at 660 nm and at 20° incidence in four bands 400-540, 480-600,590-720,900-1100 nm with the Surface Optics Corporation (SOC) InspectIR-VIS.

The specular reflectance data shown in Table 1 are dependent on the smoothness of the adhesive layer, which was not of primary concern for the generation of the prototype samples. The current primary concern is demonstrating high total reflectance and long term durability. Therefore, the lower than desired readings are not a concern at this point of the development activity.

Table 1: Silver Film Optical Properties

Sample	Total Reflectance *(initial, T=0 Readings)*	Specular Reflectance, 7-mrad *(initial, T=0 Readings)*	Specular Reflectance, 25-mrad *(initial, T=0 Readings)*
PET	87.9 to 96.5%	6.4 to 14.2	46.8 to 82.5
ETFE	78.0 to 94.7%	5.3 to 7.1	45.0 to 52.1
Melinex	94.7 to 96.9%	In progress	In progress
Teflon®	N/A	N/A	N/A

Table 2 below contains the initial accelerated testing results from the four films. For the initial screening test, it is desired to achieve 1000 hours of testing with both the QUV/A-Bulb and the salt spray without any significant degradation in optical properties. Again, the Teflon film failed during the manufacturing process; therefore, no results exist for this sample.

Table 2: Silver Film Initial Accelerated Testing Results

Film	QUV/A-Bulb	Salt Spray
PET	1000	N/A
ETFE	Failed	N/A
Melinex	650	500
Teflon®	N/A	N/A

Six different PET film prototype variations all passed 1000 hours of QUV/A-Bulb testing both with and without the protective top coating. Based on the perceived long term performance viability of the PET option compared to the other films evaluated, none of the PET prototypes were tested in salt spray.

The four Melinex film prototype variations have survived 650 hours of QUV/A-Bulb testing (with and without the protective top coating), and will continue in test for an additional 350 hours. All ETFE film prototype variations failed QUV/A-Bulb testing due to an adhesion loss of the metalized silver layer to the ETFE carrier film substrate. Given the ETFE samples failed under the QUV/A-Bulb test, the salt spray test was not performed.

The Melinex film has successfully survived 500 hours in Salt Spray testing, and will continue to be exposed for an additional 500 hours.

1.1.2 Thin Film Technology and Results

A cross section of the thin film prototype is shown in Figure 2.

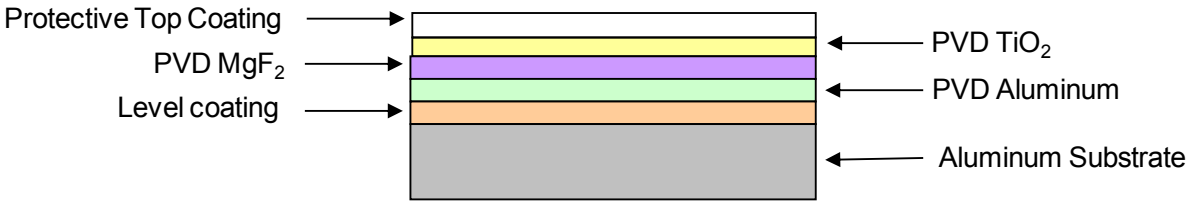

Figure 2: Cross-section of Thin Film Technology Option

The fabrication of the thin film technology product option begins with the application of a level coating to aluminum sheet substrate. Before application of the thin film stack to the aluminum sheet substrate, the surface must be as level as possible in order to achieve a high degree of reflectance on the final product. One approach is to start with bright-rolled high purity aluminum, perform a chemical or electrochemical brightening operation, and anodize it for durability purposes. Typically, the brightening and anodizing processes are done at speeds of 20 to 40 feet per minute.

The Alcoa hypothesis was to start with less expensive, mill-finish aluminum sheet substrate, and level the surface via the application of an inexpensive epoxy coating. If successful, this process has the potential to significantly reduce the manufacturing costs for the reflective surface as compared to starting with bright-rolled high purity aluminum. The leveling thickness is approximately 0.38mm (0.015") thickness and can be applied in coil form at speeds of 200+ feet per minute.

After leveling, the film stack deposition is done via Physical Vapor Deposition (PVD). To prepare the carrier film surface for the PVD coatings, plasma cleaning is initially done. The reflective layer is high purity aluminum at approximately 100 nm. The two optical enhancement layers are magnesium fluoride (MgF2) at approximately 75 nm and titanium dioxide (TiO2) at approximately 80 nm.

Ideally, once the thin film stack is applied to the coating leveled aluminum sheet substrate, it will possess adequate durability characteristics for use in concentrated solar panel applications. For added protection against UV-light and moisture, a polysilazane-based protective top coating system has been successfully tested.

The test results of the thin film stack applied to mill-finish aluminum via a continuous coil process are shown in Table 3. Sample 1 has no protective top coat while Sample 2 has a protective top coat. As with the silver film results, the total reflectance was measured at ATC and the specular reflectance measurements were performed by NREL as defined in section 1.1.1 above.

Table 3: Thin Film Optical Properties

Sample	**Total Reflectance** ***(initial, T=0 Readings)***	**Specular Reflectance, 7-mrad** ***(initial, T=0 Readings)***	**Specular Reflectance, 25-mrad** ***(initial, T=0 Readings)***
1	94.2	21.5	41.1
2	91.1	6.2	25.8

Accelerated QUV/A-Bulb performance testing was conducted on the thin film prototype material, with and without the protective top coating as shown in Table 4. The prototype sample with the protective top coating passed 1000 hours of QUV/A-Bulb testing, while the one without did not. Based on the lower than desired specular reflectance due to inadequate leveling of the level coat, salt spray testing was not initiated on the thin film prototype samples.

Table 4: Thin Film Initial Accelerated Testing Results

Film	QUV/A-Bulb	Salt Spray
1	1000	N/A
2	Failed	N/A

As a result of the above test data, the Alcoa hypothesis of starting with mill finish aluminum, which proved positive by utilizing batch processing to apply level coatings and thereby achieving acceptable specular and total reflectance after thin film deposition, could not be duplicated on a cost-effective continuous coil line. Therefore, an alternative approach was taken in which the thin film stack was applied to production-proven coating systems. More than 25 different actual coil coated aluminum samples were tested from products commercially available at Alcoa's Lancaster facility in Lancaster, Pa. Based on the ability to level as-rolled aluminum, material cost and speed of application on a continuous coil coating line, an epoxy coating system was chosen for further development.

Task 1.2: System Ideation

System ideation began with a review of the recently employed technology within the Parabolic Trough market. During attendance to Solar Paces in March of 2008, the Alcoa team visited the Nevada Solar One plant and examined the aluminum spaceframe structure. The Solar Paces symposium also served as a convenient venue for a kick-off meeting for Phase I of this program. In attendance were CSP Services, Inc, a consultant arm of Deutsches Zentrum für Luft- und Raumfahrt (DLR), the Department of Energy (DOE), and various members of the Alcoa CSP team. CSP Services was engaged as a collaborative partner by Alcoa to provide experienced based input and feedback to the design team. Led by CSP Services, the Alcoa team reviewed structural designs that relied on a central torque tube (i.e., EuroTrough) or a spaceframe (i.e., Solargenix/NSO) to provide the primary structural stiffness. In both approaches, silver glass mirrors were mounted to the structural elements, and the glass mirrors were isolated from the structure in order to limit the stresses induced in the glass. Alcoa's approach to the design of a parabolic trough collector is based on the utilization of the reflective surface as a structural member. The fundamental hypothesis tested in Phase I of this program is that the use of the reflective surface as part of the structure would lead to a more efficient use of materials and a lower cost collector trough.

After the kick-off meeting, an ideation session was held with a multi-disciplinary team. The reviewed technological approaches as well as the Alcoa CSP team's hypothesis were discussed in detail. This review session resulted in the creation of a categorization of the collector designs into 3 basic approaches: Spaceframe, Torque Tube, and Monocoque. Figure 3 illustrates these categories.

Spaceframe - Solargenix | Torqebox - LUZ | Monocoque

Figure 3: Structural Architecture Categories

The Alcoa hypothesis that the mirror surface is structural was discussed in terms of its viability as applied to each of the categorized approaches. Preliminary analysis based on Alcoa's high level engineering study prior to the DOE award revealed that high connectivity of the mirror surface within the structure would

be essential to providing a lower cost system. The current discrete connection method employed for the glass mirrors, by design, limits the utilization of the mirrors for structure. By utilizing an aluminum reflector, this design limitation is removed. The spaceframe approach with an aluminum reflector would likely result in a suboptimal system due to the structural redundancy introduced by the sheet-to-spaceframe load transfer members or the excessive sheet thickness required to reduce the need for the additional members. Therefore, it was concluded that pursuing a spaceframe approach would only result in an incremental cost savings over current spaceframe systems. The torque tube design leads to a similar end. With the torque tube, the problem would resolve to one of optimizing the portion of the structure supporting the mirror surface, and would likely lead to a spaceframe approach. The fact that the most recent designs have moved to spaceframes would tend to reinforce this conclusion.

This logic directed focus on a monocoque design. This structural design approach relies heavily on the ability of the external skins to carry load, precisely what the Alcoa hypothesis is based upon. It was during the ideation meeting that the term 'Wing Box' was first applied to the monocoque structure due to the collectors resemblance to an aircraft wing and the similarities to the structural approach utilized in the aircraft industry, i.e., optimal use of material in a high stiffness application where the outer surfaces can be utilized as load bearing members.

The result of Task 1.2 was that the Alcoa team would pursue a monocoque, or 'Wing Box', design approach.

Task 1.3: Down-Select Preliminary Concepts

This task describes the process and results of the down-selection of preliminary concepts for the reflective surface and the system design as defined in Task 1.2. The down-selection process utilized for the reflective surface development and the structural design was performed using preliminary evaluations based on both performance and cost.

1.3.1 Reflective Surface Down-Selection

For the reflector development activity, the original Phase I plan involved developing two parallel path technology efforts (silver film and thin film), conducting two iterative evaluations on these technologies, and based on testing results, choose the best technology to be incorporated into Phase II. Due to unanticipated development iterations with both surface technologies and due to the amount of time required to obtain performance testing results from these iterations, the down-selection of the optimal technology could not be performed before the end of Phase I.

The development iterations of Phase I have narrowed the focus of activities for both the silver film and thin film efforts. The silver film product with the PET and Melinex films showed promising initial accelerated life testing; however, additional Xenon arc by NREL was required before these options could be further narrowed. For the thin film option, the level coating of production grade aluminum with a protective top coat also showed promise however additional testing was required to improve the reflectance results.

Therefore, based on less than optimum sample performance results and the incomplete Xenon arc testing results, the reflector sheet down-selection process could not be performed in Phase I of this program. Given the potential success and the progress made during Phase I testing, Alcoa recommended that this development work be continued into Phase II. More specifics of this development effort are outlined in Section 5, Task 2.1.

1.3.2 System Design Down-Selection

With the main structural approach determined in Task 1.2, concept generation was performed in order to further down-select the specific approach to the Wing Box concept, as well as, to determine the rough performance and cost as compared to the Phase I goals. Concept generation began with the creation of CAD and FEA models based on the overall trough dimensions shown in Table 5. Note these trough

dimensions serve as the basis for the performance and cost comparisons and they are not necessarily final recommendations on the optimum trough size.

Table 5: Alcoa Design Overall Dimensions

Aperture Width	5.7 meters
Collector Length	8.0 meters
Collector Section Depth	0.46 meters
Focal Height	1.70 meters

The initial FEA model was constructed to perform a material optimization analyses. The model shown in **Error! Reference source not found.** is comprised of 60,711 elements. The rear panel of the structure is removed from the figure for clarity.

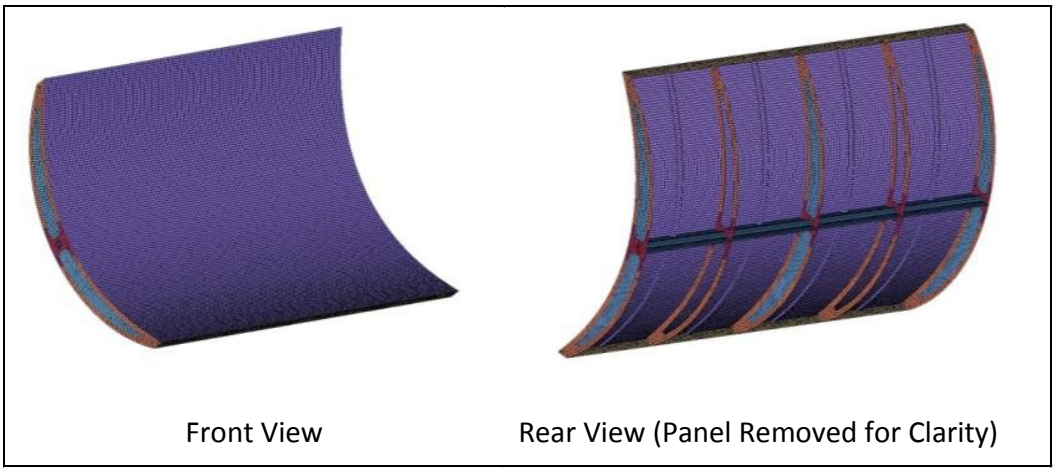

Front View Rear View (Panel Removed for Clarity)

Figure 4: Initial CSP FEA Model

The optimization analyses were based on the minimization of mass with deflection constraints under two principal load cases. The first load case applies a 1G vertical gravity load and restricts the maximum deflection of the reflective surface to 2.0 mm. The loading is illustrated in Figure 5 and is based on analyses of a single glass mirror panel under similar conditions as shown in Figure 6. The second load case applies a torsional load of 600,000 in-lbs to one end of the collector module. This is illustrated in Figure 7. The deflection restriction for the torsion load case was 50 mm and is based on data presented during the 2003 Solar Energy Systems Symposium by Solargenix for a collector based on a spaceframe construction (see Appendix B).

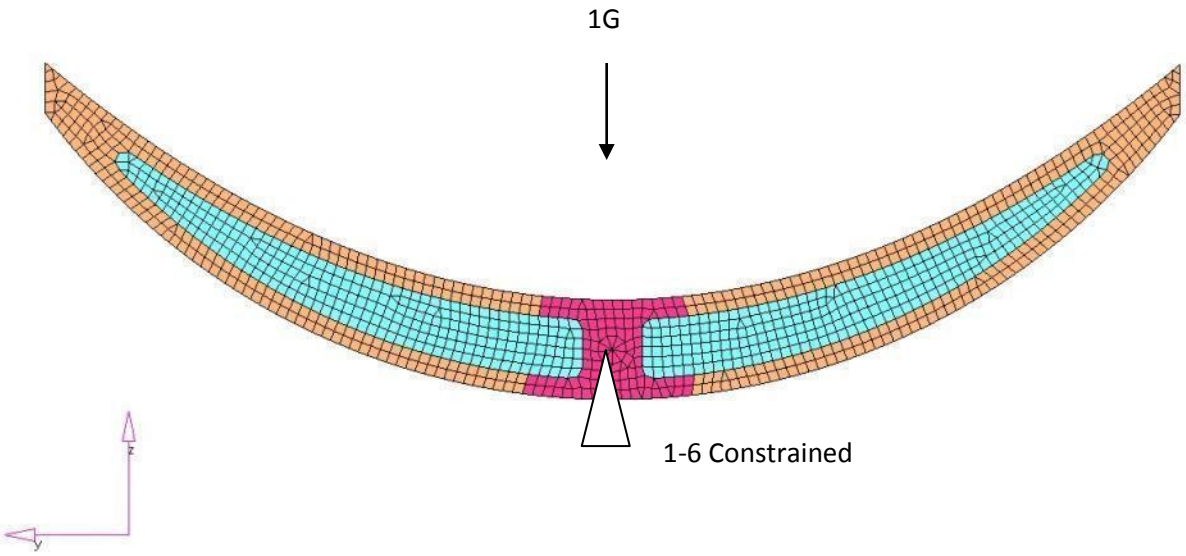

Figure 5: Orientation of Gravity Loading of Initial Model

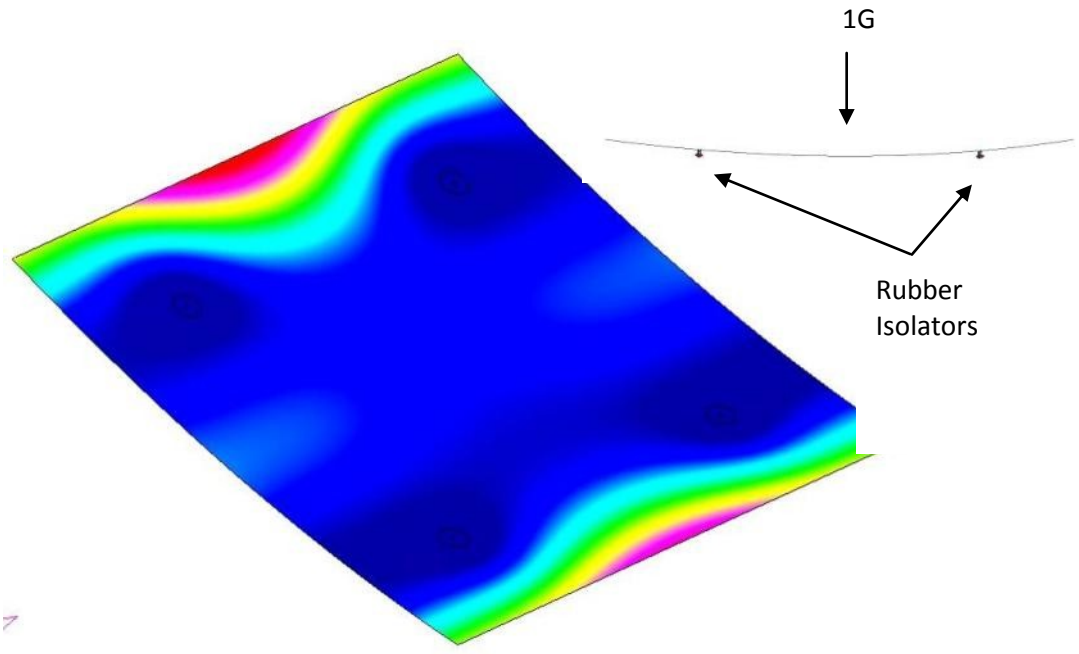

Figure 6: Deflection Contours of Glass Facet under 1G Vertical Load

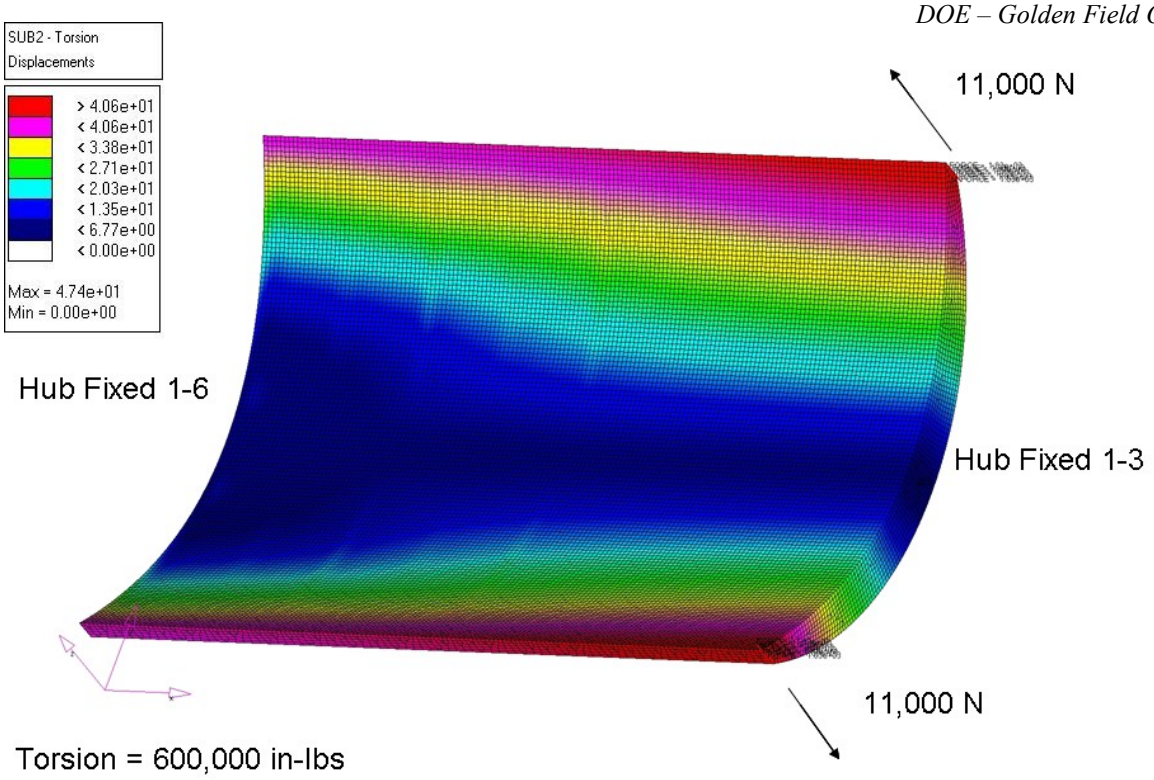

Figure 7: Torsional Load Case and Deflection Contour Plot

The results of the initial optimization analyses are shown in Table 6. These results indicated that the 'Wing Box' approach had merit due to the predicted deflection meeting the objective criteria, and that further refinement was warranted. A review of the design approach with Dr. Thomas Mancini and Greg Kolb at Sandia National Laboratories provided additional positive feedback that the Alcoa team should continue to develop the proposed concept.

Table 6: Optimization Results of Initial Model

Component	Material Thickness (mm)
Reflective Sheet	2.5
Back Close-out	2.1
End Close-out	2.1
Center Close-out	2.1
Web Member	2.1
Web Reinforcement	2.1
Hub Reinforcement	12.7
Estimated Mass	839 Kg

A more detailed model was constructed and similarly analyzed. The updated model is shown in Figure 8. The detail of the new model allowed for finer control over the material distribution throughout the structure. The design variables and their associated ranges within the optimization analyses were established with consideration for manufacturing constraints; e.g. extrusion profile and wall thickness manufacturing guidelines. The detailed model contains 240,574 elements.

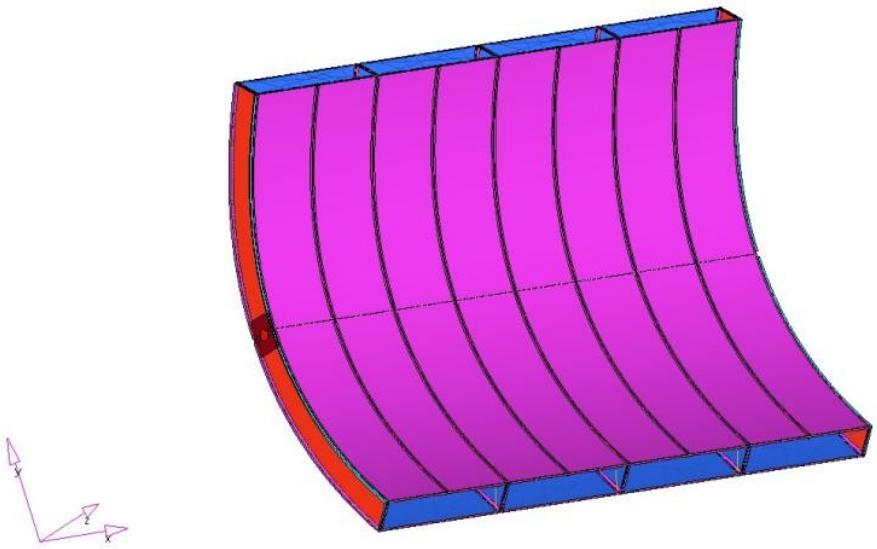

Figure 8: Detailed FEA Model of Wing Box Collector

Manufacturing and cost analyses were performed and modifications were made to the model to study the impact of the cost reduction initiatives on the structural performance of the collector. The progression of the design is illustrated in Figure 9. The manufacturing studies drove fundamental design changes to the structural sheet components other than the reflective surface, which can change little due to the principal shape requirement of the collector surface. Material utilization is the key parameter that controlled these decisions. The result is a structure with minimally higher deflections, but improved manufacturability. The higher torsional deflection can be seen in Figure 9 for optimization case 17.

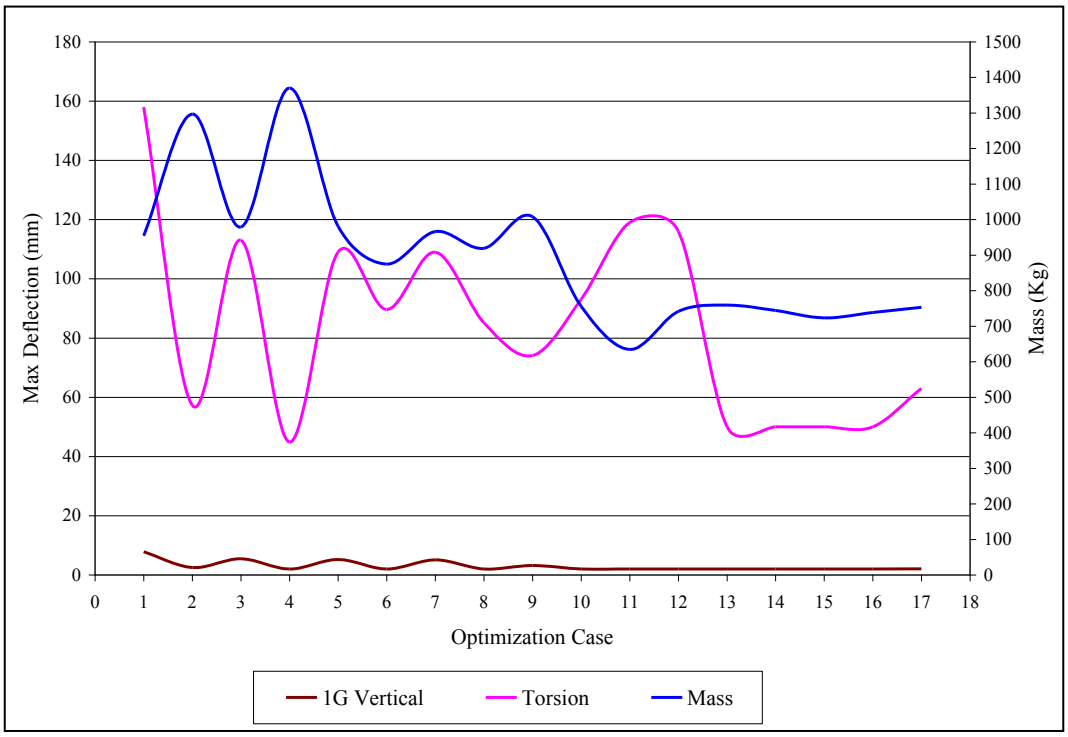

Figure 9: Optimization History – Deflection and Mass

Throughout the design analyses, CSP Services, Inc. was employed to review and comment on the resulting deflection of the reflective surface as predicted by the Alcoa FEA. One such review by CSP Services is

shown in Figure 10. Feedback from Dr. Luepfert of CSP Services indicates that the predicted error in the reflective surface is small, on the order of 0.5 – 1.0 mrad, "*Shape deviation along the collector axis is negligibly low*" – Dr. Eckhard Luepfert, shape analysis 05001852 report to Adam Schaut dated November 14, 2008 . The result of this feedback indicated that the design can be further optimized and that there is a residual error allowance for manufacturing variability.

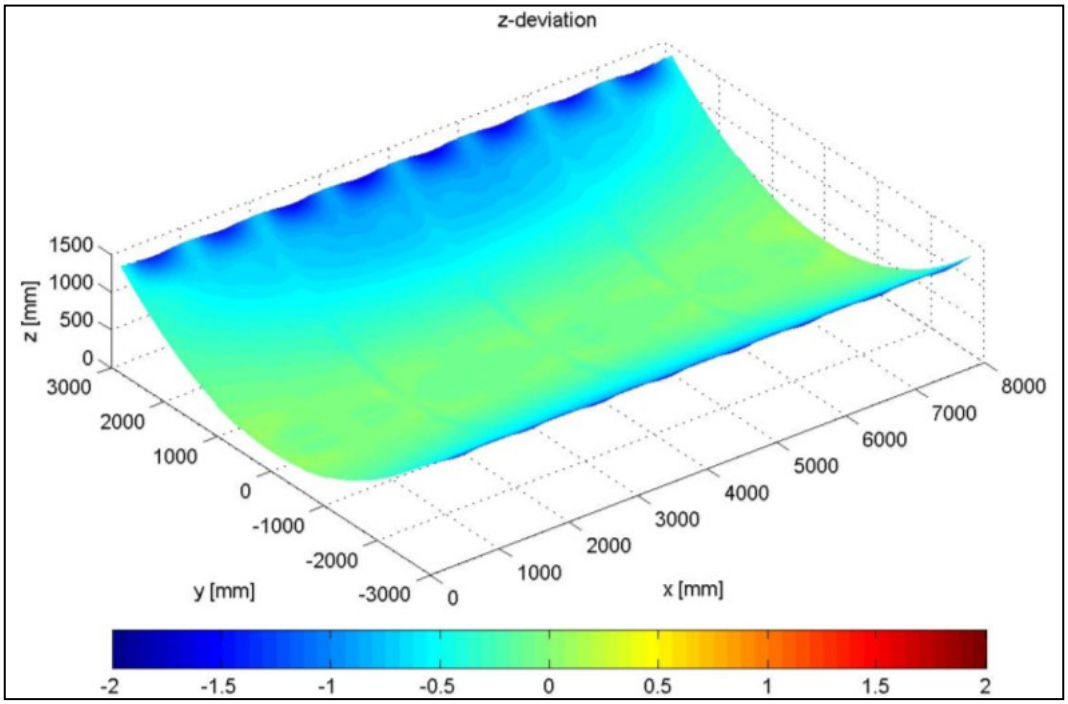

Figure 10: CSP Services Z Deviation Due to 1G Loading

Additional structural analysis of the target design was then performed utilizing the data presented in the NREL report *Wind Tunnel Tests of Parabolic Trough Solar Collectors* (NREL/SR-550-32282). As specified in this report the loading associated with an average mean wind speed of 30 mph at the collector pivot was converted to vector based gravity loading. Two cases from the report were chosen for consideration; the maximum combined horizontal and vertical loading, and the maximum horizontal loading. Table 7 provides the load information.

Table 7: G Values for Operational Wind Load Analyses

	Config	Yaw	Pitch	Cfx	Cfy	Model G's (Z)	Model G's (Y)
Max Cfx	B3	30	0	5.097	-0.034	-1.74	-1.01
Min Cfz	B3	0	60	2.107	-5.256	-2.78	-0.77

The stresses induced in the collector structure under these loading conditions are predicted to be relatively small, on the order of 20 MPa (2.9 Ksi), compared to the typical yield strength of 6000 series aluminum of 240 – 275 MPa (35-40 Ksi). The predicted deflection of the reflective surface under the wind loads was reviewed by CSP Services, Inc. Dr. Luepfert's feedback based on the wind loading analyses is consistent with the previous reviews of the gravity loading, *"In the given data, the possible losses in the intercept factor on a 70 mm diameter absorber tube are very low."* The slope error introduced by the wind loading is estimated by CSP Services to be on the order of 1.5 mrad. Appendix C contains a report from CSP Services covering the highlights of the analysis of this wind loading condition.

The resulting down-selected Phase I structural design is illustrated in Figure 11 and Figure 12. The main features of the Alcoa solar trough design are:

1. Structural reflective 2 mm thick sheets integrally assembled into the collector structure,
2. Formed aluminum extrusions that establish the parabolic shape and provide the structural attachment of the reflective sheet,
3. Sheet web panels ties between aluminum extrusions,
4. Structural aluminum panels that close out the Wing Box structure,
5. A modular design that permits factory manufacturing techniques and simplified field assembly.

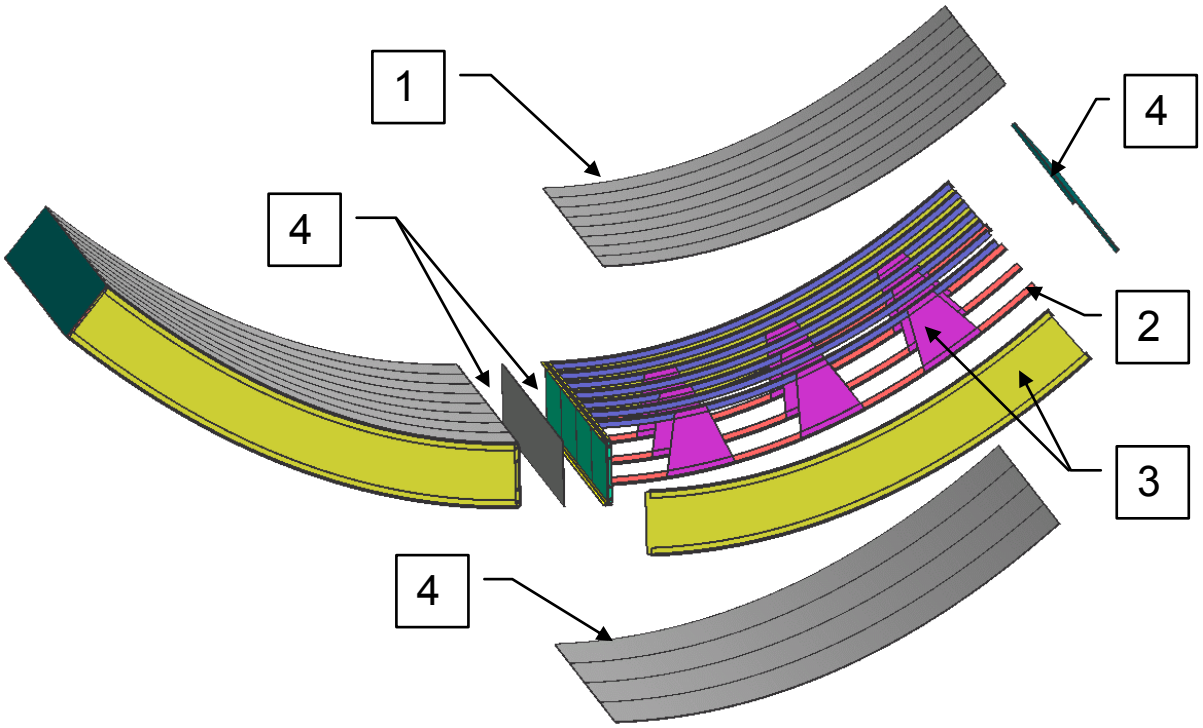

Figure 11: Exploded View of Alcoa Collector Design

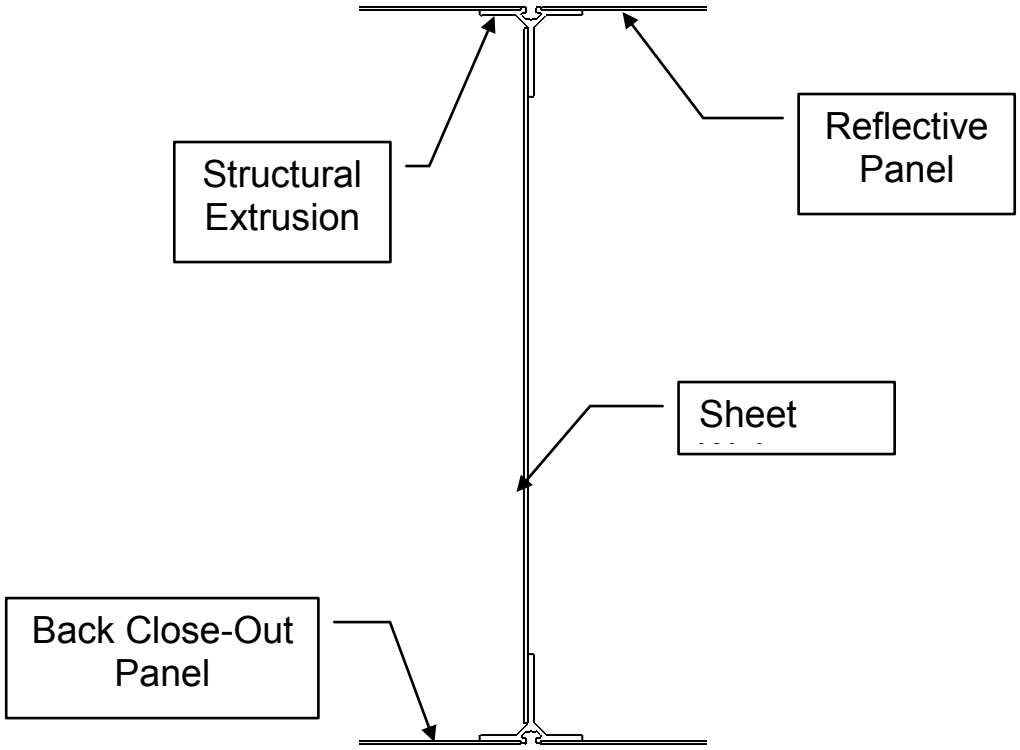

Figure 12: Section Detail of Frame Support and Web

The key differentiation created by the Wing Box design, when compared to the spaceframe approach, is the relatively shallow box section required to provide adequate stiffness. As noted above in Table 5, the section depth of the Alcoa concept is 0.46 m (18 inches). This is a fraction of what is commonly seen with the spaceframe collector structures.

The reduced section depth creates the opportunity to transport complete modules to the field, rather than the individual elements typical of the spaceframe approach. This greatly reduces the complexity presented to the assembly teams in the field, where the potential for variability is high.

The modular design and compact section create the opportunity to take advantage of highly automated manufacturing processes in the controlled setting of a factory. The collector modules can be manufactured and assembled with high precision and repeatability. Once assembled, the modules can be racked for shipment to the target installation site. A preliminary review indicates that it is possible to transport 6 complete collector assemblies on a single truck; i.e. 12 modules per truck. Figure 13 illustrates one configuration for transporting the modules.

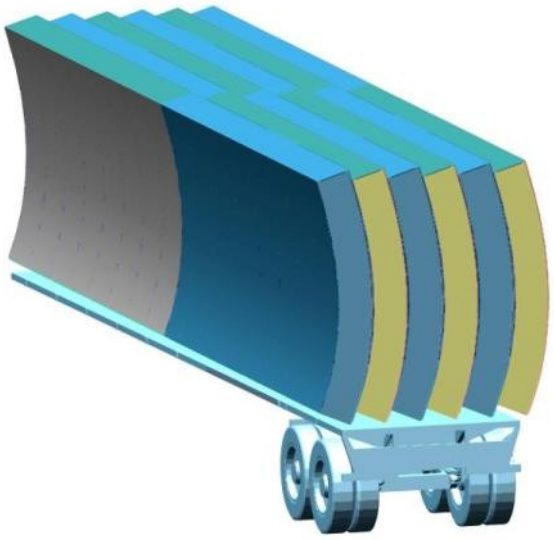

Figure 13: Alcoa Collector Modules on Flatbed Trailer

The result of Task 1.3 is the selection of a modular monocoque, or 'wing box', design that is comprised of structural sheet and extruded components. It is proposed that the collector modules be manufactured in a factory setting in order to take advantage of automated assembly processes to reduce cost and improve repeatability. Structural analyses performed as part of this task indicate that the proposed design provides sufficient stiffness and strength while manufacturing cost assessments (see section 1.3.3) support moving forward with a more detailed design phase.

1.3.3 Cost Modeling

Note: The cost modeling effort was applied concurrently throughout the reflector and system ideation and down-selection process; however, for reporting purposes the effort is being reported separated for clarity and to allow for the description of the cost modeling approach employed on this program.

A number of cost modeling tools were employed to access the impact of Alcoa's aluminum-intensive collector design approach. The objective was to quantify the impact of innovative design and materials used in conjunction with state of the art, commercial manufacturing technologies on both the solar field capital and levelized cost of energy (LCOE). Alcoa's approach employed several types of modeling tools:

- Solar Advisor Model (SAM) Version 2.0.0.2 (https://www.nrel.gov/analysis/sam/) – high level or top-down cost estimation tool developed by NREL specifically for solar applications,
- Excelergy 7-13-07 – NREL high level or top-down cost estimation tool developed that preceded SAM,
- SEER-MFG (www.galorath.com) – commercial available low level or built-up cost estimation tool that is used in the aerospace, defense, and consumer product industries.

These tools were employed in a complementary fashion such that SAM provided the baseline LCOE, capital, and field erection costs while SEER-MFG quantified the impact of Alcoa's design in reference to the baseline trough system. Additionally SAM was the primary high level costing tool, but Excelergy provided supplemental data in terms of distribution of the capital in the solar field. Figure 14 illustrates the connectivity of the tools in relation of the program.

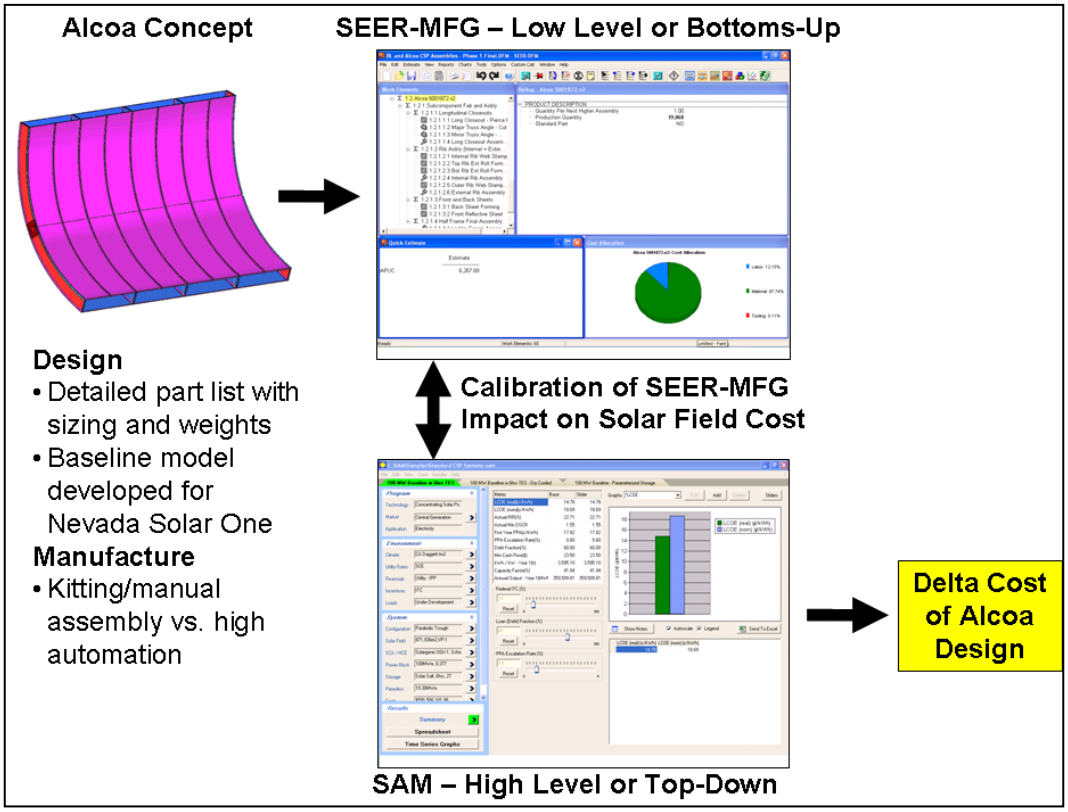

Figure 14: High Level Cost Modeling Flow Path

The general characteristics and cost structure of the baseline system was provided in SAM. SAM served as the reference and calibration tool for Alcoa's built-up SEER-MFG baseline cost model. Once the build-up baseline model was properly calibrated, the manufacturing cost savings associated with the Alcoa design could be measured. The description of the baseline system is provided in Table 8. In addition to the high level system parameters in SAM, Alcoa personnel were able to observe the baseline system directly during the tour of Nevada Solar One at SolarPaces 2008. While SAM's baseline employs NSO's solar field technology, the key difference is that it assumes a larger field size (100 MW versus 64 MW) with 6 hours of thermal storage.

Table 8: Summary of Baseline System Description in SAM

Base Case Inputs for "100 MW Baseline w 6hrs TES" in "C:\SAM\temporary\Standard CSP Systems.sam"

Technology	Concentrating Solar Power			
Market	Central Generation			
Application	Electricity			
Climate	CA Daggett.tm2			
Configuration	Parabolic Trough			
Solar Field	871,936m2,VP-1	Number of SCAs per Row	4.00	
		Distance Between Rows of SCAs	15.00	m
		Distance Between SCAs in Row	1.00	m
		Solar Multiple	2.00	
SCA / HCE	Solargenix SGX-1, Schott PTR70	Mirror Reflectivity	0.935	
		Collector Type	Solargenix SGX-1	
		# of Receivers/SCA	24.00	
		Average Focal Length	1.80	m
		SCA Aperature Area	470.30	m2
		SCA Aperature	5.00	m
		SCA Length	100.00	m
		Mirror Cleanliness Factor (field avg)	0.95	
		Solar Field Availability	0.99	
		Dust on Envelope (field avg)	0.98	
Power Block	100MWe, 0.377			
Costs	650,970,672	Solar Field per area	350.00	/m2
		Sales Tax Percent of Direct	80.00	%
		PLM Percent of Direct	3.50	%
		EPC of Direct	16.00	%
		Storage per capacity	40.00	/kWht
		Power Plant per capacity	850.00	/kWe
		Fixed O and M	50.00	/kW-yr
		Variable O and M	0.70	/MWh
		Fixed O and M Escalation	0.00	%
		Variable O and M Escalation	0.00	%
		Contingency Percent	8.40	%
		Fossil per capacity	0.00	/kWe
		HTF per capacity	150.00	/kWe
		Site Improvements per area	3.00	/m2
		Fixed (Annual) O and M	0.00	/yr
		Fixed (Annual) O and M Escalation	0.00	%

In order to understand the impact of the solar field cost on LCOE a series of sensitivity studies were performed in SAM. Table 9 shows the distribution of the direct and indirect costs for the baseline facility for three solar field costs ($350/m^2 baseline plus or minus 10%). All costs were normalized according to the baseline solar field cost. The results show that the solar field accounts for 42% to 52% of the total system capital costs, with the baseline approximately 47%. Since the solar field accounts for such a large percentage of the total capital costs, advances in design, manufacturing, and efficiency would create substantial advantages to the industry. Figure 15 also shows the cost distribution in terms of a pie chart. It is clear that the mirror and metal support structure are similar in costs to other major elements such as the power plant and storage facility.

Table 9: Capital Cost Distribution of a 100MW Plant for Various Solar Field Costs

	Major Capital Elements	Definition	Solar Field Cost, $/m^2		
			315	350	385
Direct Costs	Site Improvements	871936 m^2	0.4%	0.4%	0.4%
	Solar field	871936 m^2	42.2%	46.9%	51.6%
	HTF System	100 MWe	2.3%	2.3%	2.3%
	Storage	1749 MWht	10.7%	10.7%	10.7%
	Fossil Backup	100 MWe	0.0%	0.0%	0.0%
	Power Plant	100 MWe	13.1%	13.1%	13.1%
	Contingency	8.4% of Direct	5.8%	6.2%	6.6%
Indirect Costs	Engineer, Procure, Construct	16.0% of Direct	11.9%	12.7%	13.5%
	Project, Land, Misc.	3.5% of Direct	2.6%	2.8%	3.0%
	Sales Tax 7.75% applies to	80.0% of Direct	4.6%	4.9%	5.2%
		Totals	93.6%	100.0%	106.4%

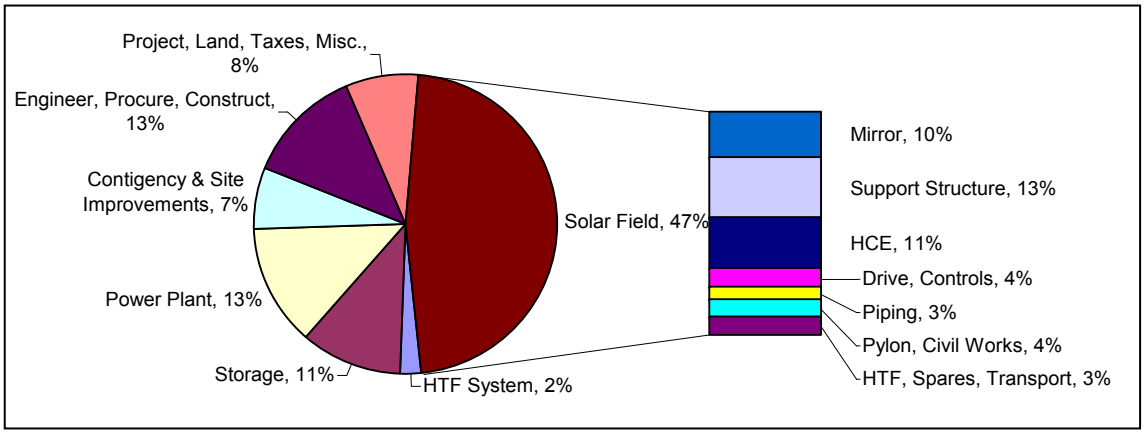

Figure 15: Cost Distribution for Baseline 100MW Parabolic Trough with 6 hours TES

Figure 16 shows the relationship between reductions in solar field versus LCOE. The figure shows in order to effect a 10 to 20% reduction in LCOE, the solar field capital costs must be reduced by approximately 18 to 35%, respectively. While mentioned previously that the solar field comprises roughly 47% of the total capital, it can further be broken down according to Table 10. This table shows the cost distribution as a function of the solar field only and the total 100MW plant costs. As illustrated in this table, the mirrors and structure account for approximately 48% of the solar field cost but only 22.5% of the total plant cost.

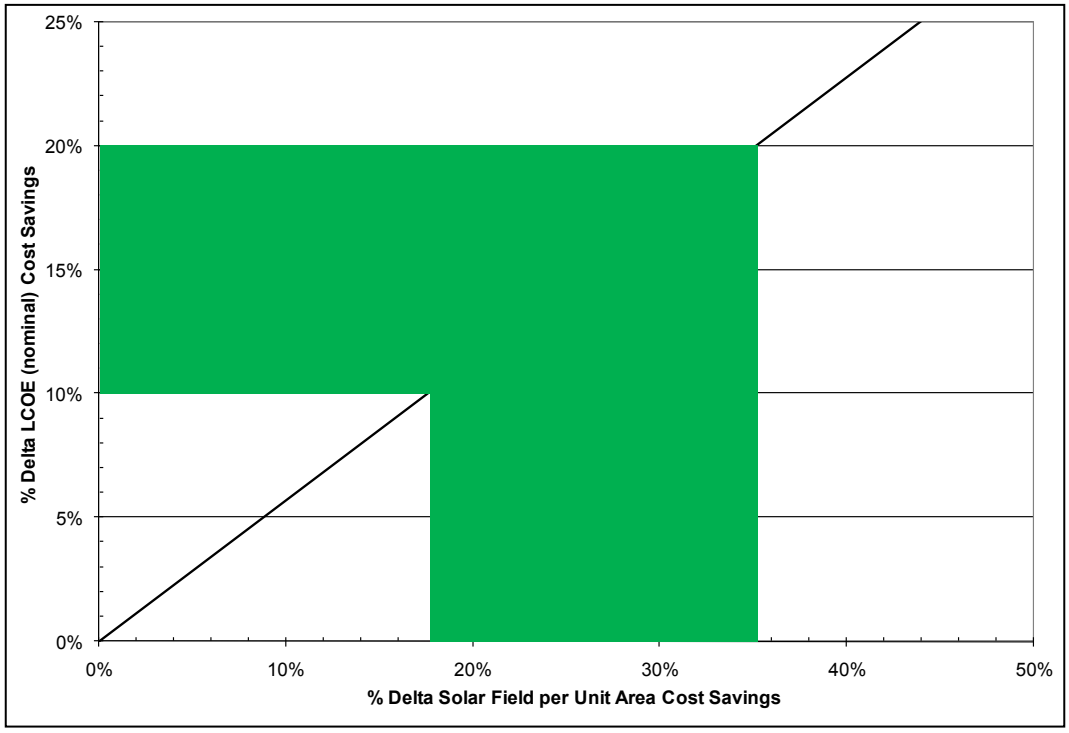

Figure 16: % Delta Solar Field Cost Savings versus % Delta LCOE Cost Savings

Table 10: % Cost Distribution for Solar Field

Solar Field Components	Solar Field Only			100MW Plant		
	Materials	Labor	Total	Materials	Labor	Total
HCE	22.8%	0.0%	22.8%	10.7%	0.0%	10.7%
Mirror	21.2%	0.0%	21.2%	9.9%	0.0%	9.9%
Metal support structure	20.6%	6.2%	26.8%	9.7%	2.9%	12.6%
Drive	5.1%	0.0%	5.1%	2.4%	0.0%	2.4%
Interconnection Piping	2.3%	0.0%	2.3%	1.1%	0.0%	1.1%
Electronics & control	3.4%	0.0%	3.4%	1.6%	0.0%	1.6%
Header piping	0.0%	3.1%	3.1%	0.0%	1.5%	1.5%
Pylon Foundations	0.0%	3.7%	3.7%	0.0%	1.7%	1.7%
Other Civil Works	0.0%	4.2%	4.2%	0.0%	2.0%	2.0%
HTF Fluid	2.9%	0.0%	2.9%	1.3%	0.0%	1.3%
Spares	2.0%	0.0%	2.0%	0.9%	0.0%	0.9%
Freight & Transportation	2.6%	0.0%	2.6%	1.2%	0.0%	1.2%
Total	82.8%	17.2%	100.0%	38.8%	8.1%	46.9%

In terms of Alcoa's design approach, both primary and secondary cost savings were realized. Primary savings were associated with the direct trough system (listed as mirror and metal support structure in Table 10). Secondary savings are influenced by the design characteristics, such as larger aperture widths, SCA lengths, etc. and the effects of equipment-based items, such as receiver couplings, pylons, drives, piping, etc. In order to maintain transparency, both types of cost savings were specified separately rather than coupled.

In order to access the impact of Alcoa's design, a built-up manufacturing model was developed for the Solargenix SGX-1 trough (NSO) system. The intention was to calibrate the results according to the high

level costs results obtained from SAM. Once the baseline model was fully calibrated against SAM, a similar assessment was conducted on Alcoa's design. The delta cost differences between the two built-up estimates was then employed to understand the influence of LCOE from SAM.

The SEER-MFG models were developed based upon part counts, sizing, and weight estimates derived by the Alcoa team. SEER-MFG is an industry leading manufacturing costing tool employed by a number of organizations such as Boeing and NASA. It allows the user to build-up the cost of a complex assembly by breaking down the manufacturing sequence required for each individual component. The manufacturing steps can include various forming, machining, joining, and inspection operations. An example of the SEER-MFG tool can be seen in Figure 17. In this figure, a work breakdown structure (WBS) is shown in the upper left hand screen. This WBS includes all the major manufacturing steps to build the final structure. Each WBS element is an individual manufacturing step that is populated with labor rates and manufacturing steps shown in the upper right hand window. The analysis is parametric in nature such that the costs are dependent upon the overall sizing, complexity, and degree of automation employed in the process. SEER-MFG produces labor hours based upon industry adopted time study results. The SEER tools are conventionally employed to develop "should costs" and the results are considered as rough order of magnitude (ROM) values since they do not necessarily include the margins and overheads associated with actual industrial applications.

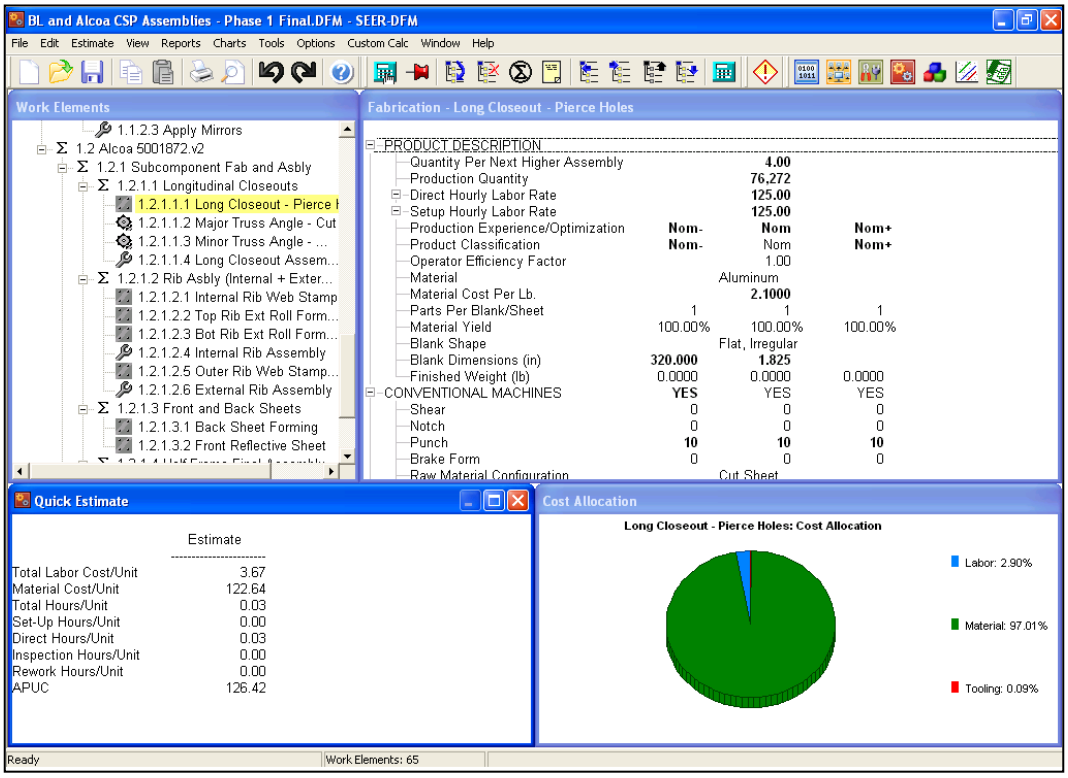

Figure 17: SEER-MFG Cost Estimation Tool

The baseline NSO model and Alcoa designs are very different in terms of the part geometry, fabrication technologies, assembly, and field erection. The SEER-MFG analysis included the materials and labor associated with the fabrication and field assembly of the mirror and metal support structures. The analysis did not include the pylons, foundations, motors, piping, and HCE. In general the trough models included the following:

Baseline Model

- Extrusion Materials, Fabrication, and Kitting – long and short (couplings) extrusions that are manually cut to size and predrilled. Parts are inspected and kitted per individual trough.

- Mirror material costs
- Field Assembly – Manual field assembly of approximately 450 parts (extrusions, mirrors, pins, blind fasteners)
- Pylon Assembly – Field erection of individual trough to pylon couplings

Alcoa

- Subcomponent Fabrication and Assembly:
    - High automation for fabrication and assembly of "half shell" troughs,
    - Employs robotic forming and joining technologies that are leveraged from automotive environments,
    - Joining employs low heat distortion technologies such as mechanical clinching, self-pierce riveting, friction stir spot/seam welding, and adhesive bonding; thus maintaining high part tolerances,
    - Aluminum product forms include extrusions and sheet,
    - Reflective surface applied at factory and costs estimated from Alcoa design team.
- Pylon Assembly – Finished half shells are transported to solar field where they are directly mounted on pylon supports, significantly reducing field assembly times.

The approach adopted from the Alcoa design leverages trends from the building and construction industries that employ highly automated processes to prefabricate large scale components. Alcoa design allows a much greater packing density over spaceframe-based systems. As a result, the Alcoa design offers an advantage of directly transporting a semi-finished trough to the site, thus eliminating the need for field assembly (see Figure 13 above).

The material and labor costs for the baseline and Alcoa designs can be seen in Figure 18. This figure shows that the primary cost of Alcoa's design is approximately 25% less expensive than the baseline. The cost saving for materials was roughly less than 10% of the baseline while the labor savings exceeded 70%. The significant labor savings was associated with high volume manufacturing technologies in conjunction with simplified field assembly and erection. While the primary cost savings shows the direct value of Alcoa's innovative structure, additional secondary improvement can also be realized (reduced pylon, drives, HCE connections, etc.). Figure 19 shows the primary and secondary savings associated with Alcoa's design. The figure shows that the primary savings could reduce the LCOE by approximately 6%. Additionally the direct secondary savings from reducing the number of pylons, drive motors, HCE couplings could contribute another 2% savings. This is a direct result of Alcoa's aperture width of 5.7 meters versus the baseline of 5 meters, thus reducing the number of troughs needed. One potential advantage of aluminum mirror systems is the ability to increase the aperture width even greater than 5.7 m. Next generation systems may increase the width to 6 m while also increasing the individual trough length from 8 to 15 m. Under those conditions an additional 3% could be further realized, thus reducing the LCOE by 11%. The cost distribution of the complete solar field for the various designs can be seen in Figure 20. This figure illustrates the various primary and secondary cost savings that were estimated by the Alcoa design.

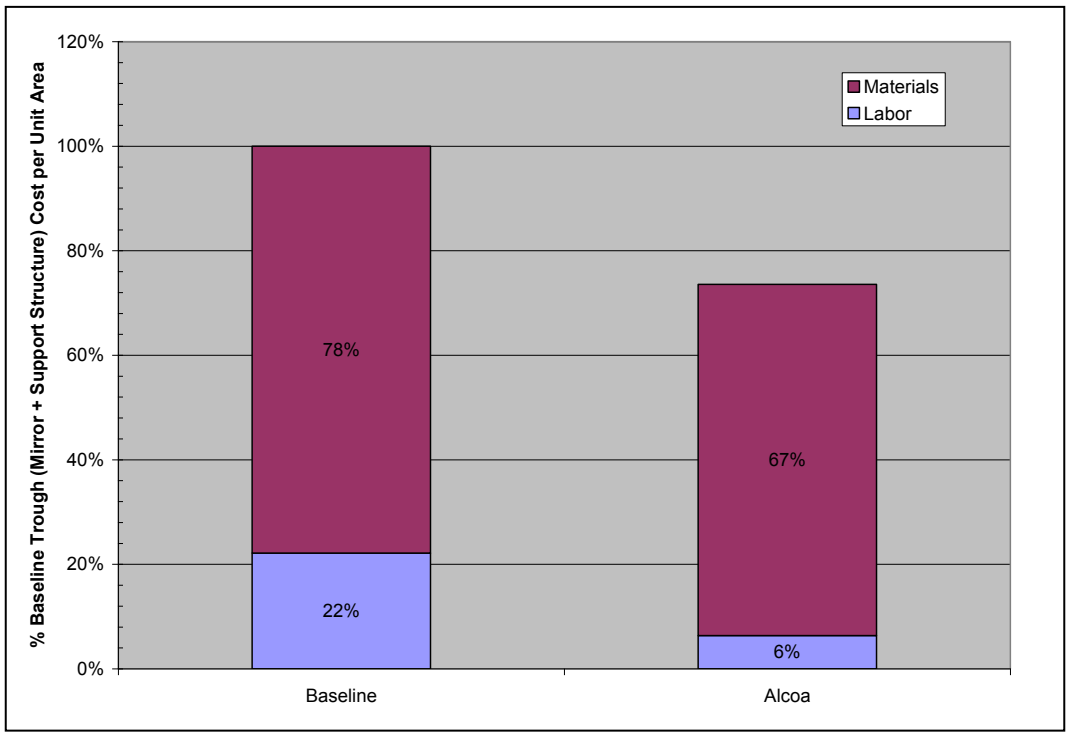

Figure 18: Percent Baseline Trough Cost per Unit Area

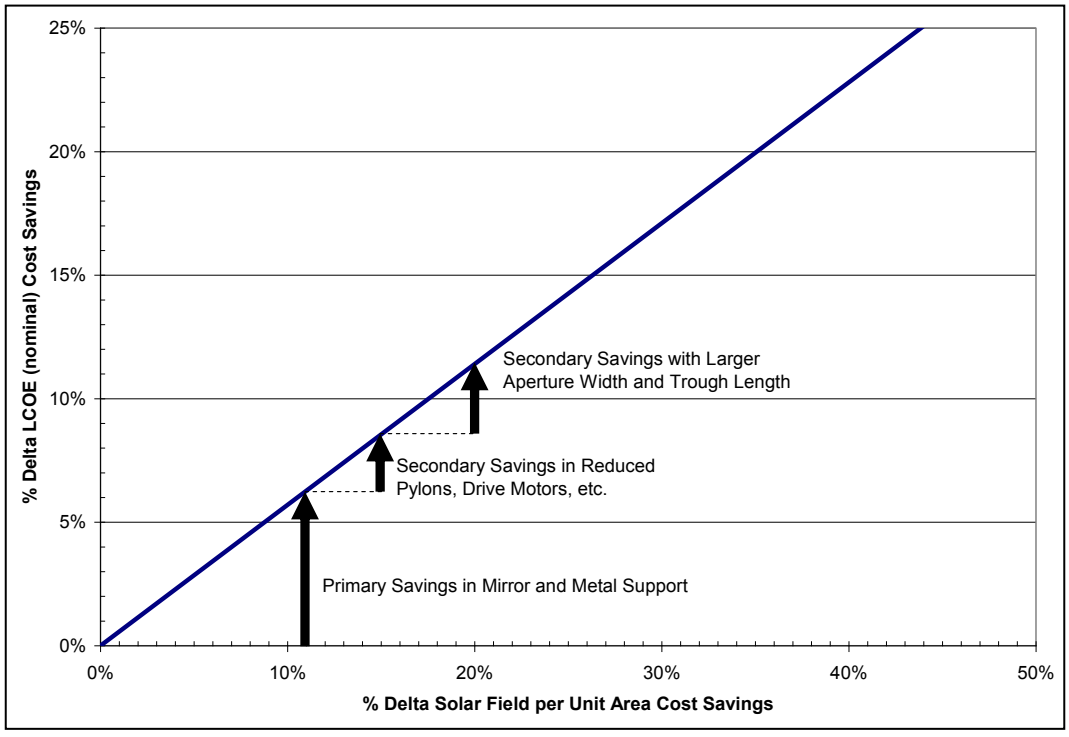

Figure 19: Primary and Secondary Solar Field Weight Savings on LCOE

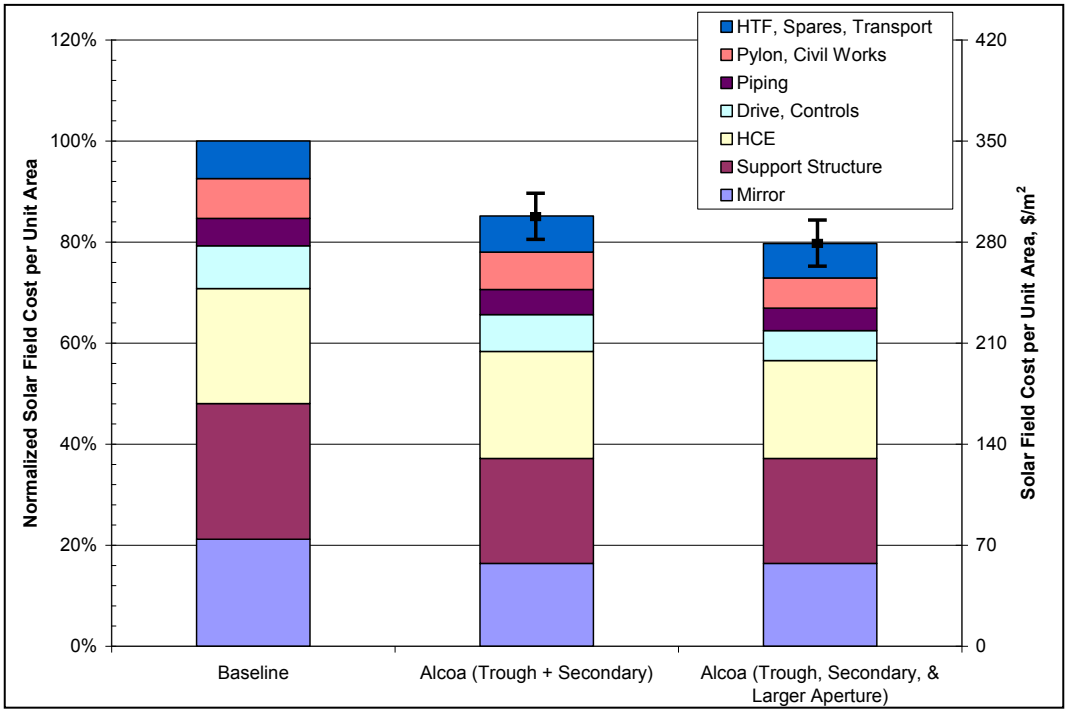

Figure 20: Cost Distribution Comparison between Alcoa and Baseline Trough System

Task 1.4: Revise Phase II Plan

This task was performed to refine the Phase II plan based on the results from Tasks 1.1 through 1.3 above. Based on the final results of the reflective surface development work, it was determined that further optimization of both the silver film and thin film product would be required in Phase II. While this optimization was not anticipated in the original Phase II plan, this activity allowed Alcoa to determine which technology has the most potential for this application. The specific activities required in Phase II are described in Task 2.1 below.

Additionally, given knowledge of the specific down-selected design, the remainder of the Phase II tasks was updated. The task description for these activities remain as proposed in the original proposal, however specifics regarding the sub-tasks and resources required to perform the work were considered in the revision. The specific activities required for Phase II are described in Task 2.2 through 2.6 below.

Table 11 below highlights the major effects of revised Phase II plan on required funding and duration as compared to the original Phase II proposal. Alcoa understands that any increased costs over the original proposal are Alcoa's responsibility as part of the Recipient total cost share.

Table 11: Summary of Revised Phase II Plan

	Original Phase 2 Plan	Revised Phase 2 Plan	Delta
Duration (months)	15	14	1
Total Labor (hours)	7331	8332	1001
Engineering Labor (hours)	*5927*	*6210*	*283*
Technician Labor (hours)	*1404*	*2122*	*718*
Labor & Burden (cost)	$ 947,203	$ 1,028,665	$ 81,462
Material & Subcontractor Cost ($)	$ 93,433	$ 102,000	$ 8,567
Travel Cost($)	$ 9,566	$ 33,118	$ 23,552
G&A Expense, B&P, COM	$ 595,582	$ 643,482	$ 47,900
Total Cost	**$ 1,645,784**	**$ 1,807,265**	**$ 161,481**

Task 1.5: Phase I Prep & Review with DOE

The final Phase I report was submitted as required on November 26, 2008. The Phase I review meeting with various members of DOE was held on December 3, 2008 at the Alcoa Technical Center. The purpose of both the report and the review meeting was to enable the DOE SETP to evaluate the feasibility of the down-selected aluminum-intensive collector concepts, assess the benefits of continued technology design and prototype development, and make an informed go/no-go decision for Phase II. Phase II of the program was ultimately approved by the DOE.

5.0 Phase II Results

The following section provides a detailed account of the Phase II tasks as defined in the Statement of Project Objectives (SOPO). This detailed account highlights the approach for each task as well as the subsequent results.

Task 2.1: Reflective Surface Optimization

Reflector sheet down-selection continued into Phase II due to the need for additional iterations to achieve optimum reflector performance as well as to complete on-going Xenon arc durability testing at NREL. During Phase I, two different reflector technologies were being explored by Alcoa, namely thin film and silver film (Figure 21). For Phase II, the focus was (a) producing a uniform level coating for the thin film stack approach to maximize specular reflectance and (b) producing an adhesive layer of uniform thickness for the silver film approach which is necessary to maximize specular reflectance.

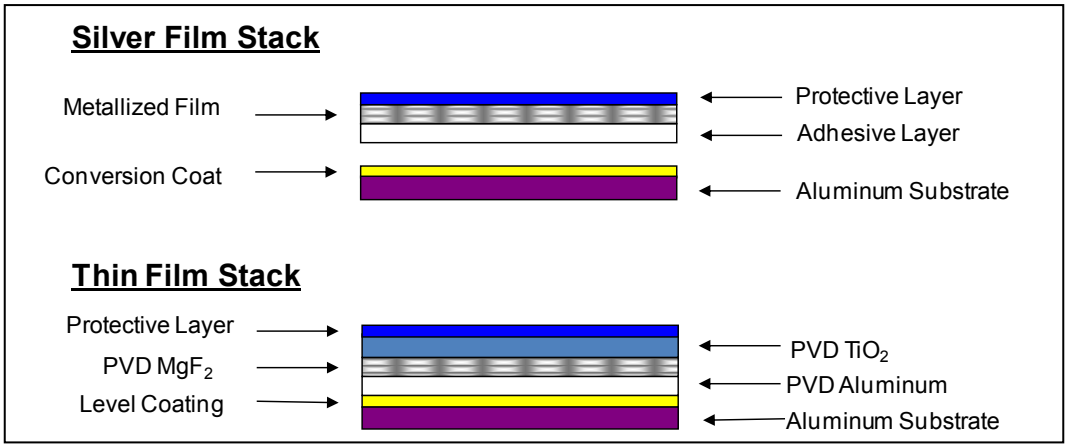

Figure 21: Silver film and thin film stack

High temperature QUV/A-bulb testing (per ASTM G53) of batch laminated silver film candidates was completed. Concurrent outdoor weatherability and accelerated tests continue at NREL. Samples were produced and tested both with and without a durable top coating to provide additional durability protection, if needed. It is anticipated that a smooth surface will be obtained through adhesive application and lamination on production equipment, thereby, maximizing specular reflectance. Significant durability improvement was noted with the application of a protective topcoat over UV-stabilized polyester silver film (UV-PET). In Figure 22, note the distinct whiting of the uncoated film after 2000 hours of exposure to high temperature QUV/A-bulb testing.

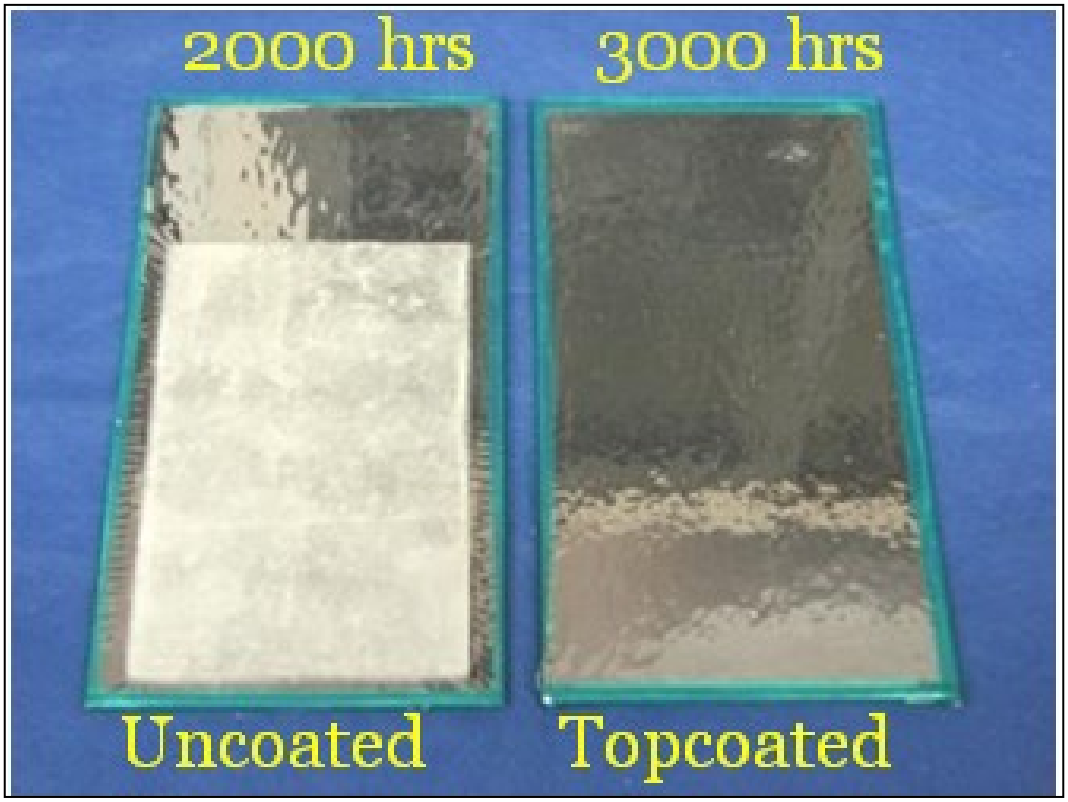

Figure 22: Batch laminated silver film samples with and without durable topcoat

After 3000 hours, the topcoated sample continued to show no sign of degradation. It should be noted that the silver film samples in Figure 22 are not intended to have high specular reflectance given they were hand laminated to the backer sheet. NREL testing continued to show consistent high total reflectivity of the UV-PET, both with and without the durable topcoat after over 8 months of outdoor exposure (Figure 23 and Figure 24).

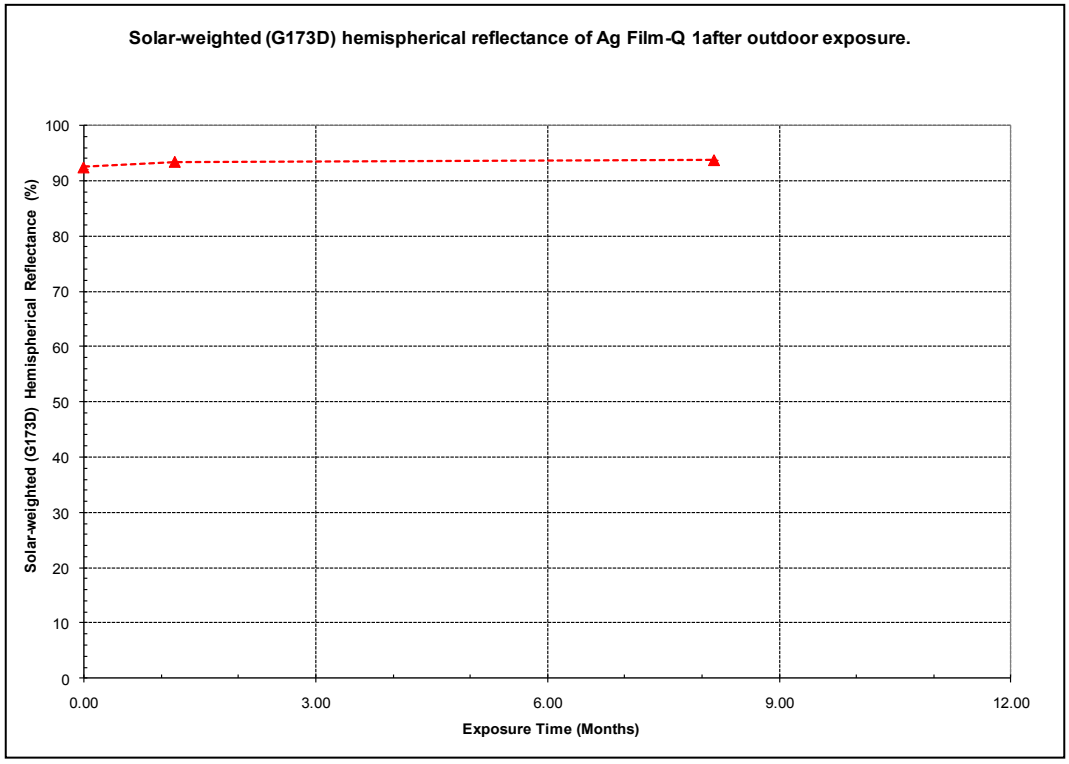

Figure 23: Silver film NREL outdoor exposure testing without topcoat

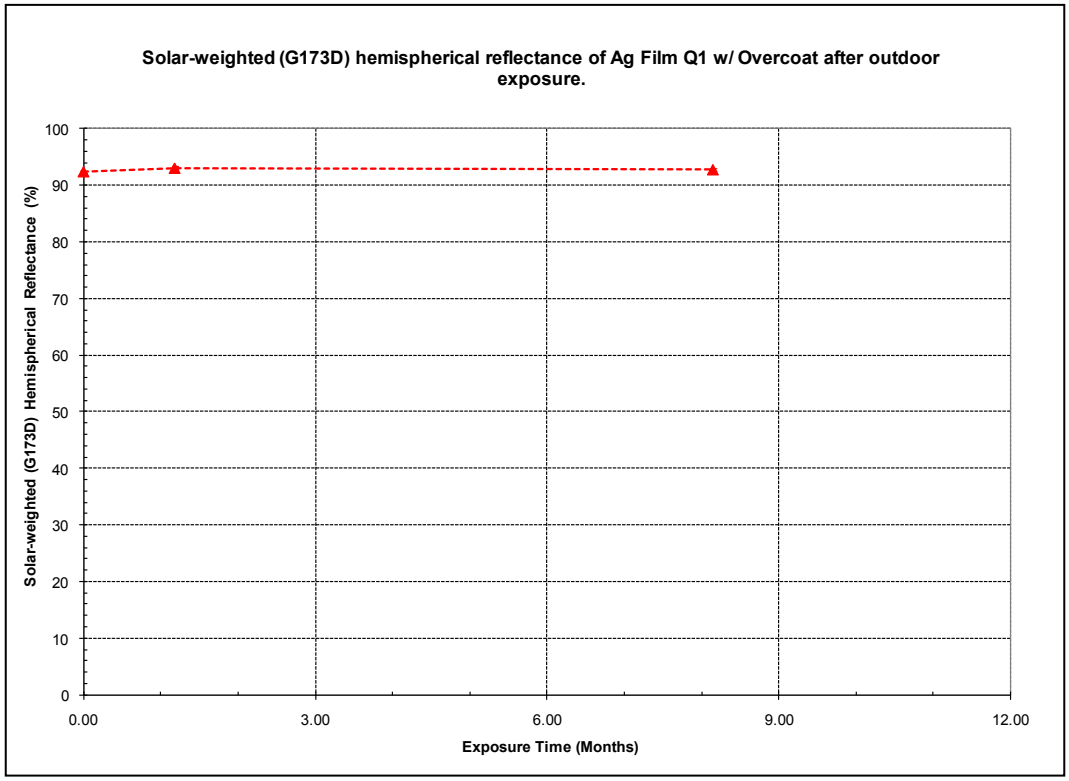

Figure 24: Silver film NREL outdoor exposure testing with topcoat

A thin film stack applied to level coated production width aluminum coil (both commodity mill finish and a smoother "preferred" mill finish) showed lower total and specular reflectivity than a commercial control (Alanod MIRO-SUN©). Level coating has not been shown to be a viable route to achieve a competitive thin film stack reflective surface. Similar to the silver film results, QUV/A-bulb testing has shown that the application of a durable topcoat over the thin film stack material improved reflectivity retention versus uncoated thin film stack samples. This has been corroborated with over eight months of outdoor weatherability testing at NREL. All uncoated thin film stack samples have shown significant reduction in total reflectivity over time, while all coated samples have maintained their reflectivity.

2.1.1 Reflective Surface Down-selection

For the silver film samples, total reflectivity is on par with commercial material, that is, ReflecTech© (Table 12). Additionally, based on Alcoa's cost modeling of the silver film manufacturing flowpath, equivalent cost would be obtained with the Alcoa UV-PET silver film (assuming durability is similar) as compared to the commercial controls. Therefore for down-selection purposes, since no cost or performance advantage was demonstrated, Alcoa chose to only consider commercial or near-commercial silver film offerings for the Phase II CSP trough prototype.

Table 12: Total reflectivity of Alcoa thin film and silver film samples compared to commercially available controls

	Glass Baseline	Thin Film Baseline	Alcoa Thin Film	Silver Film Baseline	Alcoa Silver Film
Solar Weighted Value (SWV)*	92%	92%	86%	95%	95%

* Results based on test results in April 2009

The level-coated aluminum coil stock to produce thin film-based reflector material also showed no demonstrated advantage versus commercially available thin film reflector material, that is, MIRO-SUN©. As shown in Table 12, the achieved total reflectance of the Alcoa thin film sample is lower than the total reflectance of the thin film baseline. In order to further improve the performance of the Alcoa option, more expensive substrate materials would be required, which would eliminate the cost saving potential with this reflective surface technology. Therefore, similar to the silver film results, no demonstrated cost

or performance advantage was achieved with the Alcoa thin film technology. Therefore, Alcoa again chose to consider only commercially available thin film materials for the prototype CSP trough.

A cost and performance analysis was performed on various commercial silver film and thin film reflective surfaces. A large factor in the selection was also the available weathering data. It was noted that there are many candidate materials but only a few have an NREL testing measured in years. Based on its consistent specular reflectivity and durability under outdoor and accelerated testing, Alanod's MIRO-SUN© was chosen as the reflective surface for the Phase II trough prototype. However, it should be noted that the Alcoa trough design can utilize other front reflector mirrors. The decision of which commercially available reflective surface to utilize in the future will be based on reflective performance, lifetime durability, maintainability, and cost.

In conclusion, two aluminum-based reflective surface development approaches were investigated throughout Phase I and II of the program: thin film and silver film. Given cost and/or performance parity results compared to commercially available reflective surfaces, Alcoa has currently discontinued the development of an aluminum reflective product for CSP applications.

Task 2.2: Detailed System Design

In this task and its sub-tasks, Alcoa investigated trough sizes, performed detailed design (3D CAD) and structural analysis using Finite Element Analysis modeling (FEA), cost modeling of the prototype using high-level production process modeling, and assessed the manufacturability of the prototype design. These tasks served to complete the design and prepared the Alcoa Technical Center (ATC) for building and testing the prototype. The main criteria used for selecting the prototype size were operational performance, structural performance, trough costs, and available receiver tube sizes.

2.2.1 Trough performance criteria

The primary operational performance criterion used to drive the development of the design was the need to maintain a high optical efficiency of the system throughout its operating wind load range. To achieve the desired optical performance, an intercept factor greater than 96% was specified.

As illustrated in Figure 25 there are many factors that influence the optical efficiency. The intercept factor has a tremendous effect on the system efficiency and it is a directly correlated to the geometric accuracy of the reflector. Excluding the reflectivity, the other factors are largely a function of the solar field design and the heat transfer fluid (HTF) system, which is outside the scope of this project. The choice of the reflective surface is covered in Section 5 (Phase II Results), Task 2.1.

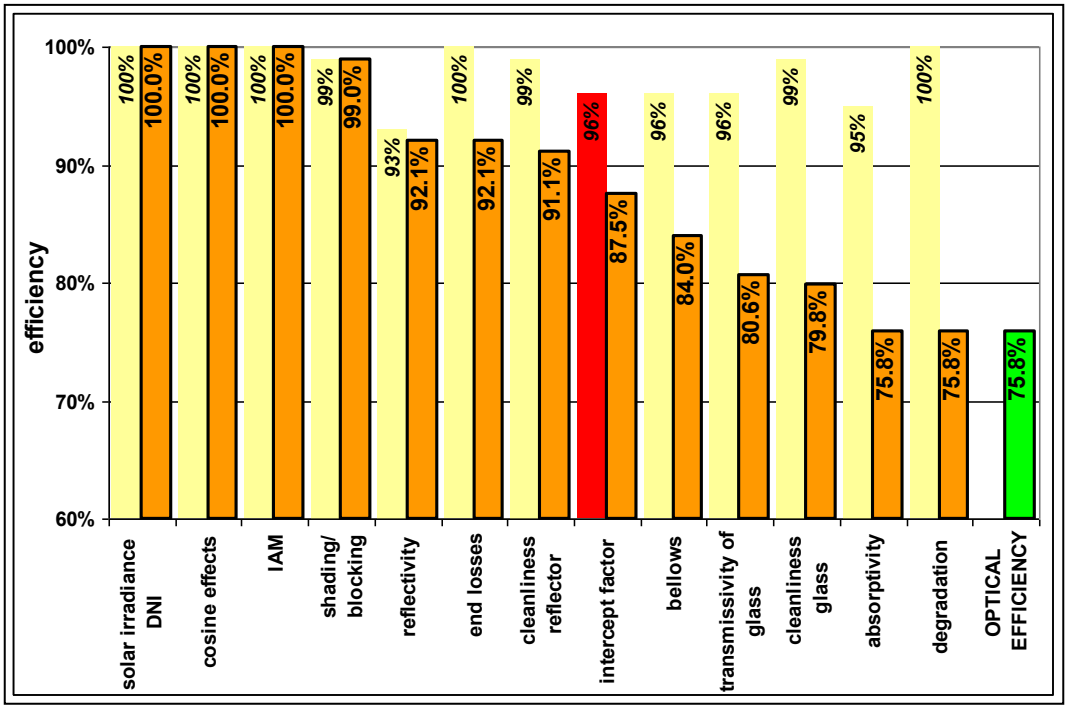

Figure 25: Parameters effecting optical efficiency in parabolic troughs (Courtesy of CSP Services/DLR)[1]

Receiver tubes with a diameter of 70 mm or 80 mm were considered for the prototype design. As illustrated in Figure 26, to achieve the desired intercept factor with a 70 mm or 80 mm diameter receiver tube, the sum of the squares deviation of the of the parabolic trough contour must be less than 8 mrad. This design criterion illustrates the importance of minimizing local distortions (waviness) of the parabolic surface. By contrast, global deflections of the surface have less of an impact on the intercept factor. For example, a 20mm global deflection on a 6m aperture trough with an 80 mm receiver tube would have insignificant effects on the intercept factor.

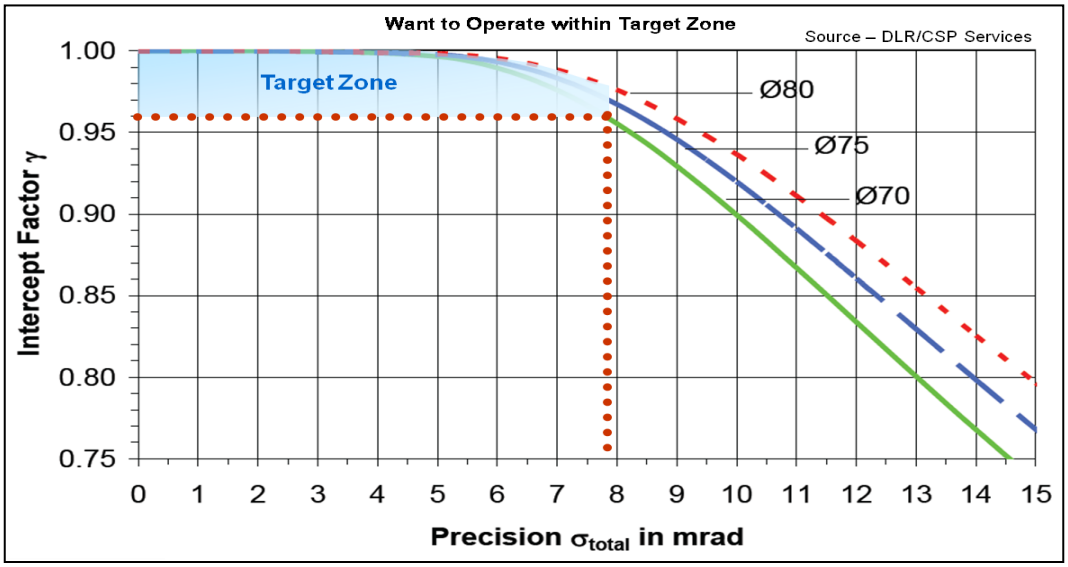

Figure 26: Intercept factor versus structural accuracy in parabolic troughs (Courtesy of CSP Services/DLR)[1]

In order to achieve and maintain a high intercept factor, the following design factors were maintained:

- The trough must be assembled with high geometric accuracy,

[1] Lüpfert E., et. al.: Parabolic Trough Analysis Techniques for Optical Performance. J. Sol. En. Eng. 2007, Vol 129, 2)

- The trough must have a global stiffness high enough to maintain the parabolic shape throughout the operational range,
- The trough must have a local stiffness high enough to resist buckling,
- The trough must remain undamaged by 'survival' wind loads.

The parabolic trough must also maintain a high intercept factor throughout its full range of operational motion, as well as under the dynamic effects of wind loading. Without any protection from the wind, the troughs at the outer edge of the solar field can experience roughly twice the wind loads compared to interior troughs (Source: NREL/SR-550-32282 *Wind Tunnel Tests of Parabolic Trough Solar Troughs)*. These wind loading effects are can be mitigated by installing a wind fence around the solar field. In order to be conservative with the first generation design (GEN-1), the prototype trough was developed as an outer edge trough without a wind fence. Two main wind loading conditions were used during the structural analysis:

- 30 MPH wind loads, with gravity effects, on an operating (un-stowed) trough
- 90 MPH wind loads, with gravity effects, on a stowed trough

For the simulation of the operating load case, the trough was oriented to the wind at a 60 degree pitch and 0 degree yaw. This corresponds to the largest total load on the trough per the NREL wind tunnel test report.

The torque loading (twist) of the trough is also an important factor to control in order to achieve a high intercept factor during operation. A load of 600,000 in-lbs applied to the corners of the trough was deemed to be the maximum allowable torque. This maximum torque condition was based on a presentation given by Solargenix at a 2003 Solar Energy Systems Symposium.

The complete set of load cases analyzed during the development of GEN-1 prototype trough was:

- Gravity loading acting on the trough pointed at the horizon,
- Gravity loading acting on the trough pointed at the zenith,
- 15 to 30 MPH wind loads with gravity effects on an operating (un-stowed) trough,
- 30 MPH wind load with gravity impinging on the back of the trough in operating mode,
- 90 MPH wind loads on a stowed trough (survival load case),
- Torsion loading due to the drive motor,
- 3g acceleration applied to module on carts
- Various rigging conditions for transportation of the prototype,
- Various static testing conditions for FEA model correlation (see Section 2.5),
- Various wind loadings corresponding to real test conditions at NREL (see Section 2.5).

2.2.2 Trough size selection

A number of different trough sizes were investigated (Table 13). The various trough sizes that were considered were based on standard trough sizes already in production and on the available lengths of commercially available receiver tubes.

Table 13: Potential trough sizes

Aperture (meter) x Length (meter)
5 x 4.0
5 x 8.0
5 x 12.0
5.7 x 4.0
5.7 x 8.0
5.7 x 12.0*
6 x 4.7
6 x 9.4
6 x 14*

The potential sizes were down-selected by the team to two possibilities: 5.7m x 12m and 6m x 14m. The initial down-selection to the two possible sizes with the largest aperture and length was made given the assumption that a larger aperture area would result in the lowest installed cost per trough by minimizing the cost of secondary solar field components such as trough foundations, piping, drive motors, etc. Upon further evaluation, the 6m x 14m trough size was chosen based on the following observations:

- Larger aperture easily accommodated with front reflector mirrors
- Larger aperture suitable to 80mm diameter receiver tubes
- 80mm receiver tubes anticipated to be standard in 2-5 years
- Easier to scale down prototype size than up for production
- More efficient with respect to installed costs
- Fewer moves during fabrication and assembly
- Faster to assemble per m^2

It should be noted that the optimum trough size for full-scale production was not determined during this phase of work. There is a limit to the assumption that “bigger is better” given there is a trade-off to maintain the accuracy (through stiffness) for a larger trough while still obtaining secondary cost savings from the larger trough size. Eventually, the cost of the trough structure required to maintain the structural stiffness will off-set the sizing benefits. The inflection point for the sizing can only be considered with an optimum manufacturing flow-path for the trough components, optimized sizing (material thickness) of the trough components, and trade-offs between manufacturing, assembly, and shipping costs. Given the main goal of this phase of the program was to validate that a Wing Box structural architecture could yield high optical efficiencies, the Alcoa team focused on validating a ‘large’ trough size knowing that a smaller trough size could easily maintain or exceed the same optical efficiencies.

2.2.3 Transportation

A high-level transportation study was performed to determine the maximum feasible dimensions of the prototype for shipping from the Alcoa Technical Center in Pittsburgh, Pa to the National Renewable Energy Laboratory (NREL) in Golden, Co. Given a monolithic 6m x 14m trough could not be transported to the NREL test facility, the team considered fabricating the prototype as a 2-module (half modules) or as a 4-modular (quarter module) design. After considering the pros and cons of each configuration (Table 14), it was determined that a 2-module configuration would potentially achieve a higher optical efficiency by minimizing the number of splice joints between the modules (see Figure 27). This configuration would also minimize the amount of assembly time required at the NREL facility. The cons with this design were mainly a result of the resources at the Alcoa Technical Center to safely handle a prototype of this size. As a result, professional riggers were contracted to move the modules during final assembly for safety reasons.

Table 14: Comparison of 2-module and 4-module designs

6 m x 14			
2-module design		4-module design	
Pros	Cons	Pros	Cons
Able to build halves in prototype shop	Professional riggers required given internal safety regulations	Easier to handle smaller modules	More handling during final assembly (potential for more errors)
Improved tolerance	Must transport halves to larger building for final assembly	Professional riggers not required by Alcoa safety	Will require more fixtures (cost and time)
Improved optical efficiency given less joints			Tolerance issues given more joint may affect operational efficiencies

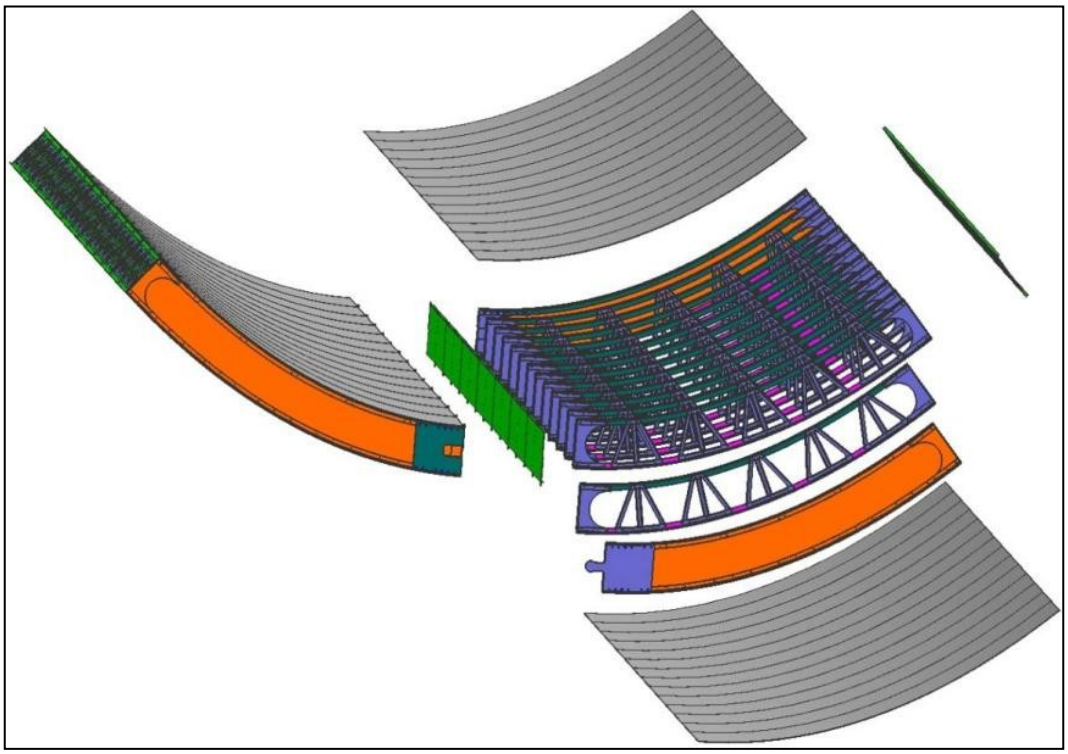

Figure 27: Monolithic Wing Box trough

2.2.4 Manufacturing

Some architectural decisions were made based on manufacturing constraints. The maximum reflector panel width was set at 1 meter, since that was the limitation of one of the Alcoa reflective surface options that was being considered. The trough's section depth remained unchanged from the Phase I concept, since it was the result of an optimization study with the same performance constraints as previously mentioned.

In an effort to minimize costs and improve the structural accuracy, several opportunities for part count reduction were identified. In some cases the functions of two parts were found compatible and a single part replaced a pair of parts. In the interest of reduced manufacturing cost and ease of prototyping, sheet product forms were used for the majority of the components. This product form also lends itself to high-volume production techniques that could easily be deployed in the future.

In order to avoid the need for a full-size assembly fixture, locating features were developed to aid in self-alignment between the two modules and to allow optical verification of alignment along the joint. Assembly fixtures consisting of adjustable carts allowed for assembly on uneven surfaces.

2.2.5 Sheet gauge

A FEA model of the proposed prototype design was developed to determine necessary sheet gauges and predict structural responses to loads. Early analysis results showed similar performance to the Phase I concept models, boosting confidence in the chosen analytical methods for Phase II of the program. Once the bill of materials (BOM) was created, structural analysis of each part was performed. In most cases, buckling performance of thin sheet parts dominated gauge and geometry decisions. Steel reinforcement plates were added to the end ribs to reduce stress concentrations on nearby sheet and extruded parts. While dissimilar materials are not a corrosion concern with this type of application, the reinforcement plates will most likely be redesigned in aluminum in future design iterations.

An early version of the prototype design had open portals in the back sheet and the outer spars in an effort to reduce weight. Analysis proved that they dramatically reduced torsional performance of the structure. However, access to the interior of each module is required to join the two modules during final assembly. For the prototype closeout panels were attached to the perimeter of the opening with machine screws. This solution turned out to be tedious during final assembly of the two modules and the approach will be revised in a next generation design.

2.2.6 Receiver tube support structure

The receiver tube support structure was developed while the trough prototype was being manufactured. Feedback from CSP Services suggested that the tube supports needed to be extremely stiff to maintain a high intercept factor. This proved to be challenging because of the flexibility of the modules at the required receiver tube support locations on the trough. The anticipated deflection was overcome by bonding bar-stock foundations to the trough's inner rib posts. Bolting the trough halves together through the foundation of the receiver tube support also provided the level of stiffness required (Figure 28).

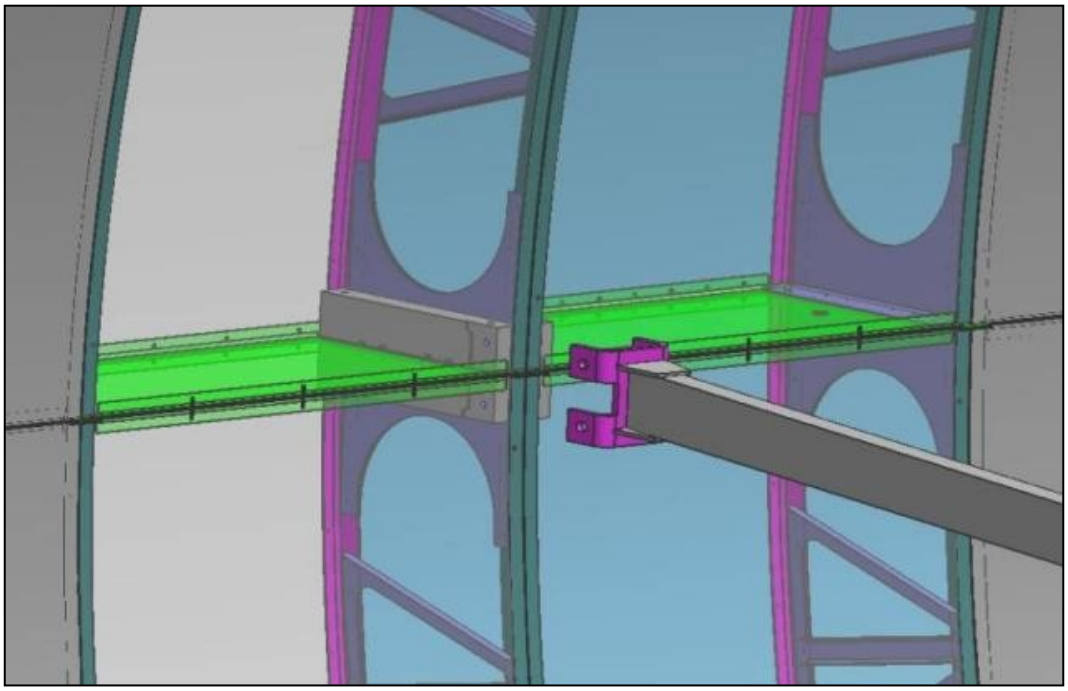

Figure 28: Strengthen receiver tube foundation

Rectangular stainless tubing was chosen for the vertical receiver tube supports because it eases manufacturing and decreases thermal conduction when compared to common steel. Some amount of free motion had to be allowed at the tube mounts because the absorbers grow in length when heated. A novel sliding bracket design provided that freedom while offering adjustment for alignment of the absorber tubes with the modular trough (Figure 29).

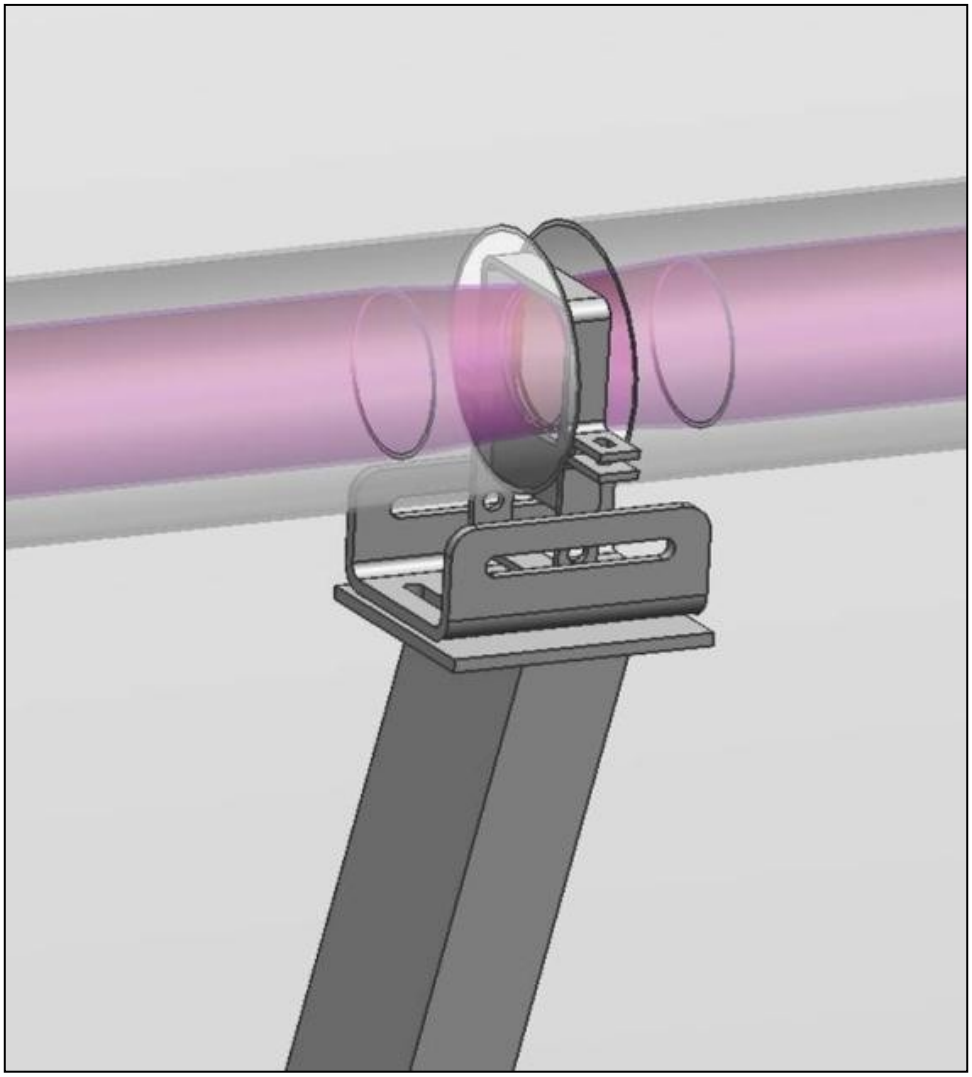

Figure 29: Receiver tube support

It should be noted that the receiver tube supports were designed mainly for function and were not optimized from a cost perspective. The main focus of Alcoa's Phase II effort was on the trough architecture and not necessarily on supporting components such as receiver tube supports and trough supporting stanchions.

2.2.7 Joining plates and trough mounting

The joining plates and trough mounting hardware were the last parts developed because of the relationship between the stub axle locations and the trough's center of mass. For safety reasons it is preferred to have the units center of mass located such that the unit wants to point to the zenith and does not try to rotate during installation. This is also desirable in the case of a free moving trough during operation. These parts were designed to be easily manufactured from steel plate and tube.

2.2.8 Final System Design

The final Phase II design for the Wing Box trough is shown in Figure 30 and Figure 31. In an effort to reduce the weight of the trough, simplify the manufacturing of the components, ease the assembly process, reduce manufacturing variability, improve optical efficiency, and to reduced costs, significant efforts were made to reduce the number of parts through unitization and commonality of components. The result is a design with a minimum number of parts and the components can be made using highly automated manufacturing techniques.

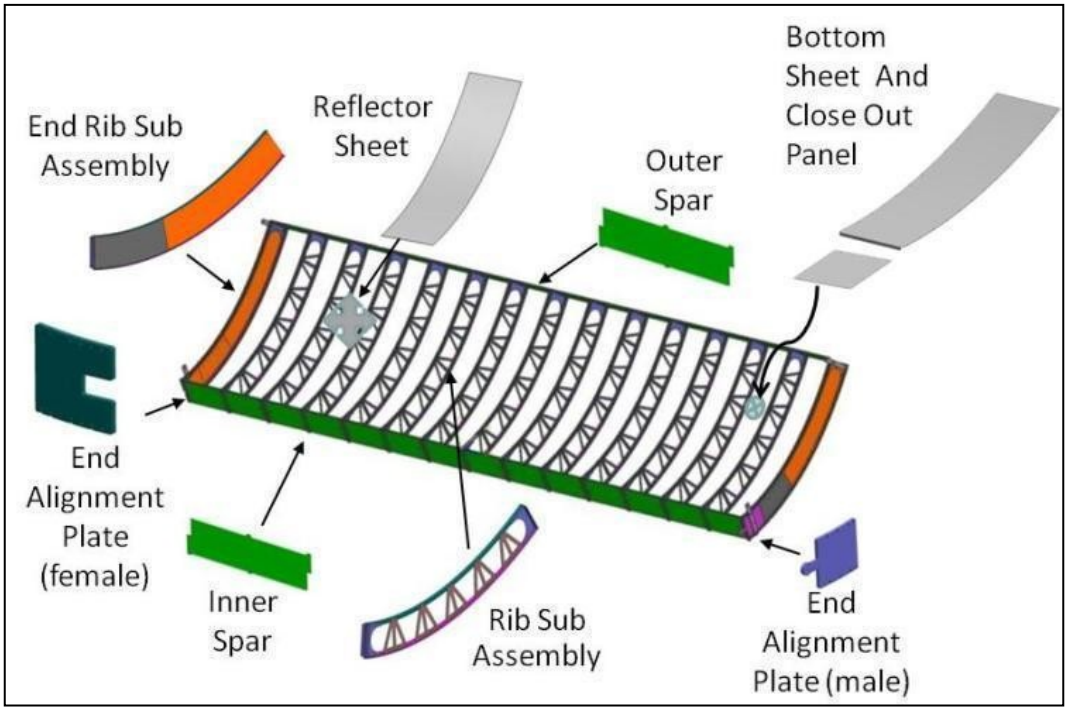

Figure 30: Half module Wing Box design

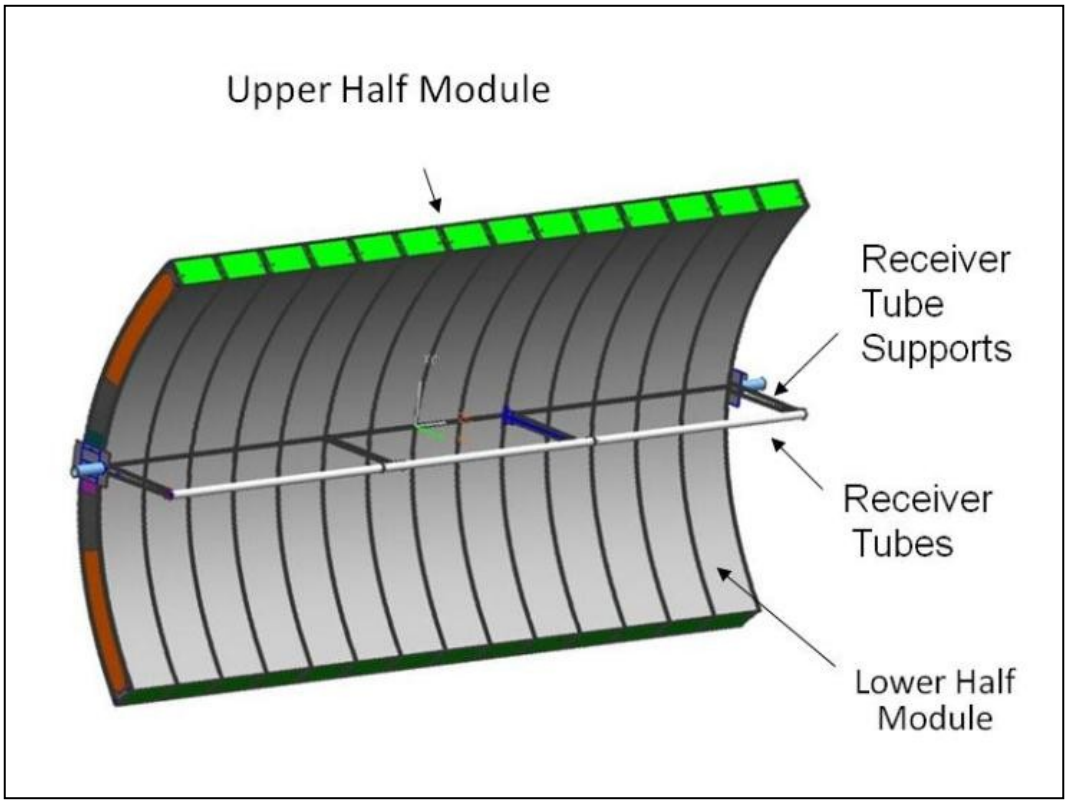

Figure 31: Fully assembled Wing Box design

Task 2.3: Internal Critical Design Review

This task highlighted an internal Alcoa milestone to review all the critical design information before officially releasing the design for prototyping.

The following were reviewed:

- Detailed prototype design
- Structural finite element analysis (FEA) results

- High level costs
- Assembly plan
- Component, subassembly and half module quality plan
- Static and dynamic test plan
- Safety issues

The main criteria and weighting used to drive the design review are listed in Table 15. This table shows the design drivers and the criticality of these drivers for the Phase II prototype build. The performance of the prototype, in terms of structural accuracy, was deemed the most important criteria for this stage of the development program. If the Wing Box design configuration cannot be manufactured to a high-level of accuracy in a prototype environment, then achieving accuracy in a production environment will be difficult. While the overall objective of this program was to demonstrate that the aluminum intensive Wing Box trough system could significantly reduce the levelized cost of energy (LCOE) for CSP troughs, the purpose of the prototype was predominantly to validate that the system would perform as designed.

Table 15: Design review criteria weightings

Design Drivers	Prototype Weighting
Performance	40%
Costs	20%
Manufacturability	20%
Schedule	20%

2.3.1 Design decisions

The Critical Design Review was performed by a diverse group of Alcoa design, manufacturing, and cost modeling personnel who are experts in a wide variety of markets and technologies. The design was presented on a component-by-component basis and FEA predictions were shared with the group. Much of the discussion centered on the expected structural performance of the design. The manufacturing process, proposed test plan and safety concerns during manufacturing and assembly given the resources at the Alcoa Technical Center were also reviewed. The results of the structural analysis were used to verify the proposed material thickness for each of the components. Material thickness for all components of the prototype were proposed and accepted based on the analysis results. For an example of this analysis, see Figure 32.

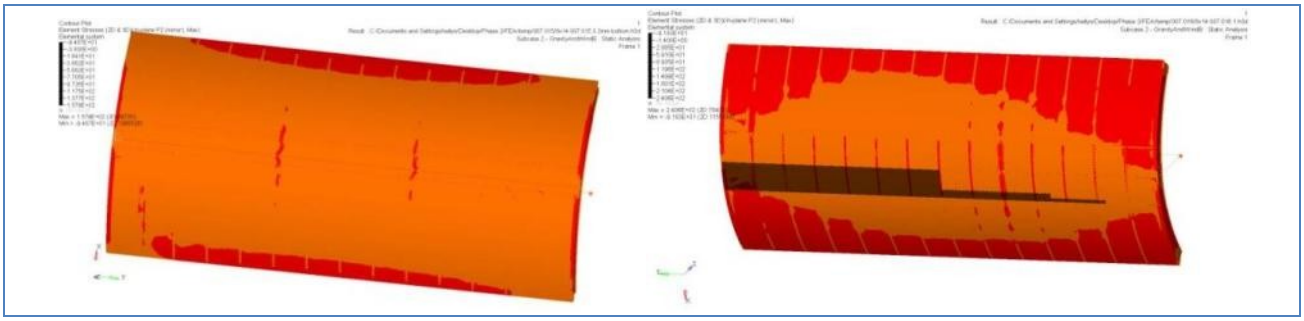

Figure 32: FEA results depicting regions predicted to buckle at high operational loads highlighted in red. Two different skin thicknesses are depicted left versus right.

In the above figure, the same loading conditions are applied to models with different skin thicknesses.

The detail design was reviewed and the following decisions were finalized:

- Design to be released with conservative sheet thicknesses for all outer skins.
- The aluminum alloys for the prototype build were established based on the required strength levels of the components and based on current availability for the prototype build.
- Rib sub-assembly inner rib post design to be fabricated from mild steel sheet for additional robustness
- to prevent fastener head embedment

- to increase the safety factor associated with the modular connection
- All trough parts designs to be released for build at specified gauges.
- Tube stand-off design to be completed while trough modules are manufactured.
- Test stanchions will be designed by ATC's engineering department.

2.3.2 Pending items

Pending items from the CDR included finalizing the static and dynamic test plan and reviewing the safety protocol with ATC's EHS group. The safety reviews included the prototype build plan and the local transport methodology for the modules and whole units. The pending items were resolved in parallel with the prototype build. The test plan is discussed in Section 2.5 of this report. The safety protocol related to the final assembly of the prototype was established prior to the completion of the modules.

Upon successful completion of the internal CDR, the detailed design was released for build and the manufacturing and assembly of the prototype trough structure commenced.

Task 2.4: Prototype Build

This section describes the manufacturing of a full-scale trough prototype including the reflective surface panels. Activities included releasing the prototype drawings, fabricating necessary tooling and fixtures, procuring materials and off-the-shelf components, fabricating system components, fabricating the reflective panels, and assembling the final prototype. The completed prototype is considered the Alcoa Generation 1 Prototype Assembly, or simply GEN-1. The prototype assembly is 14 meter long with a 6-meter aperture. Fabrication was completed during the 4th quarter 2009 and assembled at the Alcoa Technical Center (ATC).

As shown in Figure 30, the major sub-assemblies of the prototype trough are the rib sub-assemblies, the reflector sub-assemblies and the receiver tube supports. The end alignment plates were also a very critical component during the prototype build.

2.4.1 Fabrication and assembly

The assembly process developed for the components was designed to drive high precision into the fabrication of the sub-assemblies and half module assemblies.

The rib sub-assembly is shown in Figure 33. It is used to set the location of the surface of the reflective sheet. It was necessary to maintain a high degree of precision during the assembly process to assure the correct geometric surface of the reflective sheet. The inner and outer bows were fabricated from aluminum extrusions with a 'T'-profile. The extrusions were stretch bent and then checked in a check fixture to assure that the correct shape was achieved. Tight tolerance control was used to fabricate all parts that could influence the resulting geometric precision of the trough surface.

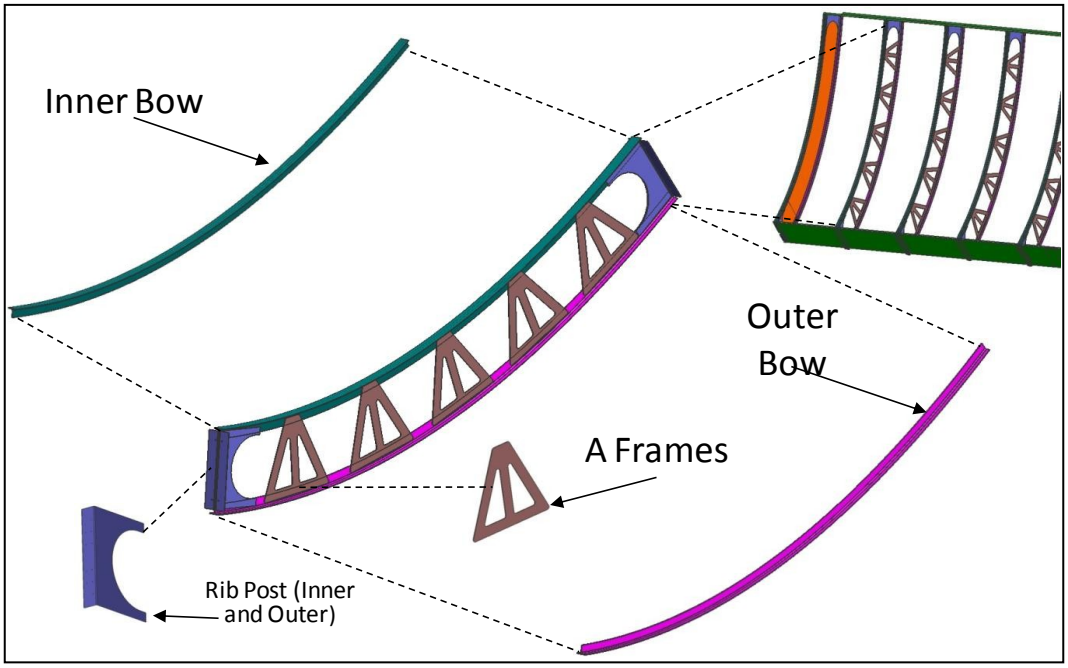

Figure 33: Rib sub-assembly conceptual design

The bows were spaced with A-frames fabricated from cut and bent aluminum sheet. They were attached to the aluminum bows with mechanical fasteners instead of welding to prevent distortions. Welding of any component was avoided if possible to minimize distortions, assuring a high level of geometric accuracy.

The outer rib posts were fabricated from cut and bent aluminum sheet. The inner rib posts were fabricated from cut and bent steel. This was done for the prototype only. Once the structural simulations had been correlated with actual results, the design would be optimized such that the inner rib posts can also be fabricated from aluminum.

The fixture used for the assembly of the rib sub-assembly was designed and fabricated at the ATC. All of the rib sub-assemblies were checked on a coordinate measuring machine (CMM) for accuracy. The rib sub-assemblies that passed quality inspection are shown in Figure 34. It is anticipated that during full-scale production, the rib sub-assembly process would include a high degree of automation. The quality control of the rib sub-assemblies will also be automated. As long as the process is in control, a low percentage of the final product would need to be spot checked.

Figure 34: Rib sub-assemblies after final inspection

The reflector sheet was composed of a commercial thin film product (Alanod's MIRO-SUN©) attached to an aluminum backer sheet. See Section 4, Task 2.1 for more details regarding the reflective surface studies and down-selection. The quality of the process used to join the reflective thin film stack-up to the aluminum backer sheet is critical to maintain the specularity of the MIRO-SUN©. The reflective sheet was adhesively joined to the backer sheet via a batch operation. For full scale production, it is anticipated that a continuous process would be used.

The receiver tube supports were another critical sub-assembly. The alignment of the receiver tubes to the reflective surface of the trough depended upon the accuracy of the build and installation of the tube supports. The receiver tube support saddles allowed the adjustment of the support during tube installation, as well as movement of the receiver tubes during operation due to thermal expansion. All receiver tube support components were made from stainless steel in an effort to maintain a high degree of accuracy and to prevent distortion during operation. An example of the receiver tube support saddle is shown in Figure 35. It is anticipated that automation would also be used to fabricate the receiver tube components, as well as the receiver tube sub-assemblies during full rate production.

Figure 35: Tube support saddle

The end alignment plates were also considered critical components for the prototype build. The end alignment plates were used to assure that the two half modules not only went together rapidly, but also accurately (Figure 38). They were the main feature that allowed rapid assembly of the trough in the field. As in illustration of this, the trough was ready to be placed on the two axis tracker at NREL within a matter of a few hours. The alignment plates were fabricated from steel for the prototype. To further reduce the weight of the trough, it is anticipated that the alignment plates would be fabricated from aluminum in future designs.

The Alcoa design was fabricated in two half modules and joined along the centerline to create the Wing Box trough (Figure 36,Figure 37, and Figure 38). The modular design would permit the use of automated factory manufacturing technique, not only during the fabrication of the prototype, but also during full rate production. The automotive and aerospace techniques incorporated into the design results in a high degree of accuracy during fabrication and allows for simple field assembly. The two halves were assembled at the ATC and underwent a Geometric Dimensioning & Tolerancing (GD&T) quality control evaluation prior to NREL's VSHOT (Video Scanning Hartmann Optical Test) evaluation of the accuracy of the reflective surface. (See Section 2.5 for more details.) For NREL to conduct the VSHOT test at Alcoa, the complete prototype was placed in stanchions so that the trough could point to the horizon (see Figure 39). Once the NREL evaluations were completed, the trough was removed from the stanchions and the two halves were disjoined and transported to NREL's Solar Industrial Mesa Test Area (SIMTA) in Golden, CO.

Carts were fabricated to transport the two half modules to the final assembly area at the Alcoa Technical Center (Figure 37). The carts were also designed to ease in the alignment of the two halves for final assembly. The carts were then used as transport fixtures during the transportation of the two halves to NREL's SIMTA test site in Golden, CO. At NREL the carts were once again used to align and join the two halves to create the final assembly. The final assembly was then mounted to NREL's two axis trackers where it underwent additional performance validation tests. See Sections 4, Tasks 2.5 for more information regarding System Validation.

Figure 36: Half module fabrication at ATC

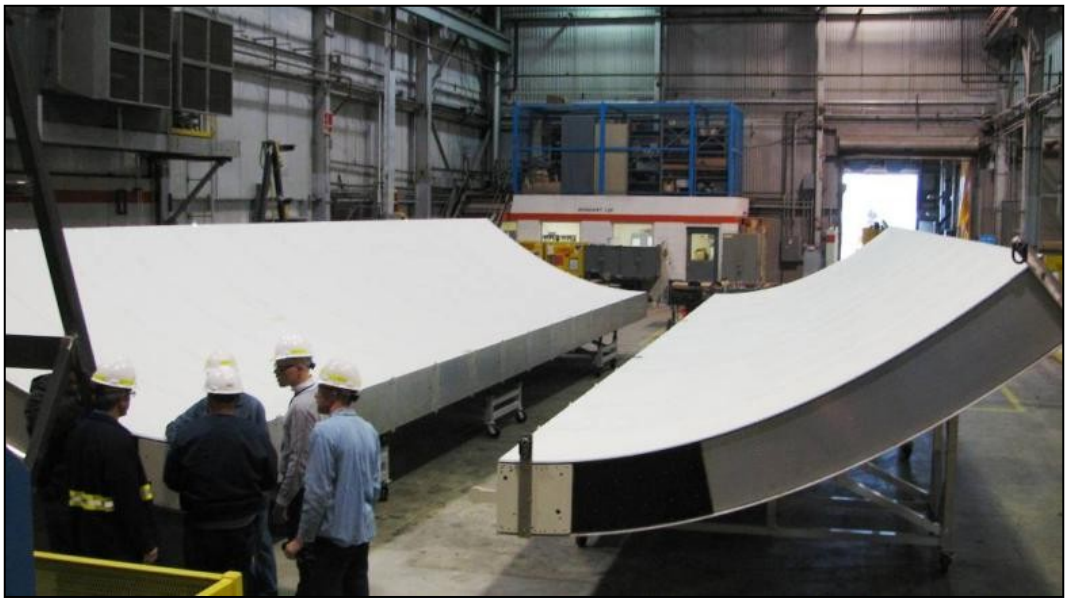

Figure 37: Two half modules mounted on the alignment carts prior to joining at Alcoa

Figure 38: Two half modules joined together at ATC

Figure 39: Prototype trough in stanchions at the ATC

Task 2.5: System Validation

This task focused on validating the performance of the prototype throughout the manufacturing and final assembly process. Geometric Dimensioning and Tolerancing (GD&T) analysis, Finite Element Analysis

(FEA), various optical tests, and cost analysis were used. GD&T was used to verify the dimensional accuracy of the components, sub-assemblies and final assembly. FEA was used to simulate the response of the prototype to various loading conditions. The simulations were then correlated with actual load tests, both static and dynamic. The Video Scanning Hartmann Optical Test (VSHOT), Distant Observer (DO) test, and Incident Angle Modifier (IAM) test were used to verify the surface contour, as well as to generate an optical efficiency value for the Wing Box design trough architecture. The SEER MFG cost modeling software was used to conduct various trade studies, as well as to compare an anticipated production cost to the incumbent technology. System validation consisted of the following major tasks:

- Measuring dimensional accuracy of the individual prototype components and the final prototype assembly,
- Documenting variations in assembly cost when compared to the build plan,
- Simulating static loading conditions at the Alcoa Technical Center,
- Measuring specular reflectance by NREL via prototype material samples,
- Simulating dynamic loading conditions (gravity and wind loading) at NREL,
- Measuring optical efficiency via VSHOT of the final assembly both at the Alcoa Technical Center and at NREL (testing performed by NREL),
- Conducting Optical Efficiency testing at NREL.

The details of the Alcoa Wing Box design performance test plan can be found in Appendix D “CSP GEN-1 Test Plan”.

2.5.1 Geometric Dimensioning and Tolerancing (GD&T)

Extensive Geometric Dimensioning and Tolerancing (GD&T) modeling and validating of the model were performed during this task. The purpose of the GD&T activities is to predict the tolerance build-up of all the individual trough components via analytical modeling and then to validate the model via physical measurement techniques. The ultimate goal is to achieve an acceptable intercept factor. The tolerance build-up of the components and the final prototype assembly can then be used to predict the expected tolerance variations during large scale production of trough assemblies. Essentially, the GD&T study is used to predict and help control the geometric accuracy, which in turn affects the intercept factor of the final trough assembly. Through this detailed analysis an understanding of the important components that affect the final optical performance of the structure can be assessed. This information can then be used to further improve the accuracy of the system in future design iterations. GD&T can also be used for cost reduction purposes to relax manufacturing tolerances on non-critical components. This analysis also helped generate the datum reference system used for positioning all components and sub-assemblies in the assembly fixtures in the prototype trough manufacturing process.

A GD&T model was developed for the half module, as well as the individual components. Figure 40 illustrates the typical results of an estimate of variation of the completed trough. It illustrates the expected 6 sigma (range) tolerances for the position of the reflective surface relative to a reference system on the center spar.

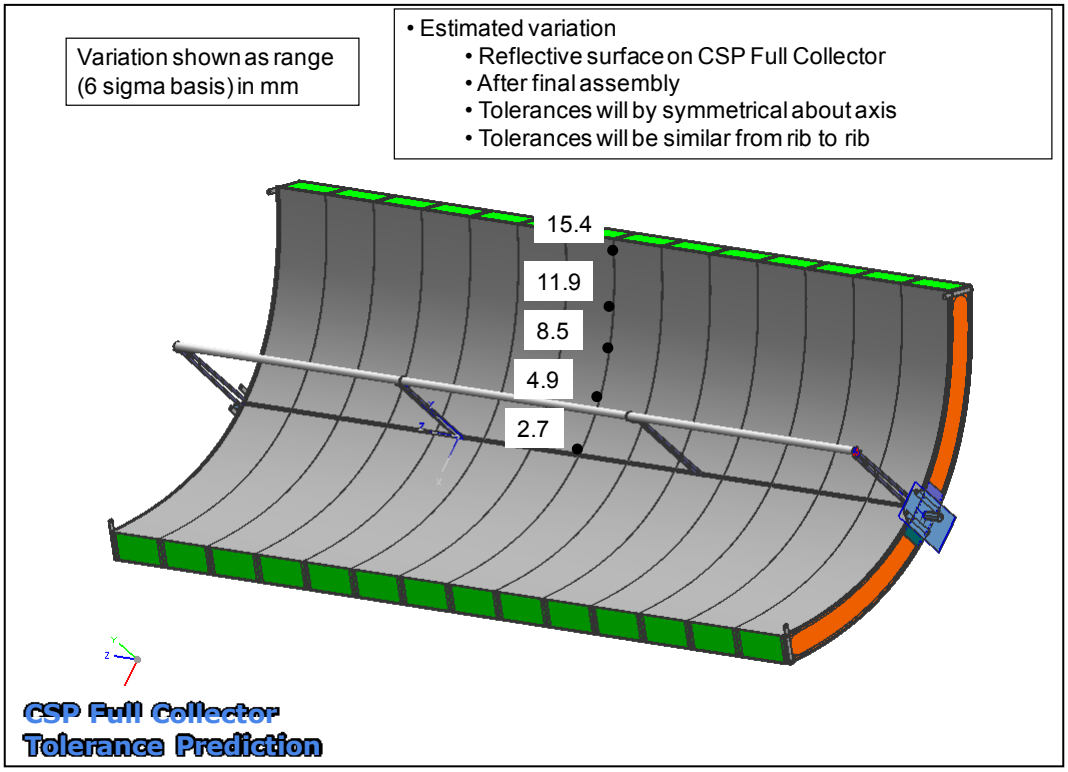

Figure 40: GD&T simulation results for the full trough

Ultimately, the optical performance of the trough is defined by the position and orientation of the reflective surface relative to the trough receiver tube. However, the trough tube is assembled and positioned in the field at final assembly. The reference system on the center spar allowed for a common reference to be used for in-process measurement on the trough halves in a manner that represented the position in the trough assembly step. As illustrated, the expected vertical (y-direction) deviations of this surface range from 2.7 mm to 15.4 mm going from the vertex to the rim of the trough. Since these are 6-sigma range deviations, 99.7% of the deviations are expected to be within this range. The maximum expected variation of 15.4 mm (~±7 mm) was then used as the target tolerance for measuring the trough halves relative to the reference system on the center spar.

The analysis was developed by establishing manufacturing datum reference systems and positional tolerances for all the major components and sub-assemblies for the trough half. Figure 41 illustrates the datum and tolerance scheme for the rib-subassembly as an example.

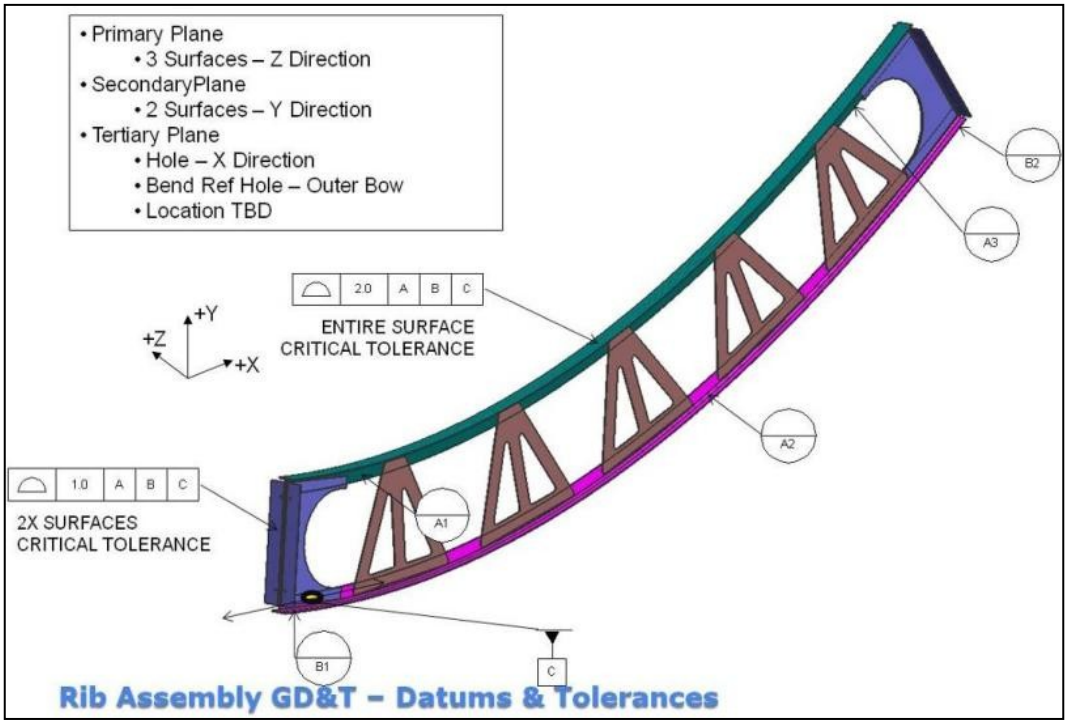

Figure 41: GD&T data and expected tolerances for the trough rib assembly

Similar to the results of Figure 40, the expected tolerance deviations of the Alcoa trough were projected for various critical locations throughout the structure. The datum reference systems and tolerance were used for inspection of the components and sub-assemblies during manufacturing. Also, the datum reference systems were used in the assembly fixtures to position the parts and sub-assemblies at each major assembly step.

As a first assessment of the acceptability of the trough variations from the GD&T study, the effective focal length error for a ±7 mm variation error at the rim was calculated. This was estimated to be ~10 mm, which is well within the expected trough tube diameter.

Given that the ultimate goal of the trough performance is to achieve a high intercept factor, it is desirable to understand how the deviations of the reflective surface from the GD&T study translate into intercept factor deviations. In order to relate the two studies, a ray tracing analysis is required. Given the point distribution (sampling rate) within the GD&T simulation was not high enough for a direct ray trace analysis. The manufacturing tolerance effects were added to the FEA model and then analyzed. The FEA model was re-run with and without the additional tolerance constraints to give a detailed mapping of the reflective surface under wind loading (Figure 42). The FEA analysis results were provided to CSP Services for ray tracing (see Appendix E, “Shape Analysis Data-Set 090426”). Under maximum wind loading conditions, the deformation at the reflector rim deviated by ~7 mrad with and without the applied manufacturing tolerances. Given the extreme load case conditions of the analysis, it was deemed that the tolerance variation predicted from the GD&T study would have little effect on the intercept factor during normal operating parameters.

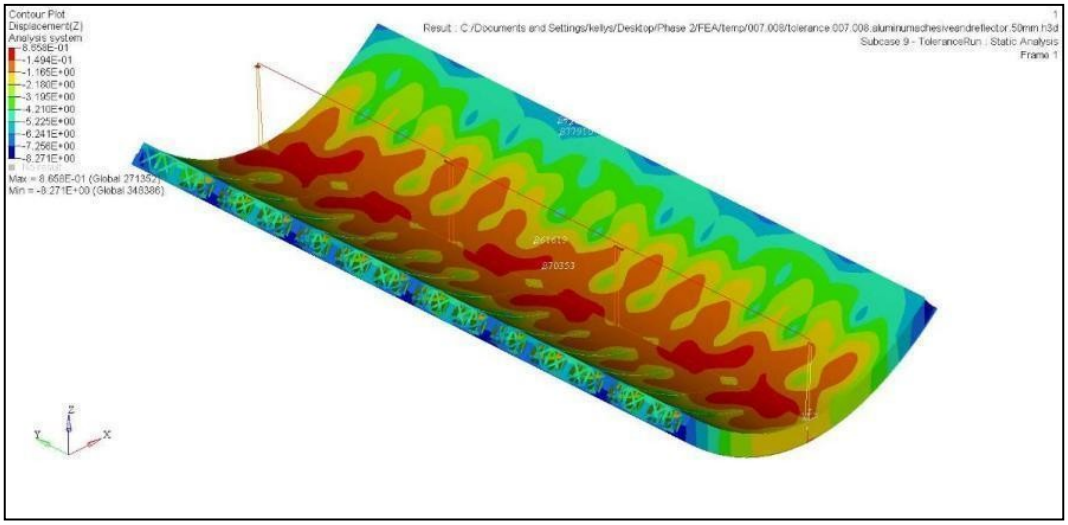

Figure 42: FEA simulation generates reflector surface with worst case tolerances

The GD&T model was then validated by performing physical tolerance measurements on the individual trough components, the trough subassemblies, and the final trough assembly. The geometric accuracy of the individual components was verified by utilizing a fabricated check fixture or a coordinate measuring machine (CMM). The subassemblies were measured using a CMM or a laser tracker unit. The final assembly was measured using a laser tracker unit (Figure 43 and Figure 44).

Figure 43: GD&T validation of trough half module assembly via laser tracker

Figure 44: GD&T validation of trough via laser tracker

Figure 45 depicts the results of the laser tracker testing of the half trough assembly. The measurements were made with the reference system on the center spar that simulated how the reflector half would be positioned in the final trough assembly. This is the same reference system used in the tolerance simulation.

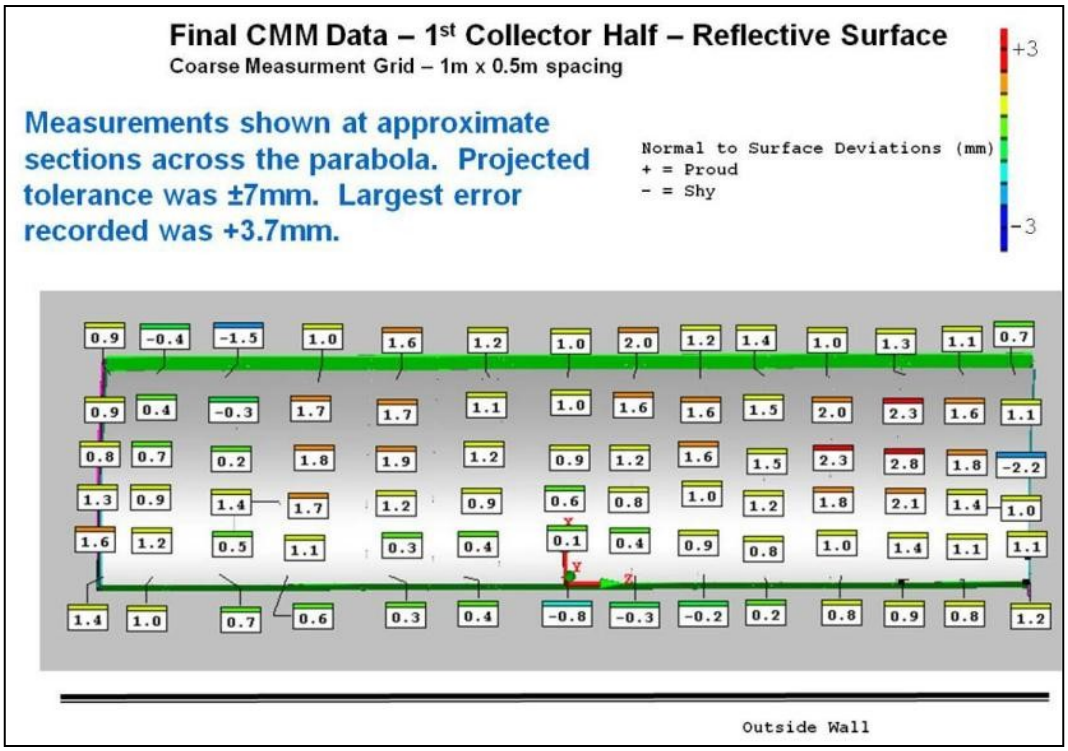

Figure 45: GD&T Laser tracker test results of half trough assembly

The values show the vertical (y-axis) deviations from a perfect parabola as measured on the reflective surface. As shown, the largest deviations were approximately 3.7 mm while the projected tolerance from

the GD&T analysis was ±7 mm indicating that the trough half was manufactured with a high degree of precision. Comparing deviations between adjacent points on the grid across the parabola gave a qualitative assessment of possible angle errors. The absence of large changes from one measurement point to the next also indicated a high degree of precision.

2.5.2 Static load testing

As part of the trough validation testing, static load testing of the half trough modules was performed to better understand the structural performance of the trough. A static test plan was developed as shown in CSP GEN-1 Test plan (see appendix D). These tests were conducted at the Alcoa Technical Center prior to assembling the two trough modules together.

To perform the test, a fixture was created to support the three corners of the half module. One of the corners was allowed to hang free. At the free-hanging corner, weight was added and corresponding deflection was measured (Figure 46). After several load and unload cycles, a linear response was obtained as weight was steadily added. The measured deflection was within 10% of the predicted response from the FEA modeling. The results show good correlation of the structural response as compared to analytical modeling.

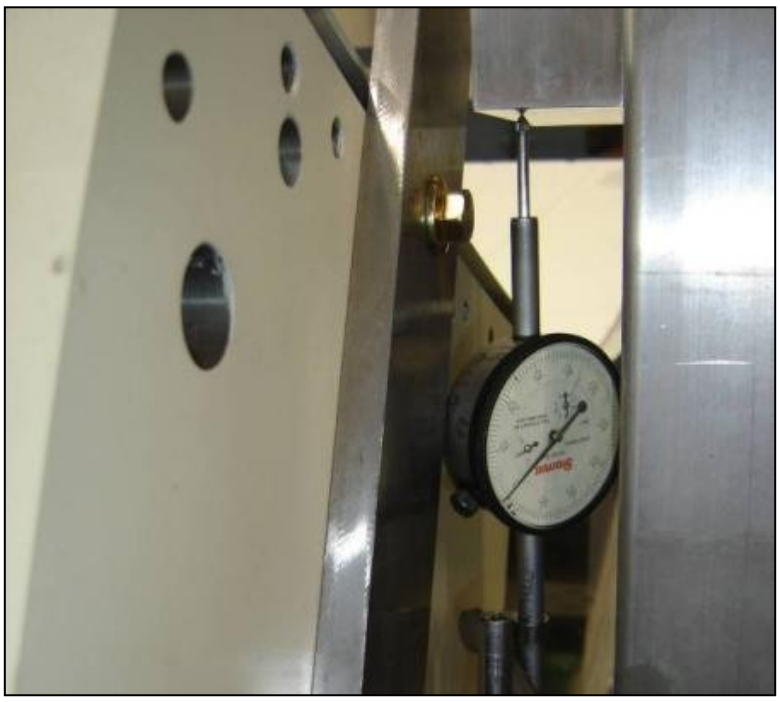

Figure 46: Static testing of half module

2.5.3 Optical analysis

VSHOT at Alcoa

In order to characterize the surface of the final assembled trough prototype, the Video Scanning Hartmann Optical Test (VSHOT) was performed by NREL at the Alcoa Technical Center (Figure 47).

Figure 47: VSHOT testing of the whole trough at Alcoa

A slope error is generated from the results of the VSHOT test. To complete the VSHOT testing, one vertical scan was taken approximately every 0.102 m (4 inches) along the length of the trough. Figure 48 illustrates the VSHOT test results for panel 2 of the trough. The slope errors (y-axis) are plotted along the arc length of the aperture (x-axis). The maximum allowable slope error is plotted in red. This allowable error is a function of the receiver tube diameter.

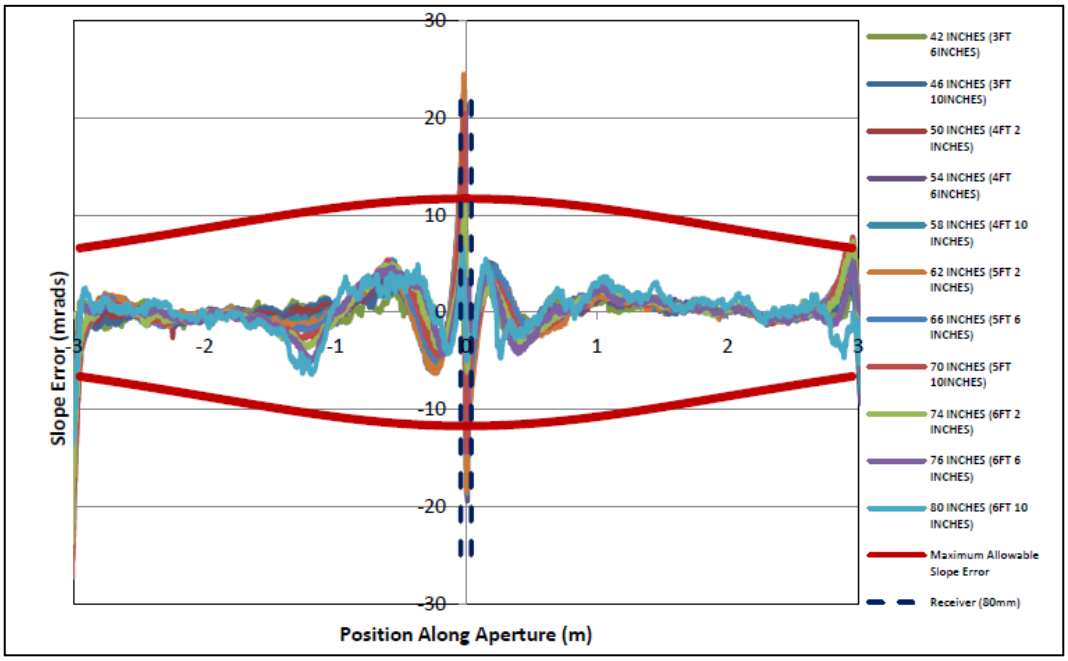

Figure 48: VSHOT test results for panel #2 with an 80 mm receiver tube

As can be seen, the largest deviations are at the vertex and the rim of the trough. The deviations at the vertex are mitigated by the shadowing of the receiver tube which is shown by the vertical dotted lines. The deviations at the vertex and the rim were a result of the joining process utilized for the reflective surface. All the deviations, albeit small, were very repeatable and can be addressed in future design iterations.

The full VSHOT test results and report can be found in Appendix F (Optical Testing of the Alcoa Parabolic Trough, NREL Milestone Report 550-47996). The major findings from the complete VSHOT testing was that the average transverse RMS slope error for the trough was 2.70 milliradians (mrad) with an intercept factor at normal incidence greater than 0.99. These results indicate a very high optical quality for the surface.

VSHOT at NREL

After the detailed VSHOT testing was completed at Alcoa, the whole unit was split along the vertex. The half modules were shipped to the NREL's Solar Industrial Mesa Top Area (SIMTA) site in Golden Colorado for further testing. The GEN-1 prototype was mounted to NREL's large payload two-axis tracker system (Figure 49 and Figure 50), and 3 Schott PTR80 receiver tubes were welded together and mounted on the receiver tube supports by NREL personnel. The receiver tubes were initially aligned using a laser distance meter mounted to the rim of the trough with a custom made mounting bracket (Figure 51).

Figure 49: Trough at NREL's SIMTA Site, Golden, CO

Figure 50: Trough mounted to NREL's two axis tracker

Figure 51: Laser Distance Meter used to conduct initial receiver tube alignment (Photo courtesy of NREL)

In order to verify that there were no issues with transporting and re-assembling the prototype, VSHOT testing was repeated at select areas of the trough. The results were consistent with the detailed VSHOT testing at Alcoa which indicates that the alignment process of the two halves functioned properly. The detailed results of the VSHOT testing at NREL can be found in Appendix F, (Optical Testing of Alcoa Parabolic Trough).

Distant Observer Test

The final receiver tube alignment was verified using the Distant Observer Methodology. The Distant Observer (DO) test is a qualitative analysis of the trough and receiver tubes as a system. The test uses the reflected image of the receiver tubes to provide diagnostic information. An aerial test is capable of providing information for a large field of troughs. More information, such as slope error, trough alignment, receiver position, and tracking accuracy can be provided if only a single trough is analyzed at a time.[2] According to Richard Wood, "The accuracy of the results is diminished if the observer is closer than approximately ten times the aperture width."[3] In order to verify the initial alignment of the receiver tubes to the trough, a Distant Observer test was conducted. The photo in Figure 52 indicated that additional tube alignment was required.

Figure 52: Distant observer evaluation at NREL's SIMTA site (Photo courtesy of NREL)

Incident Angle Modifier Test

Most trough troughs in a field are operated in a single axis fashion. As a result, their efficiency varies throughout the year as the sun position changes with the seasons, that is, incident angle. The angle that the sun strikes the trough affects the performance of the trough. The incident angle modifier is a value that represents an angular performance factor. The Incident Angle Modifier modifies the efficiency curve of the trough. Although NREL has a two-axis tracker, they were able to simulate the conditions of a single axis tracker. NREL took advantage of the vernal equinox and conducted an Incident Angle Modifier Test. By doing so on a day near the solar equinox, NREL was able to simulate an optimum day for a single axis tracker and determine the Incident Angle Modifier.[4]

Figure 53 shows a photo of the trough when the incident angle was about 35^{o} from the east. "It was advantageous doing the IAM tests near the equinox because the 2 axis tracker can simulate a single axis mode."[5] The tests were conducted at incident angles of 0^{o} through 50^{o} in 5^{o} increments. The ratio of the efficiency of the trough at the incident angle to the efficiency at 0^{o} is the incident angle modifier (IAM). The Incident Angle Modifier plot shown in Figure 25 of Appendix F is relatively flat indicating that there is little effect of the incident angle on optical performance.

[2] Distant Observer Overview for Alcoa, Presentation by Kathleen Stynes of NREL, March 8, 2010
[3] Distant Observer Techniques for verification of Solar Concentrator Optical Geometry, Richard L. Wood, P.21
[4] Incident Angle Modifier and Average Optical Efficiency of Parabolic trough Troughs, H.Gaul and A. Rabl, p. 1, July 1979.
[5] Per Keith Gawlik of NREL

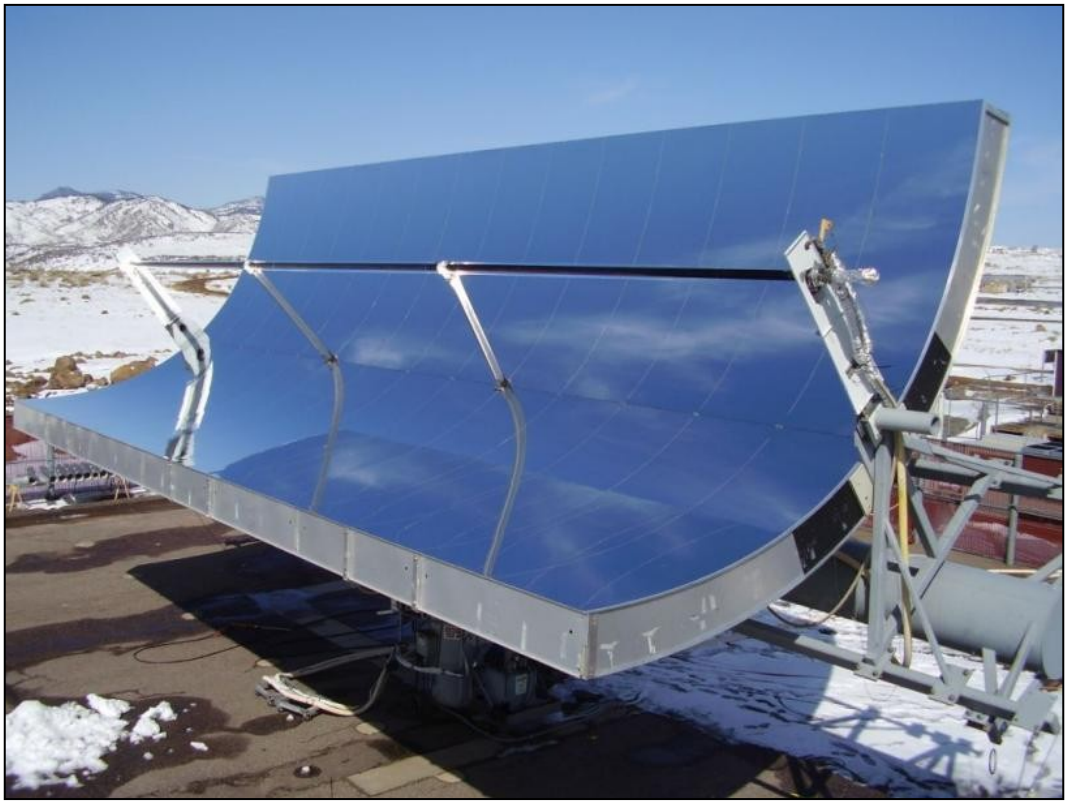

Figure 53: Alcoa trough during Incident Angle Modifier Test (Photo courtesy of NREL)

Optical Efficiency Testing

Optical Efficiency tests were also conducted on the Mesa Top using NREL's Optical Efficiency Test Loop. Results were obtained from clear days with direct normal solar radiation from 700 to 1,000 W/m2, mass flow rate of 1.6 kg/s, and receiver tube inlet temperatures from 2°C below to 2°C above ambient temperature. During tests in March 2010, the average trough optical efficiency was found to be 0.747 and 0.749± 1.7% (see Appendix F, Optical Testing of Alcoa Parabolic Trough). The test results are consistent with a trough having a high intercept factor (99%) and an aluminum mirror reflector with a 25mrad specular reflectance of 88%.

2.5.4 Wind Load Testing

While the static load testing conducted at Alcoa provided good correlation to the FEA results, the magnitude of the applied load was significantly less than the applied loading that the trough will see in operation. To improve verification of the design and correlation of the structural analysis tools, a test plan was developed to further the structural testing by collecting strains induced by various wind conditions. Due to the low stresses predicted in the structure, the static application of weights or cable-applied loads was deemed impractical given the amount of load that would be required to emulate operational loading conditions. In order to determine the structure's response and validate the FEA model, the system needed to be perturbed with large loads to generate measurable strains. The typical source of large loads experienced by a trough is high wind conditions. It was decided to develop a wind load test plan to determine the real strains experienced by the trough when real environmental conditions are applied.

The primary goal of the wind load testing was to determine the structural response of the trough to real-world loads. This data would be collected using a combination strain measurements from the trough and the pedestal of the two-axis tracker. The experimental structural response of the trough and the reaction forces of the wind loading would then be used to compare the FEA model's predictions with reality.

The decision was made to record data on the trough using strain gages mounted in various locations on the trough and NREL's two axis tracker. The gage locations were derived from analyzing the FEA results to determine the high stress and convenient areas to better allow for the experimental correlation of the analytical model. Additional gages mounted to the NREL two-axis tracker would allow for measurement

of the reaction forces from the wind loading that are transmitted to the ground (Figure 54 and Figure 55). A total of 112 strain gages and 105 signals were applied to the trough and the two-axis tracker:

- Trough; 96 strain gages, 96 signals
- Tracker; 16 strain gages, 4 signals
- Others; 5 signals

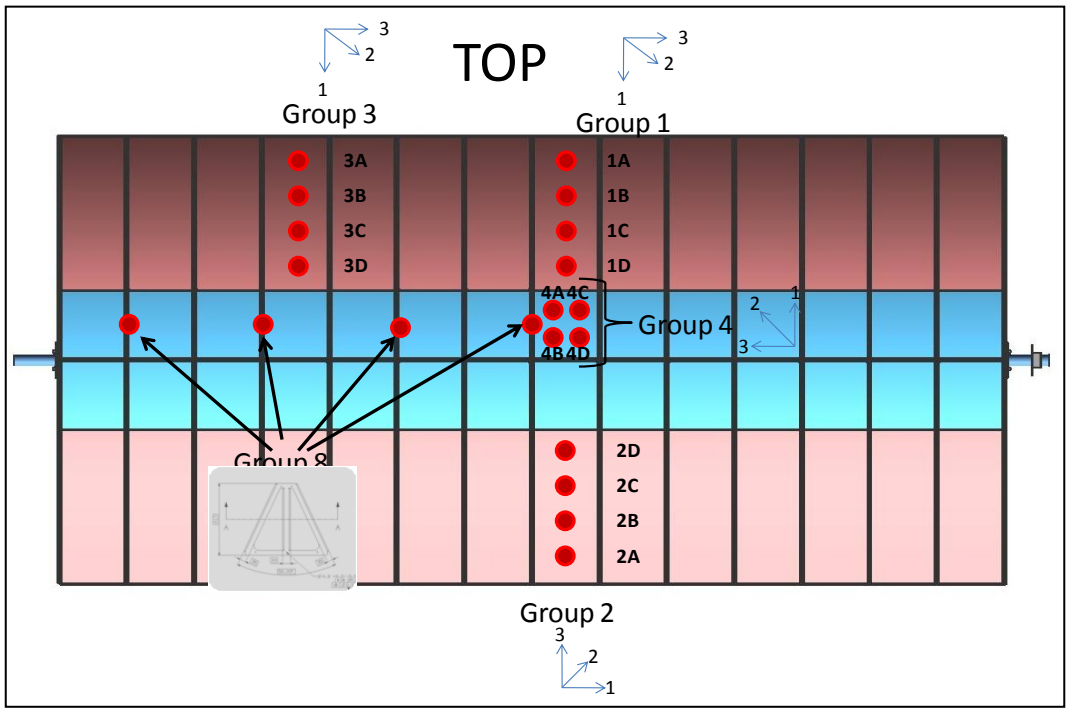

Figure 54: Strain gage locations on the Alcoa Wing Box trough

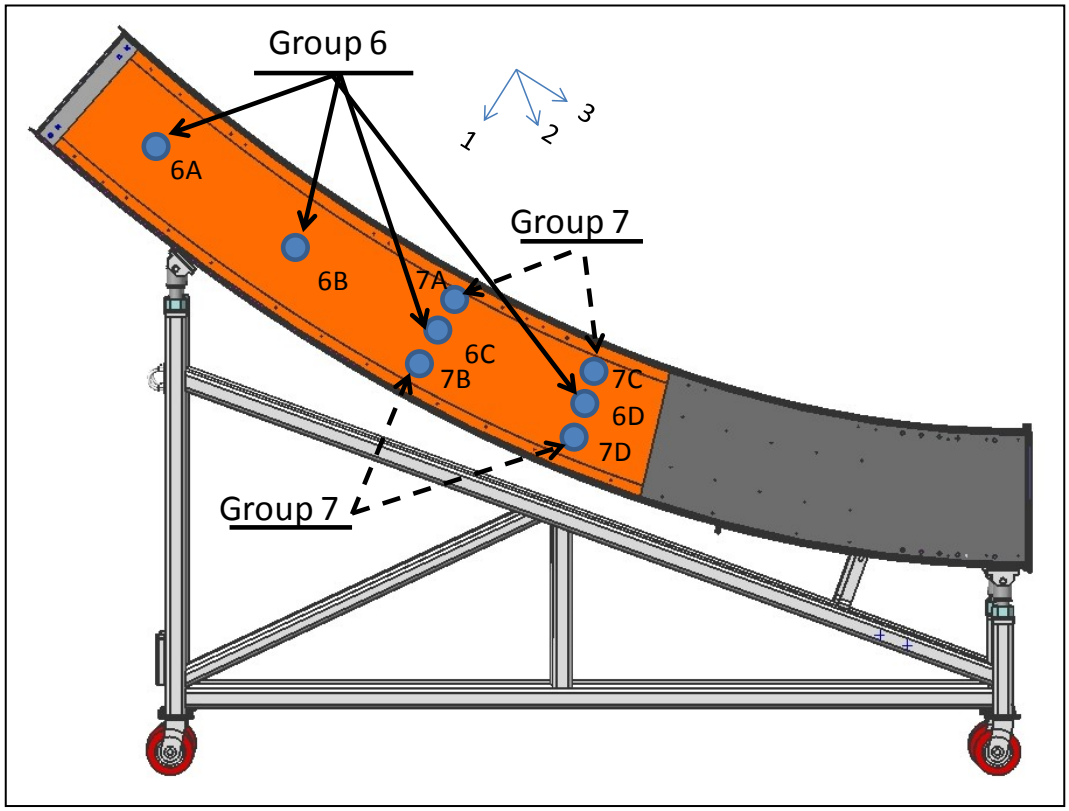

Figure 55: Strain gage locations on end of the Alcoa Wing Box trough

Over 250 wind load tests were conducted with the assistance of NREL personnel. Tests included dynamic sweeps of the tracker as well as stationary recordings of various wind loadings at different static orientations of the trough. The objective was once again to correlate the predictive FEA simulations with actual results. The correlated model will be used to optimize future designs by having greater confidence that the analysis tool predicts reality. It should be noted that this testing is beyond the original scope of the validation test plan, but it was deemed necessary to fully correlate the actual prototype performance given actual wind loading events.

Measuring the wind load forces proved to be a challenge given environmental variables involved in the testing. Some of the important test variables are as follows:

Wind Speed	Measurable, but not from the trough location. NREL's Instrument deck is closest location (~100 meters) with readings taken every 3 seconds.
Wind Direction	Measurable, but not from the trough location. NREL's Instrument deck is closest location (~ 100 meters) with readings taken every 3 seconds.
CSP Orientation	Measurable, but not able to tie into data acquisition system
Temperature	Surfaces of trough and Pedestal; Measurable

The wind loading conditions at NREL's SIMTA site proved to be a difficult variable to characterize. There is a wind speed indicator at the tracker control room, but wind direction is not recorded. There are three anemometers near the tracker control room which provide wind speed and wind direction (see Figure 56) The challenge was to decide which anemometer to use depending upon a given wind direction.

Figure 36 illustrates the variance between the three different anemometer locations. Ultimately, it was determined that the anemometer on the instrument deck correlated the best with the wind speed readings at the tracker control room (see Figure 57).

Figure 56: Anemometer locations

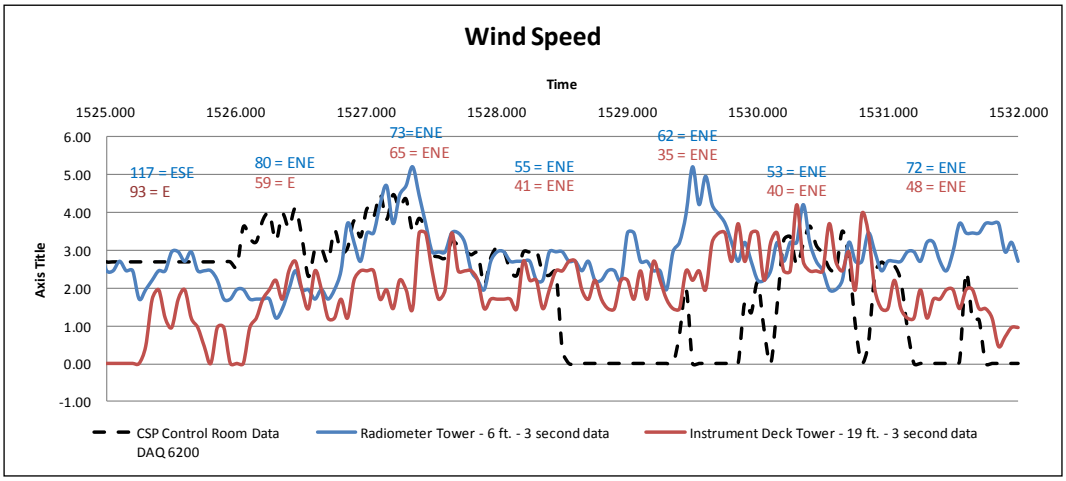

Figure 57: Low wind speed readings from different anemometers

In addition to the wind direction variance, it was also determined that temperature variations throughout the day and at various trough orientations created difficulties in collecting the desired wind loading data. A significant amount of the initial wind load testing was spent calibrating the system and performing repeatability tests to assure that strain data was logical for given tracker orientations, tracker movements, and wind load conditions. The lack of repeatability among test even at similar wind loading conditions was eventually hypothesized and validated as thermal effects resulting from the orientation of the sun to various locations of the trough.

In realistic operational environments, the trough is always oriented normal to the sun. In this configuration, a high percentage of the sun's energy is reflected from the trough to the receiver tube. While conducting the wind loading tests at the NREL SIMTA facility, the trough was often oriented to the direction of the wind and not the sun. In cases where the sun was oriented on the back-side of the trough, which is not highly reflective, a large thermal gradient between the front and back surfaces was affecting the repeatability of the strain readings.

This thermal phenomena was discovered when elastic buckling of the back panel was noticed when the sun was oriented on the backside of the trough. The strain was measured during this elastic event and the temperature difference from the front to back surfaces was measured via thermocouples. The temperature difference was found to be 60°F (15.5°C). This temperature differential was modeled via FEA. The model was able to predict the elastic buckling event which confirmed the thermal effect.

Ultimately, the solution to avoid the effects of temperature variations on the wind loading testing was to conduct the wind loading testing at night when the trough and pedestal are both at equilibrium temperature. For clarification, this temperature effect has no significant effect on the performance of the trough or its optical accuracy during normal operational procedures. This variation was only an issue in obtaining repeatable strain measurements during wind loading tests.

With the understanding of the effects of wind speed, wind direction and solar impingement, the resulting strains on the trough were collected and tested. Tests were conducted in a stationary position (static) of the trough as well as conducted with the trough moving (dynamic) from one prescribed location to another. By conducting static test the effects of wind loading on the trough can be better understood. By conducting tests as the two-axis tracker moves the trough from position to position, the gravity effects on the trough can be better understood. Together it is expected that the understanding of the wind loading and gravity effects will allow for the FEA model correlation.

While the full analysis of the wind loading testing was not completed given the complications and unforeseen variables within the testing, several interesting results are worth noting. The graphs in Figure 58 are examples of the induced maximum and minimum strains for a set of strain gages on the trough, with the trough pitched at 60°. Note in Figure 58, plot 7A, that the maximum strains are recorded at the lowest wind speed. The minimum and maximum variations are thought to be a result of the wind speed varying from different wind directions. The results indicate the strong interdependency between wind

speed and wind direction on the resulting strains. In future analysis these results can be compared and contrasted with NREL's wind tunnel test report. It is hoped that this wind load testing on a full-scale trough will further validate the results of the NREL report.

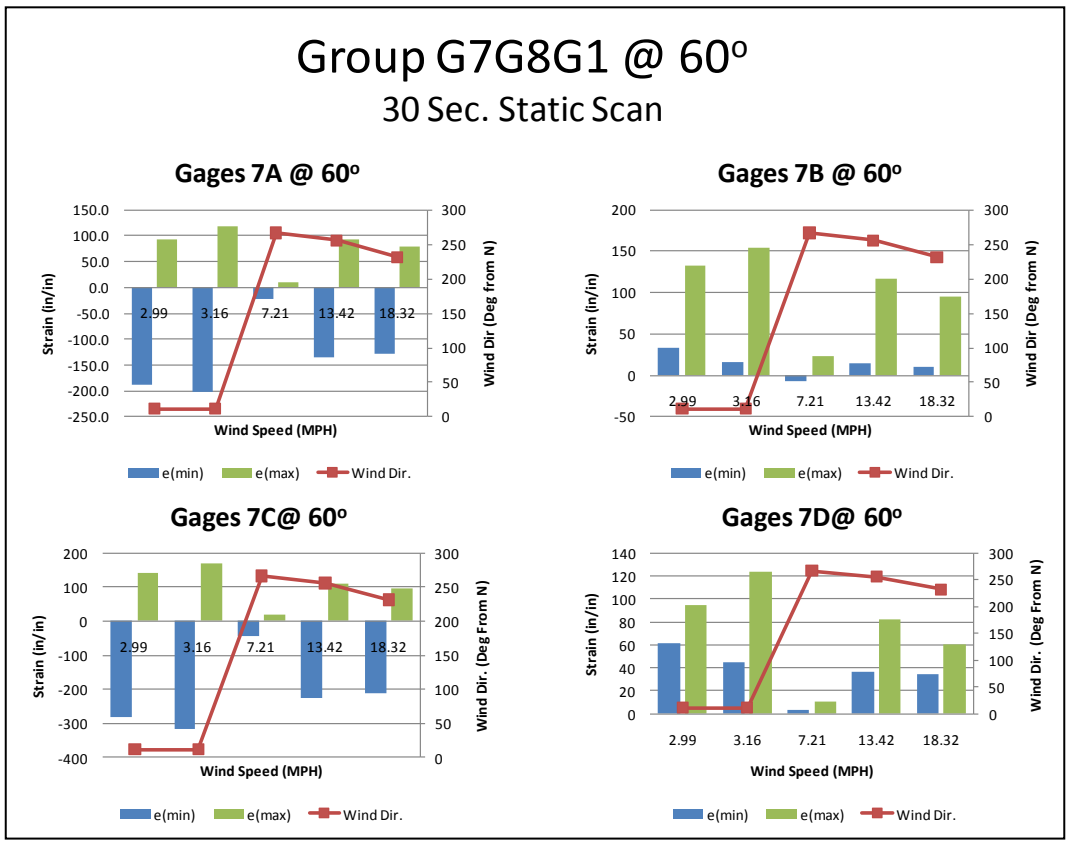

Figure 58: Static strain gage results

Strain gages mounted on the pedestal at the principal axes (N-E-S-W) provided measurement signals as directional static and wind forces were exerted on the trough and tracker structure. Figure 59 and Figure 60 shows the results of the gravity effects on the pedestal as the trough pitch was changed from stow to horizontal positions under no-wind conditions. The plotted data indicates a direct relationship between pedestal gage readings and change in pitch. Slopes for the S-N and W-E readings showed excellent agreement and repeatability, validating the measurement capability for each axis. An important observation was that temperature differences between night and day testing also have a measurable effect on strain gage sensitivity.

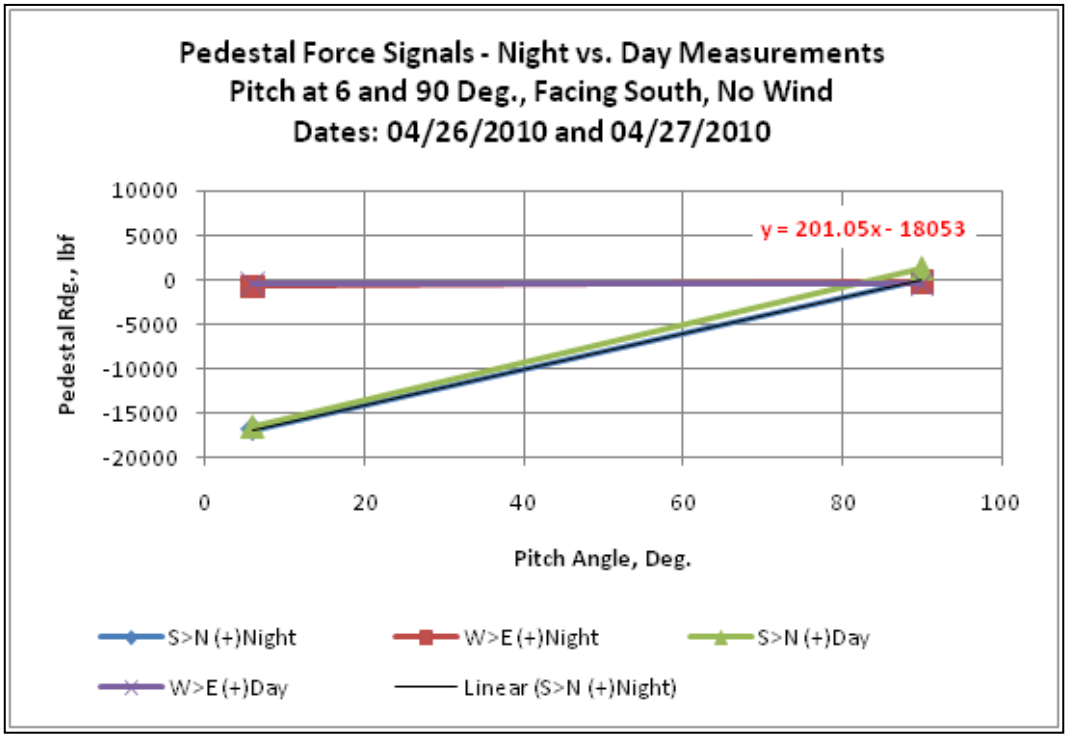

Figure 59: Pedestal reaction forces vs. pitch angle (South Facing)

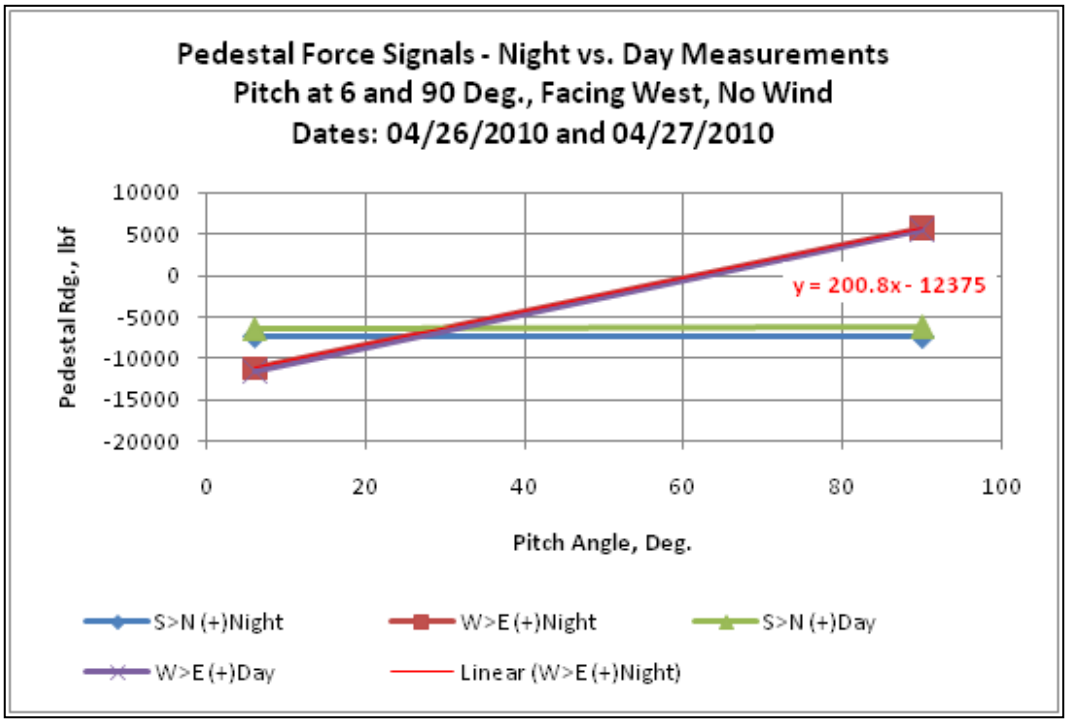

Figure 60: Pedestal reaction forces vs. pitch angle (West Facing)

Another interesting finding is shown in Figure 61 through Figure 63. The recordings taken from the strain gages mounted on the pedestal were compared to anemometer readings from the control room. In all figures, a comparison between the recorded reaction forces versus wind speed trends is shown. Figure 61 shows the raw data of the resultant pedestal versus wind speed with the tracker in stow position. Again the wide variations between the minimum and maximum strains at a given velocity are thought to be a result of the orientation of the wind to the trough Figure 62 shows the same data but filtered by taking an average of the strain measurements at a given wind speed. Figure 63 displays the filtered strain gage readings versus wind speed when the trough is pointing towards the horizon and facing the wind. It's important to note that the slope of the trendline for recordings at stow position (see Figure 62) was much

shallower than that of recordings while the trough was facing into the wind at the horizon (see Figure 63). This was consistent with our expectations and with the wind tunnel testing from the NREL report.

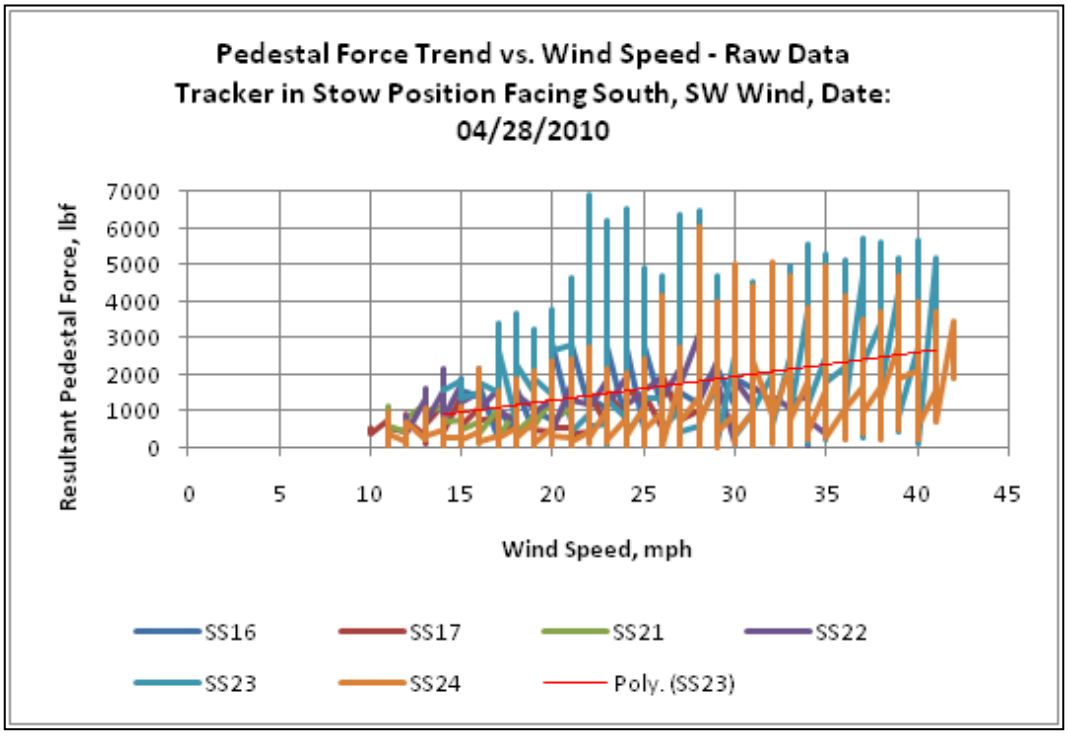

Figure 61: Trends of recorded reaction force vs. wind speed (stow position, raw data)

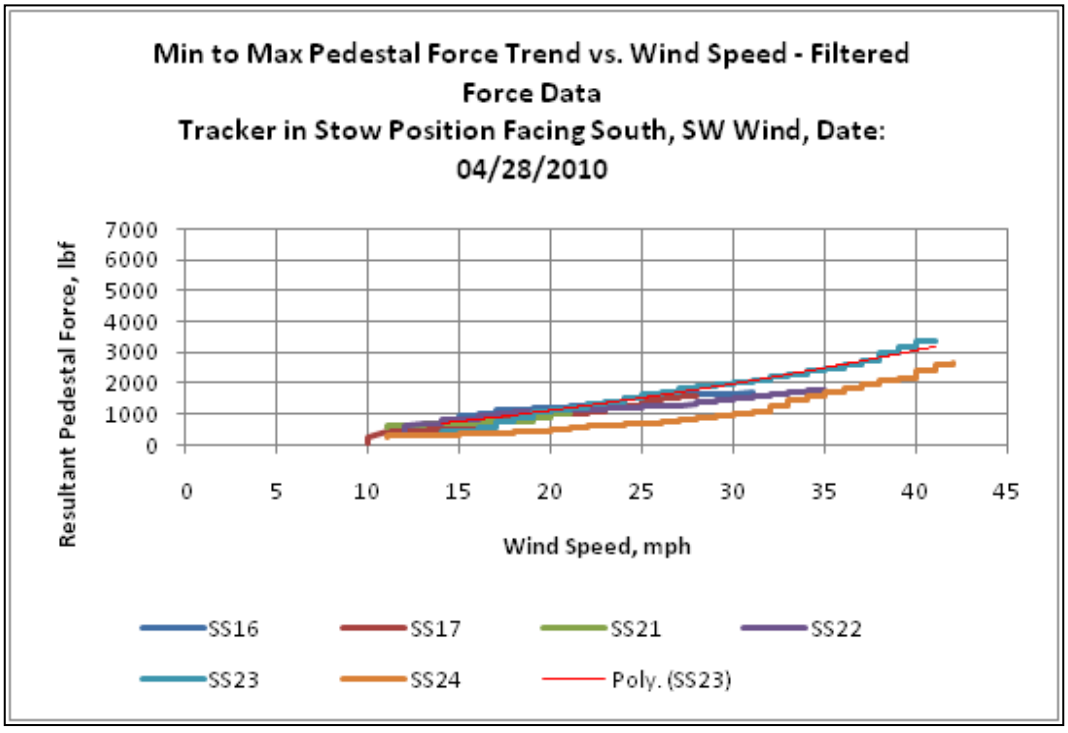

Figure 62: Trends of recorded reaction force vs. wind speed (stow position, filtered data)

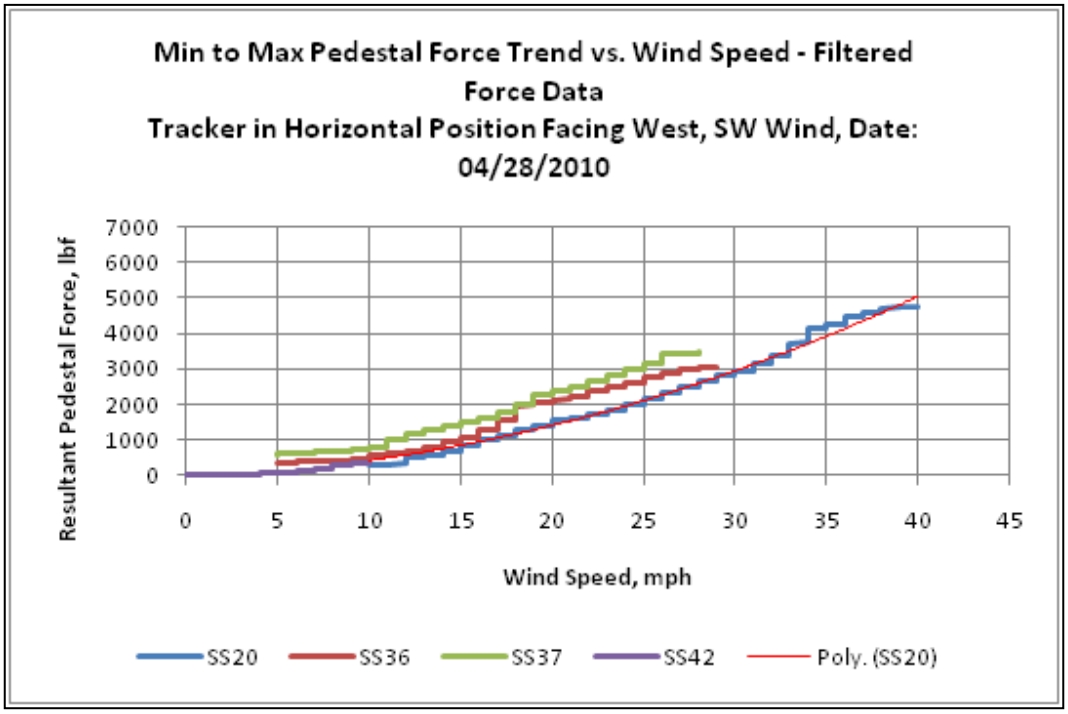

Figure 63: Trends of recorded reaction force vs. wind speed (facing wind, filtered data)

The most important learning to take from the validation testing at NREL was the fact that the first generation Alcoa CSP trough was capable of withstanding environmental conditions with no noticeable change in performance. It withstood wind, rain, snow, and hail. Optical performance did not change between the VSHOT testing at ATC and at NREL. No permanent (plastic) deformations occurred during shipment, installation, or testing.

An improved understanding of the thermal and structural loadings due to experimentation at NREL would provide the basis for a more efficient next generation design.

Over 250 scan sessions of data were recorded at NREL. Analysis of this data and correlation to the FEA model provided an improved ability to generate an optimized design through reduced conservatism. If wind load testing is repeated in the future, it is recommended to change the configuration of instrumentation on an Alcoa CSP trough in order to improve the quality of data collected during wind loading testing. There are three main recommendations for future testing:

1. Load cells integrated with the axle stubs would provide direct input of the forces applied to the trough by a wind load. This would eliminate the need for the pedestal strain gages which only produced measurable strains in the bending direction to the wind.
2. Pressure sensors distributed around the reflector would be used to calculate the forces applied by wind loads as well.
3. A wind vane and anemometer mounted near the trough would improve synchronization between recorded strains and weather conditions. This in addition to recommendation #2 would help to eliminate the wind loading variance seen in the first round of wind load testing.

2.4.5 Update cost model

Note: The cost modeling effort was applied concurrently throughout the reflector and system ideation and down-selection process; however, for reporting purposes the effort is being reported separated for clarity and to allow for the description of the cost modeling approach employed throughout this phase of the program.

Model overview

A number of cost modeling tools were employed to access the impact of Alcoa's aluminum-intensive trough design approach. The objective of this effort was to quantify the cost savings of Alcoa's innovative Wing Box trough design and the materials used in conjunction with state of the art, commercial manufacturing technologies on both the solar field capital costs and the levelized cost of energy (LCOE). Alcoa's approach employed several types of modeling tools:

Solar Advisor Model (SAM) Version 2010.4.12	high level or top-down cost estimation tool developed by NREL specifically for solar applications (https://www.nrel.gov/analysis/sam/)
Excelergy 7-13-07	NREL high level or top-down cost estimation tool developed that preceded SAM,
SAM 2010 Parabolic Trough Cost Model Rev1x	NREL detailed spreadsheet breakdown of major CSP components (released from Craig Turchi in April 2010)
SEER-MFG	commercial available built-up cost estimation tool that is used in the aerospace, defense, and consumer product industries (www.galorath.com)

These tools were employed in a complementary fashion such that SAM provided the baseline LCOE, capital, and solar field costs while SEER-MFG quantified the impact of Alcoa's design in reference to the baseline trough system. In Phase I of Alcoa's program, Excelergy was used to provide an additional level of detail regarding the distribution of the solar field capital. Recently a new spreadsheet was developed by NREL. The details of NREL's *SAM 2010 Parabolic Trough Cost Model Rev1x* (SAM 2010 Excel) was much more comprehensive than Excelergy and provided the new system cost distribution for Alcoa's internal model. Figure 64 illustrates the connectivity of the tools in relation of the program.

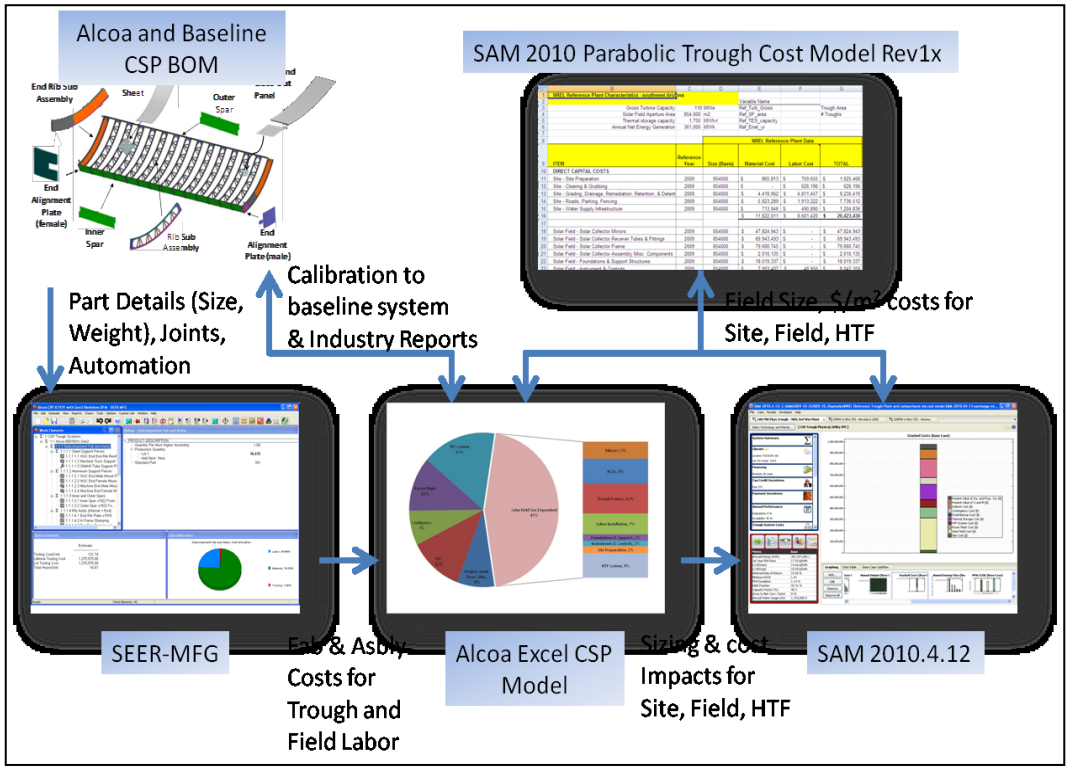

Figure 64: High level cost modeling flow path

The general characteristics and cost structure of the baseline system was provided in both SAM and the SAM 2010 Excel spreadsheet. The detailed capital breakdown provided in the SAM 2010 Excel spreadsheet was linked in a transparent fashion to the high level parametric inputs for SAM. An example of the cost elements related to the overall size of the solar field detailed in SAM 2010 Excel can be seen in Table 16 for the baseline system.

Table 16: Summary of baseline solar field size related cost parameters

Solar Field Size Related Capital	Cost Impact	Material, $/m^2	Labor, $/m^2	Total, $/m^2	% Total
Site					
Site Preparation	Secondary	1.0	0.9	**1.9**	**8%**
Clearing & Grubbing	Secondary	0.0	0.7	**0.7**	**3%**
Grading, Drainage, Remediation, Retention, & Detention	Secondary	5.2	5.6	**10.8**	**45%**
Roads, Parking, Fencing	Secondary	6.8	2.2	**9.1**	**38%**
Water Supply Infrastructure	Secondary	0.8	0.6	**1.4**	**6%**
Site - Totals		**13.8**	**10.1**	**23.9**	**100%**
Site - % Totals		**58%**	**42%**	**100%**	
Solar Field					
Solar Collector Mirrors	Primary	56.0	-	56.0	**16%**
Solar Collector Receiver Tubes & Fittings	Secondary	81.9	-	81.9	**24%**
Solar Collector Frame	Primary	93.3	-	93.3	**27%**
Solar Collector Assembly Misc. Components	Primary	2.4	-	2.4	**1%**
Foundations & Support Structures	Secondary	21.1	-	21.1	**6%**
Instrument & Controls	Secondary	9.4	0.1	9.4	**3%**
Electrical	Secondary	2.5	1.1	3.6	**1%**
Labor Installation	60%P / 40%S	-	69.1	69.1	**20%**
Fabrication tent	Primary	1.1	0.3	1.4	**0%**
Empirical Sun Tracker	Secondary	4.4	0.0	4.4	**1%**
Solar Field - Totals		**272.1**	**70.6**	**342.6**	**100%**
Solar Field - % Totals		**79%**	**21%**	**100%**	
HTF System					
Freeze Protection System	Secondary	0.4	0.1	**0.4**	**1%**
Ullage System	Secondary	0.7	0.2	**0.9**	**1%**
Pumps	Secondary	4.0	0.4	**4.4**	**5%**
Expansion & Nitrogen Blanketing Systems	Secondary	4.6	1.8	**6.4**	**8%**
Solar Field Piping, Insulation, Valves, & Fittings	Secondary	24.2	24.9	**49.1**	**61%**
Power Block Piping, Insulation, Valves, & Fittings	Secondary	0.8	0.2	**0.9**	**1%**
Foundations & Support Structures	Secondary	1.0	1.2	**2.2**	**3%**
Fluid	Secondary	15.8	0.0	**15.8**	**20%**
HTF System - Totals		**51.4**	**28.7**	**80.2**	**100%**
HTF System - %Totals		**64%**	**36%**	**100%**	
Solar Field Size Related Components (Site, Solar Field,and HTF System)					
	Total	**337.3**	**109.4**	**446.7**	
	% Primary	**34%**	**9%**	**44%**	
	% Secondary	**41%**	**15%**	**56%**	
	% Total	**76%**	**24%**	**100%**	

The highlighted values in this table were input into SAM (Figure 65) to develop the LCOE and other outputs.

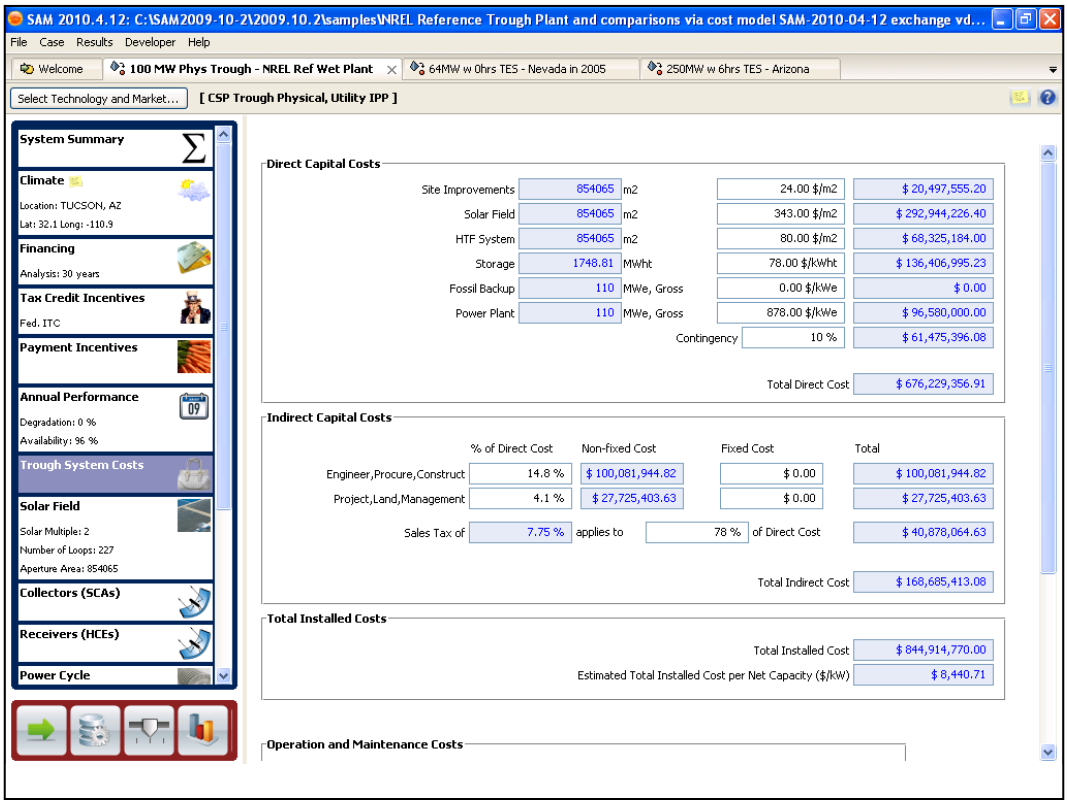

Figure 65: SAM 2010.4.12. Input Screen for Baseline 100MWe Nameplate with 6 Hours TES Cost Parameters

Additionally, Alcoa assigned each category in Table 16 as either a primary or secondary cost factor impacting the total system cost. This was intended to differentiate between trough fabrication and assembly (primary) and sizing (secondary) effects. Secondary savings are influenced by the design characteristics, such as larger aperture widths, SCA lengths, etc, and effects of equipment-based items, such as receiver couplings, pylons, drives, piping, etc. Since Alcoa's design has a larger aperture area per trough as compared to the baseline system, the model needed to include secondary effects to fully characterize the potential cost saving opportunities.

Alcoa developed a parallel Excel model based upon SAM 2010 Excel that served as a connection point between SAM and the SEER-MFG cost model. As a result the DOE cost tools served as the calibration standards for Alcoa's built-up SEER-MFG baseline cost model. Once the build-up baseline model was properly referenced, the manufacturing cost savings associated with the Alcoa design was also estimated. Additionally, the Alcoa Excel CSP model was able to quantify the secondary solar field savings due to sizing effects. In this manner cost were updated into SAM for the Site, Solar Field, and HTF cost categories.

Baseline CSP plant

Alcoa's Phase I report referenced against a baseline CSP plant that was sized to 110MWe gross output with 6 hours of thermal storage. Additionally, it was assumed that the solar field was comprised of troughs sized similar to the 5m by 8m aluminum spaceframes in Nevada Solar One (NSO). **Error! eference source not found.** shows a comparison of the assumptions and input parameters employed between the two phases. Note, the Phase II assumptions were based on the new standard defined in SAM 2010.4.12. Several cost input parameters did increase for Phase II, most notably Site Improvements, HTF, and TES systems. The net change between these three factors increased the total solar plant costs by approximately $180M (including contingency and indirect factors).

Table 17: Comparison of baseline input assumptions and cost outputs for Phase I and Phase II analysis

Baseline Cost Model Assumptions	Phase 1	Phase 2 (Current)
Climate	CA Daggett.tm2	AZ.Tucson.tm2
Nameplate Capacity, MWe	100	
Gross Output, MWe	110	
TES, hours @ Nameplate Capacity	6	
Solar Multiple	2	
Solar Field Size, m^2	871936	854065
Trough Type	Solargenix SGX-1	ET100
Aperture Width, m	5.00	5.77
Trough Length, m	8.00	12.00
Trough Construction	Al Extrusion kit, manually asbled	Prefab Steel Kit, semi-fab with tooling
Field Labor	Unskilled low wage for Boulder, NV	2010 Prevailing wage for Southwest AZ
Troughs per SCA	12	8
SCAs per Loop	8	
Receiver Type	Schott PTR70	
Field HTF Fluid	VP-1	
Mirror Type	4mm Slumped Glass	
Mirror Reflectivity, %	93.5	
Analysis Period, years	30	
Inflation Rate, %	2.5	
Real Discount Rate, %	8	
Federal ITC Credit, %	30	
System Degradation, % per year	0	
Debt Fraction, %	60	42.3
PPA Escalation, %	0.6	1.14
Availability, %	94	96
Direct Costs - Site Improvements, $/$m^2$	3	24
Direct Costs - Solar Field, $/$m^2$	350	343
Direct Costs - HTF, $/$m^2$	17	80
Direct Costs - TES, $/kWh-t	40	78
Direct Costs - Fossil Backup, $/kWe	Not Considered in Assessments	
Direct Costs - Power Plant, $/kWe	850	878
Direct Costs - Contigency, % Direct	8.4%	10.0%
Indirect Costs - EPC, % DC	16.0%	14.8%
Indirect Costs - Project, Land, Misc., %DC	3.5%	4.1%
Indirect Costs - 7.75 Sales Tax applied to % DC	Applied to 80% DC	Applied to 78% DC
O&M - Fixed Annual Cost, $/yr	0	999
O&M - Fixed Cost by Capacity, $/kW-yr	50	69
O&M - Variable Cost by Generation, $/MWh	0.7	3.0
O&M - Fossil Fuel Cost, $/MMBTU	0	6
Total Installed Costs, $M	651	845
LCOE (real), ¢/kWh	16.10	15.55
SAM Version	SAM (Nov. 2008)	SAM 2010.4.12

The overall capital breakdown for the baseline plant configuration can be seen in Figure 66. In this figure the input parameters that are a function of the solar field area have been broken out separately. The new baseline indicates that approximately 45% of the total baseline plant cost is associated with the solar field size. This agrees well with the Phase I assumption of the solar field comprising 47% of the total plant costs. While the individual categories may be slightly different from the two phases, the overall trends align relatively well.

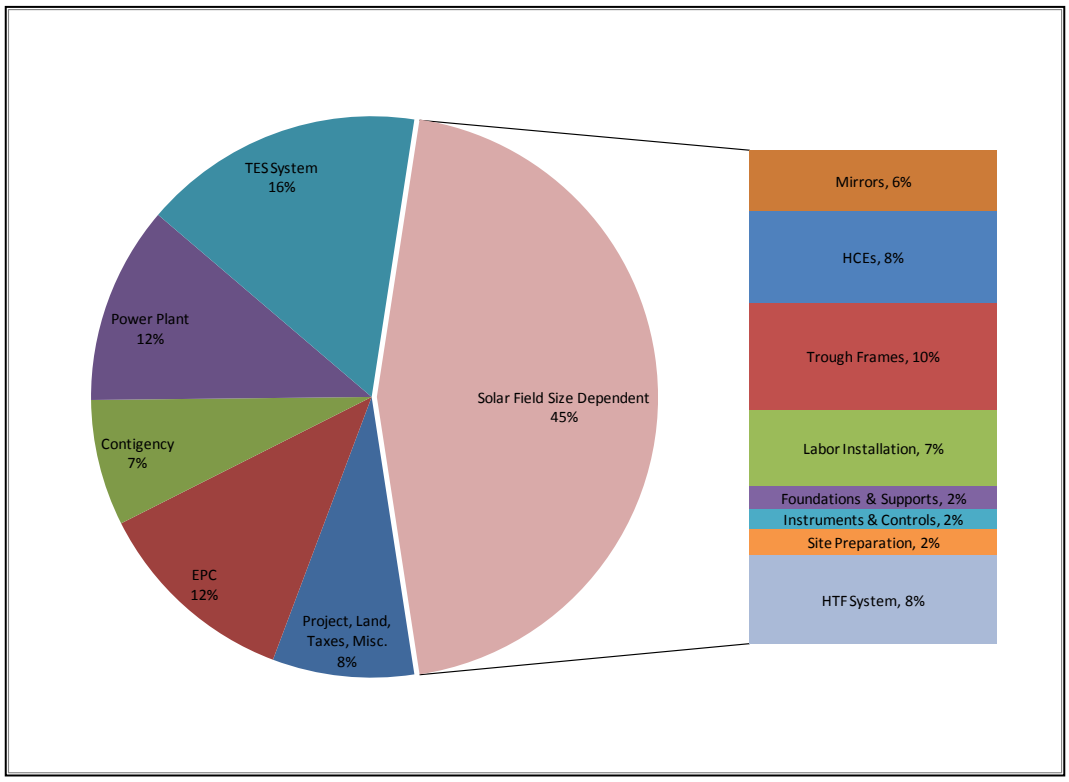

Figure 66: Cost Distribution for Baseline 110MW (Gross) CSP Plant with 6 hours TES

The impact of the capital and baseline assumptions on the LCOE can be seen in Figure 67. Solar field related capital (Site, Solar Field, and HTF System) accounts for roughly 40% of the LCOE or approximately 6¢/kWh. This does not include the indirect costs which are also influenced by the initial solar field capital. Referring back to Table 16, the Alcoa design can impact this cost portion directly by 45% (primary effects of materials, design and manufacturing) and indirectly by 55% (secondary effects of trough sizing).

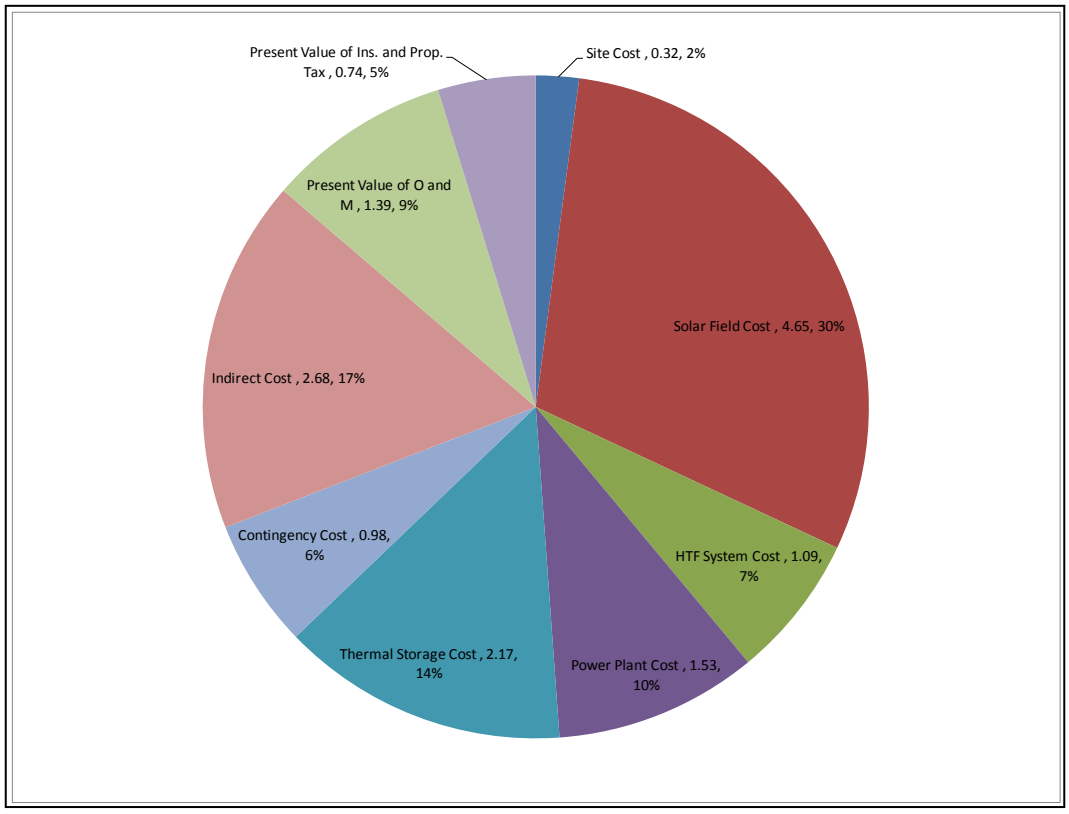

Figure 67: LCOE (¢/kWh) distribution for baseline 110MWe (gross) CSP plant with 6 hours TES

Alcoa GEN-2 trough cost assessment

During Phase I of the program, a built-up manufacturing model was developed for the Solargenix SGX-1 trough Nevada Solar One (NSO) system as a means of establishing a reference against the high level costs obtained from SAM. This baseline model was fully calibrated against SAM, and a similar assessment was conducted on Alcoa's 5m by 8m Wing Box design. In Phase II, both models were further updated for market representative consumable costs and labor rates. Additionally, the Alcoa trough design was further refined in terms of structure weight, aperture width, trough length, and part count. As a result, the Alcoa design optimized in Phase II is now referred to as "GEN-2". The Gen-2 design shares much of the same architecture as the Phase I design but has been enlarged to 6m by 14m to capture additional secondary savings. As in the first Phase, the delta cost differences between the two built-up estimates were employed to understand the influence of LCOE which was calculated from SAM.

The SEER-MFG models were developed based upon part counts, sizing, and weight estimates derived by the Alcoa team. SEER-MFG is an industry leading manufacturing costing tool employed by a number of organizations such as Boeing and NASA. It allows the user to build-up the cost of a complex assembly by breaking down the manufacturing sequence required for each individual component. The manufacturing steps can include various forming, machining, joining, and inspection operations. An example of the SEER-MFG tool can be seen in Figure 68.

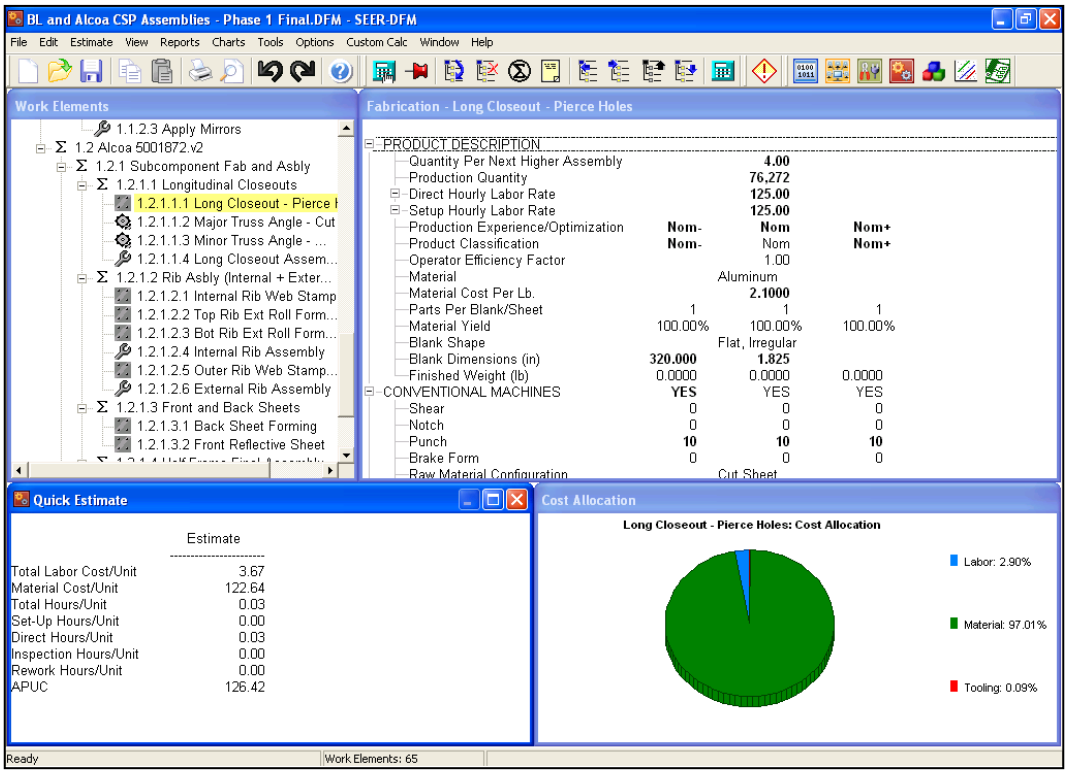

Figure 68: SEER-MFG cost estimation tool

In this figure, a work breakdown structure (WBS) is shown in the upper left. This WBS includes all the major manufacturing steps to build the final structure. Each WBS element is an individual manufacturing step that is populated with labor rates and manufacturing steps shown in the upper right. The analysis is parametric in nature such that the costs are dependent upon the overall sizing, complexity, and degree of automation employed in the process. SEER-MFG produces labor hours based upon industry adopted time study results. The SEER tools are conventionally employed to develop "should costs" and the results are considered as rough order of magnitude (ROM) values since they do not necessarily include the margins and overheads associated with actual industrial applications.

In Phase II of this program the baseline SEER-MFG cost model was updated according to market representative material prices and 2010 prevailing labor wages for Southwest Arizona. The baseline design for Alcoa's SEER-MFG analysis is a 5m x 8m SGX-1 trough that assumes the trough is assembled on-

site from an aluminum spaceframe kit with manual mirror attachment. In order to compare Alcoa's baseline model with the NREL's new baseline model of a 5.77m x 12m steel-based prefabricated truss assembly, Alcoa is making the assumption that the installed cost per unit area of the two troughs are the same. The Alcoa Excel model also takes into account sizing effects, that is, updating the secondary savings for reduction in pylons, foundations, motors, HCE, etc., caused by changes in the trough aperture and length which are currently not accounted for in the NREL cost modeling tools.

The SEER-MFG analysis included the materials and labor associated with the fabrication and field assembly of the mirror and metal support structures. The analysis did not include the pylons, foundations, motors, piping, and HCE. In general the trough models included the following:

- Baseline Cost Model (costs based on 5m by 8m but will be scaled per unit area to 5.77m by 12m)
  - Extrusion Materials, Fabrication, and Kitting – long and short (couplings) extrusions that are manually cut to size and predrilled. Parts are inspected and kitted per individual trough.
  - Mirror material costs
  - Field Assembly – Manual field assembly of approximately 450 parts (extrusions, mirrors, pins, blind fasteners)
  - Pylon Assembly – Field erection of individual trough to pylon couplings
- Alcoa GEN-2 Cost Model (6m by 14m):
  - Subcomponent Fabrication and Assembly:
    - High automation for fabrication and assembly of "half module" troughs,
    - Employs robotic forming and joining technologies that are leveraged from automotive environments,
    - Joining employs low heat distortion technologies such as mechanical clinching, self-pierce riveting, friction stir spot/seam welding, and adhesive bonding; thus maintaining high part tolerances,
    - Aluminum product forms include extrusions and sheet,
    - Reflective surface applied at factory and costs estimated from Alcoa design team.
  - Pylon Assembly – Finished half modules are transported to solar field where the two halves are joined and then directly mounted on pylon supports, significantly reducing field assembly times.

The approach adopted from the Alcoa design leverages trends from the building and construction industries that employ highly automated processes to prefabricate large scale components. Alcoa design allows a much greater packing density over spaceframe-based systems. As a result, the Alcoa design offers an advantage of directly transporting a semi-finished trough to the site, thus reducing the time for field assembly. As shown in cost flow-path (Figure 64), SEER-MFG estimates the change in manufacturing costs for the trough's (including both mirror and frame) fabrication, assembly, and field erection. This value is then input into Alcoa Excel model which contains the detailed cost distribution of all solar field related components. In this manner both the primary and secondary cost impacts can be realized and then input into SAM.

Table 18: SAM input parameters for baseline and Alcoa GEN-2 troughs

CSP Plant Cost Summary	SAM[1] Input Parameters		
	Baseline Trough (5.77m by 12m)	Alcoa Trough (6m by 14m)	Units
Direct Capital Cost			
Site Improvements[2]	23.9	< 5% Increase	$/m2
Solar Field[3]	342.6	> 20% Savings	$/m2
HTF System[4]	80.2	< 5% Savings	$/m2
Thermal Energy Storage	78.1	78.1	$/kWh-t
Fossil Backup	Not Considered in this Assessment		$/kWe
Power Plant	877.9		$/kWe
Contingency	10% Direct		of DC
Indirect Capital Cost			
EPC Costs	14.8%		of DC
Project, Land, Misc.	4.10%		of DC
DC's Sales Tax	7.75% applied to 78% of Direct		of DC
O&M Costs			
Fixed Annual Cost	999.0		$/yr
Fixed Cost by Capacity	69.0		$/kW-yr
Variable Cost by Generation	3.0		$/MWh
Fossil Fuel Cost	6.0		$/MMBTU
SAM Notes			
Note 1. SAM Version 2010.4.12			
Note 2. Solar field adjusted to account for optical efficiency differences			
Note 3. Includes trough (primary) and balance of system (secondary)			
Note 4. Larger aperture requires less loops, field piping, etc. (parasitic benefits not included)			

It should be noted that Alcoa Excel model does include a factor for the optical efficiency. The model assumes the reflectivity of the surface currently on the Phase II prototype (Alanod's Miro-Sun at 88% 25mrad specular reflectance) but also factors in the improved geometric accuracy inherent with the design as determined by NREL with VSHOT testing. As a result of the lower reflectivity, which is partially off-set by the improved structural accuracy, a small increase in the Site Improvement category is observed in Table 18. Additionally, this factor also reduces the savings observed in both the Solar Field and HTF System categories. In general a 1% change in reflectivity will reduce the total solar field costs by approximately the same amount.

The LCOE of Alcoa's GEN-2 trough as compared to the baseline system can be seen in Figure 69. In this figure, the primary savings accounts for roughly 80% of the total reduction. Overall the GEN-2 trough shows the potential to reduce the LCOE by approximately 10% or 1.6 ¢/kWh over the baseline system. While accounting for roughly 20% of the total reduction, the secondary effects could be further captured by extending the trough aperture area above 84 square meters.

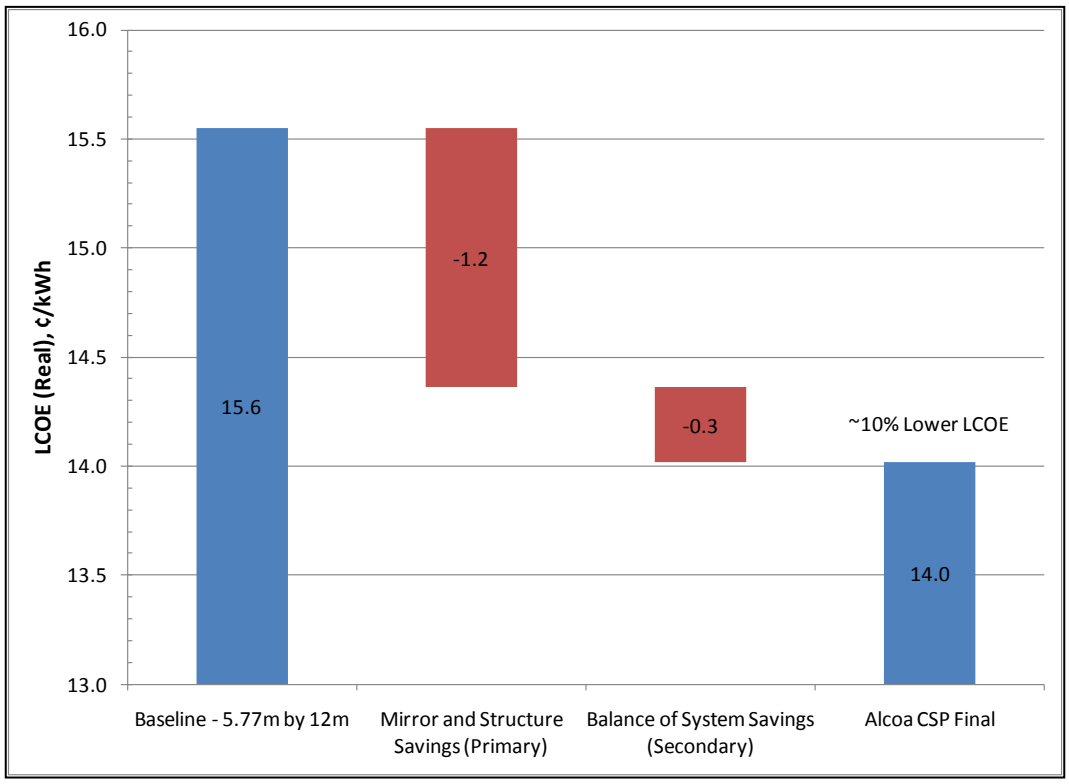

Figure 69: Cost distribution comparison for Alcoa GEN-2 and baseline trough system

The overall cost distribution for the various solar field components can be seen in Figure 70. It was estimated that the Alcoa GEN-2 trough design provides a cost savings in excess of 20% over the baseline. The savings observed in the frame and mirror components comprise roughly 80% of the overall solar field savings. The savings were achieved through design, weight minimization, and labor reductions in fabrication and assembly.

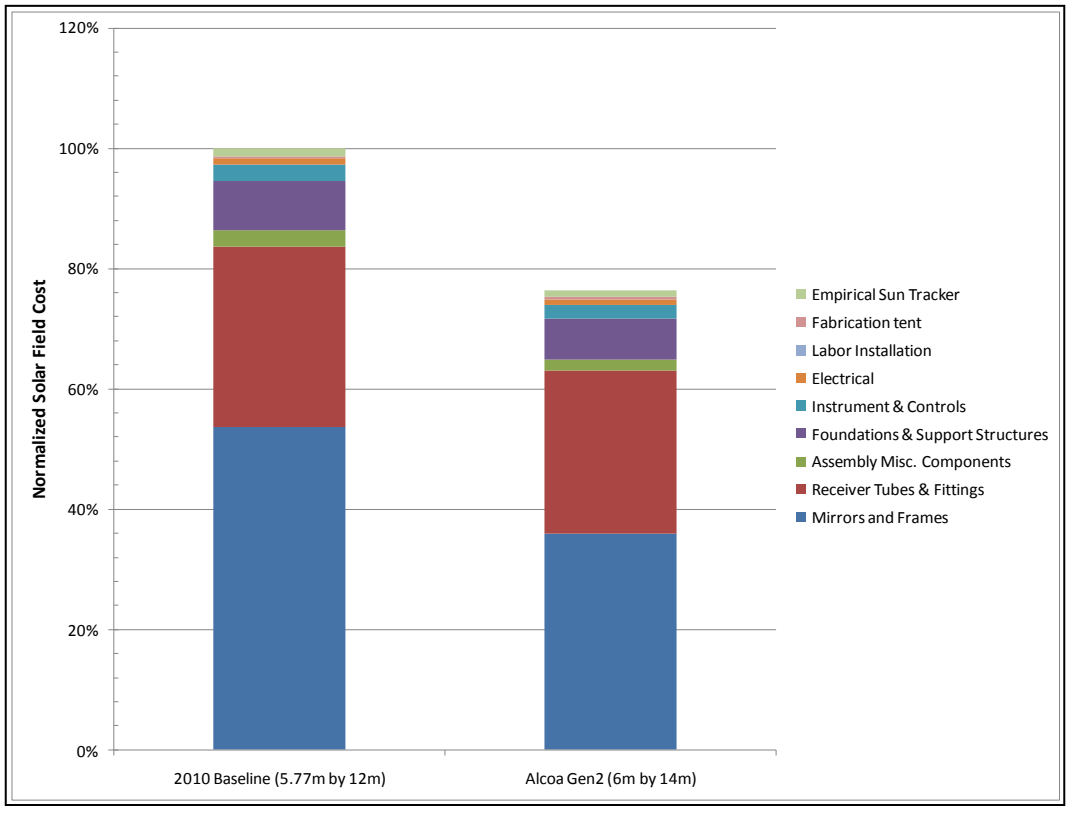

Figure 70: Solar field cost for Alcoa GEN-2 and baseline trough system

(Normalized to baseline and adjusted for optical efficiency)

Task 2.6: Develop Phase III Plan

This task was performed to redefine the Phase III plan based on the results from Tasks 2.1 through 2.5 above, and based on the activities that Alcoa feels are necessary to sufficiently develop the technology readiness of the Wing Box design for full-scale commercialization. The original statement of project objectives (SOPO) for Phase III that is outlined in the contract award (developed in 2007) proposes a commercial road mapping activity to illustrate the specifics of how the developed trough technology could be commercialized. This road mapping activity is now deemed premature as Alcoa now has a better understanding of what is required to commercialize their advanced technology within the CSP market.

Through the completion of Phase II, Alcoa successfully demonstrated that the Wing Box trough technology is technically feasible on a prototype scale in a representative test environment, that is, SIMTA facility at NREL. Before commercializing this advanced trough technology, further validation testing is required on a systems level. To better illustrate this gap in commercialization, consider the technology readiness levels (TRL) descriptions shown in Figure 71 that are used by NASA. As shown in this figure, the validation of the Alcoa Wing Box prototype in Phase II of this program is analogous to completing the TRL6 milestone. However, prior to commercialization of the technology, the technology needs to be validated on a systems level by completing the TRL7 threshold.

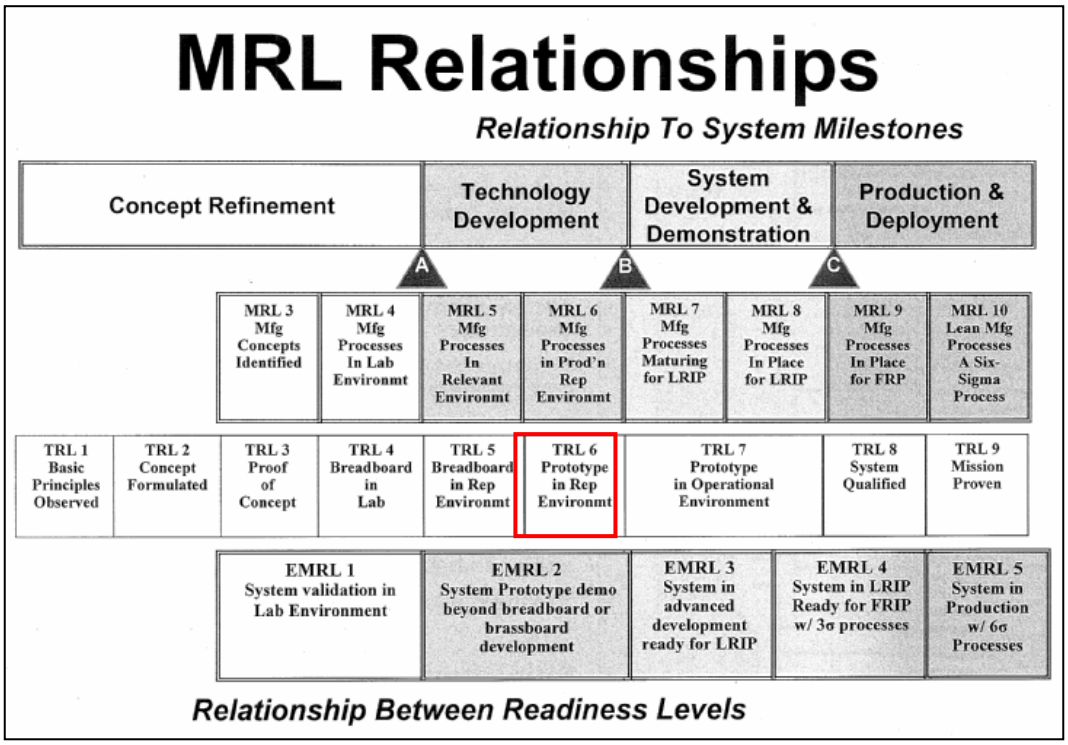

Figure 71: Manufacturing Readiness Level (MRL) Relationship to TRL

Given that a systems level test validation is required prior to commercialization, Alcoa proposed a revised Phase III plan to test the Wing Box trough via a test loop that is comprised of multiple troughs in an operational environment. Recognizing that Alcoa does not possess the systems-level knowledge and test assets to fully validate a test loop, Alcoa formed a development partnership with a major CSP integrator for Phase III of the program. This development partner will assist Alcoa in optimizing the Wing Box technology based on a systems level approach and assist in reducing the commercialization risk. The following outlines the proposed Phase III Statement of Project Objectives (SOPO) in more detail.

Per the original Statement of Project Objectives, Phase III was to consist of five major tasks and a final project review with the DOE (see Appendix A). Specific deliverables and task descriptions were to be highly dependent upon the resultant system design of Phase I and the performance results of the

prototype design in Phase II. As a result of the learning's from the first two phases, the following revised SOPO was proposed for Phase III.

Task 3.1: GEN-2 Wing Box Optimization

In this task and its sub-tasks, Alcoa will optimize the current generation of the Wing Box trough design, that is, GEN-2. Three main activities will be performed in this task:

1. Design optimization based on Phase II validation testing
2. Manufacturing flow-path optimization
3. Cost modeling update

The FEA model will be updated based on the results of the Phase II wind load testing performed at NREL (see Section 2.5). After correlating the FEA model to the testing results, a design optimization task will be performed to minimize the material utilization within the design while maximizing the structural performance of the trough.

In parallel with the design optimization, a detailed manufacturing flow-path analysis will be conducted. This analysis will determine the costs associated with the manufacturing, assembly and transportation of the all the components, the sub-assemblies, and the trough modules. Alternative manufacturing flow-paths, i.e., manufacturing processes or equipment, as well as, alternative trough component designs will be considered to minimize the installed cost of the trough.

The Alcoa trough cost model will then be updated with any changes to the material thicknesses, changes to the manufacturing of the components, or any changes to the assembly approach. This will serve as Alcoa's best estimate of the production trough costs for an optimized design based both on structural performance and optimized manufacturing and assembly approaches.

Task 3.2: GEN-3 Wing Box Optimization

During this task and its subtasks, Alcoa will work with a collaborative partner to develop the next generation design (GEN-3) of the Wing Box trough. This task will be performed in parallel with Task 3.1 and it is anticipated that the learning from Task 3.1 will concurrently inform the next generation design.

The objective of this task is to integrate Alcoa's materials, manufacturing, and prior Wing Box technology with the broad CSP systems knowledge and expertise of an established CSP Integrator. The goal is to develop an optimized systems design. Through collaboration with an experienced CSP Integrator, this next generation of the design will consider the effects of integrating the trough into a solar field and will consider any design changes to minimize costs during the systems integration. The design will also address any items that are thought to be high risk by the collaborative partner and, therefore, help to address the bankability of the system during full scale commercialization.

This task will involve setting cost and performance targets with the collaborative partner, reviewing the details of Alcoa's previous development phases, discussing pros and cons regarding the current design, performing design trades of any collaborative advanced concepts, high-level design and analysis of any new design configurations, and finally cost modeling of the collaborative design.

Task 3.3: Test Loop Decision

During this task the collaborative team will assess the GEN-3 cost saving and performance with the established targets set in Task 3.2. The team will assess the costs associated with validating the GEN-3 design via a test loop at the Integrator's facility.

This task will serve as an internal gate review between Alcoa and its collaborative partner. The goal is to make the decision to build and validate the test loop in an operational environment.

Task 3.4: Manufacture Test Loop

During this task and its subtasks, Alcoa and its development partner will perform the detailed design and manufacturing of a test loop based on the GEN-3 design solution developed in Task 3.3. It is estimated that a test loop comprised of 8 troughs should be sufficient to perform the systems validation. This number is the basis for the cost estimate for this task.

Alcoa will be responsible for the detailed design, analysis, and manufacturing of the troughs for the test loop. Our collaborative development partner will assist with the design and fabrication of the remainder of the test loop components, including the stanchions, piping, etc. Our integrator partner will install the test loop and perform the validation testing. Note that only the solar field components for the test loop will be required, as we will be leveraging the power block assets of our collaborative development partner at the test loop site.

To aid in the system validation of the test loop, Alcoa and its collaborative partner anticipate leveraging NREL's optical efficiency test assets including VSHOT testing of a trough at the Alcoa Technical Center and selected troughs at the test loop sight. In addition, reflective surface measurements would also be requested throughout the manufacturing and validation tasks.

Task 3.5: Install Test Loop

During this task and its subtasks, the test loop would be installed. This includes the foundations, troughs, received tubes, and high temperature fluid (HTF) piping. Alcoa will provide engineering support to our collaborative development partner during this task.

Task 3.6: Validate Test Loop

During this task, the test loop will be validated through a series of component level testing of individual troughs as well as full optical efficiency testing of the entire test loop. It would be desirable to utilize NREL's support during this task including VSHOT testing. Alcoa will mainly provide support to our collaborative development partner for the validation testing.

Task 3.7: Phase III Review with DOE

The final deliverable in Phase III will be an Alcoa-generated report that contains detailed technical and cost data of the design, test loop construction, and the test loop validation results. The cost estimates will demonstrate the system's impact on a CSP solar field and the corresponding LCOE.

6.0 Phase III Results

Phase II of the program was concluded on May 18, 2010 when a review meeting was held at the Alcoa Technical Center with various members of the DOE and NREL. During this meeting and in the subsequent Phase II Report, Alcoa proposed a modification to the original Phase III Statement of Project Objectives (SOPO) to accelerate the commercialization of Alcoa's Wing Box trough technology. The following SOPO items were proposed:

Task 3.1: GEN-2 Wing Box Optimization

Task 3.2: GEN-3 Wing Box Optimization

Task 3.3: Test Loop Decision

Task 3.4: Manufacture Test Loop

Task 3.5: Install Test Loop

Task 3.6: Validate Test Loop

Task 3.7: Phase III Review with DOE

The rationale behind the SOPO modification was that the Wing Box prototype testing at NREL's SIMTA facility was insufficient to fully validate the advanced trough technology for full-scale commercialization. This fact was not evident during the original DOE proposal submitted in 2007. Through the completion of Phases I and II and through discussions with various potential commercialization partners, it became evident that validation of the trough technology through a test loop at an operational CSP facility would be required prior to full scale commercialization.

During contract negotiations with the DOE, it was agreed that the proposed Tasks 3.1 and 3.2 (GEN-2 and GEN-3 Wing Box Optimization) fit under the existing SOPO Task 3.1 (Update Design to Incorporate Phase II Lessons Learned). It was also agreed that the proposed Task 3.3 (Test Loop Decision) fit under the existing SOPO Task 3.2 (Finalize Pre-Production Build Plan). The DOE would be willing to consider modifying the SOPO for Phase III only after Alcoa was successful at obtaining a supporting development partner and the required funding and the internal (Alcoa) support to pursue a test loop validation program. The program was to continue under original SOPO until the time that Alcoa was successful at obtaining the required resources for constructing a test loop at which time a SOPO modification would be reconsidered by the DOE.

Task 3.1 Update Design to Incorporate Phase II Lessons Learned

Under the original SOPO the intent of this task was to focus on integrating the Phase II results into an updated production-level system design. Detailed 3D design, FEA verification, manufacturing assessments, and detailed cost modeling were to be performed. An updated manufacturing plan for full-scale production of the system was to be generated based on consultation with potential manufacturing partners and subsequent selection of a manufacturing site.

Given the fact that a test loop validation was required prior to commercialization, it was deemed that performing detailed 3D design and performing a detailed manufacturing plan for full-scale production was premature at this point in the program. Detailed 3D design would need to be completed prior to manufacturing a test loop, i.e., the proposed SOPO Task 3.4. Additionally, the need for a detailed manufacturing plan for full-scale production would not be required until the completion of the test loop validation (i.e., proposed SOPO Task 3.6).

Therefore, this task focused on incorporating the results of the prototype trough testing into the existing trough design, i.e., GEN-2 design. Additionally, a high-level manufacturing plan was performed to further optimize the trough design configuration to better facilitate the manufacturing and assembly of a large number of troughs within an operational environment. This high level manufacturing plan was completed

through a transportation study of the major trough components to determine the optimum mix of components fabricated in a dedicated manufacturing facility versus the components fabricated and assembled at the Solar Field. After determining the optimum trough subcomponents configuration, the Wing Box trough design was further optimized via finite element analysis (FEA). This was denoted as the GEN-3 design which is the design configuration that would be validated through a test loop program.

3.1.1 GEN-2 Wing Box Optimization

As discussed in Phase II, Section 2.5.4, wind load testing was performed on the Wing Box prototype trough at NREL's SIMTA facility with the purpose of correlating the experimental results to the analytical model (FEA) results. Section 2.5.4 discusses the test procedure and data collection performed during Phase II of the program. This section discusses the correlation of the FEA model by examining the differences between predicted and recorded results. Data correlation provided validation of the structural analyses used to develop the prototype, and allowed for further optimization of the next generation design (see Subtask 3.1.2).

Arrays of strain gauges were fastened to the prototype trough before its transportation to NREL (see Figure 72 and Figure 73). Data were recorded with negligible wind velocities such that gravity was the only load source during experimentation (see Figure 74). The connected data points are the FEA predictions. The single data points are the experimental data. Data were captured exclusively at night to eliminate the effects of solar heating of the metallic structure which would result in erroneous strain measurements. As gauge calibration was not available at a zero strain state, the differences between strain records in two trough orientations were used for correlation.

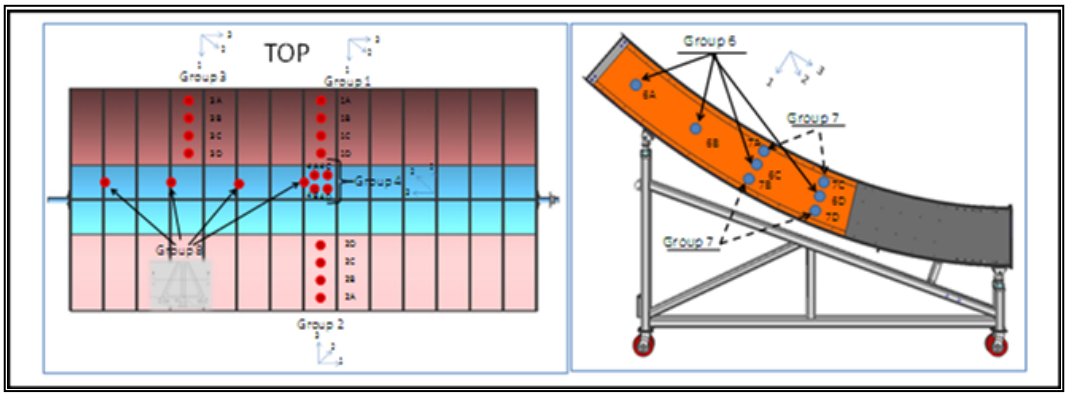

Figure 72: Strain gauge mounting locations on the Alcoa trough prototype

Figure 73: Strain Gauges Placed on Back of Trough

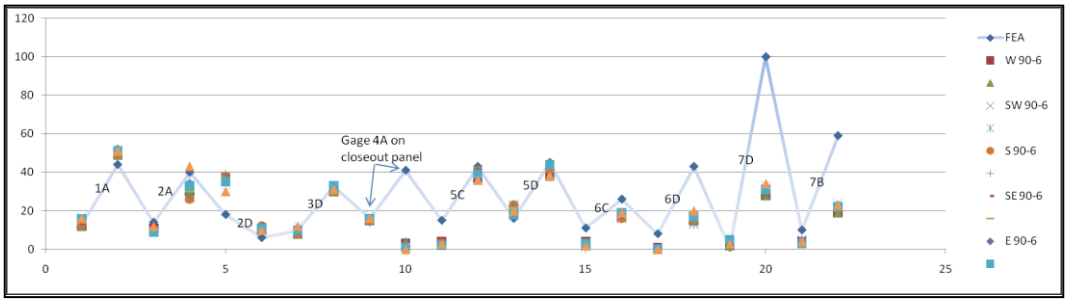

Figure 74: Gravity loading correlation

Data from the strain gauges were studied and trends were observed. Several apparent differences between the prediction and experimental results warranted further investigation. For example, the strain gauges mounted to a removable panel on the bottom of the prototype trough recorded little variation while the prediction suggested a significant strain change. Another strain gauge mounted to the permanent sheet near one of the openings recorded a differential higher than the prediction. These results were taken as evidence that the fasteners securing the panels to the trough were allowing slip rather than a rigid constraint. To address this issue, these joints were eliminated in the next generation design.

Figure 75 shows the results of 15 different strain gauge locations comparing the FEA and the experimental wind load data. A strong correlation between the recorded results and predictions was demonstrated. In the areas of poor correlation (i.e., strain gauge location #10) the causes were understood and could be explained by solar effects, instrumentation drift, non-rigid constraints, or anemometer variation. Overall, the wind load experimentation resulted in refinements to the analytical model, and the knowledge gained during the analysis provided a foundation for the advancements developed in the GEN-3 design.

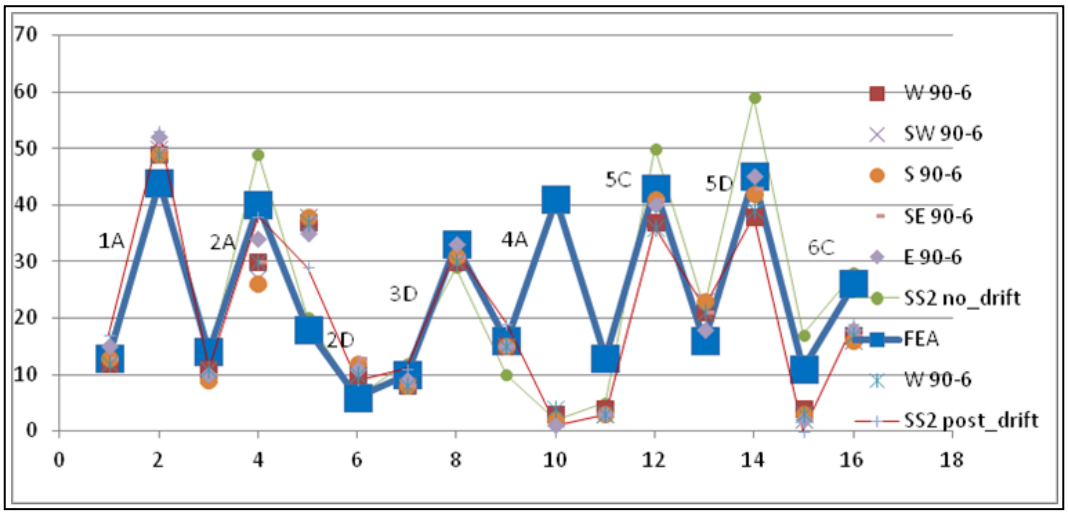

Figure 75: Plot of recorded and predicted strains in parts per million for fifteen gauges.

3.1.2 GEN-3 Wing Box Optimization

3.1.2.1 High Level Manufacturing Plan: Transportation Study

To facilitate the optimization of the GEN-3 Wing Box design a high level understanding of the manufacturing flow path was required prior to refinement of the trough sub-structure components. Given the overall size of the final assembled trough and the large quantity of troughs required for a solar field, the transportation costs would have a large influence on the final installed trough costs. Therefore, a transportation study was performed and utilized to determine the most cost effective manufacturing flow path, thus influencing the subsequent trough subcomponent design.

This section of the report is omitted from the public version of this report given it contains Alcoa Proprietary information.

3.1.2.2 Glass Feasibility Analysis

At the request of Alcoa's collaborative development partner for Phase III (see Section 3.3), Alcoa reconsidered use of a glass based reflector within the Wing Box trough design configuration. A glass-based reflector was previously considered in Phase I of the program. This was previously not considered feasible given the reflector is load bearing by nature of the Wing Box design. It was previously determined that the glass mirror would not be able to handle the loads induced during wind loading. Given the refined knowledge of the actual stresses induced into the reflective surface during wind load testing performed on the GEN-1 prototype, a more formal analysis of the glass could now be considered.

The advantages of utilizing a glass-based reflector are the following:

- Increased reflectivity over thin film, non-glass reflectors,

- Increased 'bankability' given the unknown lifetime of non-glass reflectors and the need for 20-30 year Solar Field guarantees.

An initial high-level cost study was performed to assess the use of a standard 4mm thick slumped glass mirror on the Wing Box design. The glass mirror reflectivity was assumed to be 94.5% 25mRad specular reflective. This cost analysis was performed using the GEN-2 Wing Box design configuration with a non-glass mirror with 88% 25mRad specular reflectance. Additionally, the high-level cost for a thin-glass laminate reflector was considered. For this scenario, a 1mm flat glass mirror was assumed to be laminated to a 2mm aluminum substrate.

Figure 76 shows the results of the initial cost trade study. The baseline GEN-2 trough cost, with a thin-film reflector, was normalized at 100%. Note the reflectivity cost penalty compensates for the reflectivity difference between the non-glass reflector and the glass mirror, i.e., 88% and 94.5%, respectively. The cost penalty is a result of having to increase the aperture area of the Solar Field to provide equivalent performance. As shown in Figure 76, the 4mm glass design results in a high trough cost. This is a result of utilizing higher cost 4mm thick glass mirrors (assumed ~$40/m2), increased substructure costs to support the heavier glass mirrors, and increased labor to manufacture and assembly a heavier and more fragile trough structure. As shown, the thin glass mirror laminate trough cost is in-line with the baseline trough cost. The cost is lower as compared to the 4mm slumped glass, given the lower cost of a flat, thin glass mirror (assumed ~$20/m2). Additionally, it was assumed that the trough substructure would not require significant up-gauging to support the laminate mirror. Based on this initial analysis and the potential advantages of a glass-based reflector, a more detailed cost and technical performance study was warranted.

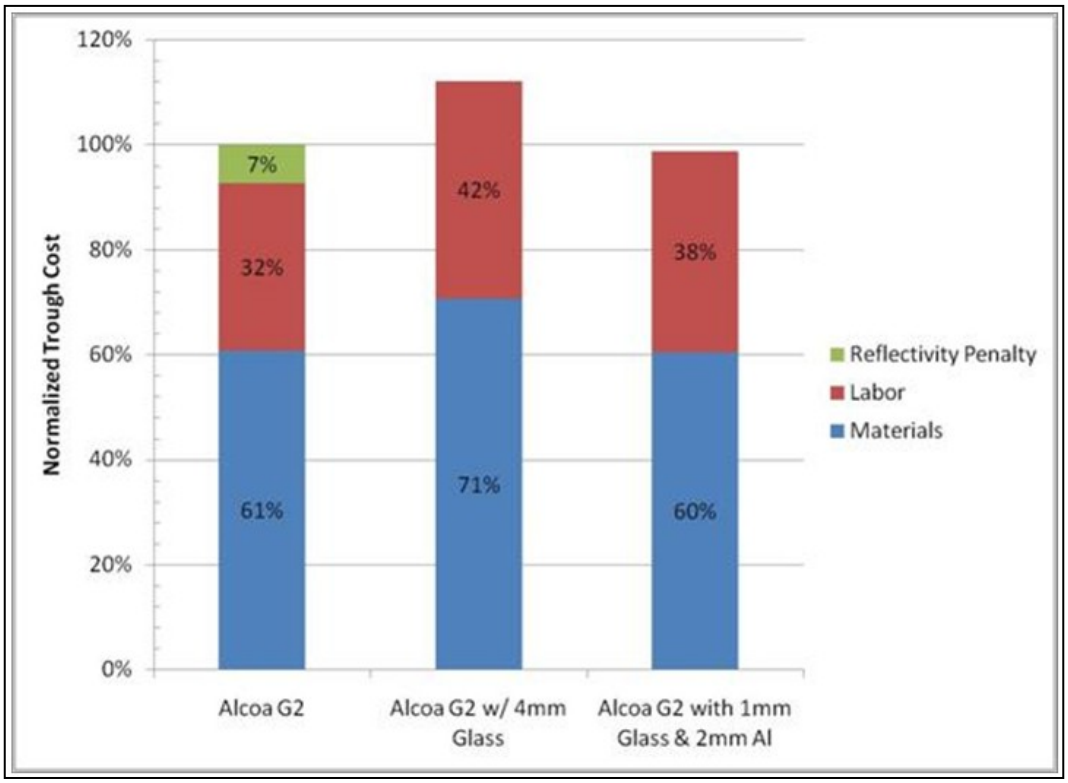

Figure 76: Cost Comparison between Glass and Non-Glass GEN-2 Wing Box Design

The technical feasibility of utilizing a thin-glass mirror was validated through experimental testing of thin-glass and aluminum laminate specimens. The purpose of the experimental testing was to determine if the thin-glass laminate could be naturally slumped into the parabolic trough curvature without breaking and without requiring pre-slumping. If pre-slumping was required, similar to that which is done with conventional 4mm glass mirrors, then the cost advantage illustrated in Figure 76 would be negated.

Test specimens were fabricated from 1mm flat solar glass laminated to 3mm aluminum substrates. Several different structural adhesives were tested for the laminate. Two different test specimen configurations were fabricated to perform a three-point bend and lap shear test (see Figure 77). The purpose of the three point bend test was to determine the maximum stresses in the laminate prior to breakage of the glass. The shear test was performed to determine the maximum stress prior to delamination of the specimen. It was a concern that the silver layer of the mirror stack-up would not be able to support the required shear loading of the reflector laminate. Both bending and shear stresses are induced into the mirror laminate during assembly of the trough (slumping the mirrors into position) and during operational wind loading of the trough. These tests would help validate that natural slumping of the mirror laminate was technically feasible and also alleviate the concerned that the silver layer within the glass mirror would not be able to withstand the shear load and delaminate. Delamination of the mirror stack-up would not only affect the reflectivity of the mirror, but also affect the load bearing capability of the laminate.

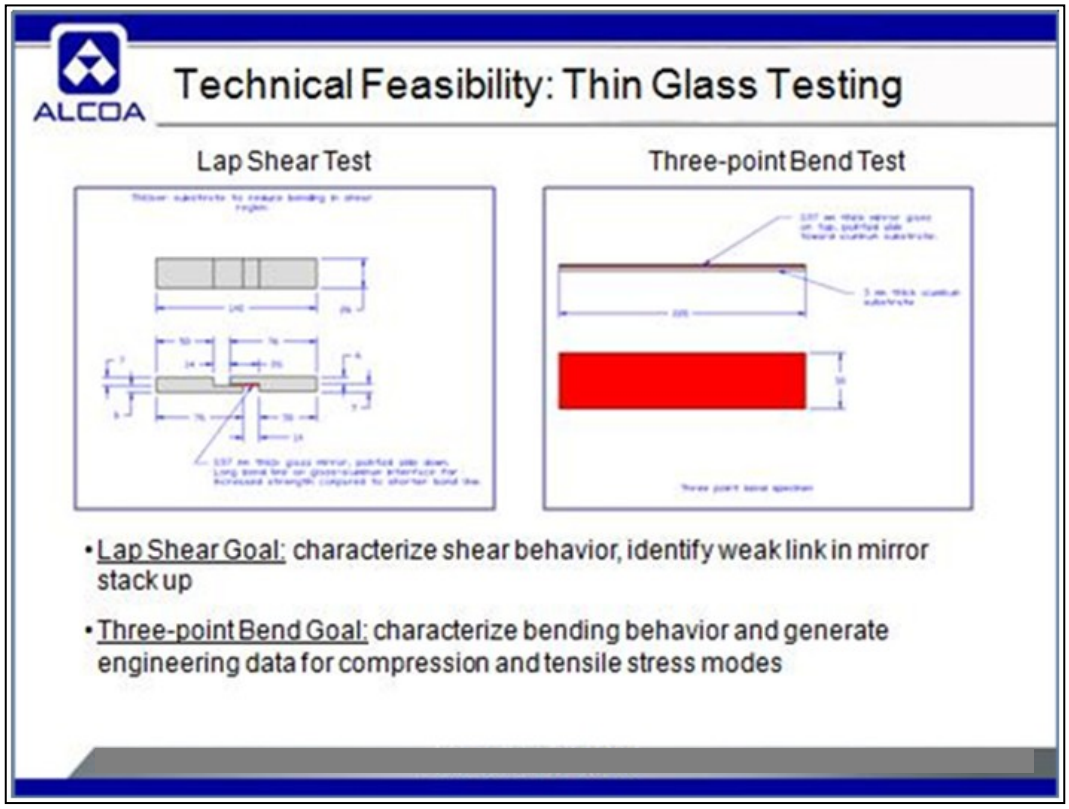

Figure 77: Thin Glass Laminate Test Specimen Configuration

Figure 78 and Figure 79 illustrate the results of the three-point bend tests with two different laminate adhesives. Figure 78 shows the amount of displacement (or deflection) of the test specimen versus the applied force. The linear portion of the force/displacement curve illustrates bending without breakage of the thin glass. The amount of displacement at which the force begins to 'roll-off' is where failure (glass breakage) is initiated. As shown in the figure, the amount of deflection before breakage significantly exceeds the calculated allowable deflections induced into the mirror laminate during assembly (or slumping) of the mirror onto the trough structure. This amount of deflection prior to breakage is also much higher than the deflections induced via wind loads on the trough. Figure 79 shows the three-point bend test set-up and an image of the test specimen at catastrophic failure (extreme displacement).

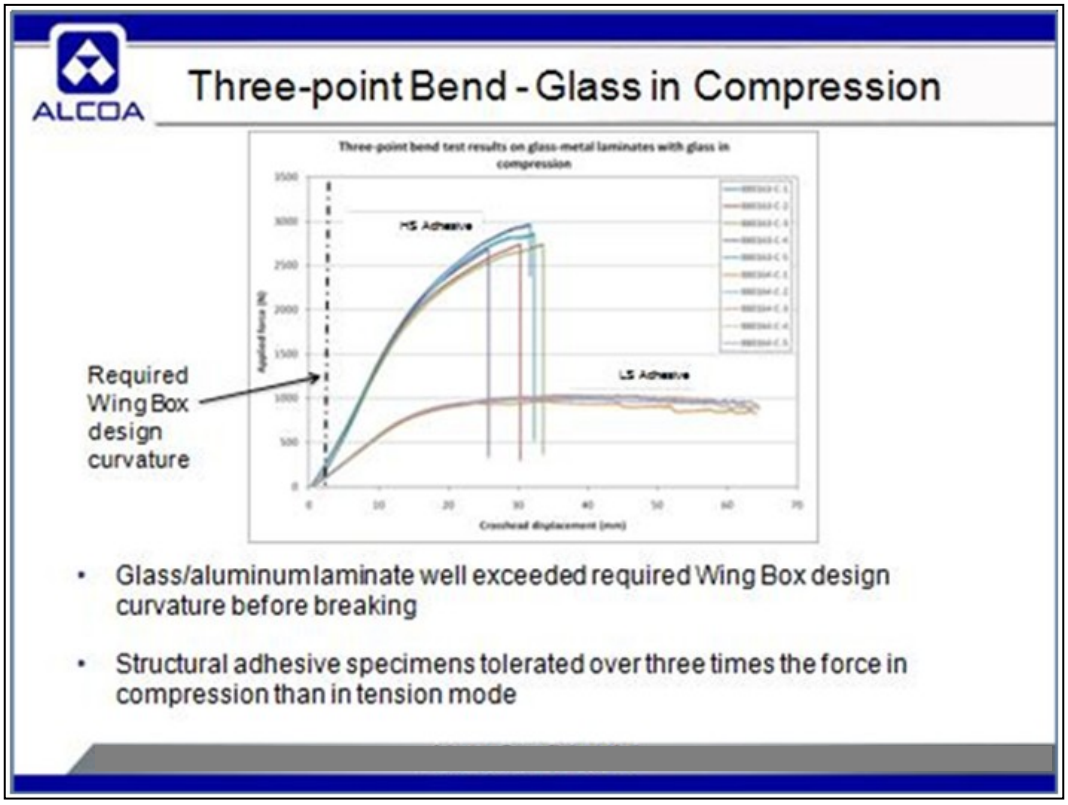

Figure 78: Three-point Bend Test Results with Two Different Laminate Adhesives

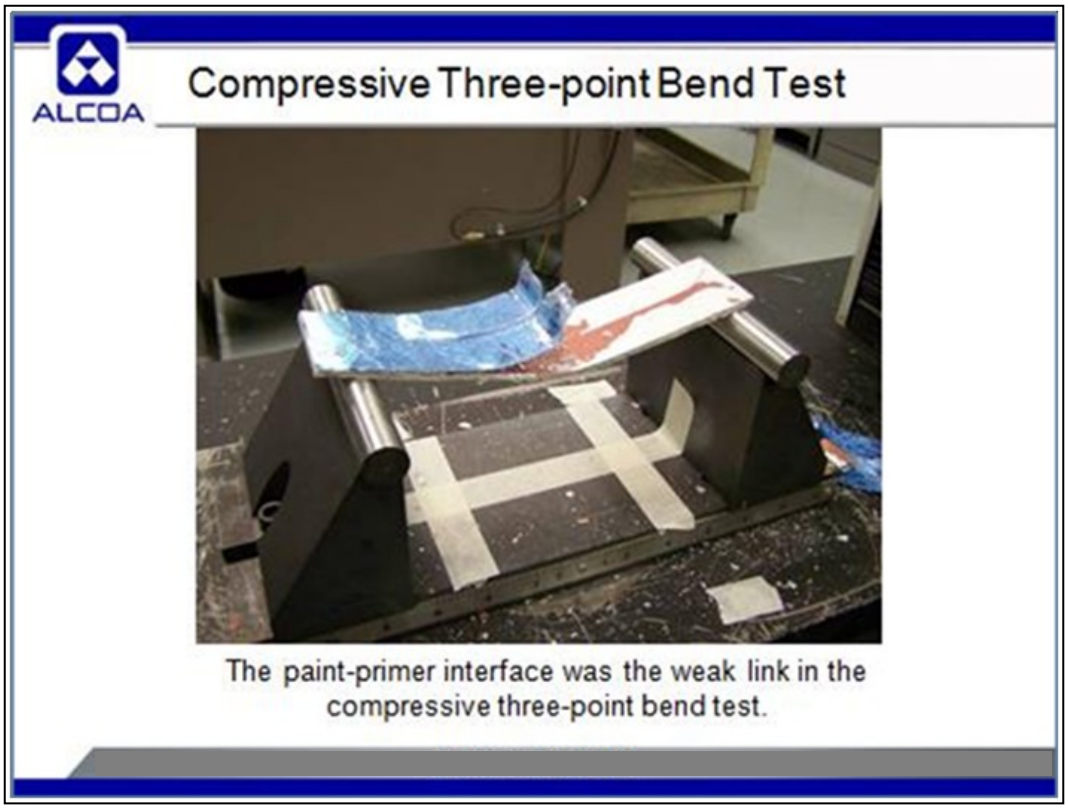

Figure 79: Three-point Bend Test Results (at Catastrophic Failure)

Figure 80 and Figure 81 illustrate the results of the lap shear test results. In this test set-up the specimens were axially pulled until failure was induced in the laminate. Figure 80 shows the resultant shear stress versus displacement. Failure, or delamination, is initiated when the applied stress 'drops-off' at a given axial displacement. For the high strength adhesive, the failure mode was the white painted surface of the

mirror and not the adhesive joint (see Figure 81). For the low strength adhesive, the failure mode was the structural adhesive. The test results were positive given that the failure mechanism was not the silver layer in the glass mirror. Based on the test results, the allowable shear stress can be managed through the choice of the structural adhesive and the stiffness of the trough substructure.

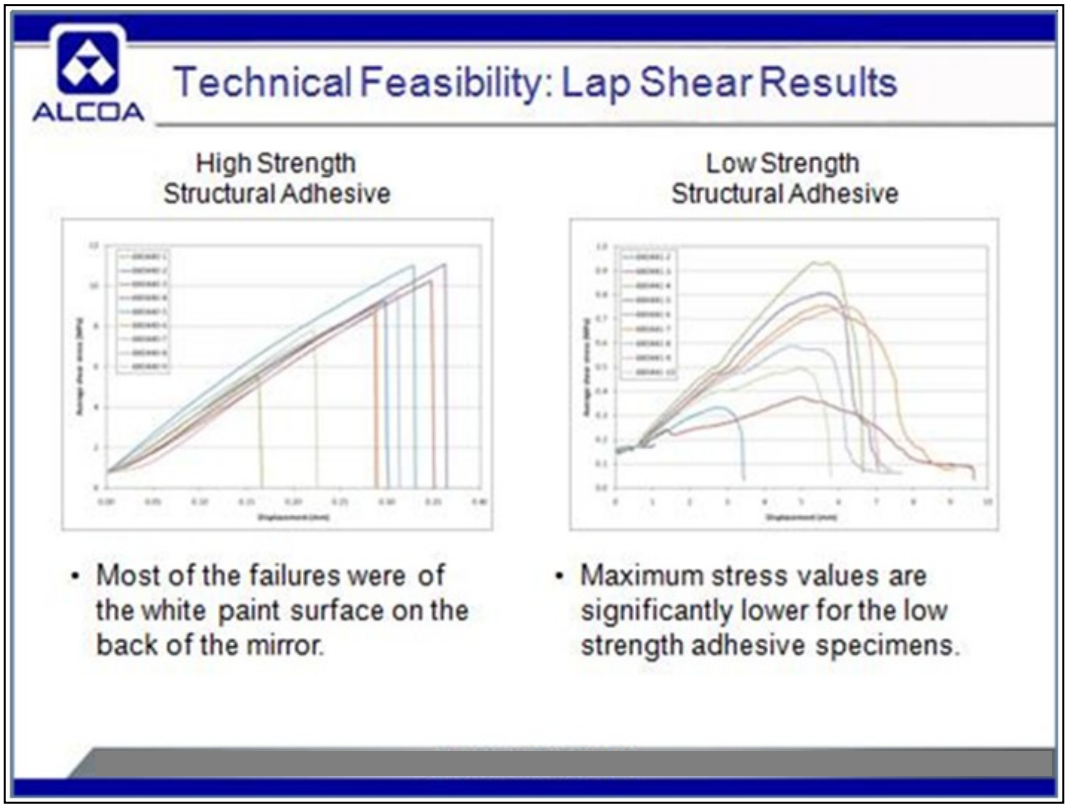

Figure 80: Lab Shear Test Results with Two Different Laminate Adhesives

Figure 81: Lab Shear Test Results (at Delamination - Failure)

Based on the experimental testing and maximum stresses within the Wing Box trough and upon the calibrated FEA model (see Section 3.1.1), it was determined that it is technically feasible to design a thin-glass laminate mirror that can withstand the loading requirements within the Wing Box design configuration.

Having established the technical feasibility, a more detailed study on the attachment mechanism of the glass reflector and further refinement of the cost study was required to assure that this solution would be economically viable. Through a series of brainstorming sessions involving Alcoa technical experts and our corporate partner, approximately 24 different glass concepts and attachment methods were ideated and down-selected (see Figure 82). The down-selection was based upon the following prioritized criteria:

1. Glass survivability (stress level in glass)
2. Bankability
3. Ease of O&M (repair, durability, replacement)
4. Costs, including:
    a) Material
    b) Manufacturing (tooling and capital)
    c) Labor
    d) Installation
5. Ease of installation
6. Area of reflective surface (% loss/gain)
7. Level of accuracy and precision

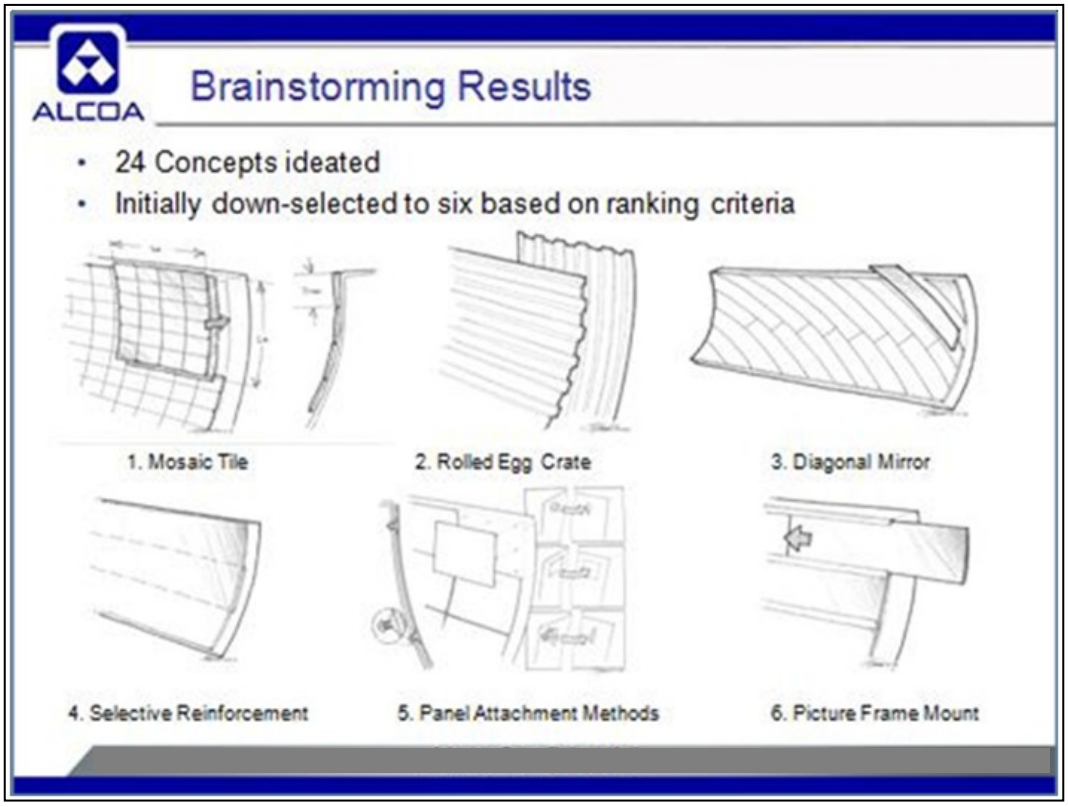

Figure 82: Initial Down-selected Glass Mirror Attachment Mechanisms

The 6 concepts shown in Figure 82 were further refined into two attachment mechanisms as shown in Figure 83. Of these two concepts, the compressive frame design was believed to be more economically viable as opposed to assembling multi-piece flat glass mirrors into the mirror panel. This concept was also perceived by the team to have lower technical risks, as compared to the faceted concept, given the results of the Technical Glass Feasibility Study. Further economic analysis of glass mirror concepts are discussed in Section 3.1.2.4, GEN-3 Cost Model Validation.

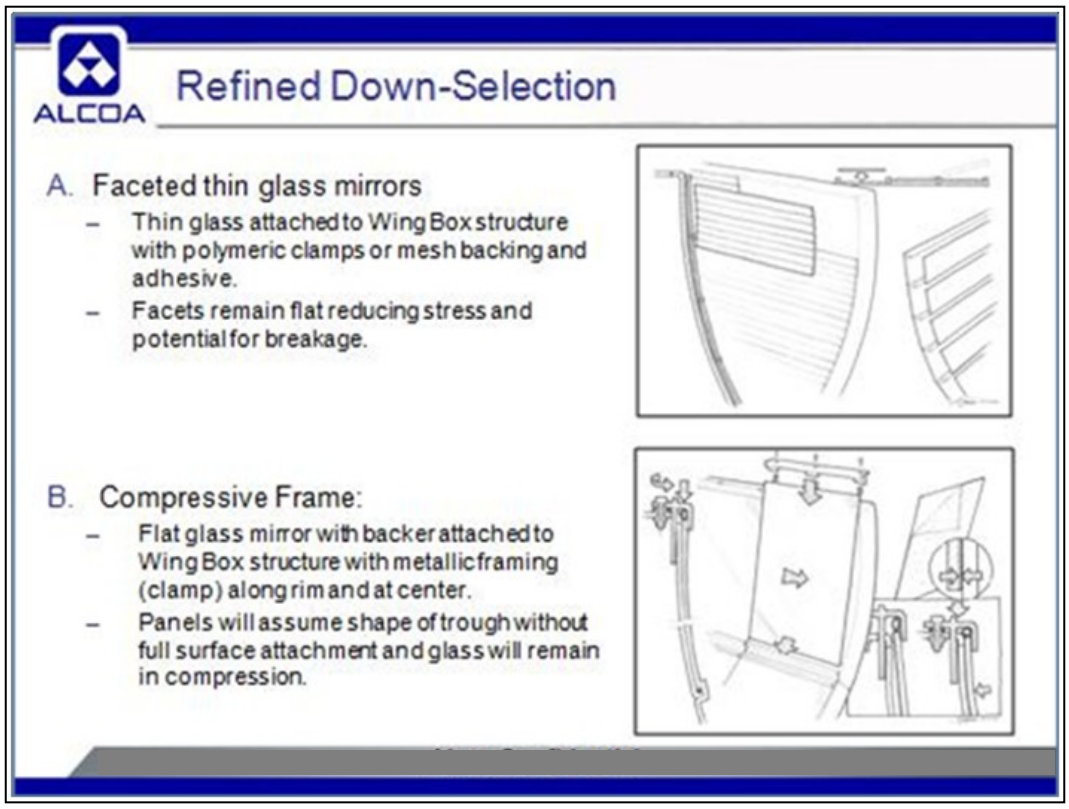

Figure 83: Down-selected Glass Mirror Attachment Mechanisms

3.1.2.3 Trough sub-component optimization

The GEN-3 Alcoa Wing Box trough design (see Figure 84) was developed based on refinements derived from manufacturing and assembling of the GEN-1 prototype, the optimized GEN-2 design (section 3.1.1), and a shipping study performed by Alcoa's Wheel and Transportation Products Business Unit. Goals of the GEN-3 design included mass reduction, optimization for transportation, ease of manufacture, ease of on-site assembly, and cost reduction.

The most substantial change in the GEN-3 trough design architecture was the elimination of modularity. The transportation study made it clear that shipping completed modules from a central location to the solar field for final assembly and installation was not cost effective. Instead components would be fabricated and shipped to a location near the field where a temporary factory would be created for rapid trough assembly. Due to the change from a modular design, the central spar and associated mass, was eliminated in the GEN-3 design (see Figure 85).

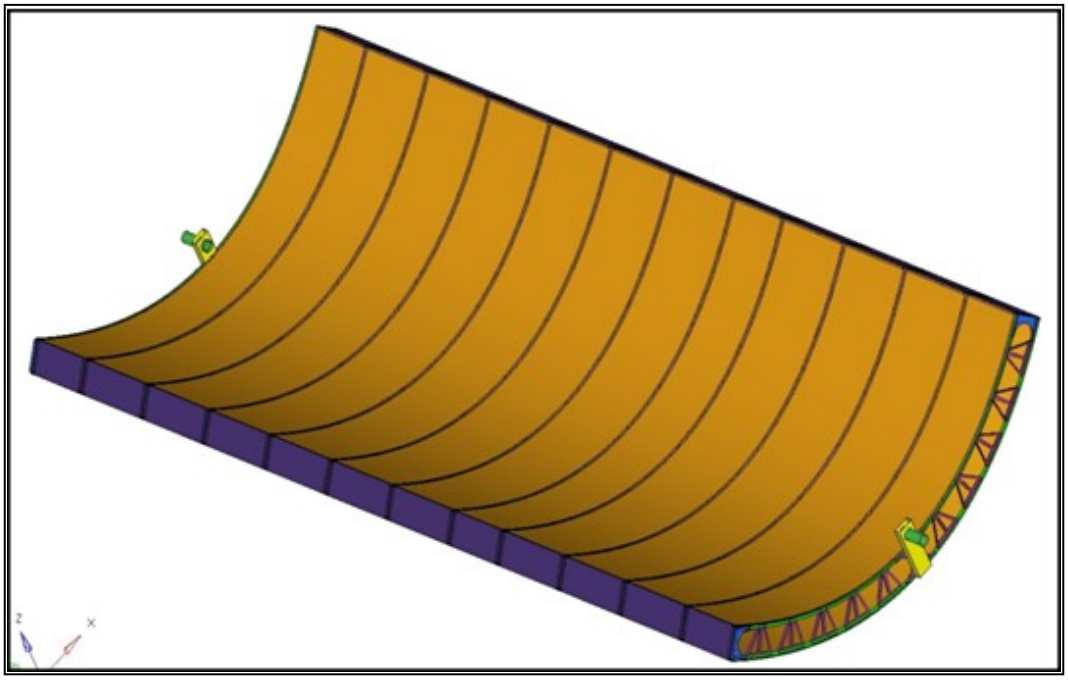

Figure 84: GEN-3 Wing Box Design

The elimination of modularity would result in improved geometric tolerances during production. In the GEN-1 prototype design, the geometric relationship between the reflector surfaces of the two modules was controlled by the tolerances of the inner spar surfaces. Each GEN-3 trough would be assembled on a single fixture such that the reflector surface location could be controlled within the required tolerance.

In order to reduce the number of ribs inside the trough structure their spacing was altered to use the maximum available reflector sheet width. This resulted in several different bay widths for a 14m trough, but provided a path for mounting the receiver tube support structures directly to the ribs. The receiver tube supports were modified from the GEN-2 prototype design by eliminating the sliding connection at the clamps and by adding a flexure near the reflector surface. The flexure allowed for the thermally-driven expansion of the receiver tubes.

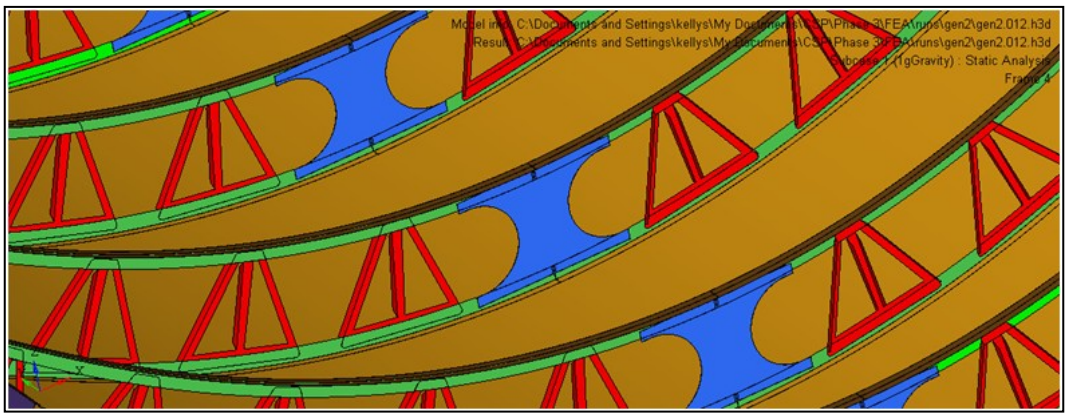

Figure 85: GEN-3 inner rib support without spar

Several different extrusion profiles are designed for the rib bows. This allowed thicker bows at the receiver tube supports and at the ends of the trough where higher strengths are required. Lighter extrusion profiles are designed for use in the other locations allowing a net reduction in weight. The thicker bow profiles provided a wider flat mounting surface. This allowed the receiver tube supports to be mounted to the trough without requiring additional steel supports and eliminated a trimming operation of the reflectors. Modified inner rib post designs were developed to better match the design goals of each location.

As a result of the optimization, the GEN-3 Wing Box design is more producible from a high-volume manufacturing and assembly perspective. The substructure architecture is optimized for manufacturing in a dedicated facility, shipping to the solar field, and on-site final assembly. While additional on-site assembly is required for this design over the GEN-2 configuration, these costs are off-set by the efficient utilization of material, the consolidation of components, and the transportation cost savings.

3.1.2.4 GEN-3 Cost Model Validation

Cost assessments were performed on the GEN-3 Wing Box trough (see Section 3.1.2.3) and the refined glass laminate concepts (see Section 3.1.2.2). The cost estimates followed the same methodology presented in Phase I and II. Additions or changes from the GEN-2 model were as follows:

- Lower structural trough weight for GEN-3 (~10%)
- Reduced part count
- Increased aluminum LME price (~14%)
- Updated transportation costs of subassemblies and individual parts
- Updated CAPEX costs for the manufacturing sites including the satellite, subassembly, and part plants

The results of these changes increased the GEN-3 cost by approximately 3% over the GEN-2 estimate. Gains in the base metal LME, transportation, and CAPEX were offset partially by reductions in both the structural weight and part count. The GEN-3 estimate is within the uncertainty associated with cost assessment techniques and therefore the results would be considered statistically similar as GEN-2. As a result the GEN-3 Wing Box trough would be expected to deliver a similar LCOE reduction as previous results, i.e. approximately 10% reductions over the baseline, 5.77m by 12m glass mirror trough. It is important to note that the GEN-3 estimate has much greater fidelity in the transportation and CAPEX assessments since significant work was devoted to mapping out the supply chain and infrastructure as compared to GEN-1 and GEN-2 estimates.

As a result of increased confidence in the GEN-3 design based on the Wing Box prototype testing and FEA model correlation, a further study was conducted to explore the integration of thin glass within its architecture as a means to improve the efficiency over non-glass mirrors. It was noted previously that a high level cost assessment on the GEN-2 design indicated similar costs may be achieved if a thin glass mirror was employed. Several glass laminate attachment concepts (Figure 82) were evaluated and high level designs were developed for each. Three concepts were down selected for cost estimates and the leading candidate was compared to the current GEN-3 costs with a non-glass mirror.

Figure 86 shows the results of the refined cost analysis comparing the GEN-3 Wing Box trough design with a non-glass reflector with 88% 25mRad specular reflectance compared to a thin-glass laminate reflector utilizing the compressive frame attachment mechanism (Figure 83). The thin-glass mirror was assumed to have 95% specular reflectance.

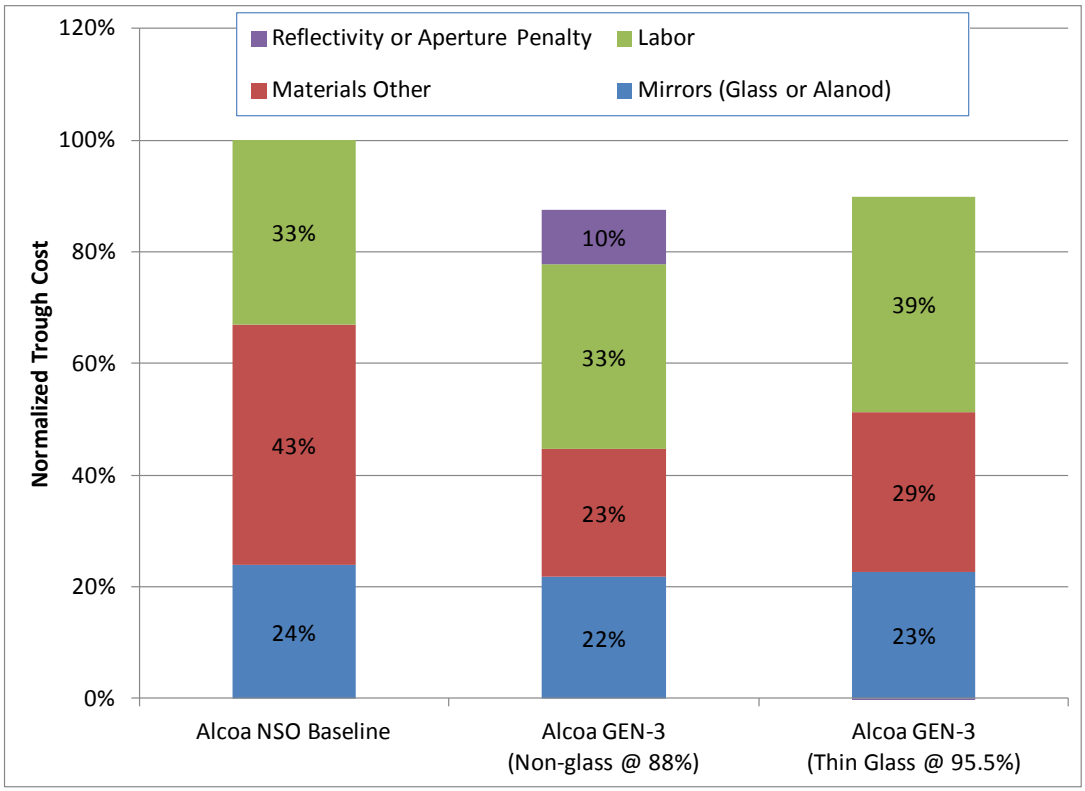

Figure 86: Normalized Cost of Non-glass (88% Reflectivity) Versus Glass Laminate Wing Box Design, 5m by 8m Trough

Figure 87 shows the results if the reflectivity of the non-glass mirror is increased to 92%. Note that 92% reflectivity was chosen as a conservative reflectivity that could be achieved with commercially available silver-film reflectors, and possibly achievable with next-generation thin-film reflectors.

This refined cost analysis illustrated that while a glass laminate solution is technically viable, it is not economically viable if the reflectivity of the non-glass reflector is greater than 90%. Additionally, a glass laminate reflector presents higher technical risks as this has not been technically validated at a large scale. Additionally, a commercially viable laminating process does not currently exist. Given the economic disadvantage and the potential technical risks, it was determined that the use of a non-glass reflector was still the optimum choice for a Wing Box design configuration where there is load sharing between the structure and the mirror/reflector.

Figure 87: Normalized Cost of Non-glass (92% Reflectivity) Versus Glass Laminate Wing Box Design, 5m by 8m Trough

Task 3.2: Finalize Pre-Production Build Plan

Under the existing SOPO, this task involved the continued refinement and update of the pre-production build plan, with a specific focus on determining the best locations and most appropriate partners for fabrication, assembly, and installation of the full-scale validation system. As agreed upon with the DOE during the Phase III contract negotiation, Alcoa was to make the decision to install a test loop using the Wing Box trough design during this task.

During Phase II, Alcoa performed an internal business analysis which was a requirement to justify the continued support of the Alcoa cost share funding under this DOE program. This internal business analysis outlined the market opportunity for CSP troughs, as well as, the commercialization potential for Alcoa through various supply chain positions for the Wing Box trough design. Figure 88 outlines the various scenarios that were considered.

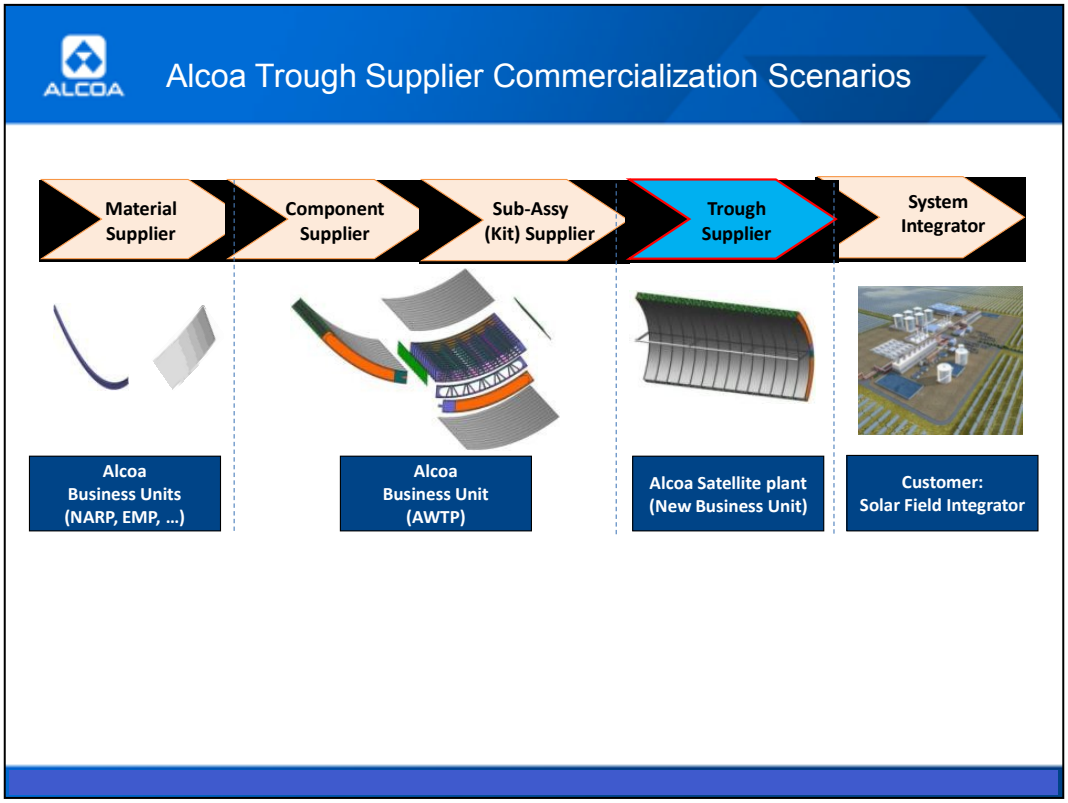

Figure 88: Supply Chain Scenarios for Commercialization of Wing Box Trough Technology

The internal study analyzed the options for raw material supply, component supply, subassembly or kit supply, and the supply of fully assembled troughs to a Systems Integrator. As a result of the study, it was determined that Alcoa would pursue the option of supplying fully assembled troughs to maximize the value to the customer and to Alcoa.

As described in Section 3.1.2, Alcoa would source raw materials from its existing Business Units including North American Rolled Products (NARP), Alcoa Engineered Milled Products (EMP), and Alcoa Fastening Systems (AFS). These raw materials would be fabricated into subassemblies and kitted at one of Alcoa's fabrication facilities under the Alcoa Wheel and Transportation (AWTP) Business Unit. To incubate the new trough business, it was determined to initially utilize a fabrication facility in Auburn, Indiana. This facility, while not strategically located within the Southwest USA, would minimize the capital investment required given existing manufacturing and assembly equipment. Once the business could be further justified, alternative Alcoa facilities could be utilized that are more strategically located within the Southwest US, i.e., Phoenix, Arizona. Once the subcomponents were fabricated and assembled at the dedicated facility they would be shipped to the Solar Field for final assembly. This shipping would most likely occur via a combination of rail and tractor trailers. Through the AWTP Business Unit, Alcoa would install a temporary fabrication facility at, or near, the Solar Field. At this facility, Alcoa would manage the final assembly of the trough units utilizing low cost, automated assembly equipment and dedicated assembly fixtures. By controlling the entire supply chain, Alcoa could better control and guarantee the accuracy, and therefore the performance, of the final assembled troughs. This temporary fabrication facility could then be easily transferred and utilized at the next Solar Field.

Task 3.3: Finalize Pre-Production Field Validation Plan

This task was to include the continued refinement and update of the full-scale test plan, with a specific focus on determining the best location and most appropriate solar power partner from the southwestern area of the USA to conduct field validation of the pre-production system.

A customer analysis was performed to identify potential trough customers as well as, potential partners for validating the Wing Box trough technology through a test loop.

After identifying a suitable development partner and after extensive technical and business related discussions, a Collaborative Development Agreement (CDA) was signed between Alcoa and Targeted Development Partner with the intention of jointly validating the Wing Box trough technology for full-scale commercialization. While Alcoa and the Targeted Partner were having technical discussions to make the decision to pursue the test loop together, the Partner went through a major restructuring which resulted in a change in their corporate strategy for developing Solar Field technologies, e.g., troughs. As a result of this new corporate strategy, the Partner made the decision to cancel the CDA with Alcoa. This decision was made on the basis of their technology development strategy to in-source proven trough technologies as opposed to internally developing advanced technologies. The decision was not a reflection of the potential of Alcoa's Wing Box trough technology.

Several discussions were made with alternative development partners to complete the test loop. One of the alternatives were willing to work with Alcoa to retrofit a 'loop' (row of SCAs from header to header) at their existing facility. While promising, this was an expanded scope over the validation approach previously anticipated with Targeted Development Partner. With the initial Targeted Development Partner, it was deemed that validation through a single SCA was sufficient rather than an entire loop. After reassessing the cost required to validate the trough technology with an alternate development partner and given the current economic environment, Alcoa made the decision to not pursue the test loop validation at this given time. As a result, Alcoa made the decision to not pursue a modification to the existing SOPO of the DOE program, and to conclude Phase III of the DOE program.

As a result of the need to further validate the trough technology prior to full-scale commercialization, a more formal pre-production field validation plan, beyond what was presented within this report, was considered to be premature given the current Technology Readiness Level of the trough technology. A more formal build plan and field validation plan can only be developed once the final trough configuration is known and validated.

Task 3.4: Internal Critical Design Review

This task highlights an internal Alcoa milestone to review all the critical design and commercialization information with Alcoa management.

After the termination of the Collaborative Development Agreement with the Targeted Development Partner and after researching alterative test loop development options, a meeting was held with Alcoa management to discuss the continuation of the program. The decision to discontinue the test loop program was made based upon the following factors:

- Added cost to validate a loop of Wing Box troughs, i.e., multiple Solar Collector Assemblies (SCA), versus 1 SCA proposed under the Targeted Development Partner agreement,
- Alcoa 'Cash Conservation' strategy given current Global economic uncertainties,
- CSP market uncertainties given economic financing, regulatory, and environmental permitting challenges,
- CSP trough market uncertainties given technical advances and cost advantages of competitive technologies such as Power Tower and Photovoltaic (PV).

As a result, Alcoa made the decision not to pursue a test loop program under the existing DOE program, and to conclude Phase III of the program. Alcoa plans to remain active in the CSP market as there is a significant potential for future growth of both aluminum and Alcoa sales within this market. The decision to pursue a test loop with the Wing Box technology will be reassessed when a suitable development partnership can be established and/or when the economic climate is more positive.

Task 3.5: Final Reporting

Upon completion of Phase III tasks, Alcoa will deliver a report to the DOE detailing all aspects (rationale, size, location, U.S. suppliers, etc.) of limited-scale production and field validation to ensure the concept's improved design will perform reliably in a realistic operating environment and to accurately predict future costs and operating characteristics. As part of this report, Alcoa also will present a final technology commercialization roadmap to assist the DOE as it explores next steps for an aluminum-intensive collector in a CSP system for the future.

This final report provides an overview of the potential value Alcoa's advanced Wing Box trough technology in meeting DOE SETP goals, and outlines the possible commercialization approach to realize these performance improvements and cost savings within the CSP market. The specific details of the production and field validation plan have yet to be developed given the need to fully validate the trough technology via a test loop prior to commercialization. As previously explained, this additional technology validation step was not anticipated during the original proposal submission in 2007.

Task 3.6: Phase III Review with DOE

As the final milestone for this project, a final discussion of the outcomes and next steps will be provided to the DOE upon request.

7.0 Patents

Date	Invention Title	Inventors	Application Filed
3/10/09	CSP Trough Design and Method of Production	Trent Chontas, John Cobes, Glenn Jarvis, Sean Kelly, Matthew Kiley, Robert Speer, D.J. Spinella	No
5/13/11	Compressive Clamp for CSP Trough Reflector Attachment	Sean Kelly, Steve Leonard, Adam Schaut, Philip Smith	No

8.0 Government Property

- Wing Box Prototype Trough (6m x 14m)
- Schott 80mm Receiver Tubes (quantity 2)

9.0 Publications

No publications issued

10.0 Presentations

Date & Location	Presentation	Presenter	Purpose
Telecoms			
March 2008- September 2011	Monthly review meeting	A. Schaut, S. Kelly, D. Smith, P. Smith C. Retarides, D. Serafin, M. Kiley, D.J. Spinella	Monthly update call with DOE
5/13/09	Conference Call	A. Schaut, D. Smith	Review of NREL Test Results with Cheryl Kennedy
5/18/09	Conference Call	P. Smith, R. Speer	Review of V-shot Test methodology with Allison Gray
6/4/09	Conference Call	P. Smith, P Gacka, S. Kelly, A. Schaut, T. Chontas	Review of Tracker Mounting Details and Tracker Testing
Attended Meetings			
4/22-24/08 Austin, TX	DOE annual solar meeting	A. Schaut	Present overview of Alcoa's proposal and activities
12/3/08 Pittsburgh, Pa	Phase I final review meeting	A. Schaut, D. Serafin, M. Kiley, D. Spinella, C. Retarides	Phase I final review meeting at Alcoa

10/30/09	State of Art - CSP Technology	Dr. Eckhard Luepfert of CSP Services	Review of current CSP technology
12/7/09	V-shot Testing and Methodology Conference Call	Allison Gray of NREL	Review of NREL's V-shot technology and testing procedures.
2/9/10 – 2/11/10	DOE Annual Review Meeting	Adam Schaut	Annual Review meeting with DOE/NREL.
5/18/2011, Golden, CO	CSP Program Award Review	Adam Schaut	Annual Review

11.0 Travel

Date & Destination	Purpose	Participants
3/3/08 Las Vegas, NV	Project technical kickoff meeting and SolarPACES symposium	A. Schaut, M. Kiley, D.J. Spinella, J. Cobes, D. Smith, E. Lüpfert (DLR/CSP Services)
4/22-24/08 Austin, TX	DOE annual solar meeting	A. Schaut
6/4/08 SNL, Albuquerque, NM	Review team capabilities, competencies, resources; discuss technical approach and status of structural design activities	A. Schaut, M. Kiley, D.J. Spinella
7/17/08 Alcoa Technical Center (ATC)	Tommy Ruekert visit to ATC to review capabilities and assess progress to date	A. Schaut, D. Serafin, M. Kiley, C. Retarides
9/30/08 NREL	Tour NREL and discussed current design and reflective surface status and results	A. Schaut, M. Kiley, D. Serafin
6/29/09 Alexandria Extrusion Alexandria, MN	Visit Alexandria Extrusion to observe extrusion of BOWS	Bob Speer
10/1/09 - 10/2/09 NREL Golden, CO	Visit NREL to discuss reflective surface analysis results, testing procedures, assembly procedures and mounting details.	Philip Smith, Philip Gacka
1/25/10 – 1/29/10 NREL Golden, CO	Visit NREL to assemble Alcoa's prototype trough and mount to NREL's 2 axis tracker	Bob Speer, Philip Smith
2/1/10 – 2/5/10 NREL Golden, CO	Visit NREL to install strain gages to 2 axis tracker and conduct wind load test.	Sean Kelly, Pete Vranka, Philip Smith
2/8/10 – 2/11/10 NREL Golden, CO	Visit NREL to conduct wind load tests.	Philip Smith
2/9/10 – 2/11/10 Sandia National Labs Albuquerque, NM	DOE annual review meeting	Adam Schaut
3/15/10 – 3/19/10 NREL Golden, CO	Visit NREL to discuss project validation status and results	Adam Schaut, D.J. Spinella
4/26/10 – 4/30/10 NREL Golden, CO	Visit NREL to conduct wind load tests	Sean Kelly, Pete Vranka
5/18/2011 Golden, CO	CSP Program Award Review – Annual Reveiw	Adam Schaut
11/10/2010 – 11/15/10 Golden, Co and Albuquerque, NM	Coordinate transfer of solar trough from NREL to Sandia NL.	Philip Smith

12.0 Major Task Schedule

Task Number	Task Description	Task Completion Date				Progress Notes
		Original Planned	Revised Planned	Actual	Percent Complete	
1.1	Reflector surface optimization	11/6/08	11/6/08	11/6/08	80%	Optimization work to continue in Phase II as per Task 2.1
1.2	System ideation/ structural development	5/19/08	6/1/08	6/1/08	100%	
1.3	Down-select preliminary concepts	8/8/08	8/29/08	8/29/08	100%	
1.4	Develop Phase II plan	11/13/08	11/13/08	11/13/08	100%	
1.5	Phase I prep and review with DOE	11/20-26/08	11/20-26/08	11/20-26/08	100%	Go/No Go meeting scheduled for December 3rd at the Alcoa Technical Center
2.1	Reflective Surface Optimization	8/6/09	8/5/09	8/5/09	100%	The durable top-coat utilized in Alcoa's thin film and silver film development surfaces is still being tested internally and by NREL. Top coat has potential applications on future solar/CSP applications. Commercially available reflective surface utilized on trough prototype.
2.2	Detail System Design	4/15/09	5/20/09	5/20/09	100%	GEN-2 design activities and FEA model correlation will continue throughout Phase II.
2.3	Internal Critical Design Review	4/20/09	5/15/09	5/20/09	100%	Completed 5/20/09
2.4	Prototype Build	10/8/09	11/5/09	11/20/09	100%	Final assembly complete
2.5	System Validation	11/06/09	3/12/10	4/30/10	100%	V-shot, Distant Observer, IAM, Optical Efficiency and Wind Load testing complete at NREL
2.6	Update Phase III Plan	3/16/10	4/16/10	4/30/10	100%	Phase III plan updated
2.7	Phase II Prep and Review with DOE	3/25/10	4/27/10	5/18/10	100%	Held at the Alcoa Technical Center (ATC)
3.1	Phase III Update Design To Incorporate	7/13/10	10/13/10	10/13/10	100%	GEN-2 design updated based on Phase II wind

	Phase II Lessons Learned					load tests. GEN-3 design created based Phase II overall learning's and a high-level MFG/transportation study.
3.2	Finalize Pre-Production Build Plan	8/24/10	10/31/11	10/31/11	100%	High-level plan created. Detailed validation plan premature given need for further technology validation prior to commercialization of Wing Box trough
3.3	Finalize Pre-Production Field Validation Plan	8/31/10	10/31/11	10/31/11	100%	Test loop validation options identified and assessed.
3.4	Internal Critical Design Review	9/7/10	10/15/11	10/15/11	100%	Decision made to not pursue test loop validation program at this point in time given several economic and market conditions
3.5	Final Reporting	3/22/11	12/31/11	12/31/11	100%	
3.6	Phase III Review with DOE	3/29/11	Upon Request	Upon Request	100%	

13.0-A Final Spending Summary*

Calendar Quarter	Year	A. Federal Share Initial Plan	B. Federal Share Updated Actuals & Plan	Cumulative Federal Share	C. Recipient Share Initial Plan	D. Recipient Share Updated Actuals & Plan	Cumulative Recipient Share
Q1	2008	$102,288	$0	$0	$44,889	0	$0
Q2	2008	$145,889	$229,601	$229,601	$64,028	98,974	$98,974
Q3	2008	$122,016	$163,721	$393,322	$53,546	70,904	$169,878
Q4	2008	$36,170	$0	$393,322	$15,925	238,634	$408,512
Q1	2009	$248,210	$349,561	$742,883	$113,718	149,786	$558,298
Q2	2009	$135,922	$304,329	$1,047,212	$62,273	128,205	$686,503
Q3	2009	$184,369	$366,628	$1,413,840	$84,469	156,002	$842,506
Q4	2009	$496,064	$334,697	$1,748,537	$227,272	143,886	$986,392
Q1	2010	$203,292	$30,358	$1,778,895	$93,138	288,778	$1,275,170
Q2	2010	$267,423	$14,235	$1,793,130	$231,676	94,209	$1,369,379
Q3	2010	$199,096	$35,303	$1,828,433	$263,918	46,361	$1,415,740
Q4	2010	$110,966	$51,461	$1,879,894	$147,094	$67,996	$1,483,736
Q1	2011	$118,619	$19,036	$1,898,930	$157,239	$24,988	$1,508,724
Q2	2011	$37,017	$12,935	$1,911,865	$95,709	$17,004	$1,525,728
Q3	2011	$0	$17,945	$1,929,810	$0	$23,776	$1,549,505
Q4**	2011	$0	$13,201	$1,943,011	$0	$17,392	$1,566,897
Q1***	2012	$0	$25,975	$1,968,986	$0	$34,618	$1,601,515
Q2	2012	$0	$0	$1,968,986	$0	$0	$1,601,515
Q3	2012	$0	$0	$1,968,986	$0	$0	$1,601,515
Q4	2012	$0	$0	$1,968,986	$0	$0	$1,601,515
Totals		**$2,407,340**	**$1,968,986**	$1,968,986	**$1,654,895**	**$1,601,515**	$1,601,515

*As of November, 2011
** Includes estimated December costs
*** Estimated Q1, 2012 and includes shipment of trough to ATC
Note: An estimated $438,354 allocated for Federal Share Phase III and an estimated $545,000 allocated for Recipient Share Phase III will not be spent

13.0-B Final Spending Summary – SF424*

Object Class Categories Per SF 424a	Approved Phases I, II & III	Project Expenditures Cumulative to Date (Phases I, II & III)
a. Personnel & Fringe Benefits	$1,992,458	$1,985,823
b. Travel	$113,420	$35,100
c. Equipment	$0	$0
d. Supplies	$44,421	$80,943
e. Contractual	$256,337	$245,109
f. Construction	$0	$0
g. Other (shipping)	$2,000	$7,442
h. Total Direct Charges (sum of a to h)	$2,408,636	$2,354,417
i. Indirect Charges	$1,653,599	$1,185,351
j. Totals (sum of i and j)	**$4,062,235**	$3,539,768
DOE Cost Share	$2,407,340	$1,950,723
ALCOA Cost Share	$1,654,895	$1,592,046
ALCOA Calculated Cost Share Percentage	40.74%	44.98%

*As of December, 2011

14.0 Cost Share Contributions – Phase I, II and III*

Funding Source	Approved Cost Share (In-kind)	This Quarter - Oct-Dec 2011 (In-kind)	Cumulative to Date (In-kind)
ALCOA Phase I	$178,388	$0	$408,512
ALCOA Phase 2	$628,940	$0	$922,530
ALCOA Phase 3	$847,567	$27,788	$273,694
Total	$1,654,895		
		Phase I ALCOA Cost Share Contributions	$408,512
		Phase 2 ALCOA Cost Share Contributions	$922,530
		Phase 3 ALCOA Cost Share Contributions	$273,694

*As of December, 2011

15.0 Appendixes

Appendix A: Statement of Project Objectives (SOPO)

STATEMENT OF PROJECT OBJECTIVES (SOPO)

Alcoa Inc.

Reflector Technology Development and System Design for
Concentrating Solar Power (CSP) Technologies

A. PROJECT OBJECTIVES

The objective of Alcoa's project is to demonstrate that significant life cycle cost savings and subsequent levelized cost of energy (LCOE) reduction are achievable through the design optimization of aluminum-intensive collectors (supporting structure and reflector).

B. PROJECT SCOPE

To support DOE Solar Energy Technologies Program (SETP) goals of lowering the cost of major trough system components and establishing U.S.-based manufacturing capabilities for these components, Alcoa proposes to develop an aluminum-intensive collector (supporting structure and reflector) that will provide a superior (lower) total life cycle cost of energy compared to current baseline collectors.

Alcoa anticipates that its proposed approach to developing both the reflector and the supporting structure design will result in a 25-50% cost savings for the solar field, which includes the collector assembly but excludes the CSP power plant. This cost savings would result in at least a 20% reduction in the LCOE. The capabilities for mass assembly and production of aluminum-intensive collector components exist in the U.S.; therefore, an additional benefit of an aluminum-intensive collector is its strong potential to substantially and positively impact the U.S. manufacturing base.

C. TASKS TO BE PERFORMED

BUDGET PERIOD 1 (Phase 1: Technical Feasibility Study)

Task 1.1: Reflector Surface Optimization – Phase 1 begins with the preparation and testing of aluminum sheet products that Alcoa believes will provide the necessary reflectivity and durability attributes for use in CSP applications. Technologies to be investigated will include silver metallized lamination and thin film deposition directly onto aluminum sheet. Alcoa will prepare surface coatings; test performance internally per QUV-A/humidity, corrosion, scratch resistance, and visible light reflectivity; and provide samples to the National Renewable Energy Laboratory for full-spectrum reflectivity measurements.

Given the short duration of Phase 1 (9 months) and the time required to prove durability performance, even under accelerated conditions, Alcoa will report reflectivity at $t = 0$ and the latest durability results as of the completion of Phase 1. Alcoa will use the following reflectance and durability criteria when conducting its internal tests:

- Initial ($t = 0$) hemispherical reflectance is $\geq$93%.
- Initial ($t = 0$) spectral reflectance is $\geq$90% for 25-mrad reading and $\geq$87% for 7-mrad reading.

Task 1.2: System Ideation – This task and its sub-tasks will begin with acquiring or defining the baseline CSP system, specifically EuroTrough. The baseline design information will include the architecture, performance (input and output), and cost. Once the baseline is established, conceptual designs will be generated through ideation sessions with knowledge experts from various industries, manufacturing backgrounds, academic institutions, and research organizations. The output of these ideation sessions will be used to further evaluate and rank preliminary concepts on their estimated cost, weight, and high-level structural performance.

Task 1.3: Down-Select Preliminary Concepts – This task and its sub-tasks involve down-selection of preliminary concepts defined in Task 1.2. Down-selection will occur based on the results of earlier reflector surface coating optimization tasks. Additional down-selection will take place using structural and specular reflectance performance and LCOE estimates. With this information, Alcoa will choose the most promising preliminary concepts for consideration in Phase 2.

Task 1.4: Develop Phase 2 Plan – This task and its sub-tasks will be utilized to develop a refined Phase 2 plan based on the down-selected concept from Task 1.3. Given knowledge of the down-selected design, including specific alloys and product forms, Alcoa will present the DOE SETP with a final Phase 1 report and refined plan for Phase 2 activities, which will include the statement of work, work breakdown structure, and costs. The refined Phase 2 plan will reflect any necessary changes to specific tasks and their duration and the labor, material, and subcontracting required to complete the phase.

CRITICAL MILESTONE (GO/NO-GO DECISION)

Task 1.5: Phase 1 Prep & Review with DOE **(9 months from project start) –** As a final deliverable to Phase 1, Alcoa will provide the DOE SETP with a comprehensive design/analysis report that presents reflector surface coating performance test results, baseline design and performance requirements, preliminary conceptual designs, initial modeling results, and estimated costs for the down-selected preliminary concepts. This report will enable the DOE SETP to evaluate the feasibility of the down-selected aluminum-intensive collector concepts, assess the benefits of continued technology design and prototype development, and make an informed go/no-go decision for Phase 2.

BUDGET PERIOD 2 (Phase 2: Design and Prototype Development)

Task 2.1: Detail System Design – In this task and its sub-tasks, Alcoa will perform the detailed design (3D CAD) and structural analysis (finite element analysis or FEA), detailed cost modeling of the prototype and production process, and manufacturability assessments. These tasks will serve to fully optimize the prototype design and prepare for prototype build later in the phase. Using the resultant optimized design, Alcoa will finalize an assembly strategy, prototype build plan, and testing plan.

Task 2.2: Internal Critical Design Review – This task highlights an internal Alcoa milestone to review all the critical design information before officially releasing the design for prototyping.

Task 2.3: Prototype Build – This task and its sub-tasks outline the manufacture of a full-scale collector prototype including the application of the optimized reflective and durable coating. This task includes releasing the prototype drawings, fabricating necessary tooling and fixtures, procuring materials and off-the-shelf components, fabricating system components, applying the reflective surface and durable coating, and assembling the final prototype system.

Task 2.4: System Validation – This task and its sub-tasks will focus on validating the completed prototype as defined in the previously developed test plan. Validation will be completed by:

- measuring dimensional accuracy of the final prototype assembly,
- documenting variations in assembly cost when compared to the build plan,
- measuring specular reflectance, and
- simulating static and dynamic loading conditions.

Task 2.5: Develop Phase 3 Plan – In this task and its sub-tasks, Alcoa will incorporate all validation results into its final Phase 2 report to the DOE SETP. Included with the report will be Alcoa's proposed commercialization roadmap for the collector (supporting structure, reflector, and reflective surface technology), which will outline Alcoa's plan to commercialize its aluminum-intensive collector by 2020 with the required low-cost power generation and storage requirements set by the DOE SETP. Refined plans for Phase 3 activities also will be presented for discussion with the DOE SETP.

CRITICAL MILESTONE (GO/NO-GO DECISION)

Task 2.6: Phase 2 Prep & Review with DOE **(24 months from project start) –** The final deliverable in Phase 2 will be an Alcoa-generated report that contains detailed technical and cost data on design, prototype construction, and prototype evaluation; high-level manufacturing estimates for production; and a preliminary commercialization roadmap to demonstrate the concept's impact on CSP system cost and LCOE. The Phase 2 report will enable the DOE SETP to make an informed go/no-go decision for the field validation planning in Phase 3.

BUDGET PERIOD 3 (Phase 3 – Field Validation Plan)

Phase 3 consists of five major tasks and a final project review with the DOE. Specific deliverables and task descriptions are highly dependent upon the resultant system design of Phase 1 and the performance results of the prototype design in Phase 2. The high-level SOPO is included below; however, this will require updating before Phase 3 award.

Task 3.1: Update Design To Incorporate Phase 2 Lessons Learned – This task and its sub-tasks focus on integrating Phase 2 results into an updated production-level system design. Detailed 3D design, FEA verification, manufacturing assessments, and detailed cost modeling will be performed. An updated

manufacturing plan for full-scale production of the system will be generated based on consultation with potential manufacturing partners and subsequent selection of a manufacturing site.

Task 3.2: Finalize Pre-Production Build Plan – This task involves the continued refinement and update of the pre-production build plan, with a specific focus on determining the best locations and most appropriate partners for fabrication, assembly, and installation of the full-scale validation system.

Task 3.3: Finalize Pre-Production Field Validation Plan – This task includes the continued refinement and update of the full-scale test plan, with a specific focus on determining the best location and most appropriate solar power partner from the southwestern area of the U.S. to conduct field validation of the pre-production system.

Task 3.4: Internal Critical Design Review – This task highlights an internal Alcoa milestone to review all the critical design and commercialization information with Alcoa management.

Task 3.5: Final Reporting – Upon completion of Phase 3 tasks, Alcoa will deliver a report to the DOE detailing all aspects (rationale, size, location, U.S. suppliers, etc.) of limited-scale production and field validation to ensure the concept's improved design will perform reliably in a realistic operating environment and to accurately predict future costs and operating characteristics. As part of this report, Alcoa also will present a final technology commercialization roadmap to assist the DOE as it explores next steps for an aluminum-intensive collector in a CSP system for the future.

Task 3.6: Phase 3 Review with DOE – As the final milestone for this project, a final report detailing outcomes and next steps will be presented to the DOE.

Appendix B: Torsional Stiffness Data Presented by Solargenix

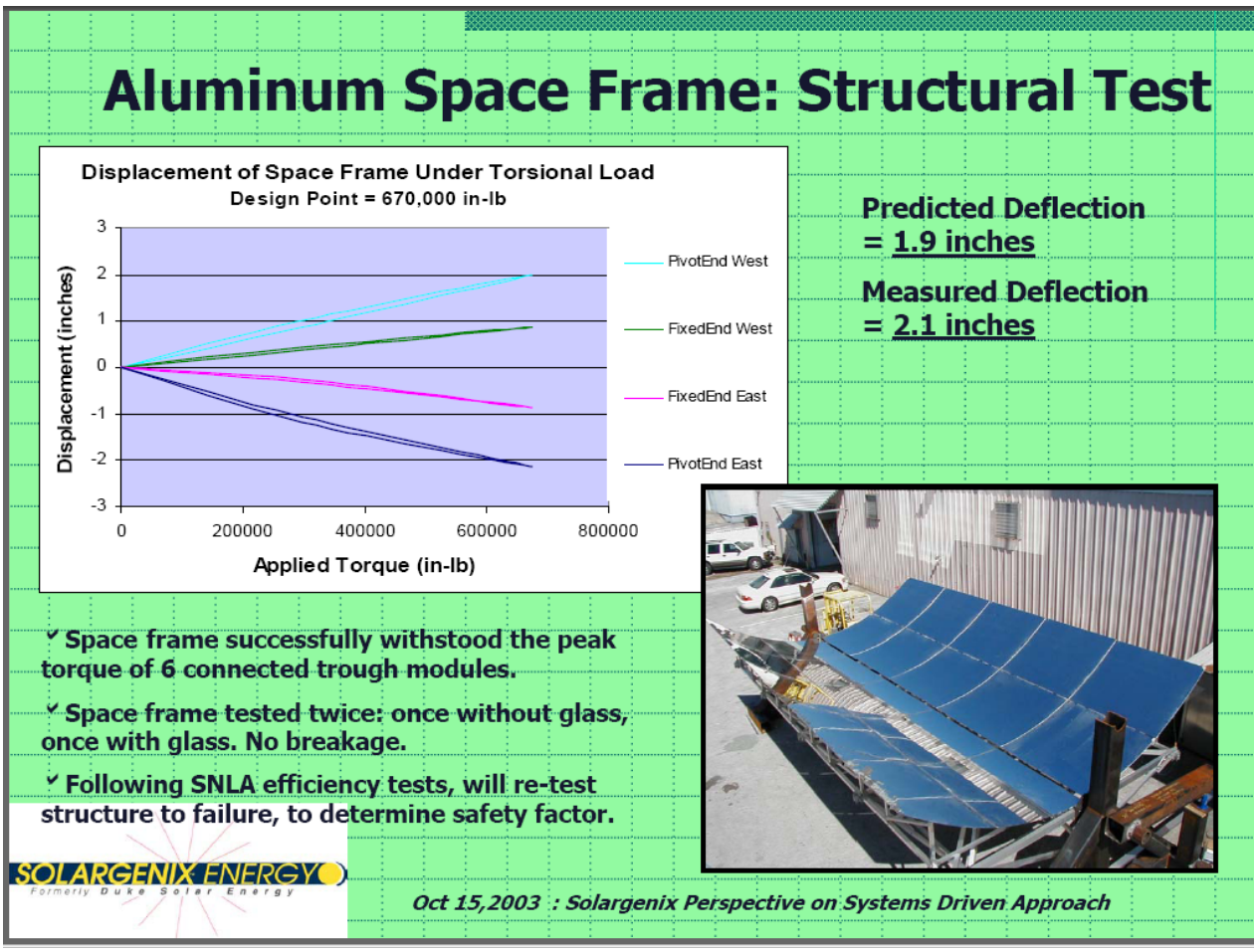

Figure B-1: Torsional Stiffness Data Presented by Solargenix

Appendix C: CSP Services Analysis Report

CSP Services GmbH, Köln, Germany

CSPS Technology Report

– Approved for Public Release –

Client: Alcoa –
Alcoa Technical Center, PA, USA

Shape Analysis 05001852
Cases 016, 017 and 018

---

1. Case 016 high resolution (1G Zenith no wind)

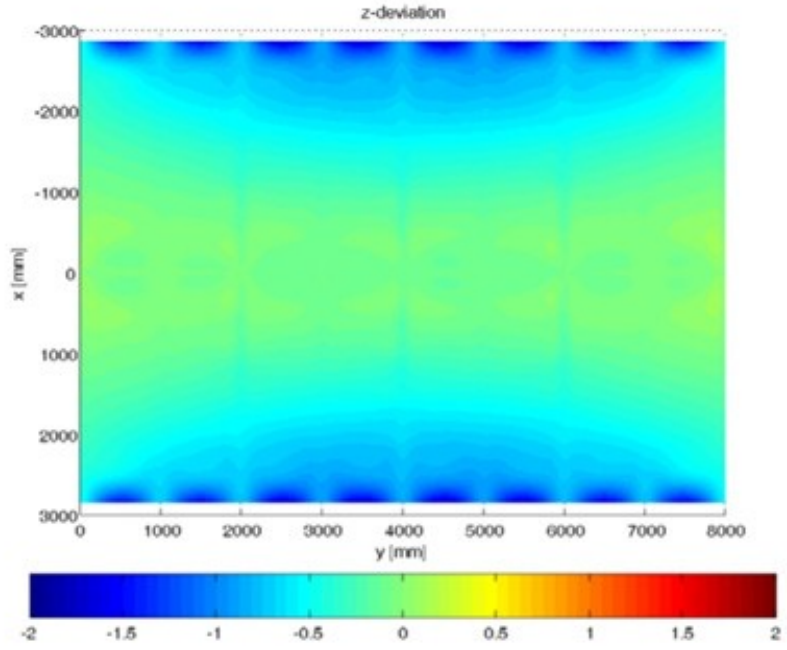

Figure C-1. Height deviation of reflector

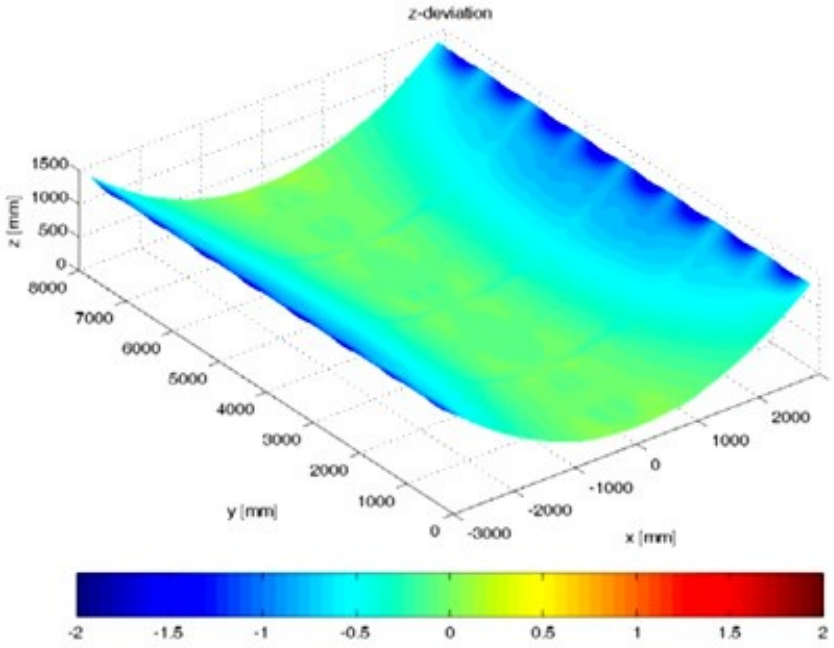

Figure: C-2. Height deviation, 3-D view

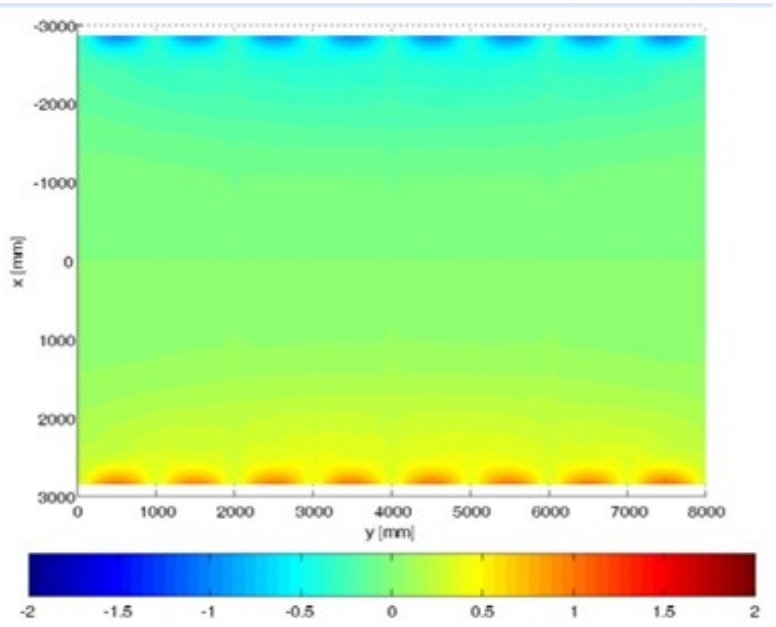

Figure: C-3: Width deviation of reflector

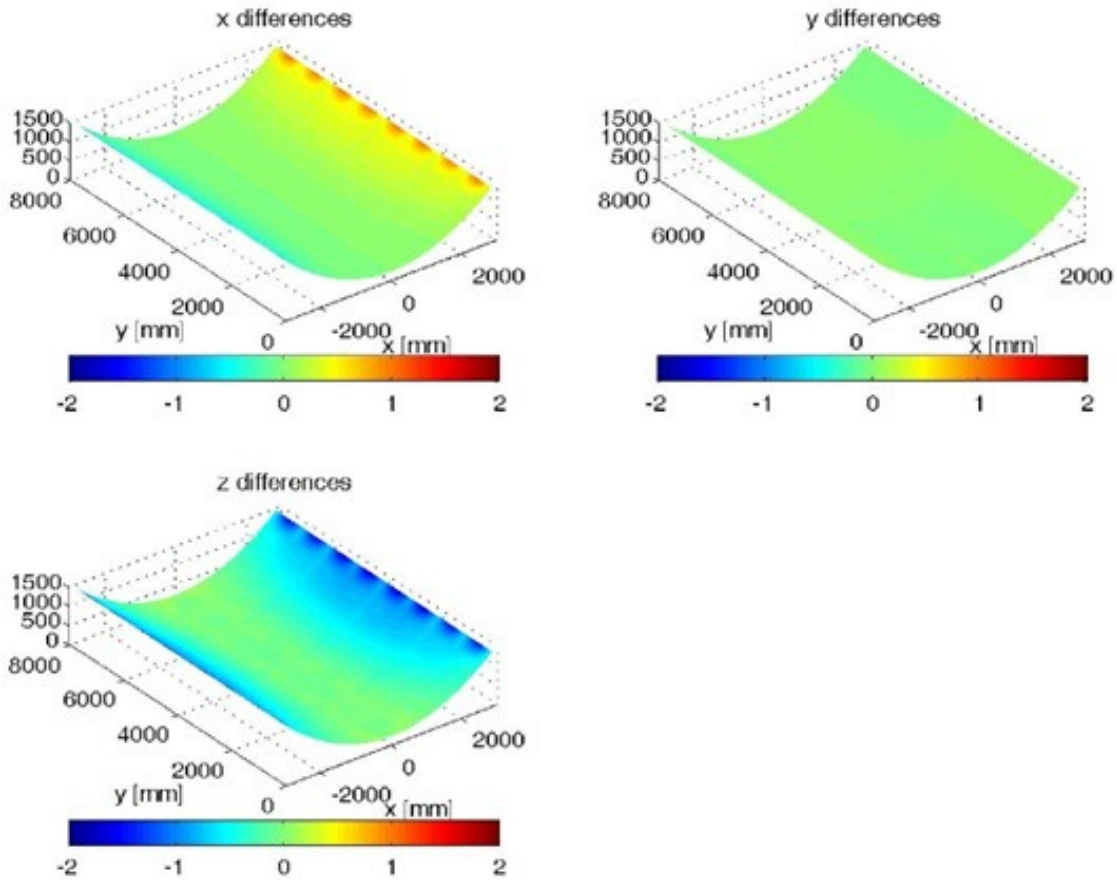

Figure: C-4: Deformation summary sheet

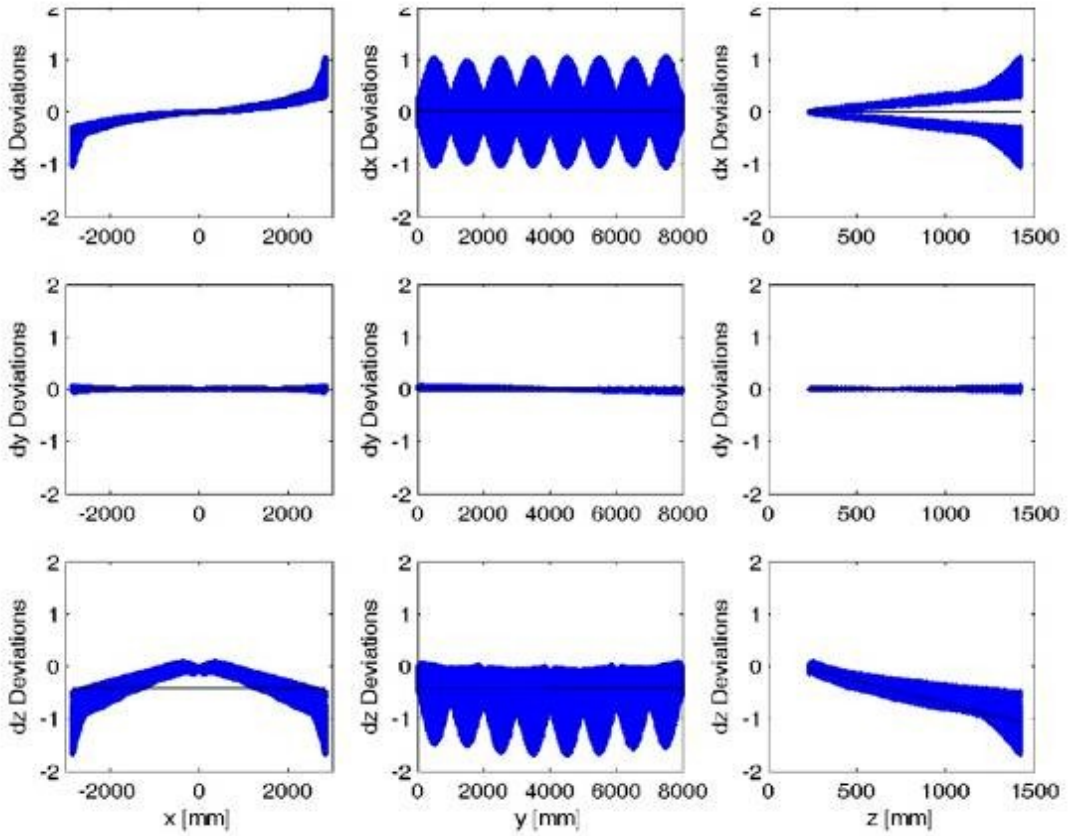

Figure: C-5: Shape deformation analysis sheet

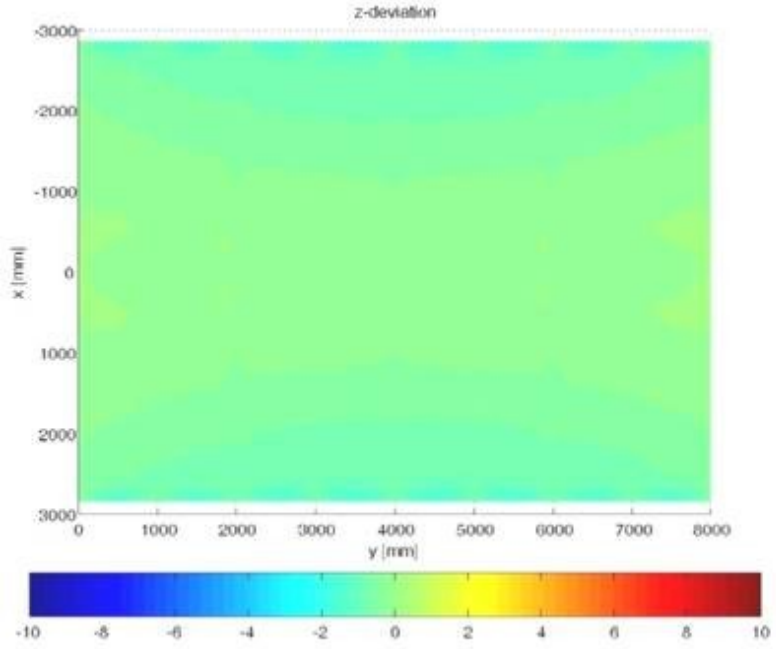

Figure: C-6: Height deviation of reflector

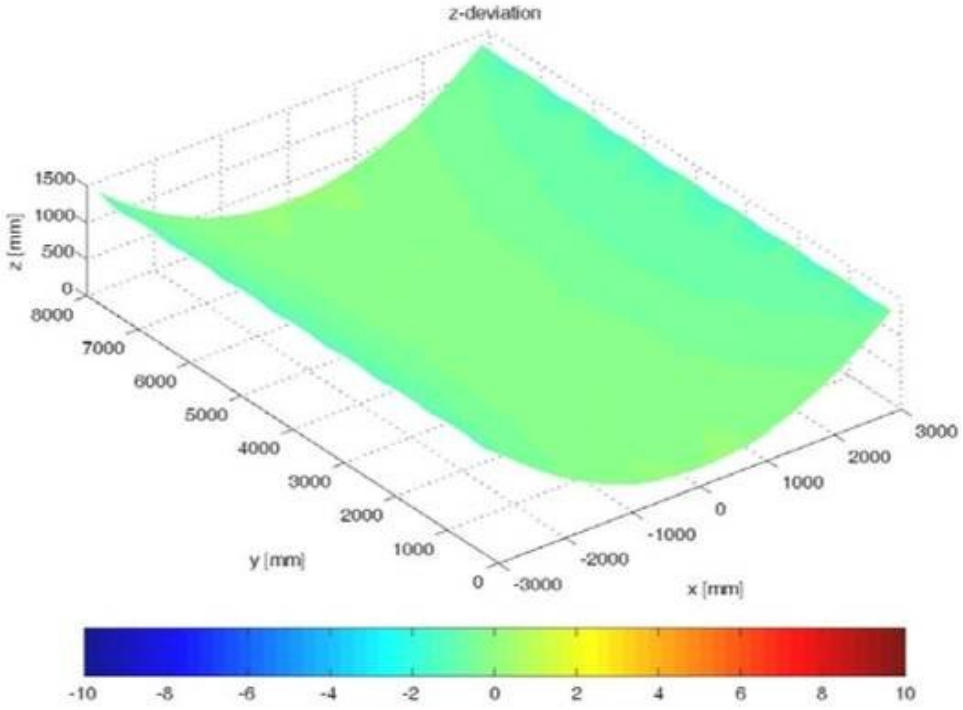

Figure: C-7: Height deviation, 3-D view

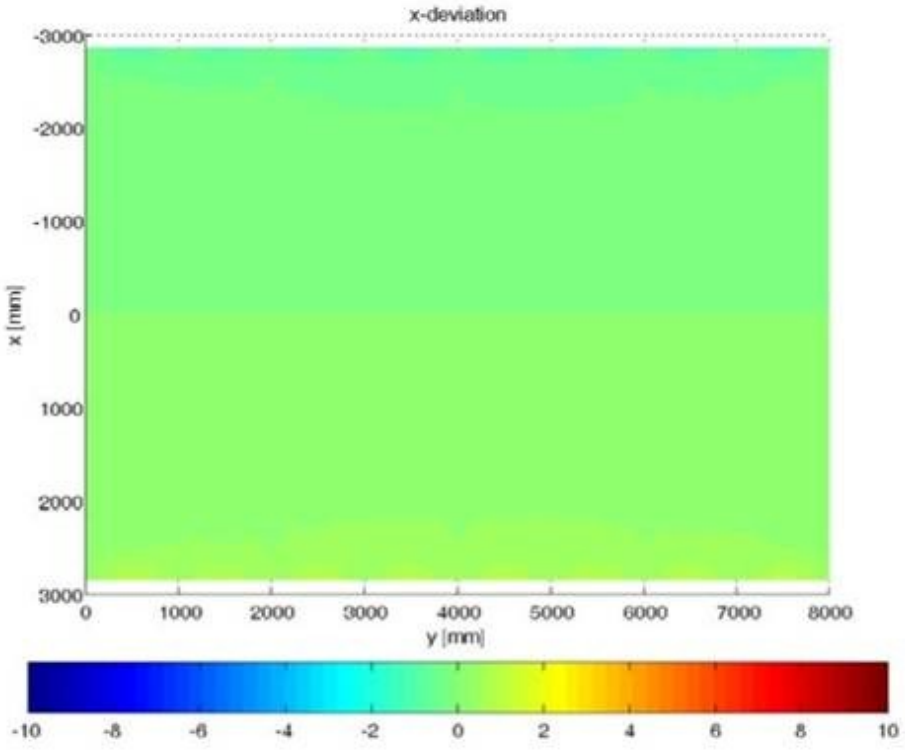

Figure: C-8: Width deviation of reflector

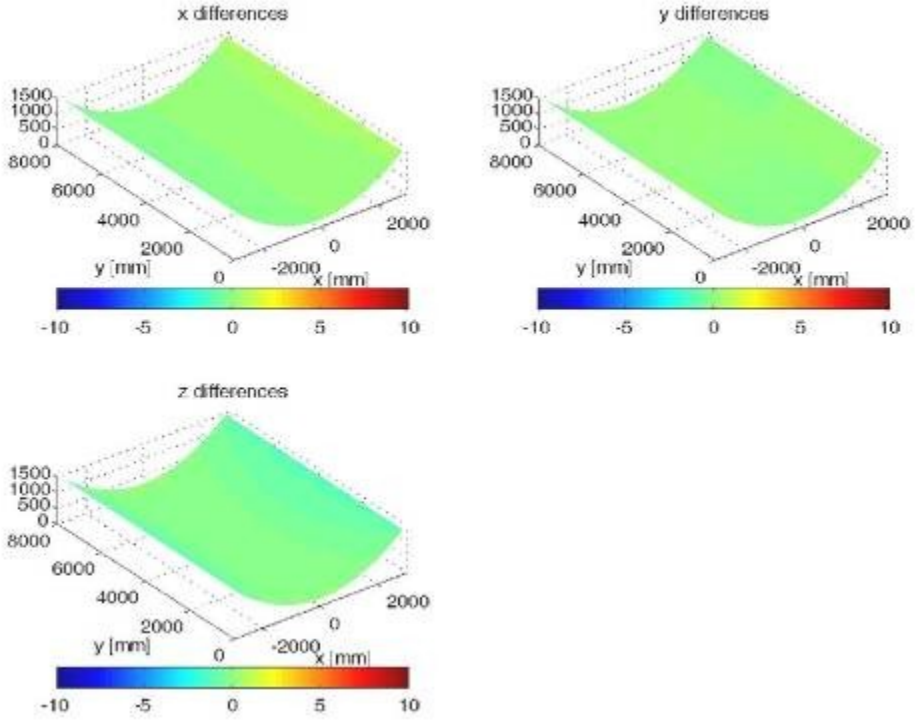

Figure: C-9: Deformation summary sheet

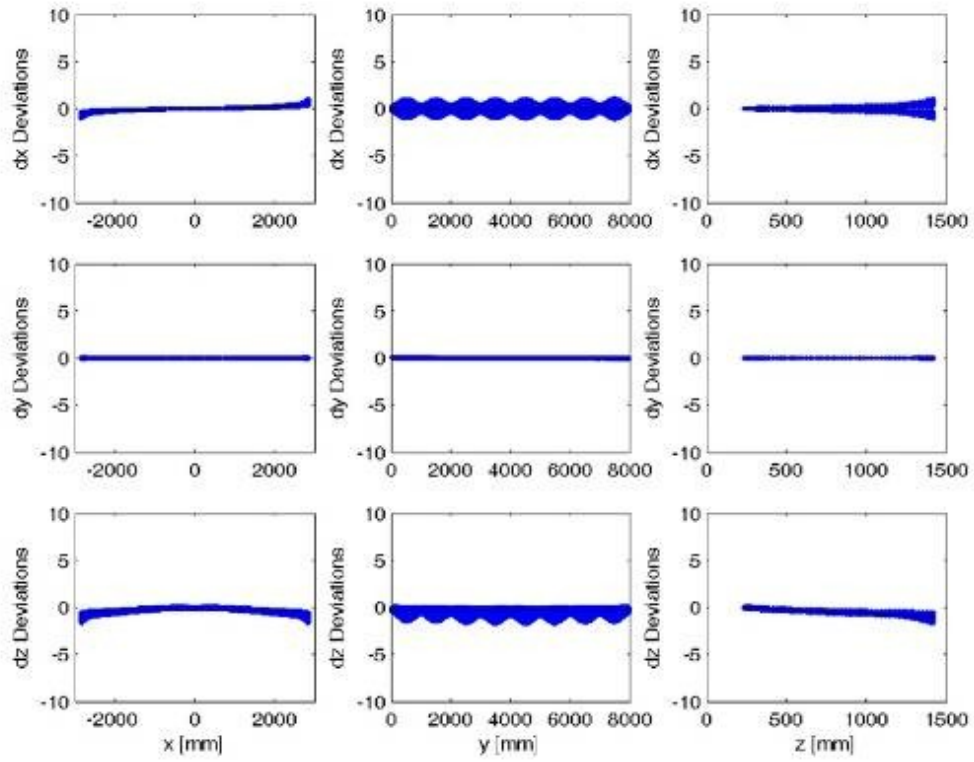

Figure: C-10: Shape deformation analysis sheet

1.2. Observations

The graphs in Figures 1 and 2 show the principal behavior of the reflector shape in height of the parabola. The detailed analysis is made on the basis of Figure 5, which gives the absolute shape deviations in all three coordinate directions along all three axes. Such graphs can be used to analyze in particular systematic effects for the deflection analysis.

There is a noticeable effect of widening of the parabolic shape with reference to the ideal original shape. This widening, or sagging, occurs on the outer rim of the parabola, and between each of the supporting ribs. However the maximum sag is of less than 1 mm. There is an overall widening effect of the parabola supporting structure, whose effect is of less than half a millimeter.

The resulting shape deviations of the mirror surface are of less than 0.5 mrad for the supporting structure, and of little more than 1 mrad as peak value on the outer edges of the reflector sheet between the supporting structural elements.

Shape deviation along the collector axis is negligibly low.

This kind of shape deviation under load seems very low. Maximum reflector shape deviations of about 1 mrad on the outer rim of the reflector have an effect of shift of the focal area of about 6 mm, which is low in comparison to the absorber tube radius of 35 mm. In particular the stiffness along the x axis (collector axis) can be further reduced with the objective to save material. A sagging of the overall structure of a few millimeters can be allowed without important performance loss for the concentrating solar collector, but material use (figures are not provided for this analysis) is to be minimized in order to keep production cost low.

2. Case 017 (case 4 B3, 1G 60°, 30 mph wind)

Modeling conditions (Alcoa): pitch angle of 60 degrees above the horizontal (case 4, configuration B3, exterior collector without protective fence – largest negative Z force, largest resultant X and Z force). Mean wind speed of 30 mph at the collector pivot. The result is a total loading of approximately 2.88G at a vector of -0.96 Z and -0.27Y in my FEA model coordinates.

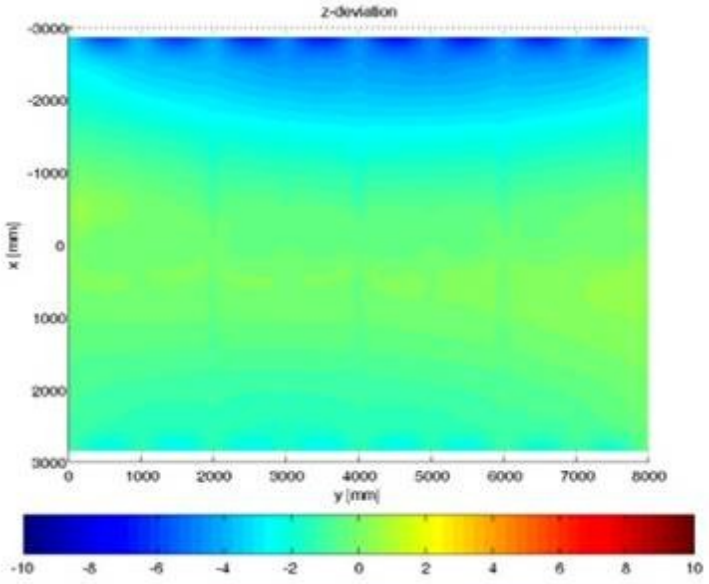

Figure: C-11: height deviation of reflector

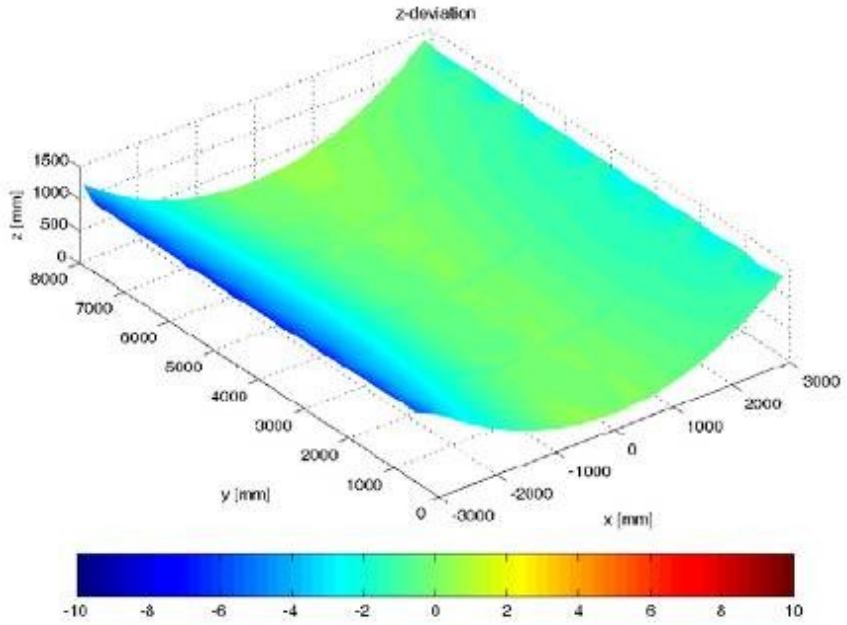

Figure: C-12: Height deviation, 3-D view

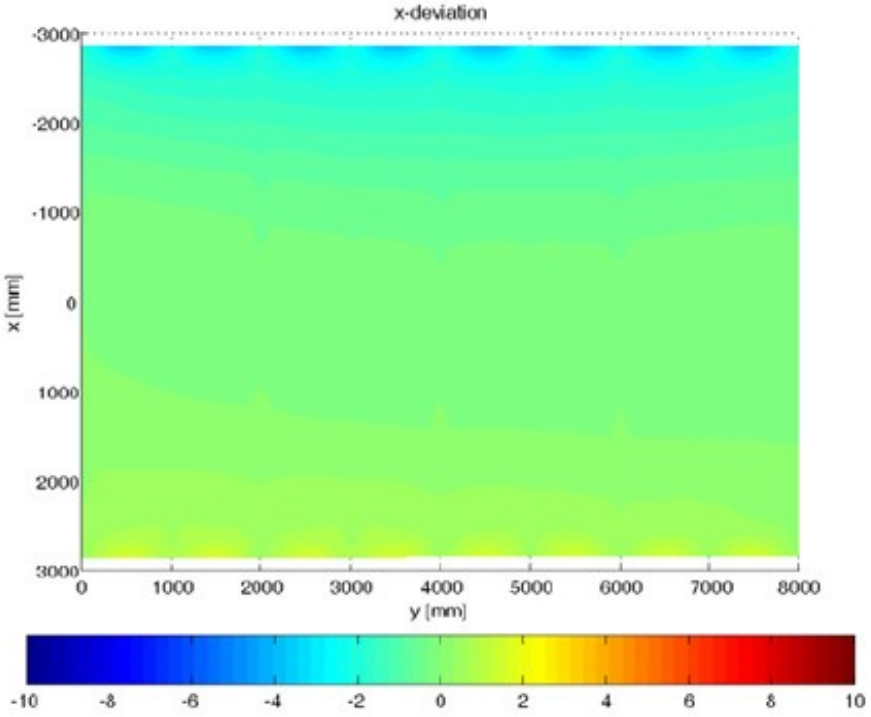

Figure: C-13. Width deviation of reflector

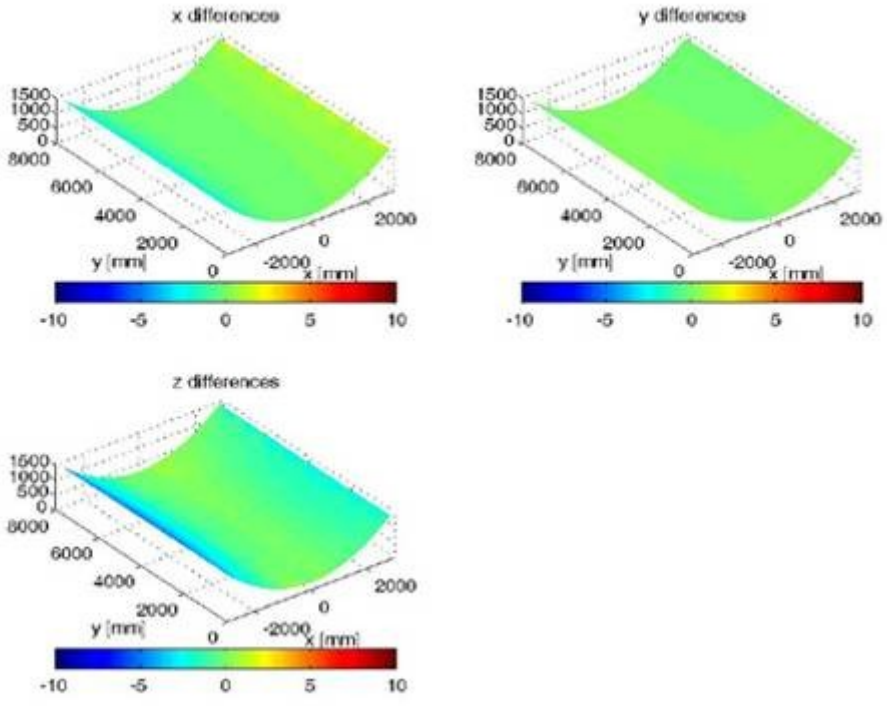

Figure: C-14: Deformation summary sheet

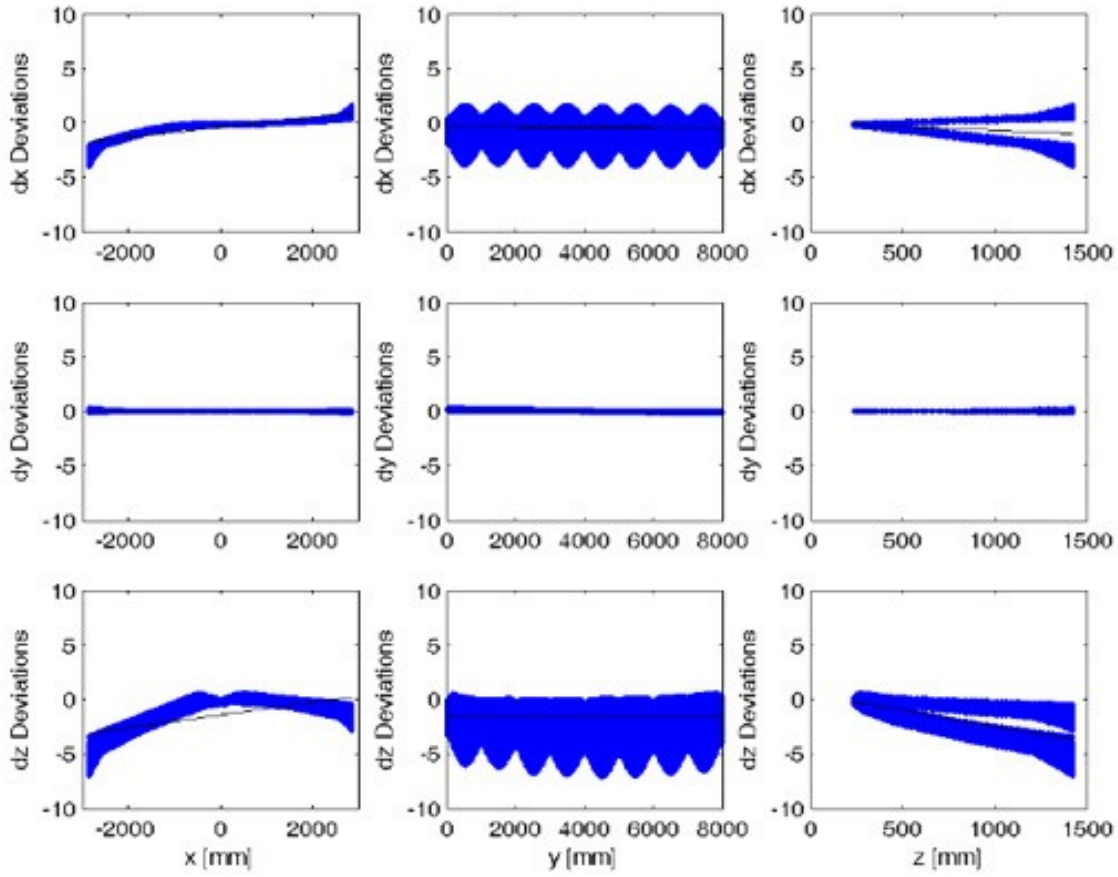

Figure: C-15: Shape deformation analysis sheet

2.1 Observations

This load case is characterized by the asymmetric load on the upper rim of the trough. The maximum deviation is 7 mm. The slope deviation of the “upper” part of the collector is 2 mrad, on the rim slightly more. This is an uncritical deformation of the module. The module is not twisted (probably due to the load case). The bending of the structure is negligible.

3. Case 018 (case 1 B3, 1G Horizon, 30 mph wind)

Modeling conditions (Alcoa): pitch angle of 0 degrees above the horizontal (case 1, configuration B3, exterior collector without protective fence – largest Horizontal force. Mean wind speed of 30 mph at the collector pivot. The result is a total loading of approximately 2G at a vector of -0.864 Z and -0.502 Y in FEA model coordinates

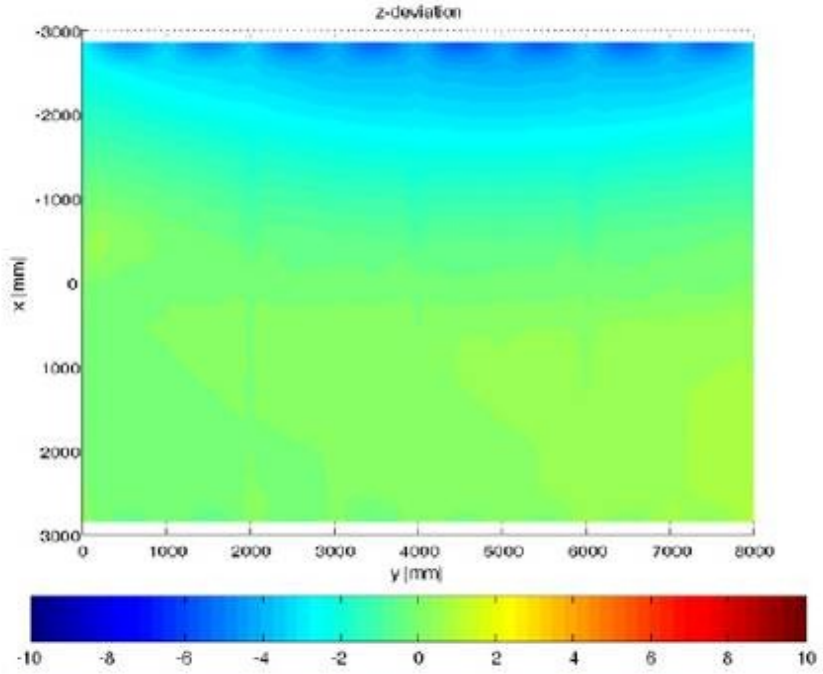

Figure: C-16: height deviation of reflector

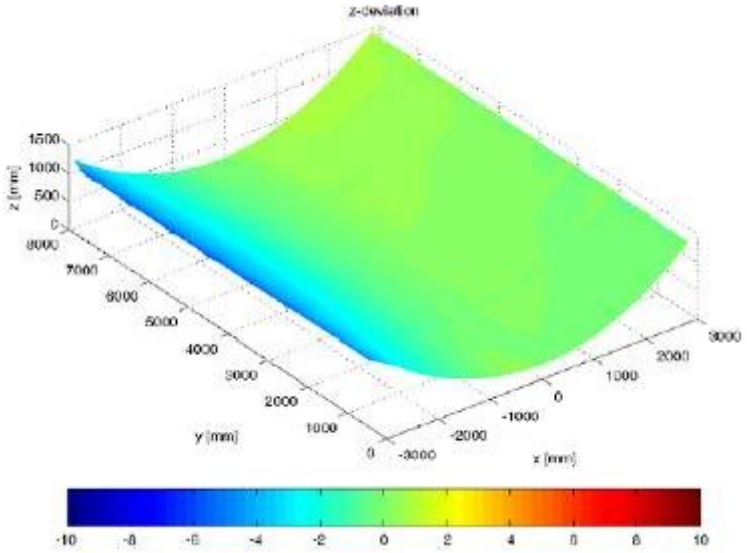

Figure: C-17: Height deviation, 3-D view

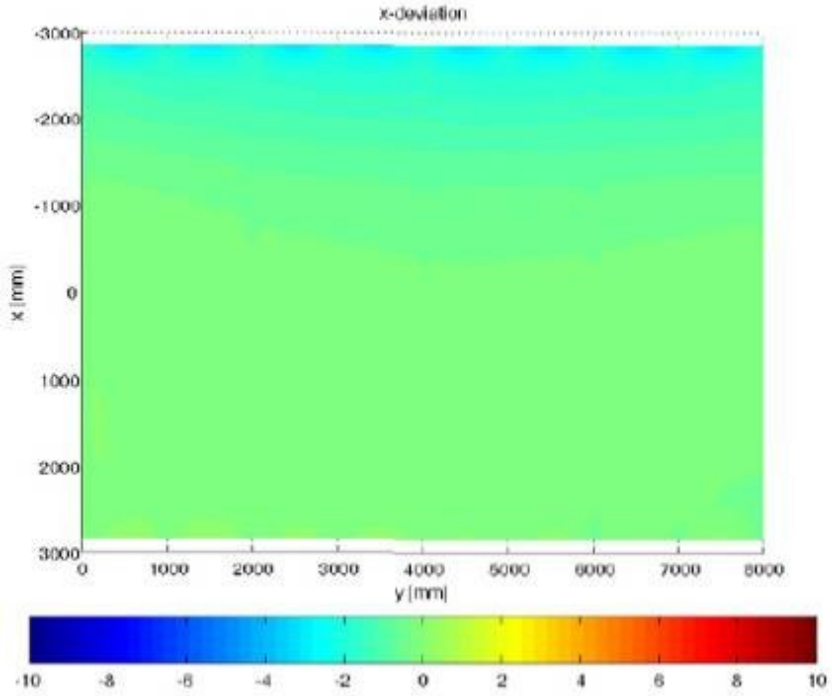

Figure: C-18: Width deviation of reflector

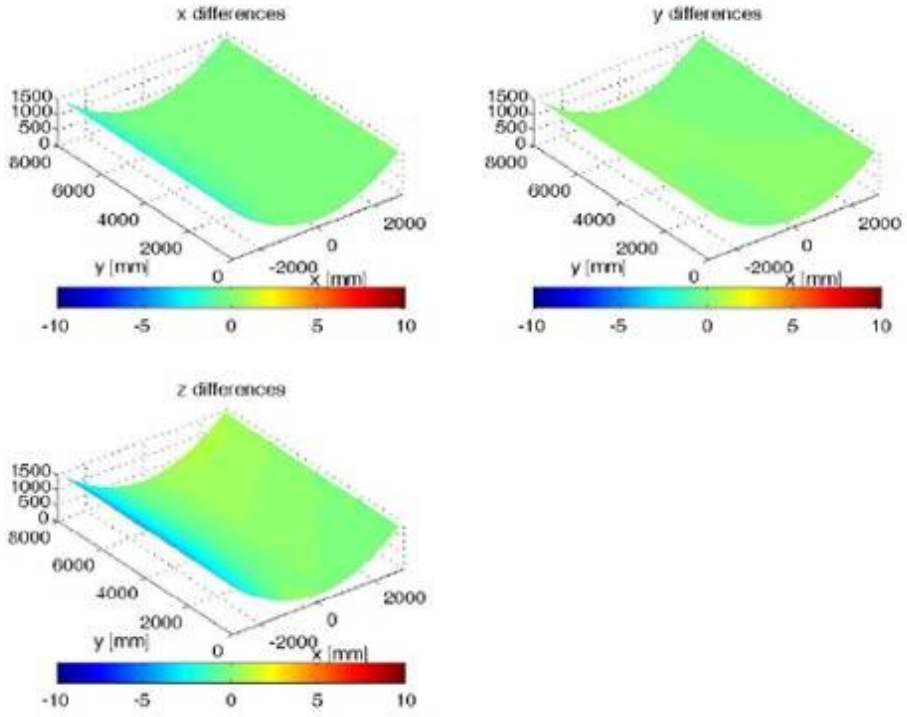

Figure: C-19: Deformation summary sheet

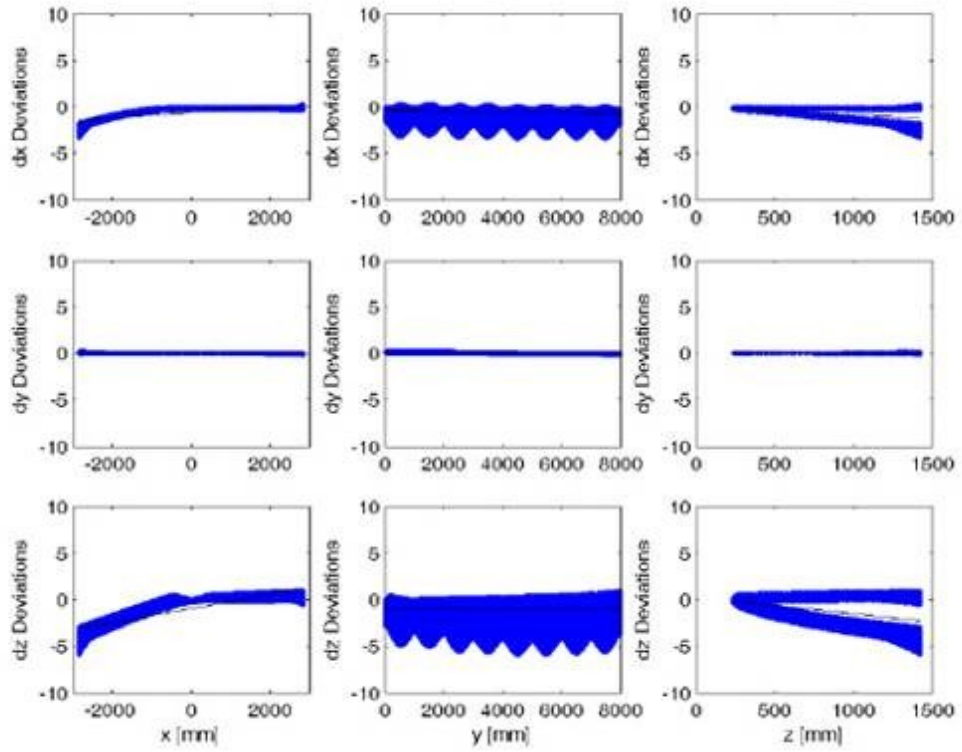

Figure: C-20: shape deformation analysis sheet

3.1. Observations

This load case is characterized by the asymmetric load on the upper rim of the trough. The maximum deviation is 5 mm. The slope deviation of the "upper" part of the collector is 1.5 mrad, on the rim slightly more. This is an uncritical deformation of the module. The module is not twisted (probably due to the load case). There is no bending of the structure in this load case.

4. Evaluation of the results

For the analysis of the collector, three load cases on a single module are available. These are in zenith angle (90°) without wind, and at pitches of 60° and 0° (horizontal) with a wind speed of 30 mph (14 m/s). Load induced deformation coordinates of the reflector from the design surface have been submitted by Alcoa to CSPS. The deformations are displayed in various views to enable interpretation of the data.

The graphs show the composition of the reflector surface of 8 stripes, which are obviously not in a stiff connection, but only supported on kind of ribs. The substructure seems to withstand the

loads from dead weight as well as the 14 m/s wind with only minor deformations, up to 7 mm on the outer rim of the mirror support ribs, and negligible bending of the total structure.

Only one collector module is modeled. No twist of the collector is noticed. This might be due to the modeled load case or due to a stiff substructure. In the given data, the possible losses in intercept factor on a 70 mm diameter absorber tube are very low. Details of the intercept factor have not been modeled.

The three data sets include typical operating conditions for a concentrating collector and thus probably allow a first estimate of the load dependent influence on optical performance of the collector. From the available information there is almost no influence on the optical performance. This is unusual for such load cases for concentrating collectors and should lead to questions regarding the load assumptions and regarding the designed stiffness of the collector module. If stiffness is as expected from the data, a further reduction of the material use for the design might be considered. However in most designs it is not the operating performance at 14 m/s that determines the structural design requirements, but the maximum wind load case of the stowed collectors such as for a 50 years wind gust.

Appendix D: CSP GEN-1 Test Plan

Team Members:
Bob Speer – ATC Team Lead
Philip Gacka – ATC
D.J. Spinella - ATC
Sean Kelly - ATC
Philip Smith - ATC
Adam Schaut – ATC
Allison Gray – NREL
Keith Gawlik – NREL

Date of Original Plan: July 12, 2009
Date of Revision 1: July 17, 2009
Date of Revision 2: July 22, 2009
Date of Revision 3: November 9, 2009
Date of Revision 4: March 1, 2010
Date of Revision 5: April 29, 2010

The following test plan includes the **ATC Geometric Dimensioning and Tolerance** (GD&T) analysis of individual components, subassemblies and the final testing. The test plan includes the **ATC Static Load Testing** of the final unit to verify the accuracy of the Finite Element Analysis (FEA) used to size the components and analyze the robustness of the design. The test plan also includes:

- Notes from conversations with Allison Gray of NREL regarding her requirements and desires for **V-shot Testing** at the Alcoa Technical Center (ATC).
- Notes from conversations with Allison Gray of NREL regarding her requirements and desires for **V-shot Testing** at the National Renewable Energy Laboratory (NREL) in Colorado.
- Notes from conversations with Keith Gawlik of NREL regarding the **Mounting Details** for the prototype collector onto the 2 axis tracker at NREL, Colorado.
- Notes from conversations with Keith Gawlik of NREL regarding the details regarding **Efficiency Testing – 2 Axis Tracker**.

<u>ATC GD&T Test Plan:</u>

1. Individual Components – The use of check fixtures or a Coordinate Measuring Machine (CMM) will be used to verify the manufacturing accuracy of individual parts.
    a. Extruded bows will be checked using a check fixture at the extrusion facility – 100%
    b. All other individual components will be checked with a CMM – 10%
2. Subassemblies – The use of a CMM or Laser Tracker unit will be used.
    a. Rib subassemblies will be checked with a CMM – 100%
    b. Tube Standoffs subassemblies will be checked with a CMM – 100%
    c. Reflective panel subassemblies – adhesive of panel to bows will be verified with coupon validation – 10%
    d. Half Panel subassemblies will be checked with a laser tracker – possibly 1st half only = 50%. If time permits 2nd half will be tested as well = 100%. Detailed plan to be supplied by Phil Gacka.
3. Final Assembly – The use of the Laser Tracker will be used to verify the accuracy of the final build. Detailed plan to be supplied by Phil Gacka.

ATC Static Load Test Plan:

1. Goal of static load testing is validation of FEA model against prototype
2. Half-collector should be tested before final assembly in order to validate FEA model
    a. Half-collector module must be raised above fixture due to non-removable center blocks
    b. Module should be supported at three points
    c. Once the collector is in a stable position, measure deflection with respect to loading
3. Specifics:
    a. The half-collector will be lifted off the fixture using jacks or engine hoists
    b. Three corners will be fixed to the ground via the fixture (more details coming)
    c. The fourth corner will be allowed to hang free
    d. Indicators will be set up at all four corners and set to zero with only gravity acting on the collector
    e. Several steps of loading and measurement will occur either using a jack with a pancake load sensor or via adding weights
4. A correlation factor between the test results and FEA model will be developed for each load step. The final correlation factor will be the average of these.
5. Full collector testing could occur on pylons – similar technique: add weight, measure response

V-Shot Optical Test:

1. At ATC by Allison Gray of NREL. See telecom notes in appendix.
2. At NREL (Colorado) by Allison Gray of NREL. See telecom notes in appendix.

Mounting Details – 2 Axis Tracker:

1. At NREL (Colorado) by Keith Gawlik of NREL. See telecom notes in appendix.

Efficiency Testing – 2 Axis Tracker:

2. At NREL (Colorado) by Keith Gawlik of NREL. See telecom notes in appendix.

NREL Structural Testing

It was determined that the data gathered from the 'ATC Static Load Test Plan' described above was not sufficient to correlate the collector's structural response with the Finite Element Analysis (FEA) conducted during the design of the collector. As a result, a number of strain gauges were attached to the collector prior to shipment to NREL (Golden, CO) where the collector was to go through field testing. The strain gauges were to be monitored during various wind loading conditions. The data collected would then be added to the database of information in an effort to correlate actual loads and responses with simulated finite element analyses.

Strain Gauge placement:

Measurement Location	Group	Rosette	Gage Element	Orientation	Signal No.
Back Upper Center	1	A	1	L	1
			2	45	2
			3	T	3
		B	1	L	4
			2	45	5
			3	T	6
		C	1	L	7
			2	45	8
			3	T	9
		D	1	L	10
			2	45	11
			3	T	12
Back Lower Center	2	A	1	T	13
			2	45	14
			3	L	15
		B	1	T	16
			2	45	17
			3	L	18
		C	1	T	19
			2	45	20
			3	L	21
		D	1	T	22
			2	45	23
			3	L	24

Back Upper Quarter	3	A	1	L	25
			2	45	26
			3	T	27
		B	1	L	28
			2	45	29
			3	T	30
		C	1	L	31
			2	45	32
			3	T	33
		D	1	L	34
			2	45	35
			3	T	36
Back Upper Center Close-out Panel	4	A	1	T	37
			2	45	38
			3	L	39
		B	1	T	40
			2	45	41
			3	L	42
		C	1	L	43
			2	45	44
			3	T	45
		D	1	L	46
			2	45	47
			3	T	48
Right Upper Outer Spar	5	A	1	T	49
			2	45	50
			3	L	51
		B	1	T	52
			2	45	53
			3	L	54
		C	1	T	55
			2	45	56
			3	L	57
		D	1	T	58
			2	45	59
			3	L	60

Right Upper End Rib Center	6	A	1	T	61
			2	45	62
			3	L	63
		B	1	T	64
			2	45	65
			3	L	66
		C	1	T	67
			2	45	68
			3	L	69
		D	1	T	70
			2	45	71
			3	L	72

Measurement Location	Group	Rosette	Gage Element	Orientation	Signal No.
Right Upper End Rib Edges	7	A	1	T	73
			2	45	74
			3	L	75
		B	1	T	76
			2	45	77
			3	L	78
		C	1	T	79
			2	45	80
			3	L	81
		D	1	T	82
			2	45	83
			3	L	84
Left Upper Middle A-Frames	8	A	1	U	85
			2	M	86
			3	L	87
		B	1	U	88
			2	M	89
			3	L	90
		C	1	U	91
			2	M	92
			3	L	93
		D	1	U	94
			2	M	95
			3	L	96
Orientation Designation: U = Upper Beam, M = Middle Beam, L = Lower Beam on A-Frame Sections					

Measurement Location	Force Direction	Polarity	Signal No
Pedestal and Base	North - South Bending	(+) = North	97
	East - West Bending	(+) = East	98
	Thrust	(+) = Up	99
	Torque	(+) = C-W	100
All Signals Are Full Bridge Configurations			

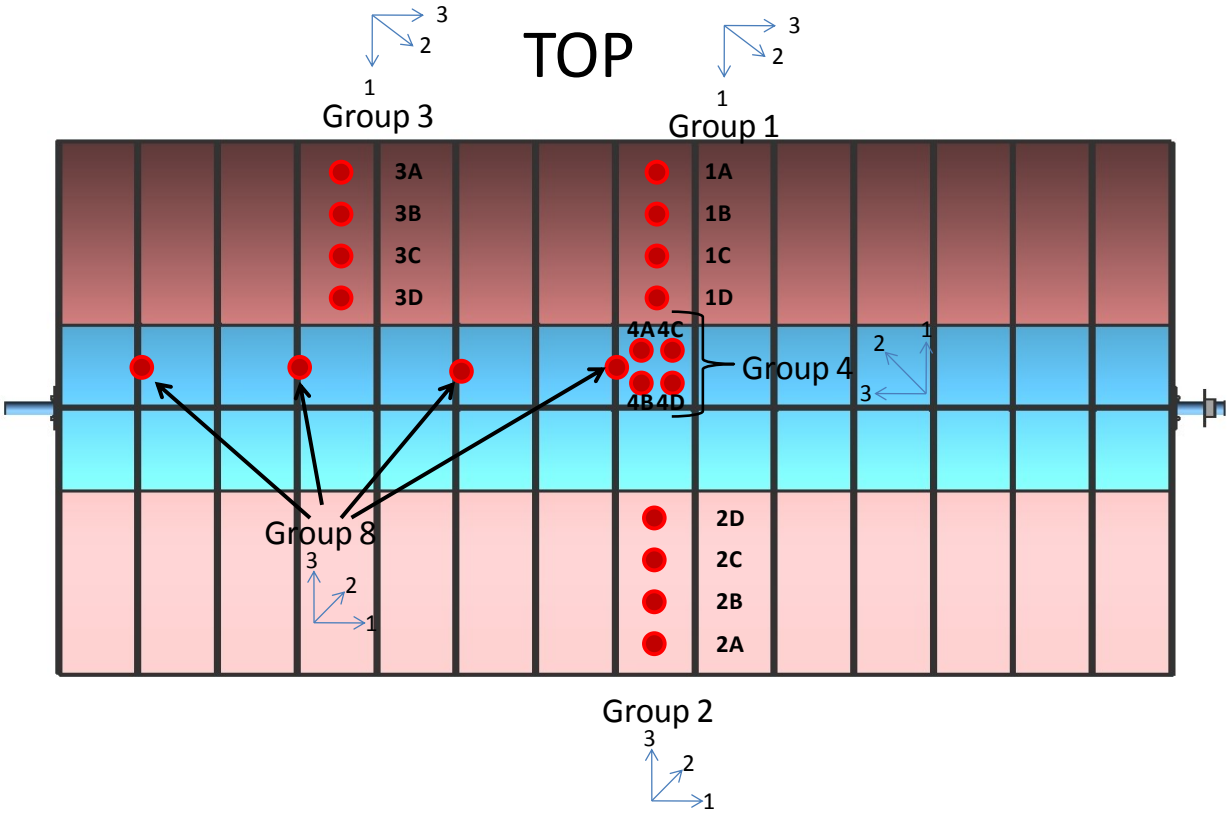
TOP
Group 3
Group 1
3A
3B
3C
3D
1A
1B
1C
1D
4A 4C
4B 4D
Group 4
Group 8
2D
2C
2B
2A
Group 2

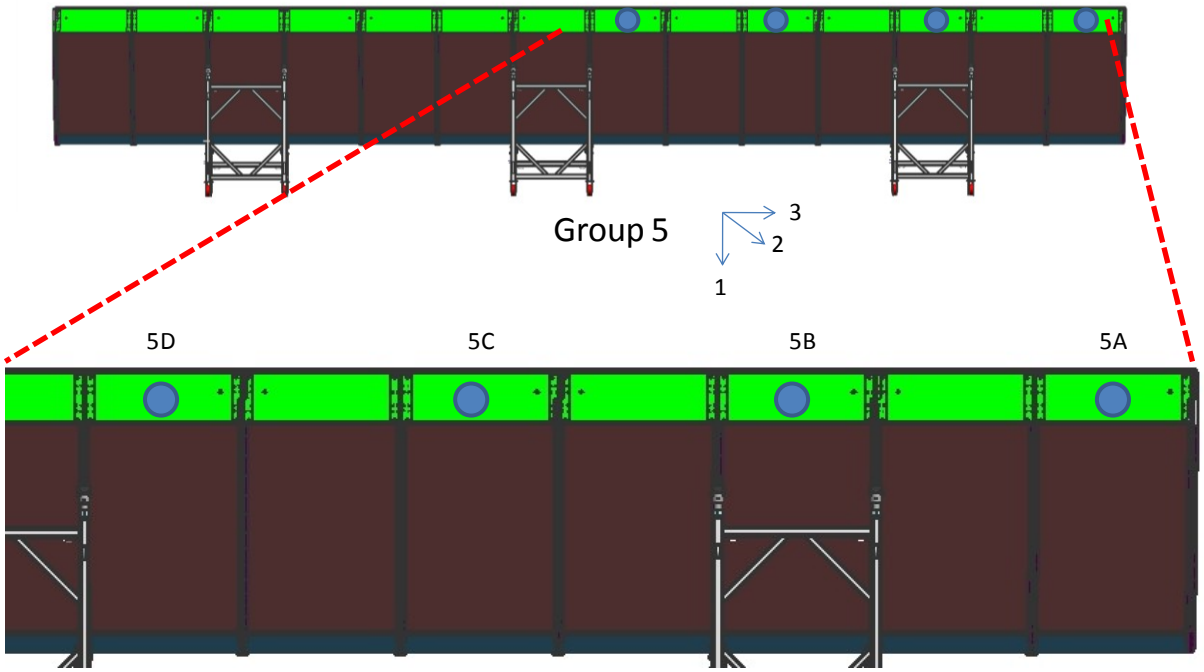
Group 5
5D
5C
5B
5A

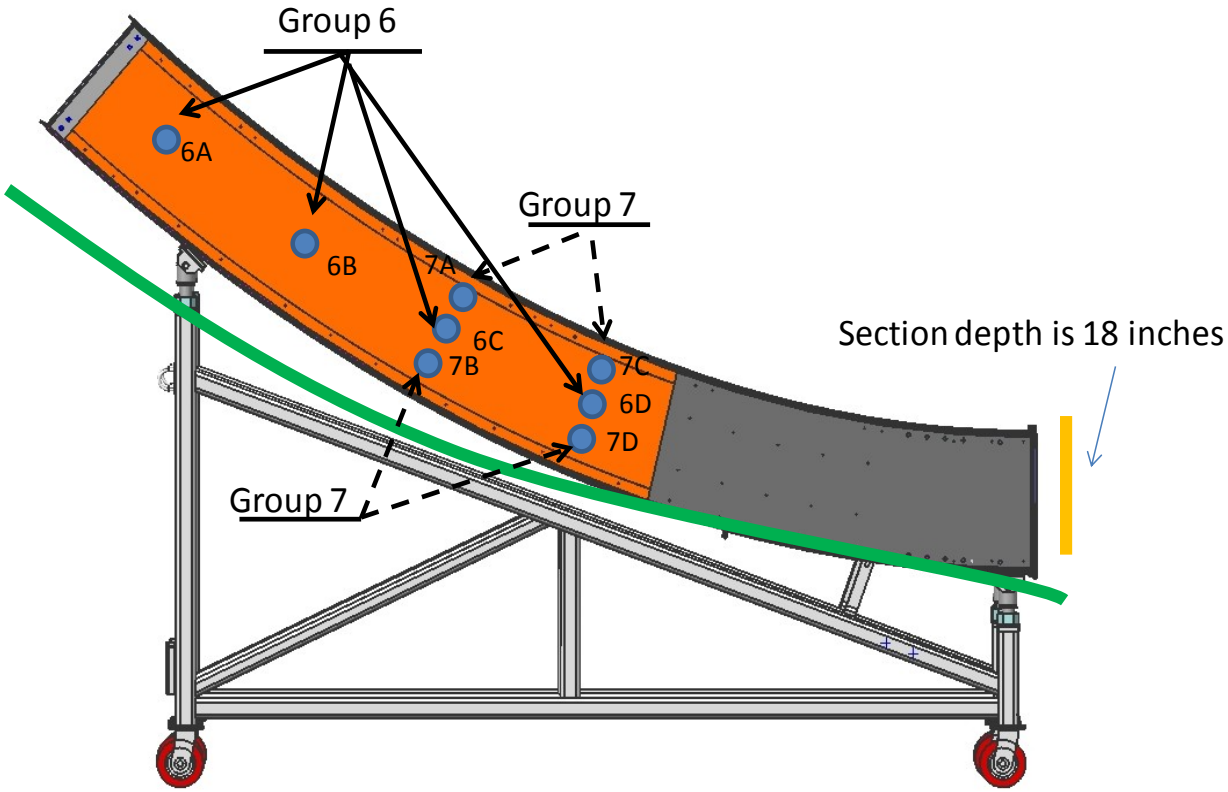

length of collector bottom (curve marked roughly in green) is 12 feet

Group 8

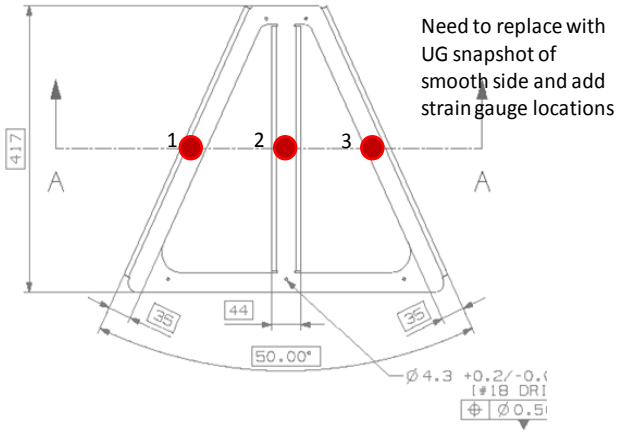

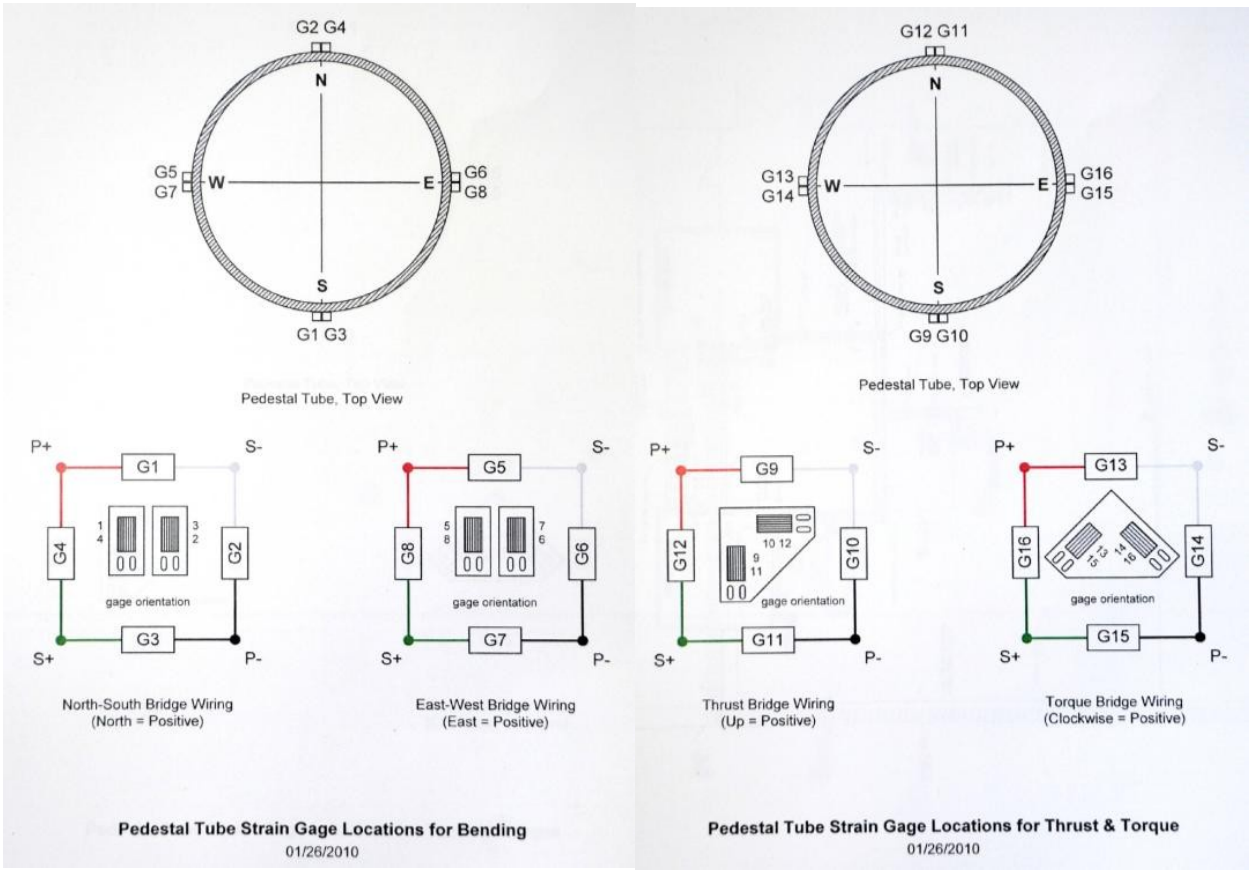

Testing Methodology:
With strain gauge instrumentation provided by Pete Vranka, documented in "CSP Wind Load Test Data.xls":

Notes on capturing calibration data:

- Collect pedestal data with the collector set at 90 degrees pitch and tracker facing cardinal directions (E, S, and W).
- Collect data for the cardinal directions at minimal pitch (~7 degrees)
- Collect data for the cardinal directions at pitch = 60 degrees
- Collect data at all three pitches for any interesting arbitrary tracker direction (e.g. NxNW on day 1)

Procedure for capturing structural data:

1. Collector should be pointed in one of the three available cardinal directions (E, S, or W) where the reflector faces the wind and preferably E or W.
3. Collector should be inclined 7 degrees above the horizon.
4. Wind speeds should be a minimum of 10 mph but ideally in the range of 15-40 mph.
5. After each scan session wind direction and collector orientation should be recorded in excel file "CSP Wind Load Test Data.xls"
6. The order of priority for the data groups are:
    a) G1G2G3 with 5 scan sessions desired
    b) G5G6G7 with 3 scan sessions desired
    c) G3G4G5 with 3 scan sessions desired

d) G7G8G1 with 2 scan sessions desired

7. Once verified recordings for the above orientations have been captured, a repeat of the above test pattern at 60 degrees pitch should be completed.

Example of testing:

An ideal data recording day might see a 15-40mph wind coming out of the NW. In that case the collector would be best oriented to 7 degrees pitch facing due west. Five ~20second bursts of data would be collected from gage group G1G2G3 with varied wind velocities. The wind direction and scan session ID for each recording would be logged to the Excel file "CSP Wind Load Test Data.xls". Once that data was captured, the group G5G6G7 would be recorded three more times with the same orientation.

Then the wind might shift and come from the SW. In this case ideally the collector orientation would not change as data captured while the collector faces east or west are preferred over those from a south-facing orientation. If the wind were to shift and come consistently from S-SW to E-SE direction, the collector would be rotated to face due south. Recordings would be captured for G1G2G3 then G5G6G7 and then G3G4G5 and G7G8G1 if conditions permit.

Once those data were captured and verified, the same procedure would be followed at the 60 degree pitch.

Notes

Notes from Telecom with Allison Gray of NREL:

1. Telecom Date – May 18, 2009
   - Collector is tested in the horizontal position
   - Allison requested the assistance of two ATC employees during testing at ATC
   - Large wooden platform (8' x 12') required for holding test equipment at proper elevation and location
   - Pallet jacks have been used in past to move wooden platform along length of collector
   - If testing outside, minimal wind is required such that equipment is not affected
   - The effect of cold temperature on the equipment is unknown
   - Output of laser is located approximately 3x the focal length
   - Laser/Scanner head moves vertically to scan surface of collector
   - Equipment is translated along platform to next scan location; 2", 4" or 6" increments depending upon desired resolution
   - Results of scans will provide an accuracy factor which can be used to develop an intercept factor
   - Once equipment reaches end of platform the platform is moved and equipment restaged at beginning of platform
   - Collector is scanned with receiver tubes off
   - Need a method of knowing location of each scan along the length of the vertex. Allison recommended permanently attaching a tape/scale along the center line length.
   - Allison recommended starting with a 2" resolution along length. If results look good then move to a 4" resolution. In center go back to a 2" resolution for X".
   - Testing will require 2.5 – 3 days using a 4" resolution. Testing will require 4.5 – 5 days using a 2" resolution.
   - Allison is aware that we desire her services during the November 30 – December 15, 2009 timeframe. She has allocated the time for testing at ATC.
   - Allison is aware that we desire to repeat the testing at NREL, Colorado. Testing at the site has not been done before. She has not committed to the testing at NREL in January.

2. Telecom Date – June 18, 2009
   - Trough needs to be aligned with horizon within 0.25^{O}
   - Vertex height – target height = height of platform
   - Scanner head makes an 80^{O} sweeps. Smallest vertical resolution is 0.01". A 0.25" resolution is typical. 1" is possible.
   - Equipment is recalibrated after each move along the horizontal axis
   - V-shot will not identify sags along horizontal axis
   - Allison is going to send :
     1. Papers w/r/t Testing of Parabolic Trough
     2. Papers w/r/t optic efficiency calculations
     3. Paper w/r/t allowable error along slope angle
     4. Details of test stand
   - Allison's Deliverables from V-shot Test at ATC:
     1. Raw data dump – before leaving ATC
     2. Immediate Summary Report – before leaving ATC
     3. NREL Report – Confidential Report or CRADA Report?
     4. Post processed data

Notes from Telecom with Keith Gawlik of NREL:

1. Telecom Date – June 4, 2009

   Mounting and Efficiency Testing Details

   - Keith to supply desired shaft diameter
   - NREL needs a reference surface so they know when they are horizontal
   - The tubes support and tubes will be installed when trough is pointed to the horizon
   - ALCOA will supply supervision and NREL will supply technicians
   - NREL will align the trough with ATC's guidance/assistance
   - ATC to sign off on final installation
   - There is a staging area near tracker where the two half subassemblies can be joined to create the final assembly
   - A crane will be supplied by NREL
   - Tube support installation methodology to be determined
   - Keith to supply photos of typical tube supports - done
   - In the past the tubes have been installed with scissors jacks
   - Inside of tubes are smooth
   - A 50/50 mixture of glycol and water is used as the heat transfer fluid
   - Coolant flow rate is related to the aperture area
   - Any spreader bars used for assembly must be preapproved by NREL . Most spreader bars are usually supplied by the crane company.
   - NREL will weld and mount receiver tubes
   - ATC to arrange for the receiver tubes to arrive at NREL at the same time as the trough
   - If receiver tubes warp in use they will break easily
   - Tubes will be tested at close to ambient or be shaded
   - When the sun is "off sun" 50/50 glycol/water coolant will be sent through the tube until no sun is able to reach the receiver tubes. Then the receiver tubes will be shaded.
   - Ambient temperature can vary from -25 ^{O}F to 80 ^{O}F
   - Gusts over 80 mph have been experienced at the test site.
   - The tracker is designed to handle a 16 meter trough up to 100 mph
   - Testing is stopped when winds exceed 25 mph
   - The trough is tilted straight up during high winds
   - Keith to send website of weather data up on mesa where test site is located – done
     http://www.nrel.gov/midc/srrl_bms/
   - When "on sun", coolant flow is monitored to make sure flow rate is maintained and is adequate.
   - Keith will verify with Allison Gray if she is able to repeat the V-shot test at the NREL test site prior to mounting the receiver tubes – done.
   - Keith described the Distant Observer Methodology of alignment. Keith is to send paper addressing topic – done.
   - Frank Burkholder – Another facility where they run the tube up to elevated temperature to measure the thermal efficiency of the tubes.
   - Shipping address:
     16253 Denver West Parkway
     Golden, CO 80401

Appendix E: Shape Analysis Data-Set 090426

CSP Services GmbH, Köln, Germany
CSPS Technology Report
– Approved for Public Release–
Client: Alcoa –
Alcoa Technical Center, PA, USA
Shape Analysis Data-Set 090426

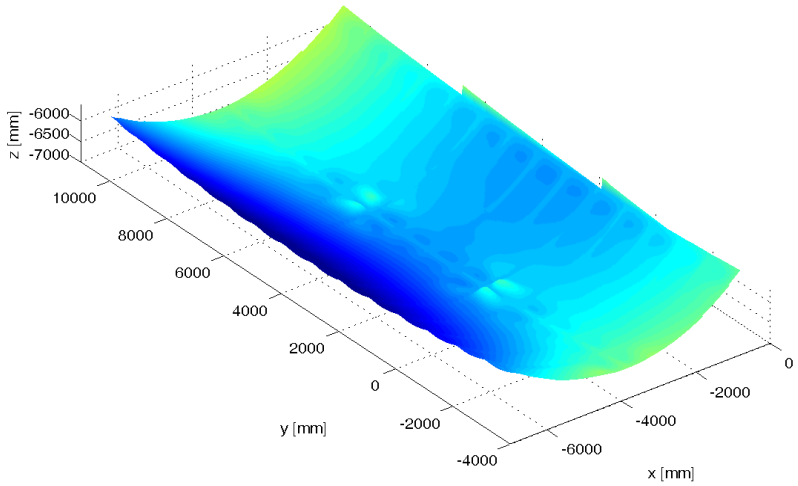

Technology Analysis Part II – Collector Shape analyses

Alcoa Purchase Order # 4000104905 (21-Jan-2009) Item#1

Study Report

Introduction and Description of the Data

Alcoa is developing a parabolic trough collector based on a proprietary aluminum design, using aluminum sheet as cover for the reflector area.

Objective of the analysis by CSPS is the comparison of the calculation results of finite-element-modeling by Alcoa to the criteria for a performance efficient parabolic trough collector.

Three data sets have been provided on 27-Apr 2009, in Ascii format.

Following description can be given:

Dataset 1:	**undeformed reflector"**	**deformed. reflector.non**	**toleranced reflector**
Knot numbers from	1210651	1210651	888063
to	1366901	1366901	1044179
transversal coordinates			
min	-6034.670	-6039.63	-6045.23
max	-0.93930	-0.4223	4.9507
longitudinal coordinates			
min	-3016.456	-3016.30	-3016.27
max	+10983.448	10984.4	10984.5
height coordinates			
min	-6999.9998	-7006.93	-7009.08
max	-5668.1405	-5666.71	-5673.38
Vertex of the parabola front end:			
x	-3017.805	-3017.8 ?	-3017.805
y	-3016.456	-3016.17 ?	-3020?
z	-7000.000		
Absorber			
Knot numbers from	720772	720772	721897
to	724403	724403	888062
x	-3017.909		
z	-5289.996		

Graphical results “deformed”

Deformed

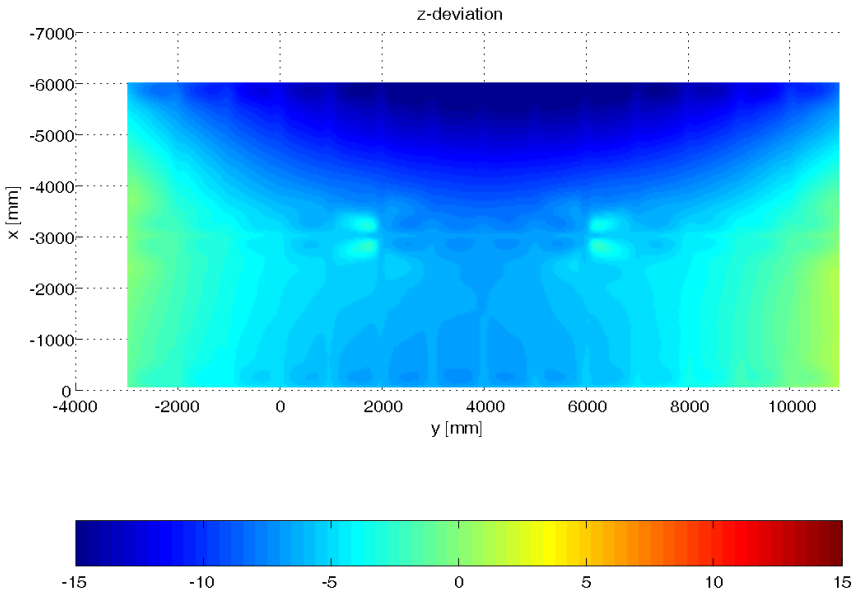

Figure 89: Height deviation of reflector

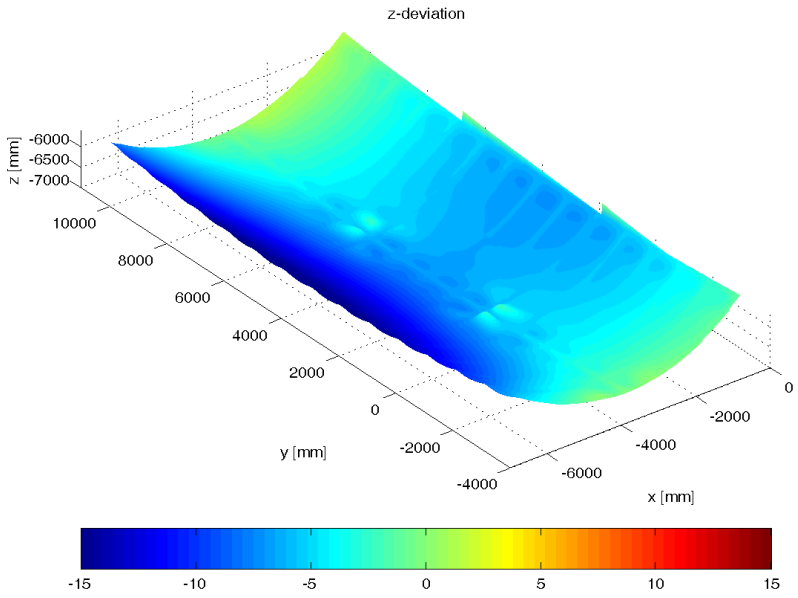

Figure 90: Height deviation, 3-D view

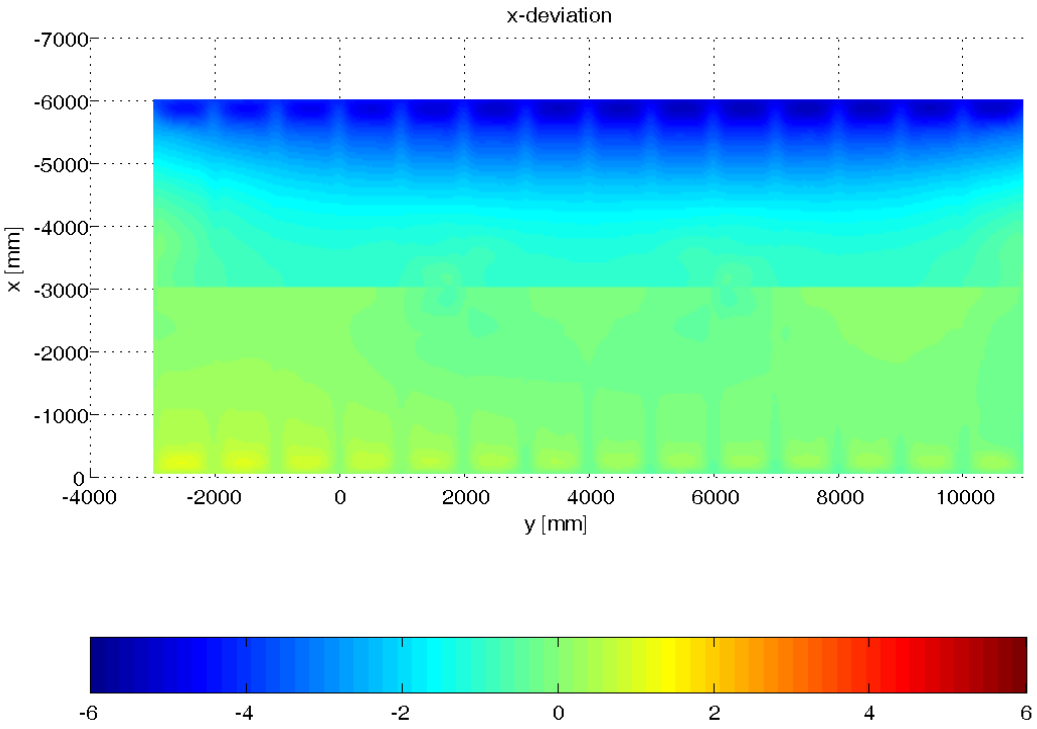

Figure 91: Width deviation of reflector

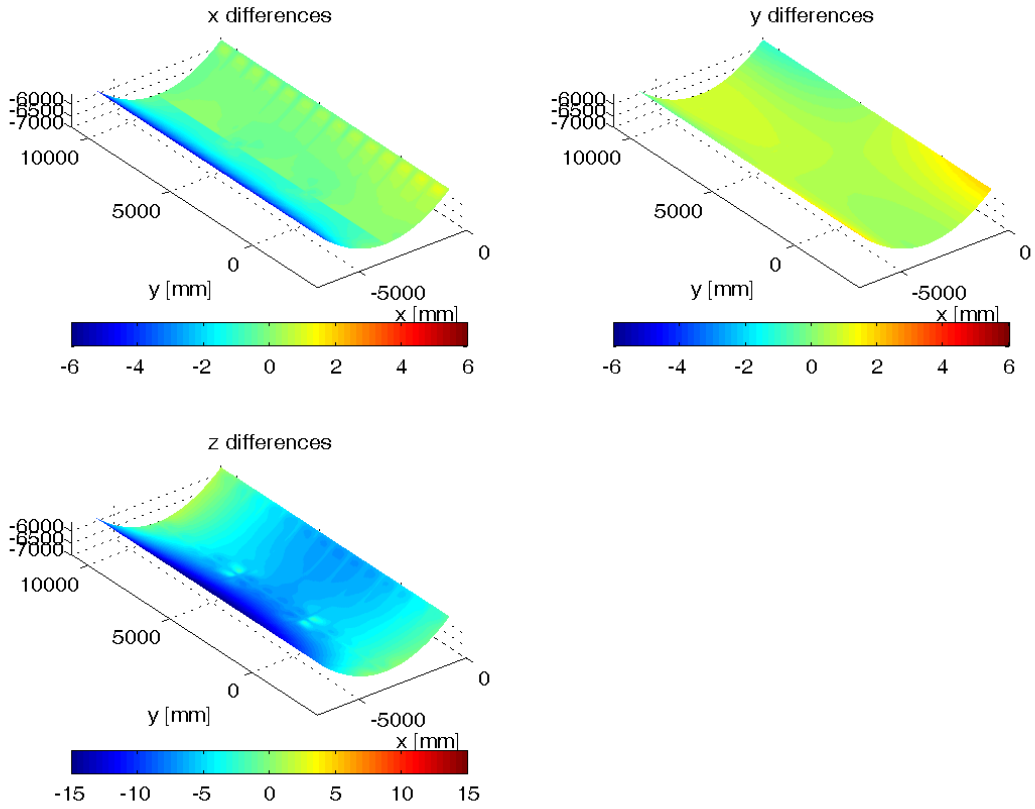

Figure 92: Deformation summary sheet

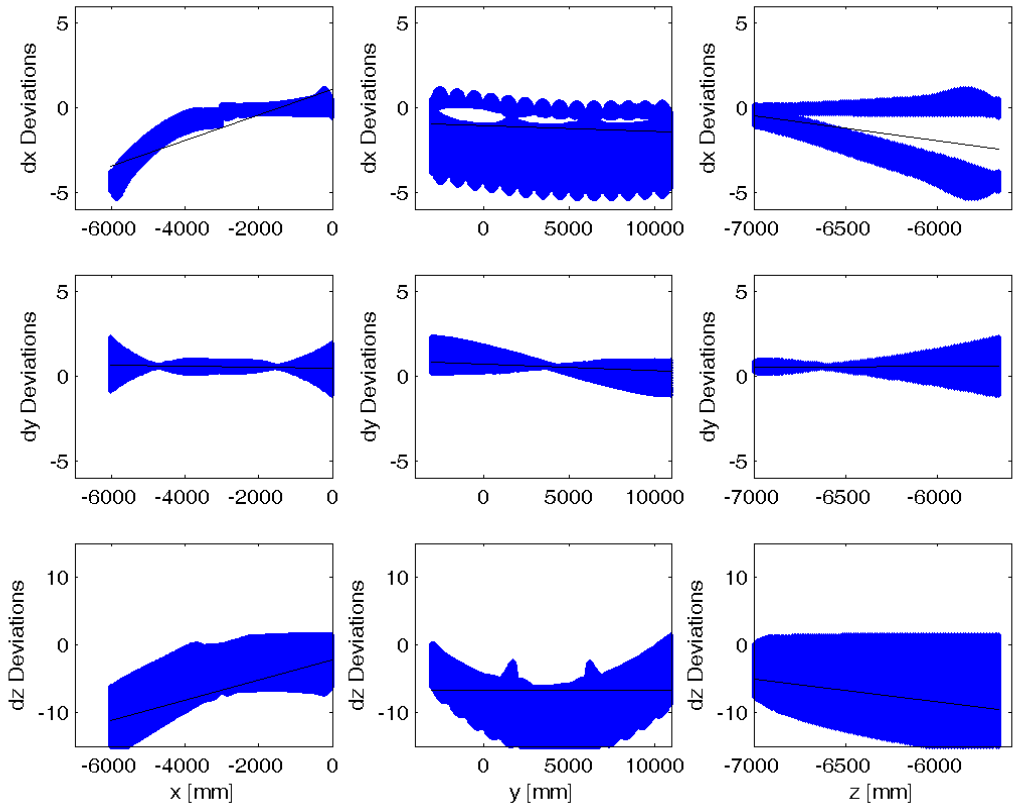

Figure 93: Shape deformation analysis sheet

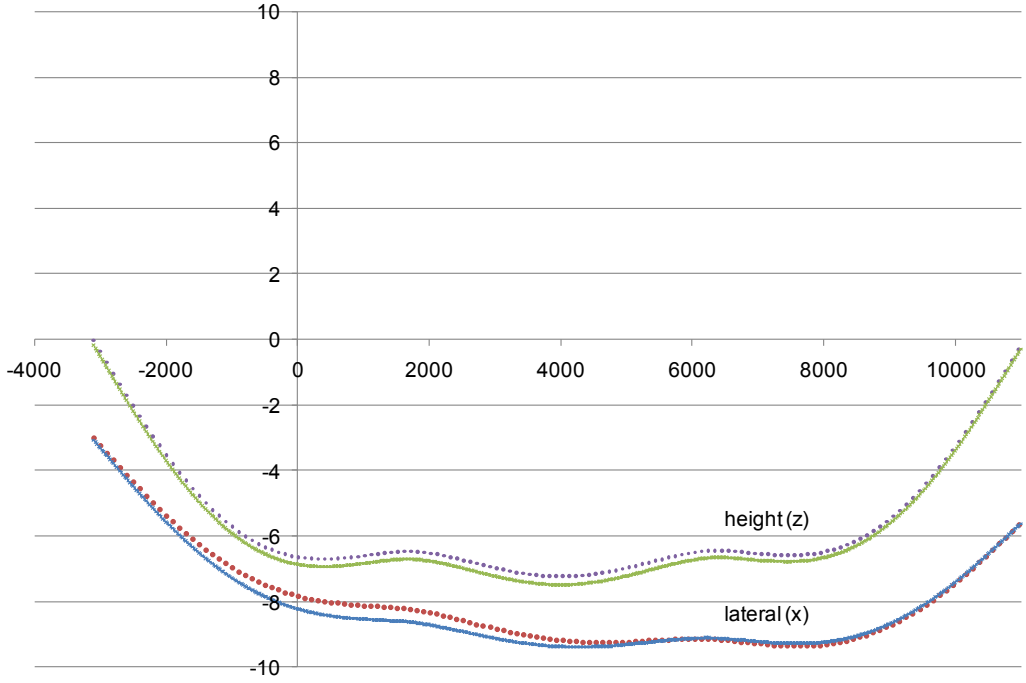

Figure 94: Deviation of absorber tube data from the ideal straight line, in mm

Comparison to parabola

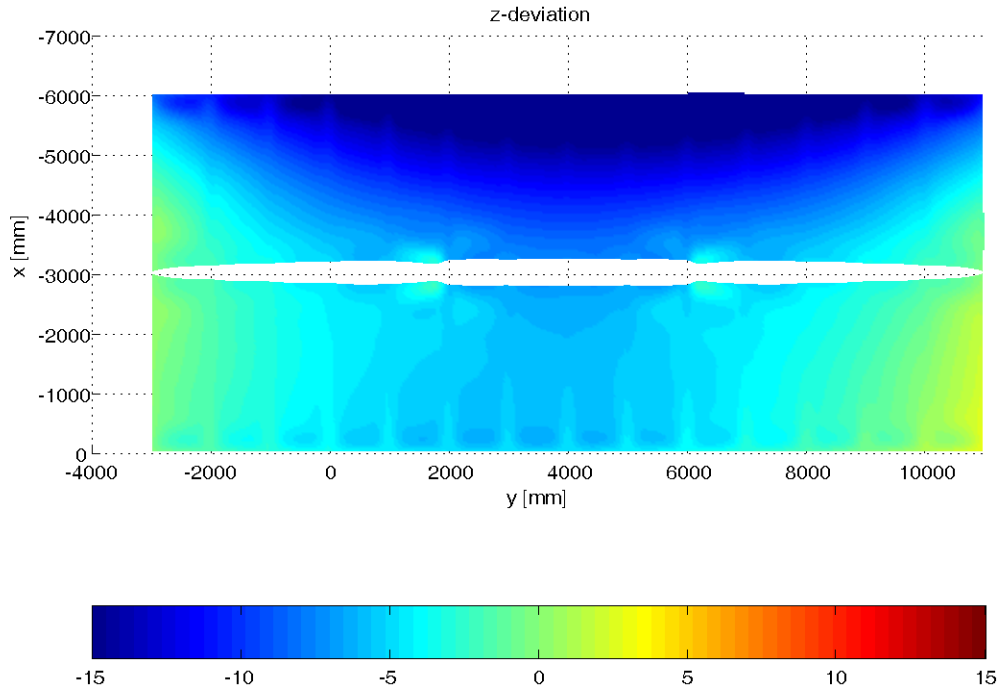

Figure 95: Height deviation of reflector

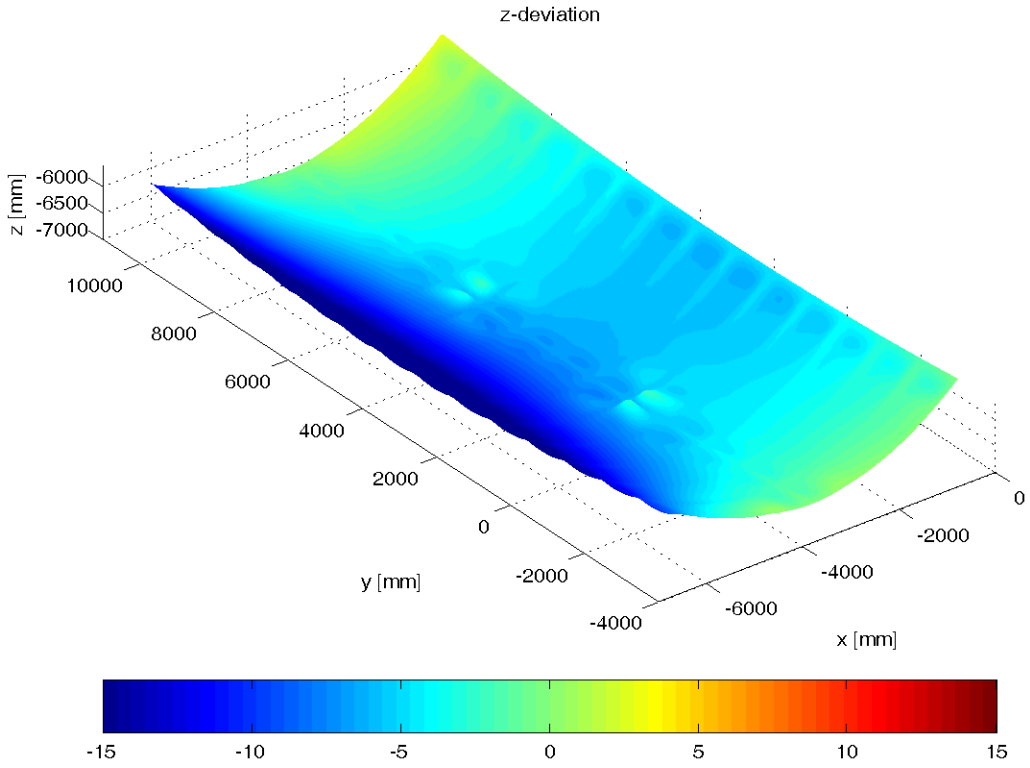

Figure 96: Height deviation, 3-D view

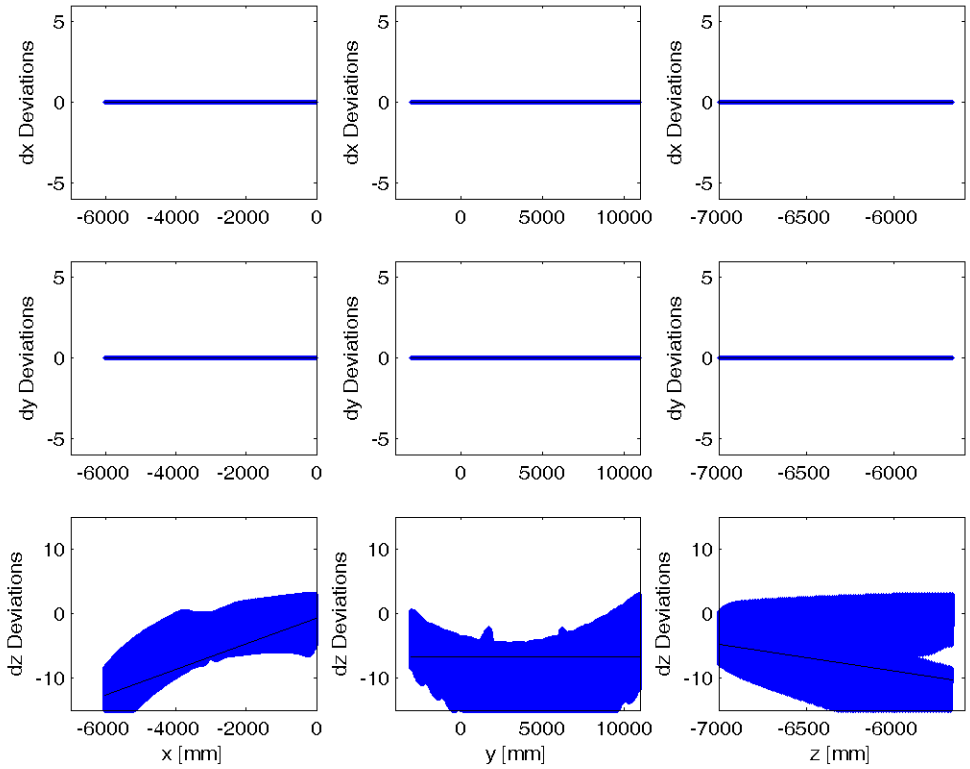

Figure 97: Shape deformation analysis sheet

Tolerated

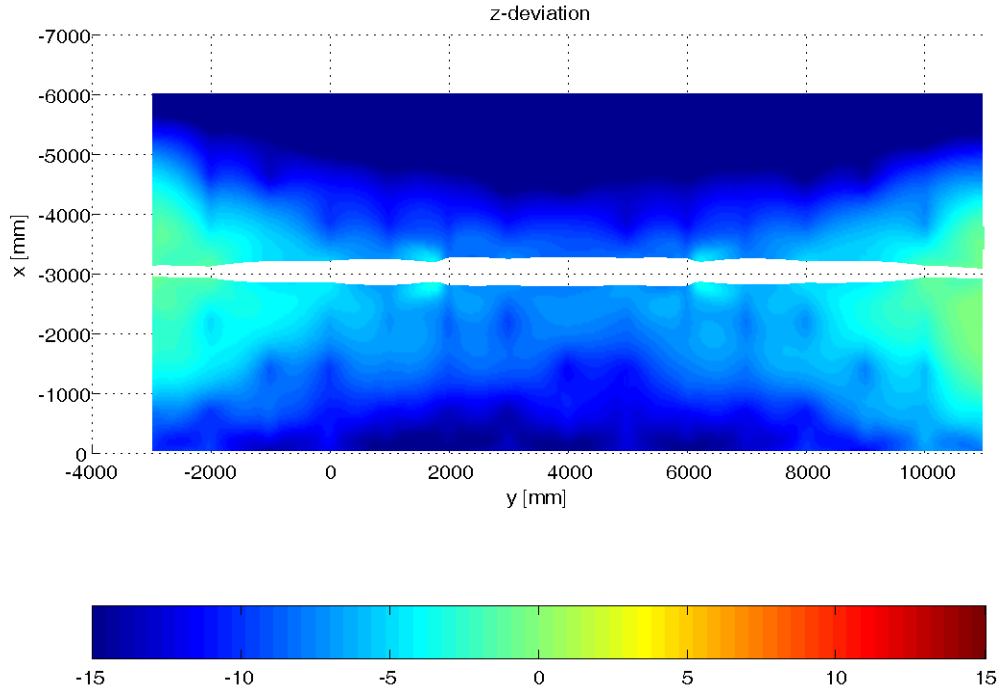

Figure 98: Height deviation of reflector

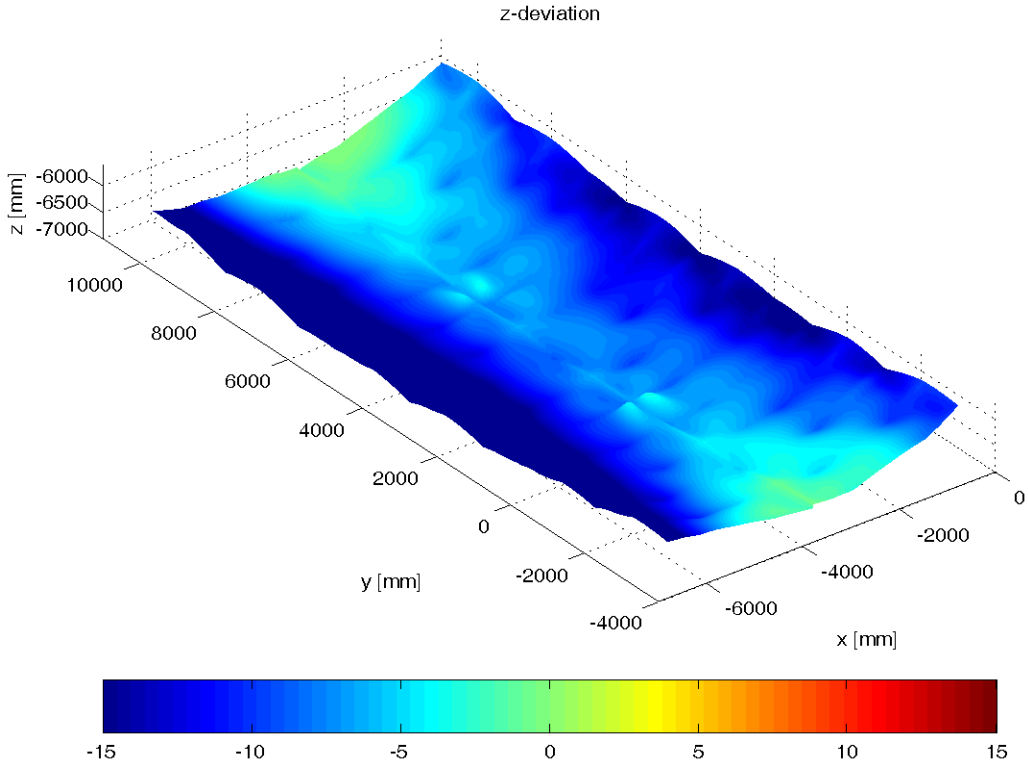

Figure 99: Height deviation, 3-D view

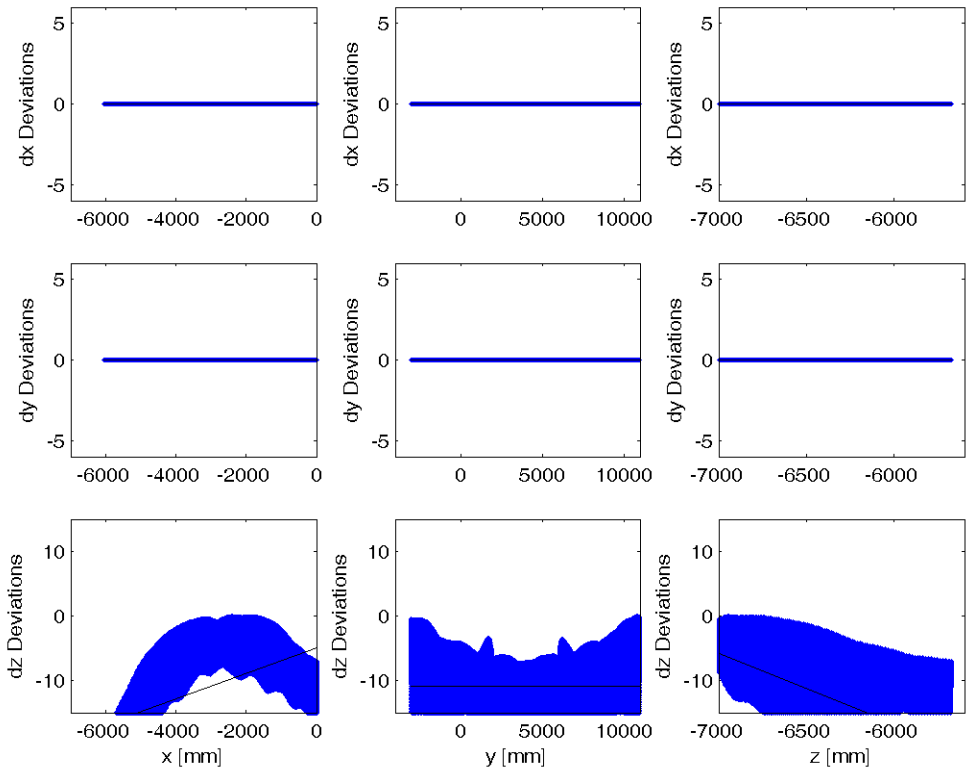

Figure 100: Shape deformation analysis sheet

Evaluation of the results, observations

(Raytracing, Intercept and summary data)

The evaluation of the data for the collector in 60° tilt from zenith at a given load case of 30 mph (13.5 m/s) shows symmetric deviations in the center of the trough element. The resulting deformations of the module can be summarized as follows:

1. The module bends 7 mm in the center relative to the support pylons. This deformation obviously includes the dead load of the module itself.
2. The outer rims of the collector receive an additional deformation due to the wind pressure of 0 to 10 mm. The deformation is in particular on the side of negative x-values, probably the upper part of the collector.
3. Deformation along the collector axis described in the first point has a very small effect on the intercept factor, because the absorber tube is supported twice on the collector and follows this bending line. Remaining relative displacement between reflector and tube of about 1 mm is negligible for the performance. At large incidence angles the effect can still be considered as very low.
4. Deformation of the reflector at the outer rim is of max 3 mrad for the 2nd case (deformation) and possibly up to 10 mrad for the 3rd ("tolerated") case. Both deformation values are very low for this load case which probably represents one of the maximum cases under regular operating conditions.
5. The absorber tube obviously performs the same relative movement. This means that the effect of the deviation is only with the weight of an alignment error, and not with the (double) effect of a reflector slope error.
6. The evaluation of the data shows only minimal effects of torsion of the collector module. This is not typical and might be due to the definition of the load case.
7. The reflector seems to reveal to locations where the absorber tube is supported. This deformation of several millimeters is almost as much as the bending and is a surprising effect. It might be connected with the lateral displacement of the absorber tube, but the values of the effect do not fit.

Conclusion

The collector module surface data supplied by Alcoa for a 30 mph wind load case shows only small deformations of several millimeters of the reflector and the absorber tube. The collector does not suffer relevant intercept losses in these conditions. At such wind speed, which would be for one of the existing trough solar fields already at the boundary of the operating conditions, larger deformations of the collector modules could be tolerated. With the level of analysis possible for the data and the supplied information it seems that the stiffness of the collector module is over-designed and leaves room for weight reduction. However it should be checked in a follow-up step, if the modeled load case includes all pressures forces and torques applicable to the wind operation situation or if too mild simulation conditions for the modeling have been applied. It will be worthwhile looking at and comparing some key figures such as pressures, size of module, specific weight, torsional rigidity of the test case and the collector design. If all such evaluation parameters are crosschecked and no relevant savings can be identified, the detailed design can continue with a quite positive evaluation result of the wind deformation analysis.

Appendix F: NREL Report – "Optical Testing of the Alcoa Parabolic Trough"

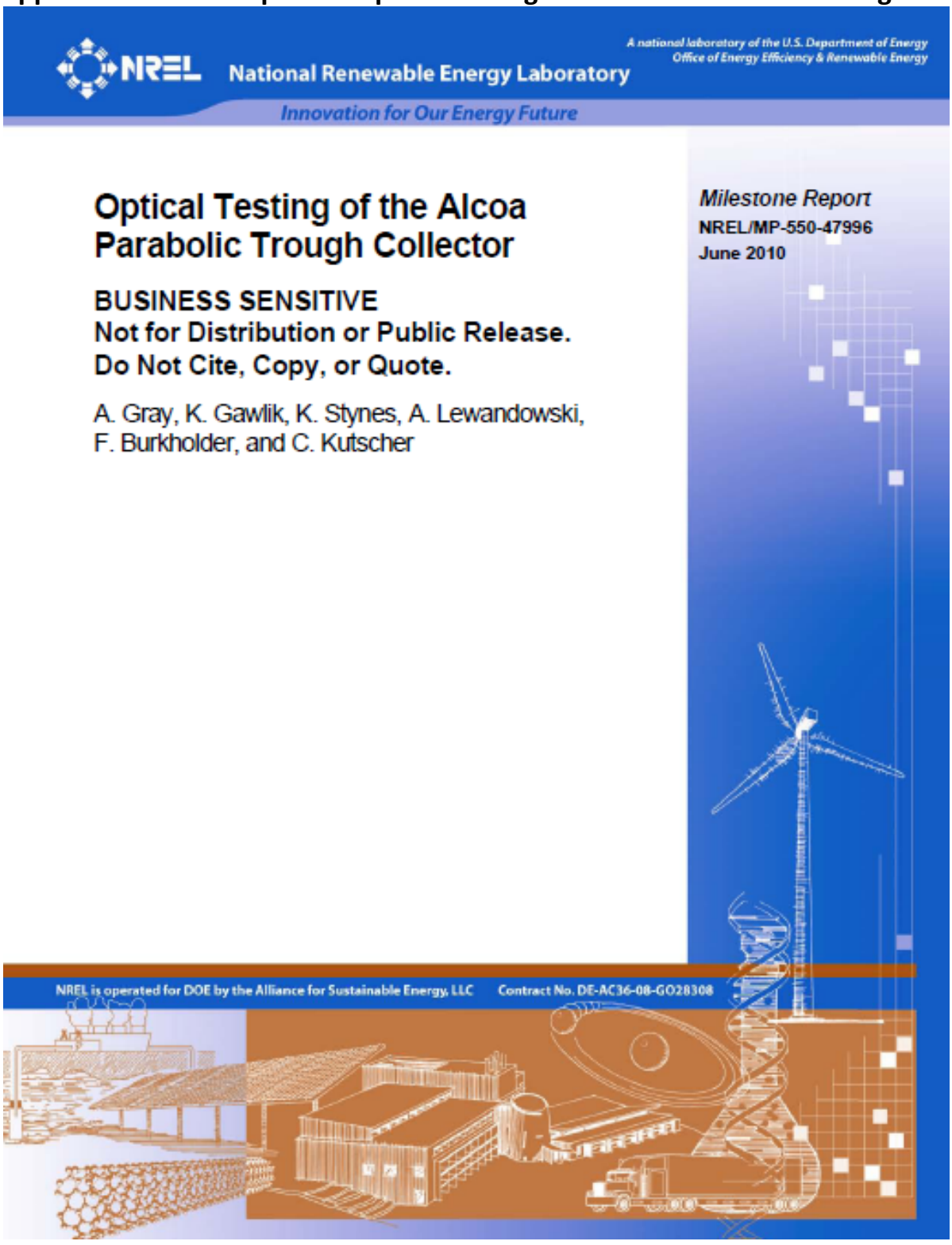

Table of Contents

Summary

Alcoa is developing a parabolic trough collector for use in utility-scale solar thermal electric power plants. NREL used its optical testing capabilities to support this development. In December 2009, the Video Scanning Hartmann Optical Tester (VSHOT) was used to characterize the surface contour of a module assembled at the Alcoa Technical Center in Pennsylvania. In February and March 2010, the same module was installed at the NREL Solar Industrial Mesa Top Area (SIMTA) with a receiver to determine its optical efficiency. Additional VSHOT testing was conducted on this module in April 2010 to verify surface contour following shipping and reinstallation.

The Alcoa collector is 14 m long with a 6-m aperture and a 1.71-m focal length. This module consists of two halves − each one representing half of the aperture width. There are 14 1-m, non-glass reflective panels on each half. A photo of the collector installed at the SIMTA is shown in Figure 1.

For VSHOT testing in December 2009, one vertical scan was taken approximately every 0.102 m (4 inches) along the length of each panel beginning as indicated schematically in Figure 2. The average transverse RMS slope error for the collector was 2.70 milliradians (mrad) with a calculated intercept factor at normal incidence greater than 0.99 for an 80-mm diameter receiver tube. The largest deviations from the ideal parabolic shape exist near the vertex and near the edges of some panels but they have very little impact on performance. The additional VSHOT testing conducted in April found very consistent results with some local differences in slope errors near the vertex compared to the December 2009 results.

The module with three Schott PTR-80 receivers was tested at NREL's Optical Efficiency Test Loop. Results were from clear days with direct normal solar radiation from 700 to 1,000 W/m^2, mass flow rate of 1.6 kg/s, and receiver tube inlet temperatures from 2°C below to 2°C above ambient temperature. During tests in March 2010, optical efficiency was found to be 0.747 and 0.749± 1.7%. Incidence angle modifiers were calculated over a range of angles from 0^o to 50^o. Separate laboratory receiver heat loss tests were then combined with the optical efficiency data to generate collector efficiency as a function of fluid operating temperature.

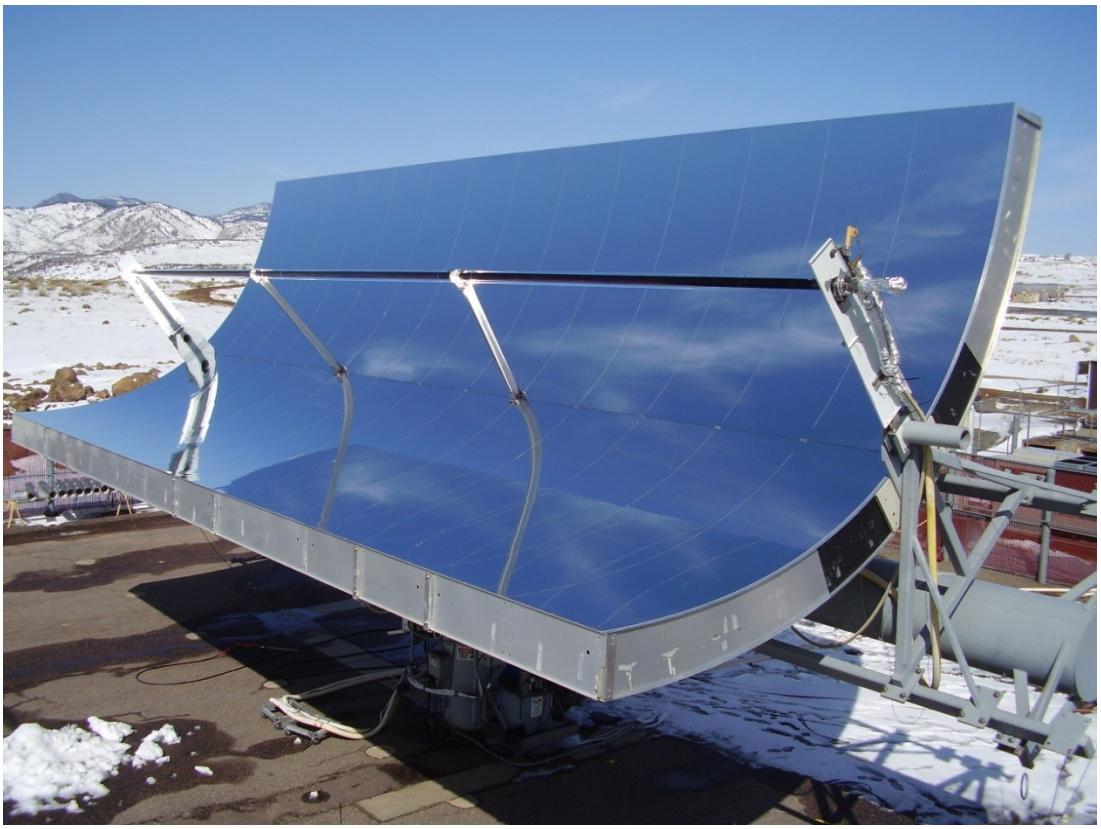

Figure 101: Alcoa collector with installed receivers on the Large Payload Solar Tracker at NREL's SIMTA. The Optical Efficiency Test Loop was used to characterize overall optical performance of this collector.

VSHOT Testing

Test Description and Background

The schematic of the Alcoa collector in Figure 2 shows the basic panel layout and the orientation of the VSHOT scans along the transverse direction. Scans were taken approximately every 0.102 m (4 inches) along the length of each 1-m-wide panel and 0.013 m (0.5 inch) from each edge of each of the 14 panels for a total of 159 scans.

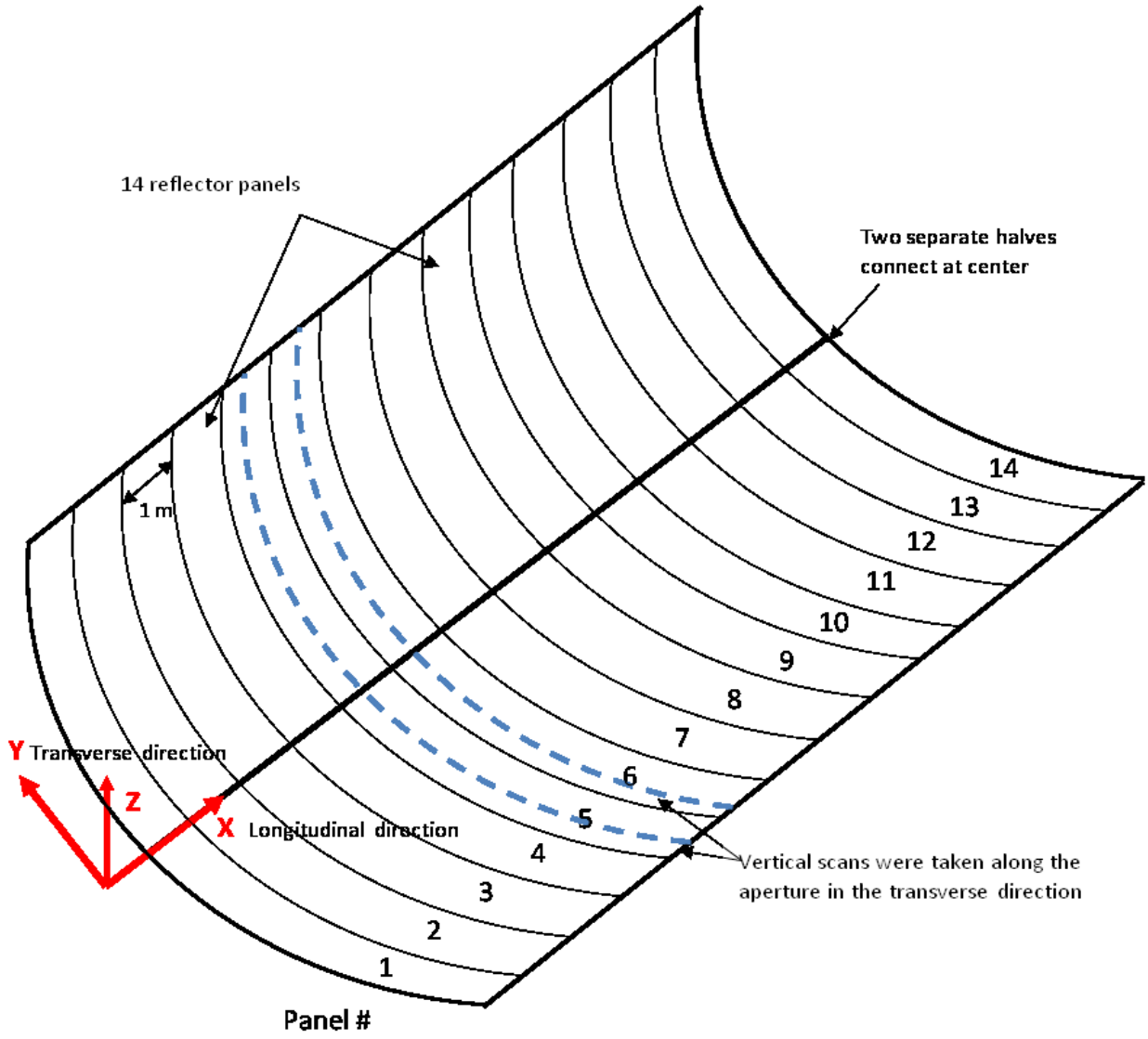

Figure 2. Schematic of the Alcoa collector showing general layout and orientation of VSHOT scans.

The modules were tested with the aperture facing the horizon (vertical aperture). The VSHOT [1] system (shown in Figure 3) was located at approximately 4.5 m from the vertex. Either

eleven or twelve vertical scans were taken on each panel with roughly 1,000 points per vertical scan. Each data point is determined by the origin of the laser beam, its output angle, α_y in the vertical direction and the position of the reflected beam on the target. This is shown superimposed in the photograph in Figure 3. A camera images the reflected laser beam location on the target. The VSHOT software uses this image data to determine the vertical location (H_y) of the reflected beam. All the data points for a given scan are collected and analyzed to produce slope data. This data is then fit to a 2nd order Zernike Polynomial to mathematically describe the surface. A 2nd order Zernike is expanded below in its 3-dimensional form.

$$z(x,y) = B_{0,0} + B_{1,0}y + B_{1,1}x + B_{2,0}y^2 + B_{2,1}xy + B_{2,2}x^2 \quad (1)$$

The data is collected in single vertical scans so it only needs to be analyzed in two dimensions. With this constraint the Zernike Polynomial can be simplified so that z is a function of only y, and assuming a second order surface, the equation is;

$$z(y) = B_0 + B_1 y + B_2 y^2 \quad (2)$$

The computed coefficients represent specific parameters of interest:

$B_2 = \frac{1}{4FL_y}$ where FL_y is the focal length,

$B_1 = \tan(tilt)$ about the horizontal axis and

$B_0 =$ z axis position error

Slope errors are generated by comparing the measured location of the reflected rays on the target to that of an ideal parabola of the design focal length. Final results are presented as a slope error at each data point and an overall RMS of the slope errors for each scan, panel or set of panels. The RMS, also referred to as standard deviation, is defined in the equation:

$$RMS = \sqrt{\frac{\sum_{i=1}^{N} R_{y,i}^2}{N}} \quad (3)$$

where $R_{y,i}$ are the individual slope errors. The RMS is a valuable indicator of optical performance. The intercept factor is the fraction of the available solar radiation incident on the receiver tube. There are several methods to estimate the intercept factor, including analytical and

more detailed ray-tracing. One ray-tracing code, Soltrace [2], can directly input some VSHOT data files[1] to yield a very accurate prediction of intercept.

[1] Soltrace can accept VSHOT data files only from scans of entire panels and not from vertical slices. This requires a laboratory setting with a much larger target than is practical for field testing.

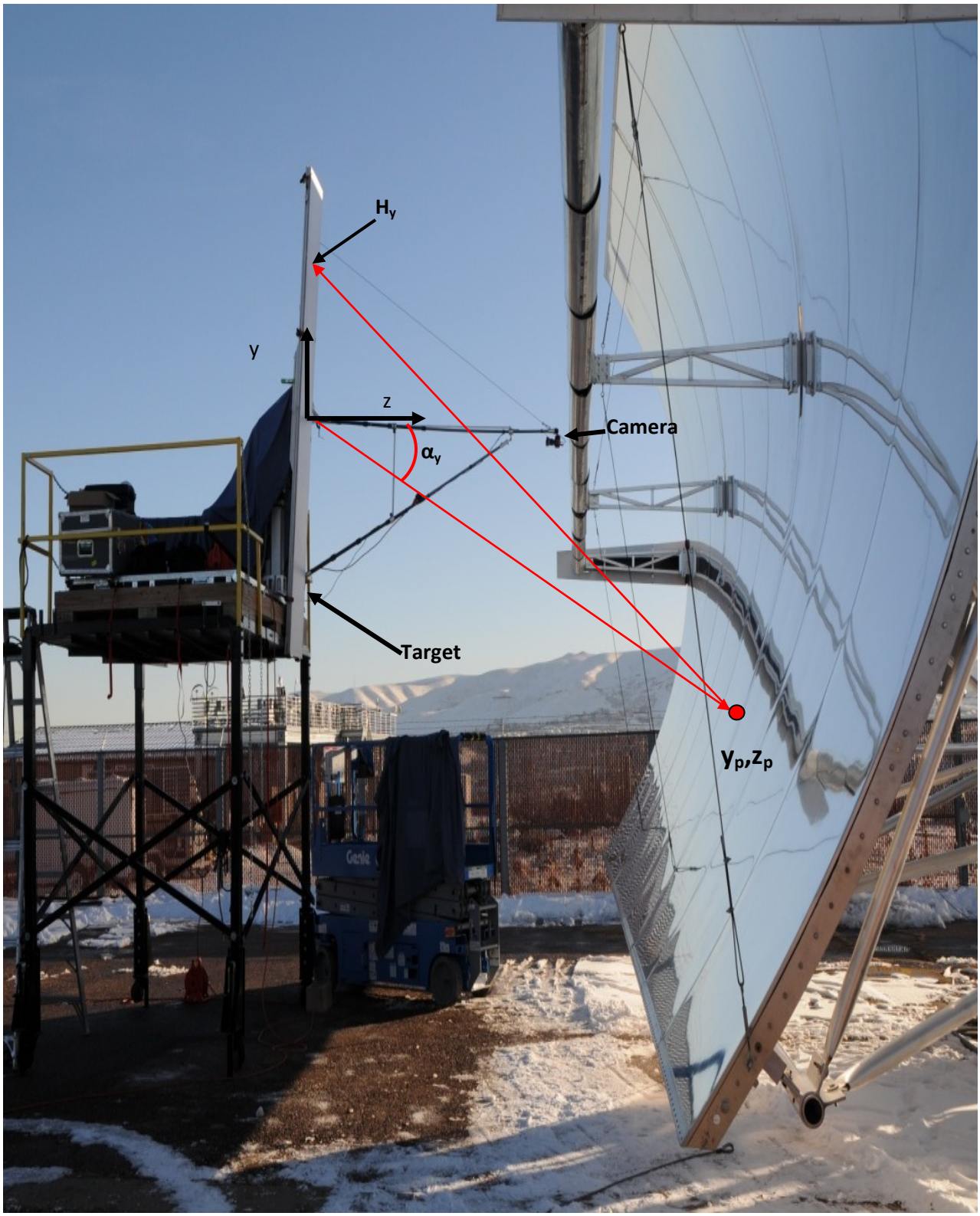

Figure 3. Image of VSHOT TO-GO system testing a collector. TO-GO refers to the portable version of VSHOT used for field measurements. This photograph was taken at NREL during testing of a different manufacturer's collector.

For a parabolic surface, the distance from the surface to the focal point increases from the vertex to the rim. The same slope error will have a greater negative impact on intercept at the rim than at the vertex. Figure 4 illustrates this effect for a trough with LS3 focal length (1.71 m) and a slightly wider aperture, 6 m to match the Alcoa design.

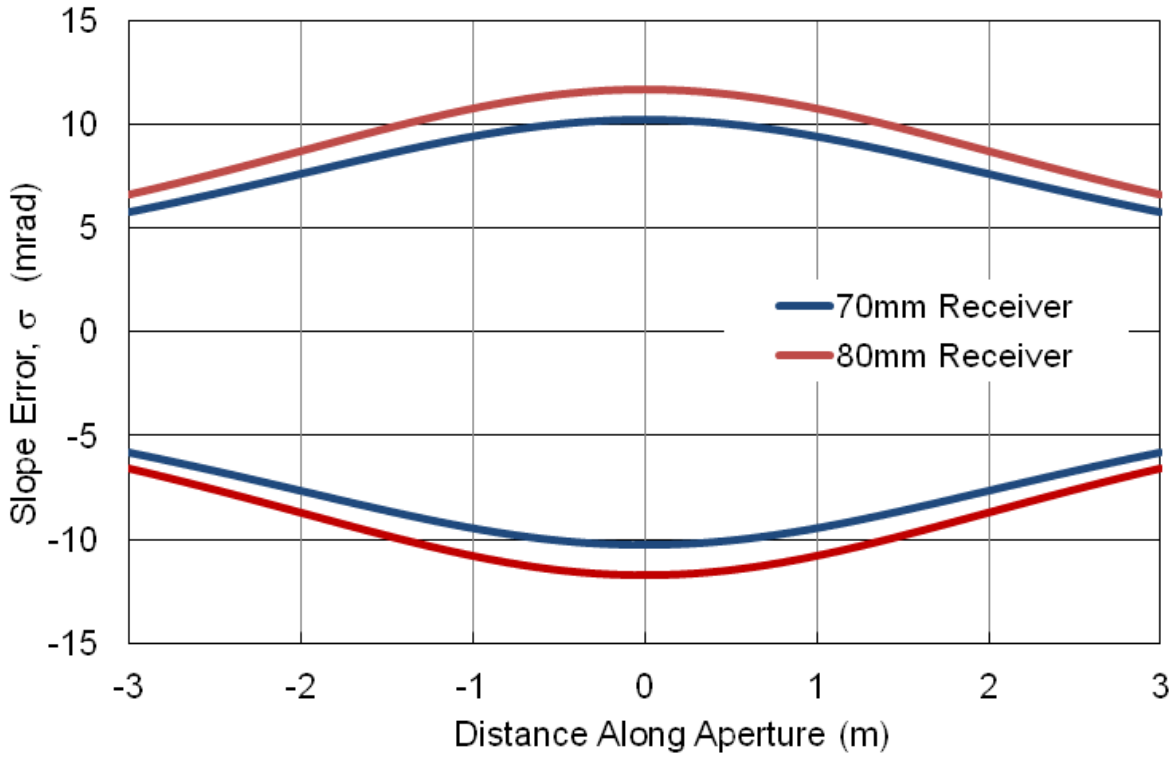

Figure 4. The maximum slope error allowable so that a normal ray at the aperture location intercepts the receiver for a collector with a 6.0-m aperture, 1.71-m focal length, and 70-mm and 80-mm diameter receivers. This calculation does not include the effect of sun shape which will decrease the intercept by a small amount.

Ray-tracing is used to analyze the effect of the transverse slope error on the intercept factor, with the following assumptions and limitations:

- Errors in the longitudinal direction were neglected.
- The reflecting surface has perfect reflectance and specularity.
- Slope errors measured by VSHOT are applied at the intersection of the outgoing ray and the ideal surface.
- The receiver has perfect absorptance.
- There is no glass envelope surrounding the absorber.
- The receiver diameter was 80 mm, and it was placed 1.71 m from the collector's vertex.
- A point sun at an infinite distance (parallel rays) and a typical clear day sunshape were used as the source.

- 56,000 rays normal to the aperture were traced[1].

When longitudinal errors are neglected the RMS slope errors become only a function of the transverse errors and are redesigned as $\sigma_{\perp}$.

Results

VSHOT Testing at Alcoa

Table 1. Summary of Nominal VSHOT Test Conditions for Data Collected.

Date and time	12-10-09 8:00-18:00 ET 12-11-09 8:00-18:00 ET 12-14-09 8:00-18:00 ET
Test location	Alcoa Technical Center
Collector Position	Horizon
Aperture Length	6 m
Collector Length	14 m
Average RMS	2.70 mrad
Average Intercept Factor (parallel rays)	0.992
Average Intercept (DLR Sun Shape)	0.991

The measured and processed VSHOT data (taken at Alcoa in December 2009) and analysis results are presented in tables and plots. The tables include RMS slope error, $\sigma_{\perp}$, and the estimated intercept factor, γ. Table 2 is a summary of results for each of the 14 panels. The 11 scans (or 12 scans for Panels 1 and 14) are averaged to generate the RMS slope error, intercept for parallel rays and an intercept for a typical clear day sun shape. Only selected ray-trace and slope error plots are shown. Tables presenting data for each scan are in Appendix 1, along with representative ray-trace and slope error plots.

Table 2. Averaged results for Alcoa collector for receiver diameter 80 mm.

Panel Number	Average RMS Slope Error (mrad)	Average Intercept parallel rays	Average Intercept DLR sun shape
1	2.61	0.994	0.993
2	2.34	0.994	0.993
3	2.45	1.00	1.00
4	2.32	0.994	0.993
5	2.72	0.998	0.997
6	2.69	0.988	0.987
7	2.51	0.994	0.992
8	3.34	0.977	0.976
9	2.83	0.995	0.994
10	2.65	0.995	0.995
11	3.29	0.981	0.981
12	3.08	0.986	0.983
13	2.73	0.995	0.994
14	2.21	1.00	0.999
Average	**2.70**	**0.992**	**0.991**

[1] This number of rays is relatively arbitrary but is sufficient to reduce any random error in the ray trace methodology to an acceptably small value.

The results in Table 2 indicate that, except for three panels, the RMS slope errors are relatively small with consequently high intercept factors. Overall, the slope errors are small enough so that including the effect of sun shape from Neumann, et. al. [4] does not have any dramatic effect on intercept. This shows that almost all rays are well inside the receiver diameter. Average intercept does not exactly correlate with average slope error because of the distribution of those errors across the aperture. For example, a panel could have high errors near the vertex but within the bounds of the envelope (as shown in Figure 4 and a few smaller errors at the rim that would be outside the envelope. However, even for those three panels with relatively higher slope errors, the intercept factors are also high.

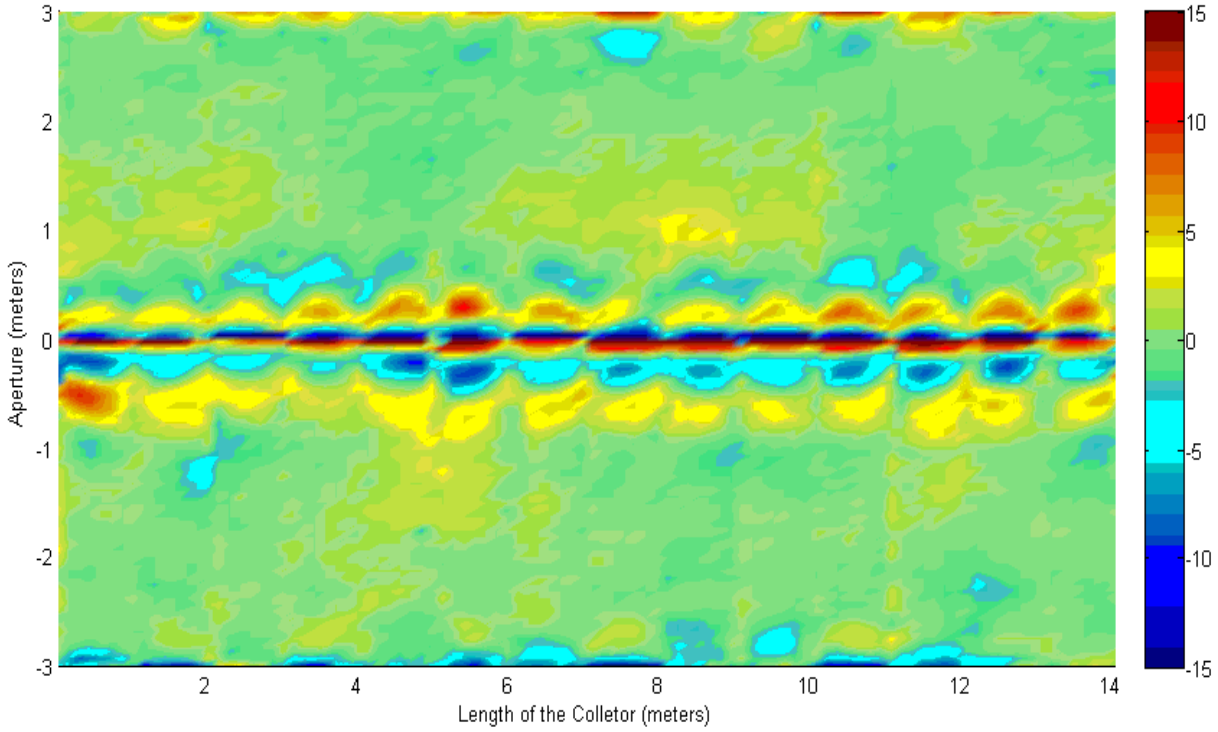

Figure 5. Contour plot of the slope errors over the collector. The color scale is from ±15 mrad.

Figure 5 shows the 159 scans as a contour map and highlights the areas with both high and low slope errors. The area along the vertex of the module represents the greatest area of high errors (both positive and negative). The impact of this would be somewhat mitigated by the receiver, its glass envelope, and the incident rays that are blocked by their shadow on the reflective surface. The ray tracing conducted for this report does not have the capability of modeling refractive surfaces, so this effect was not included. The end result based on other trough modeling efforts shows that rays refracted through the glass envelope will reflect off the concentrator surface but will not return to the absorber tube. Therefore no rays that are within the diameter of the glass envelope provide any useful concentrated energy to the receiver. However, those rays that pass through the glass coming directly from the sun will provide a small energy gain.

Two scans from the set of 159 are shown below. One is representative of a scan with relatively high errors and one with very low errors. Red rays in the plots indicate rays that miss the receiver and therefore decrease the intercept factor for that slice. In the slope error plots, the following convention indicates whether the slope of the mirror is too steep or too shallow,

depending on the sign (±) of the mirror aperture position. Too steep means that the ray will pass under the receiver tube and too shallow means it will pass over the tube. These plots were generated assuming an 80-mm diameter receiver tube with no glass envelope modeled in the ray trace. In the field, the glass envelope will block additional rays from reaching the reflective surface. Those rays that do transmit through to the reflective surface will be refracted and will not be reflected to the receiver tube. This reduces the effective reflective area near the vertex by the diameter of the glass envelope.

Mirror aperture location	**+** slope error indicates	**-** slope error indicates
- (to the left of the vertex)	**Mirror steep**	**Mirror shallow**
+ (to the right of the vertex)	**Mirror shallow**	**Mirror steep**

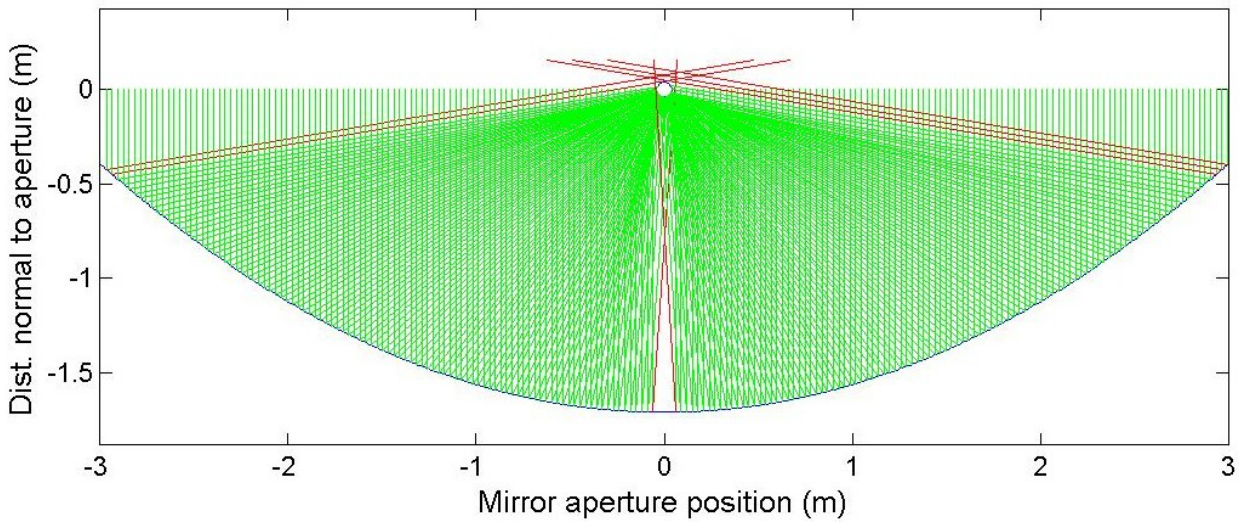

Figure 6. Ray trace results for scan of Panel 8 at 24 ft 8 inches, RMS = 4.32 mrad, γ = 0.964.

Figure 6 shows the ray-trace plot for a scan at 24 ft 8 inches (about ¼ the way along Panel 8). This scan shows high slope errors along the outer edges with slope that are too shallow so that these rays pass over the receiver. In this case, the high slope errors near the vertex pass under the receiver, indicating the slope is too steep.

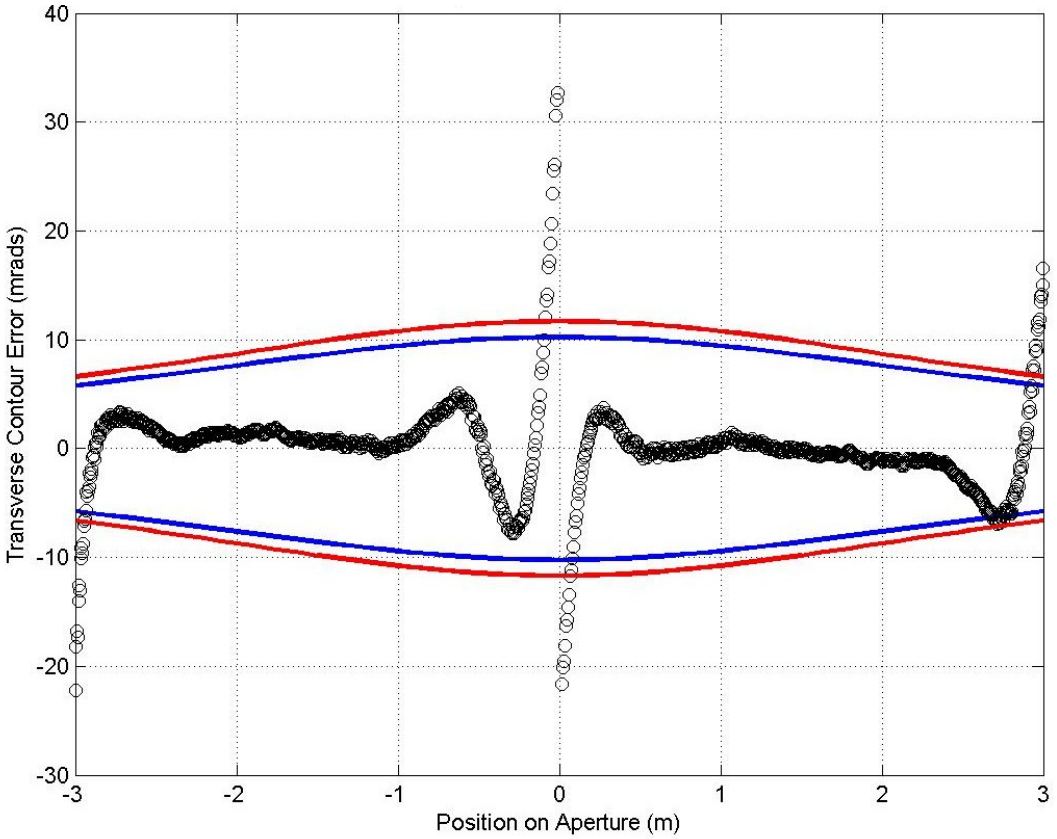

Figure 7. Slope errors along the aperture of Panel 8 at 24 ft 8 inches, RMS = 4.32 mrad.

Figure 8 shows the slope error plot for the Panel 8 scan at 24 ft 8 inches. Those locations along the aperture where the error falls outside the bounding intercept curves represent areas where rays will miss the receiver tube. For this scan, the slope errors are very small at all areas except for near the vertex and near the outer edges. This may be a result of how the reflective surface is attached at those locations. It may also be caused by some structural support details in those areas.

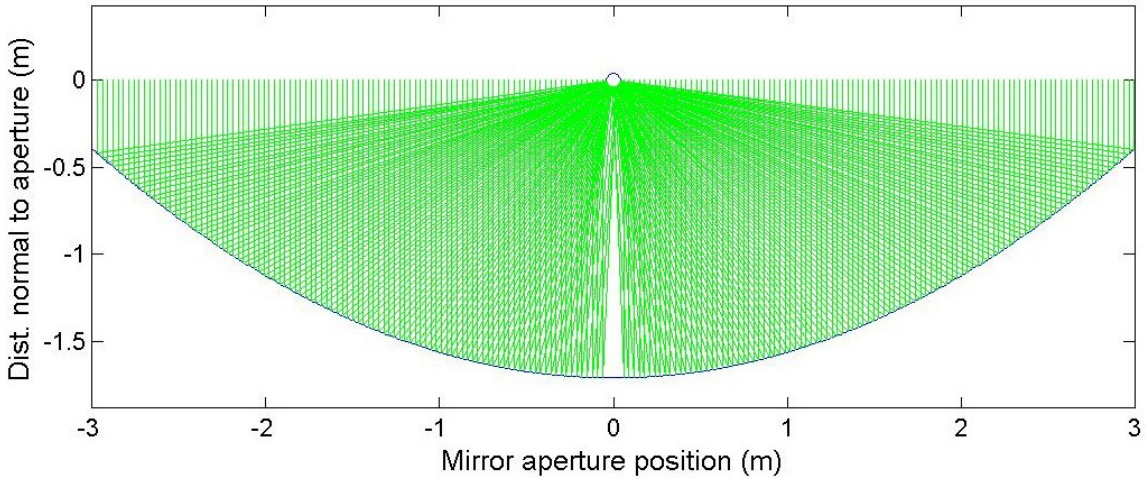

Figure 8. Ray trace results for Panel 9 at 29 ft 9 inches, RMS=1.34, γ =1.00.

Figure 9 shows a ray trace for Panel 9 at 29 ft 9in, just at the left edge of the panel. This panel has extremely low RMS slope error and would result in an intercept of 1.00 for receiver sizes of well under 80 mm.

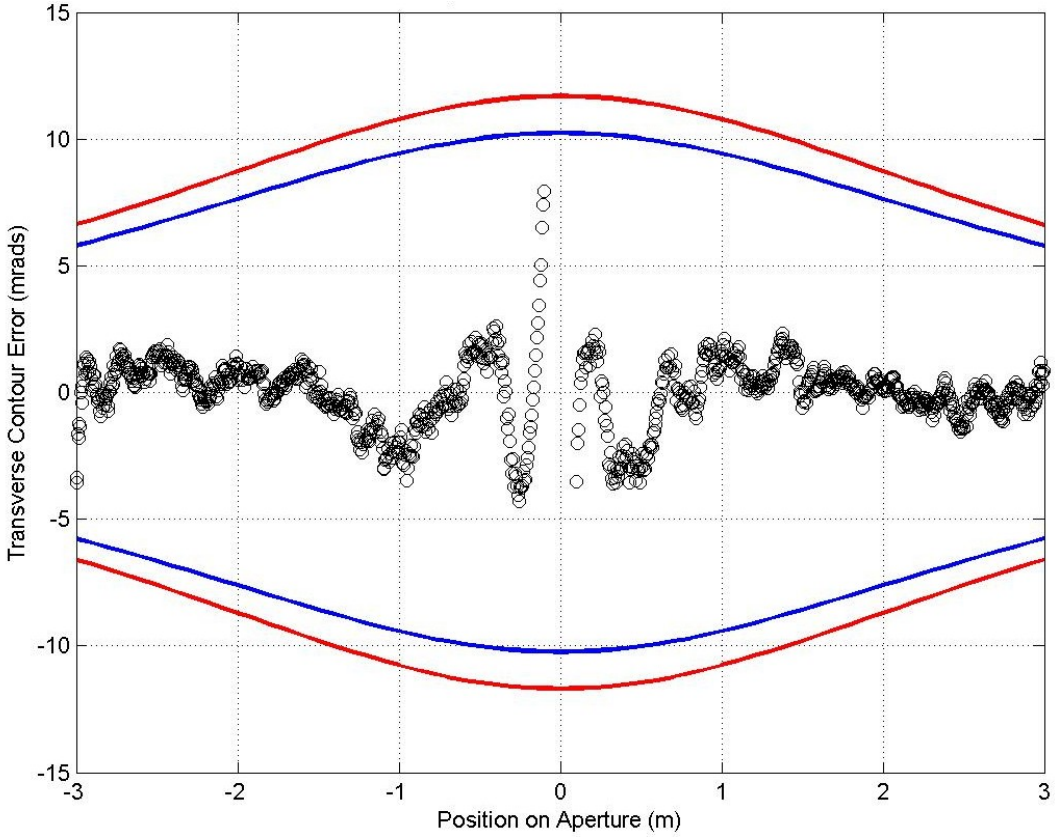

Figure 9. Slope errors along the aperture of Panel 9 at 29 ft 9 inches, RMS = 1.34 mrad.

Figure 9 shows slope errors along the aperture for Panel 9 at 29 ft 9 inches, just at the left edge of the panel. Note that the scale for slope errors is considerably smaller than for Figure 8. In this case there are very few areas along the aperture with errors greater than 2 mrad. Those areas with greater than 2-mrad error are limited to near the vertex.

VSHOT Testing at NREL

Additional VSHOT data was taken at the NREL SIMTA in April 2010 following completion of the optical efficiency testing. In setting up for the VSHOT testing, a small tilt of ~5 mrad relative to vertical was introduced into the aperture orientation. This tilt was removed during the data processing.

Table 3. Summary of Nominal VSHOT Test Conditions for Data Collected.

Date and time	4-08-10 8:00-23:30 MT
Test location	SIMTA
Collector Position	Horizon
Aperture Length	6 m
Collector Length	14 m
Average RMS	1.79 mrad
Average Intercept Factor (parallel rays)	1.00
Average Intercept (DLR Sun Shape)	1.00

Panel 1 was retested to verify that the collector's reflector surface had not changed during shipping and reassembly. Four scans were taken on Panel 1 at approximately 0.13, 0.25, 0.51, 0.76 m (5, 10, 20, and 30 inches) from the edge of the collector. A receiver tube cover is used to protect the receiver from stray light when there is no fluid flow. The diameter of the cover is approximately 0.25 m (10 inches). The cover was on the receiver during VSHOT testing. This caused a gap of about 0.28 m (11 inches) on either side of the vertex where the laser was blocked by the cover.

Table 4 shows the RMS slope errors, intercept factor for parallel rays, and intercept factor for a typical sunshape using the same processing and ray trace methods as described earlier.

Table 4. Slope and intercept data using an 80 mm diameter receiver tube.

File Name	RMS Slope Error (mrad)	Intercept Parallel Rays	Intercept DLR Sun shape
AA p1 05nches.csv	1.77	1.00	1.00
AA p1 10nches.csv	1.65	1.00	1.00
AA p1 20nches.csv	2.15	1.00	1.00
AA p1 30inches.csv	1.59	1.00	1.00
Average	1.79	1.00	1.00

The receiver tube cover prevented slope error data near the vertex from being collected. The vertex area is where the slope errors exceeded the acceptance window in the previous test at Alcoa. Elimination of much of this vertex area in the SIMTA tests caused a reduction in the RMS slope errors and slightly higher intercept factors.

A ray trace plot was generated for each of the four scans. Figure 10 shows the plot for Panel 1 at 5 inches. For each of these plots, no rays miss the receiver and the intercept was 1.0. None of the other plots are shown as they are essentially duplicates

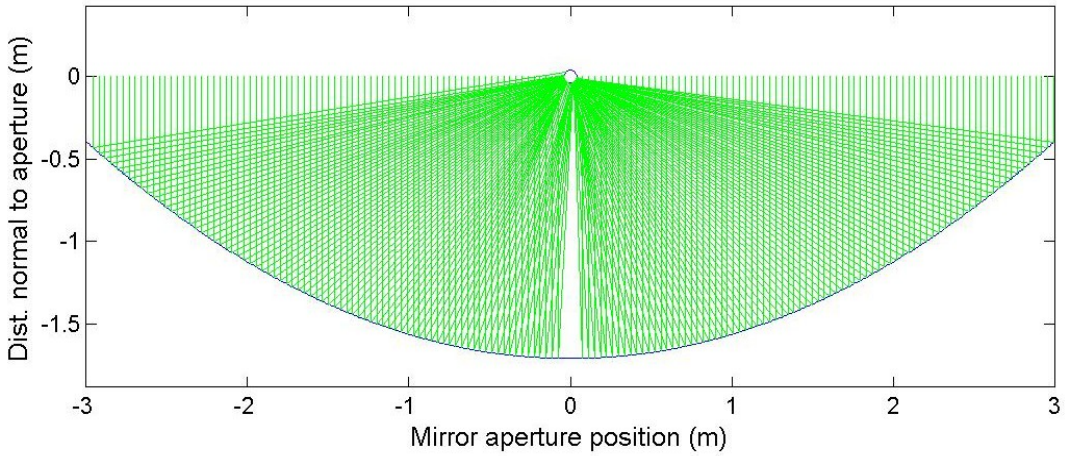

Figure 10. Ray trace results for Panel 1 at 5in, RMS=1.77, γ =1.00.

Figure 11 through Figure 14 compare the scans taken on Panel 1 at the SIMTA with scans taken at Alcoa in regions close to the SIMTA scans. Due to the receiver cover blockage of the vertex area, it is difficult to assess the potential differences in that area. However, in areas near the vertex there are some small differences. For the four scans taken at the SIMTA there also seems to be a small reduction and less variation in slope errors very near to the edge of the aperture.

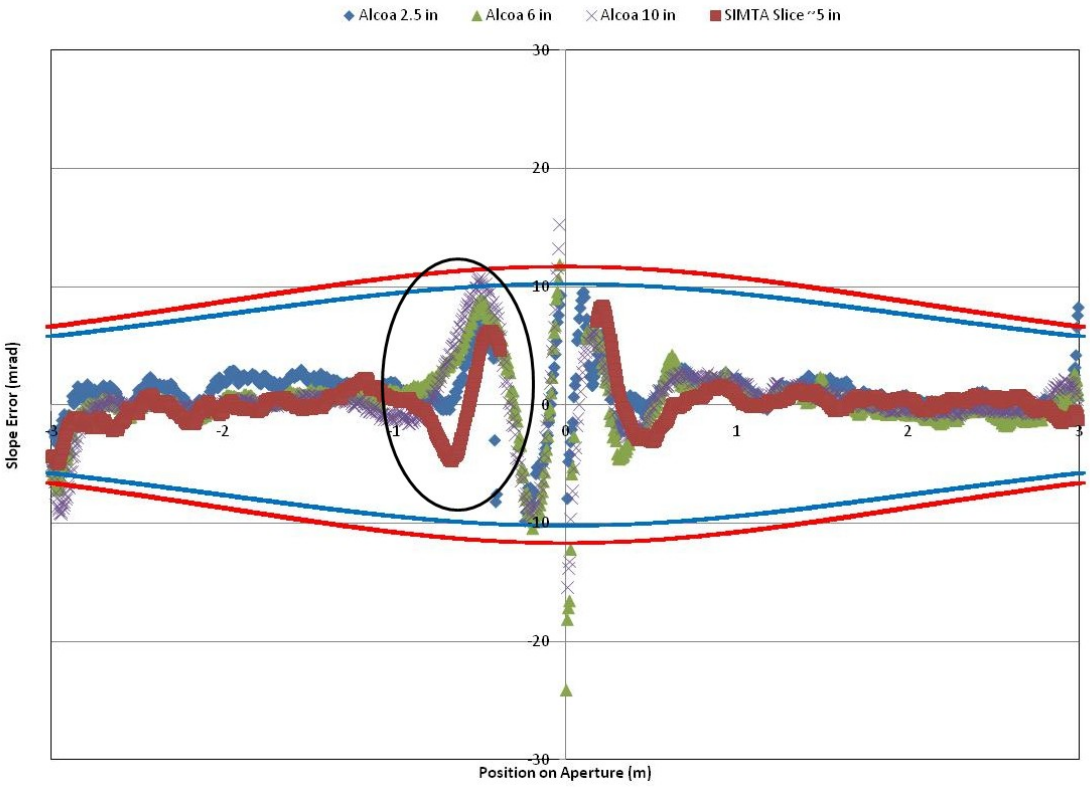

Figure 11. Comparison of scans taken at the Alcoa and SIMTA at 5 inches from the edge.

Figure 11 is a plot of the scan taken 5±3 inches from the edge of the collector at the SIMTA and the scans taken in this region at Alcoa. The slope error results correspond well with the data taken at Alcoa. There is a variation between the slope errors close to the vertex on the negative side of the aperture (circled in black). Within that region the scan taken at the SIMTA has slope errors that reach -4.5 mrad and the ones taken at Alcoa were not less than -0.5 mrad. At the positive side of the aperture, near the edge, the scan taken at SIMTA remains reasonably constant, whereas those taken at Alcoa tend to increase nearest the edge.

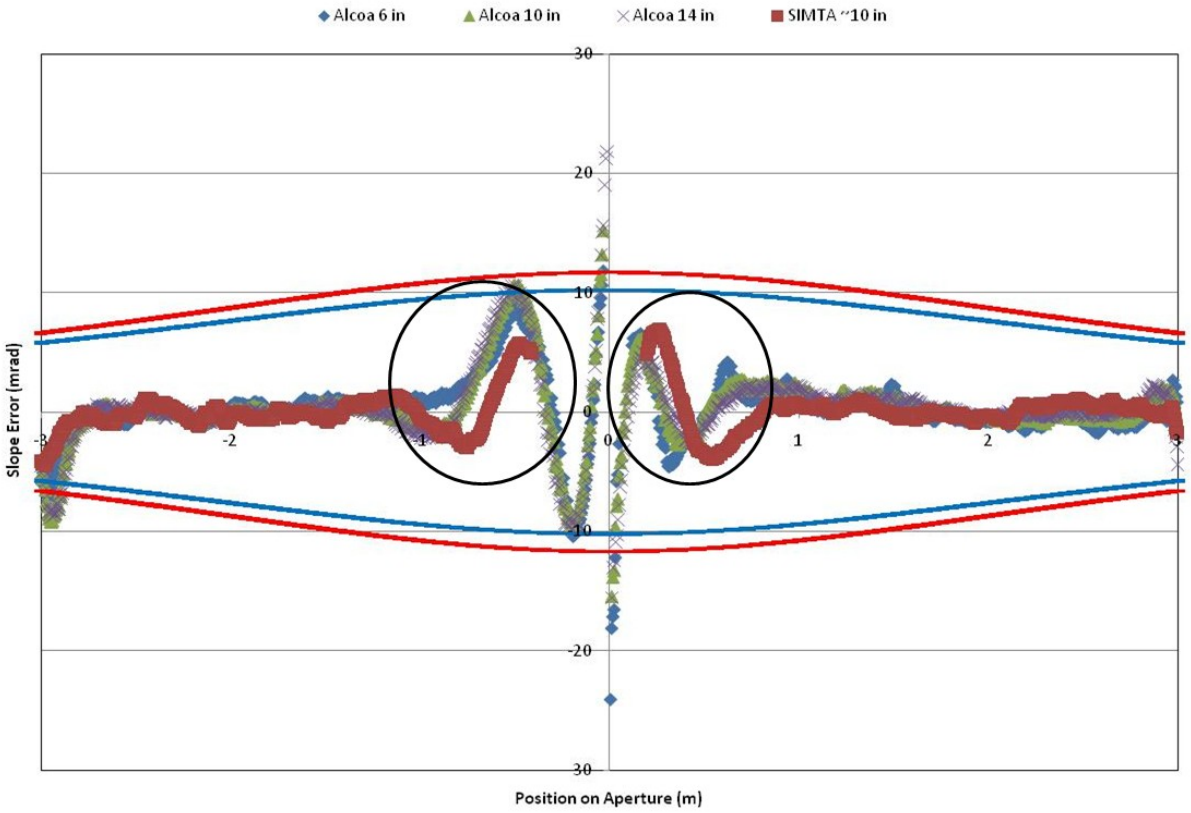

Figure 12. Comparison of scans taken at Alcoa and SIMTA at 10 inches from the edge.

Figure 12 is a plot of the scan taken 10± 4 inches from the edge of the collector at the SIMTA and the scans taken in this region at Alcoa. The slope errors taken at both facilities correspond well. There is a small variation between the slope errors close to the vertex on the negative and positive side of the aperture (circled in black). The slope error for the scan taken at the SIMTA appears to be slightly shifted to the right in these two regions.

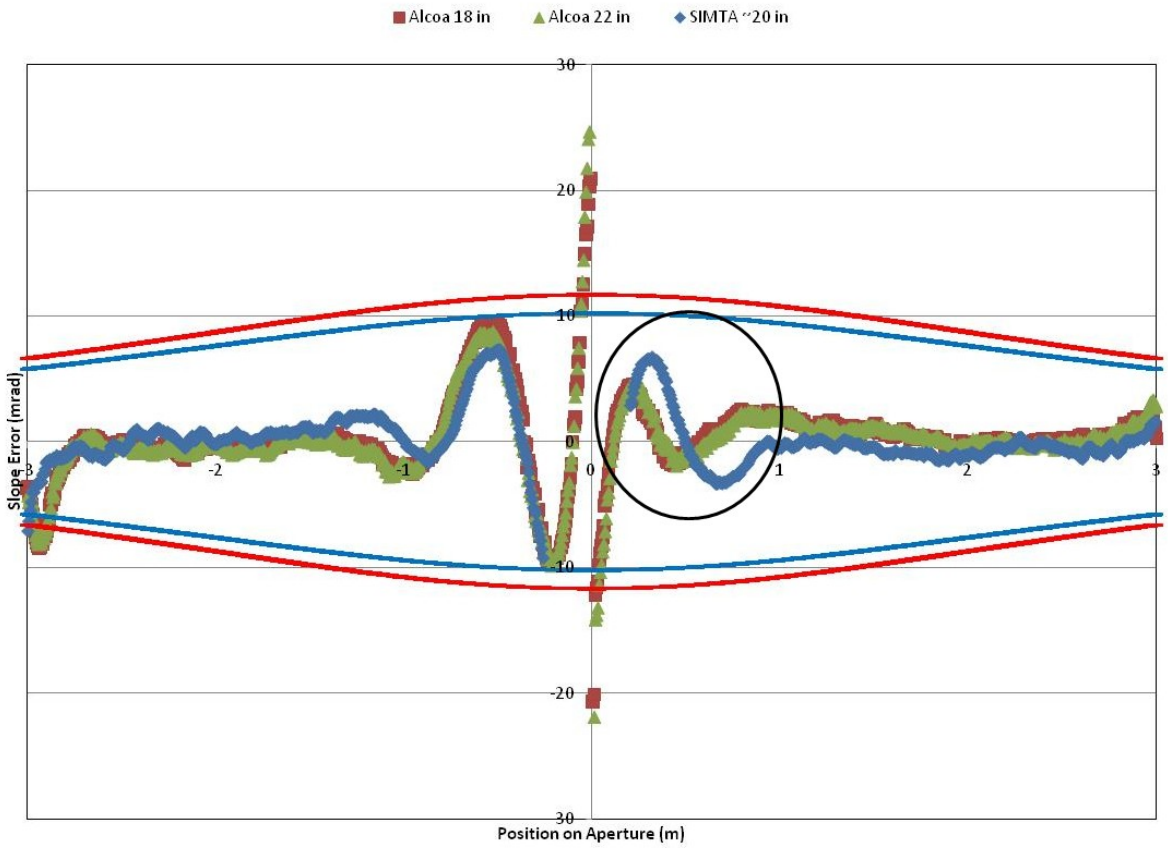

Figure 13. Comparison of scans taken at Alcoa and SIMTA at 20 inches from the edge.

A scan was taken 20±4 inches from the edge of the collector at the SIMTA and is plotted in Figure 13 along with two scans taken at Alcoa in this same region. The slope errors in this scan correspond well with the ones taken at Alcoa. There is a variation between the slope errors close to the vertex on the positive side of the aperture (circled in black). The slope error for the scan taken at the SIMTA appears to be slightly shifted to the right in this region.

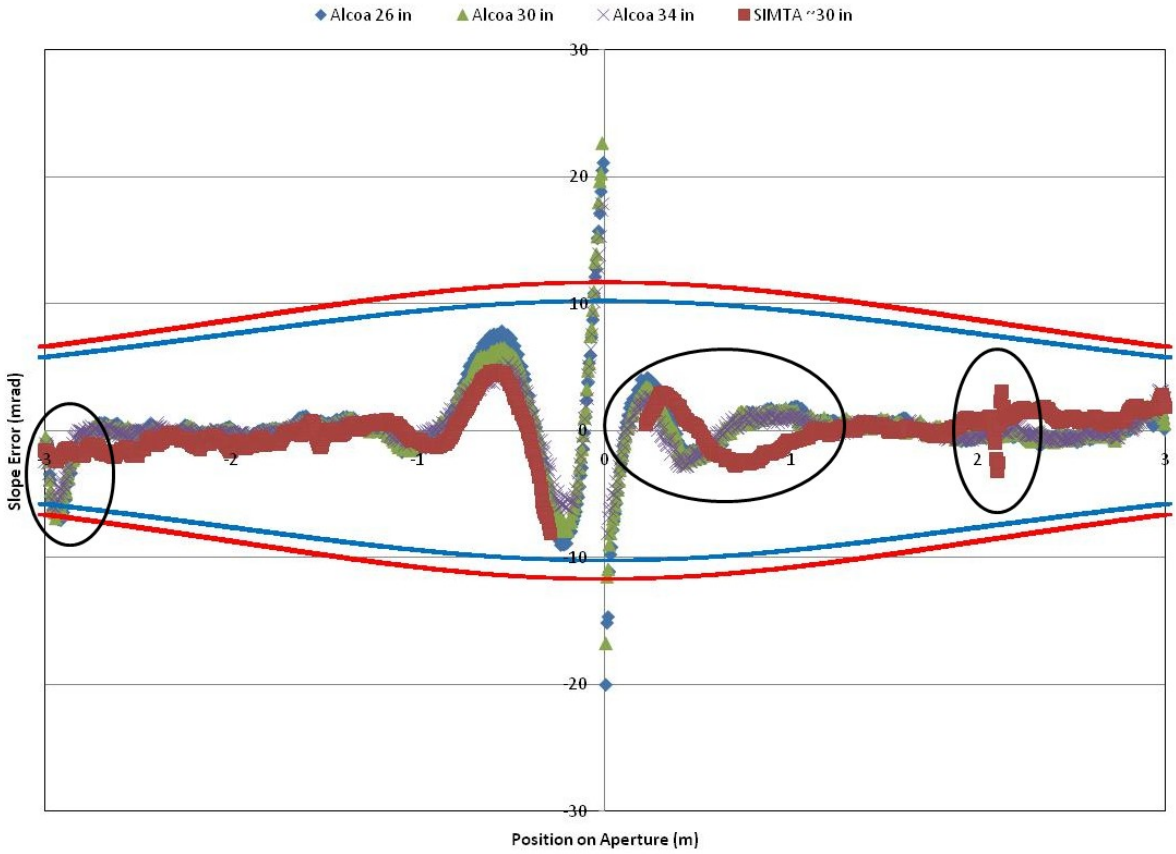

Figure 14. Comparison of scans taken at Alcoa and SIMTA at 30 inches from the edge.

A scan was taken 30±4 inches from the edge of the collector at the SIMTA. The slope errors in this scan correspond well with the ones taken at Alcoa as indicated in Figure 14. There is a variation between the slope errors close to the vertex on the positive side of the aperture (circled in black). The slope error for the scan taken at Alcoa appears to be slightly shifted to the right in this region. There was a ding on the collector at ~+2.1 m that appears in the scan taken at SIMTA. At the negative side of the aperture the SIMTA scan shows far less variation than the previous scans.

Additional Ray Trace Results

In addition to processing the VSHOT results for slope error and intercept factor, three additional studies were completed. These three include intercept for a variety of receiver tube sizes, receiver tube misalignment, and tracking errors. Each of these studies generated average intercept factors for each of the scans on the 14 panels. The results are shown averaged for each panel.

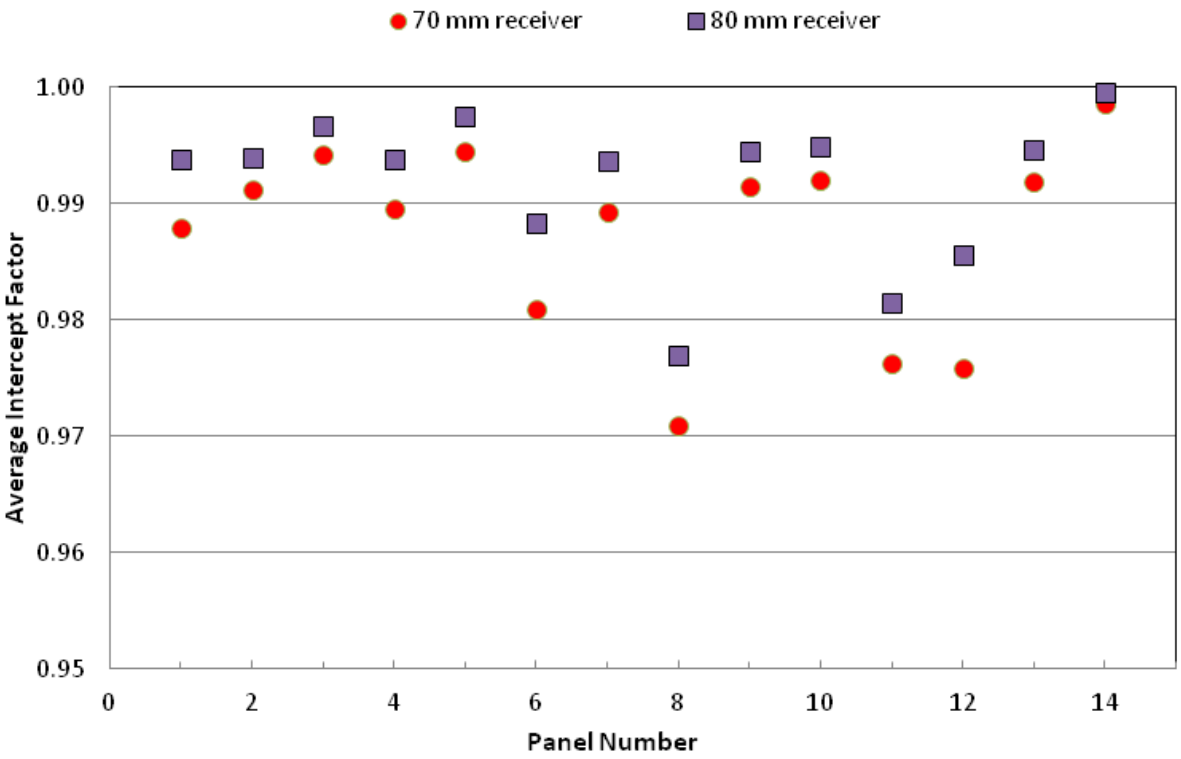

Figure 15. The average intercept factor (parallel rays) for each panel is plotted for receiver tube diameters of 70 mm and 80 mm.

Figure 15 shows the average intercept factor for 70 mm and 80 mm diameter receiver tubes when parallel rays from the sun are used. The results indicate a potential improvement in intercept for an 80-mm diameter receiver of between 0.0025 and 0.01, depending on the panel. This variation is due to the different distributions of errors in the various panels. Note the difference between the predicted intercept for Panels 11 and 12. Panel 12 clearly has a greater proportion of errors near the bounding envelope and thus increasing the receiver diameter has a greater impact.

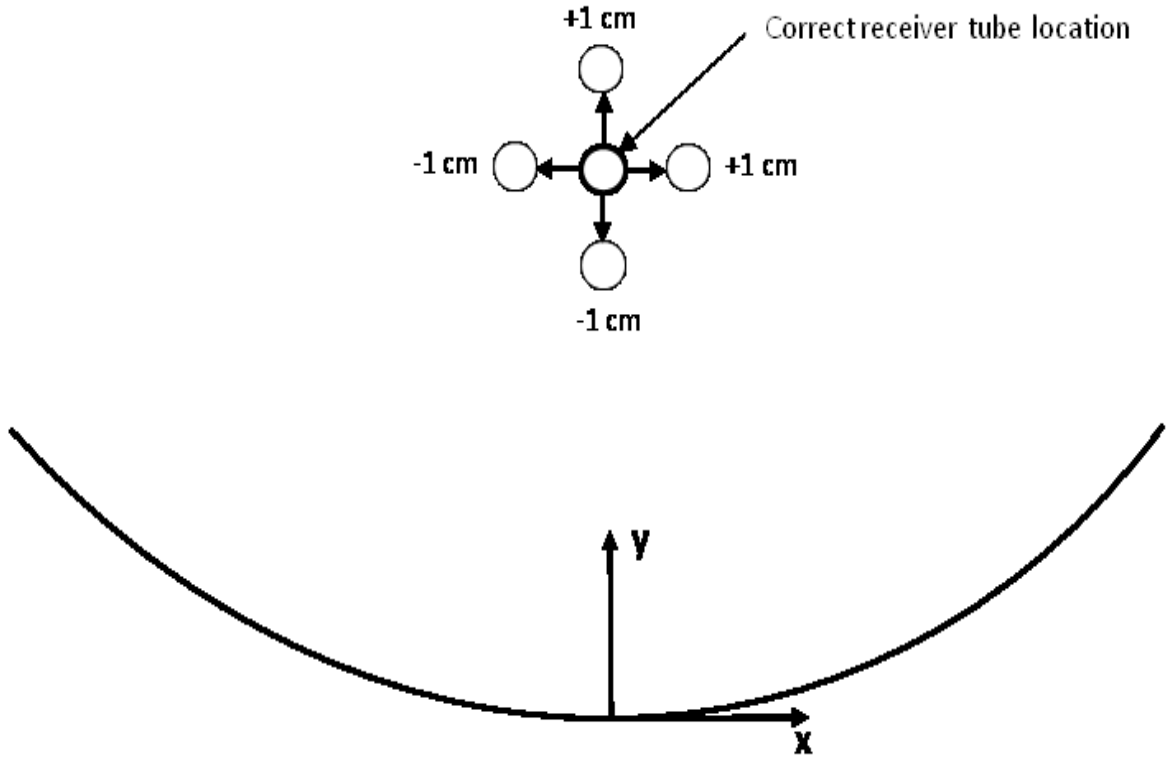

Figure 16. Ray traces were generated for 5 receiver positions corresponding to the positions in the figure.

The location of the receiver tube relative to the design can have a significant effect on optical performance. Receiver tubes can sag up to 1 cm between supports and can be mounted in the wrong location. There can be structural deformation that is a function of elevation angle or there can be thermally induced distortions that cause the receiver to be misaligned. Figure 16 shows the receiver tube positions that were considered.

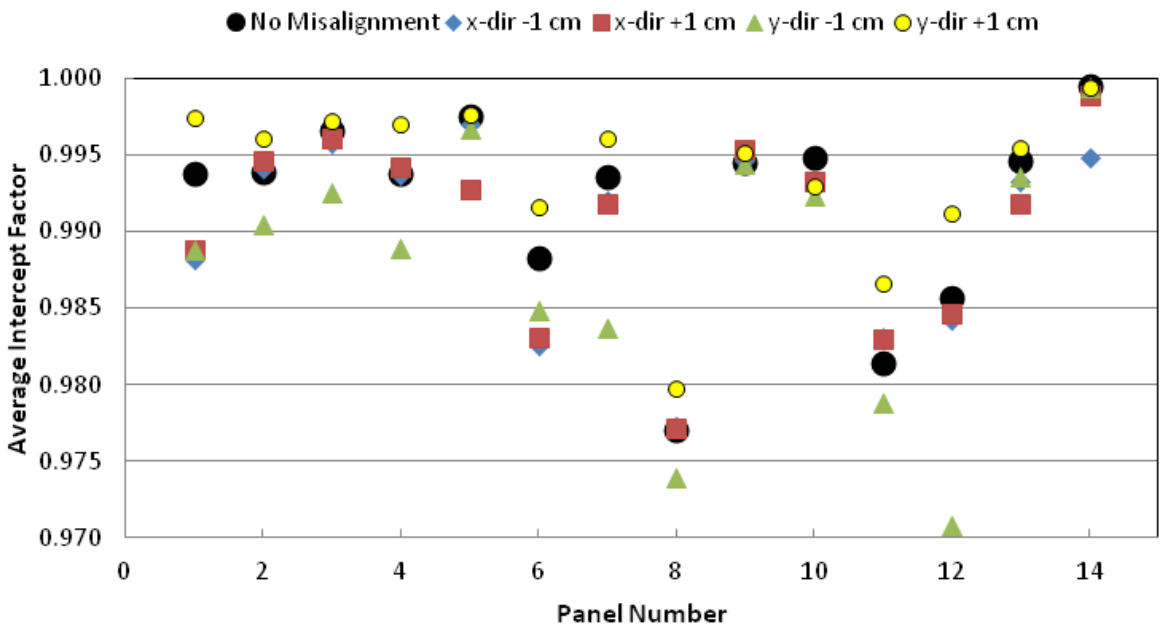

Figure 17. Average intercept factors for various receiver positions.

Figure 17 shows the impact of receiver position on average intercept for the 14 panels. Some panels, notably Panel 9, show almost no impact of receiver misalignment. Note also the wide range in average intercept for Panel 12. These results do not generally correlate with the average RMS slope errors. Both panels have relatively high values of slope error so these results must be a function of the particular distribution of slope errors for the scans collected. It is interesting to note that for this collection of scans, a receiver position +1 cm higher in the y direction almost always results in an improved intercept. This is caused by those errors that would miss the receiver in its nominal position miss above. The +1 cm movement does not result in more rays missing below.

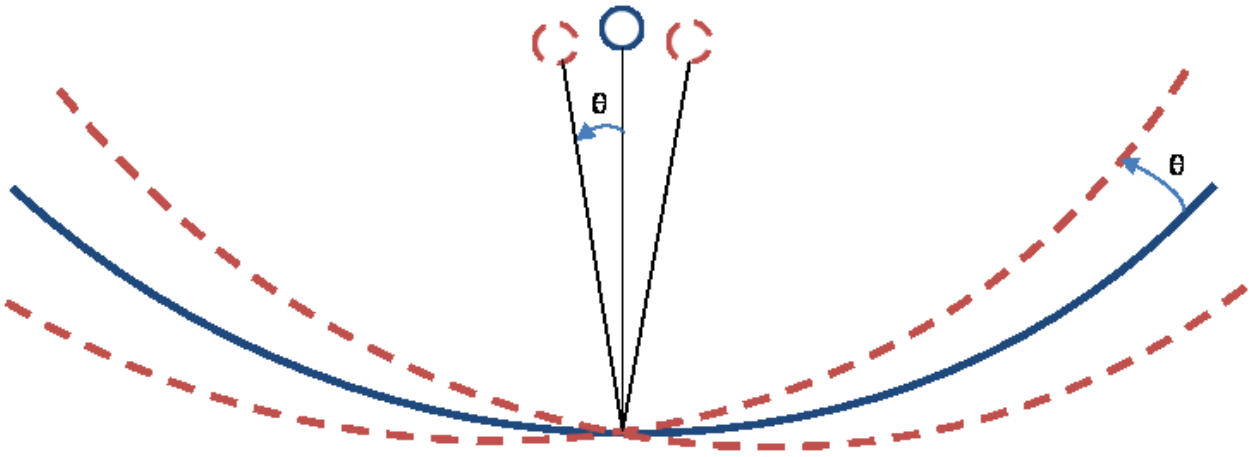

Figure 18. Tracking errors in the transverse direction can decrease the intercept factor.

Tracking errors were modeled by moving the sun relative to the module/receiver at five different transverse angles: 0 (no tracking error), ±0.1° (1.75 mrad) and ±0.2° (3.49 mrad) as indicated in Figure 18.

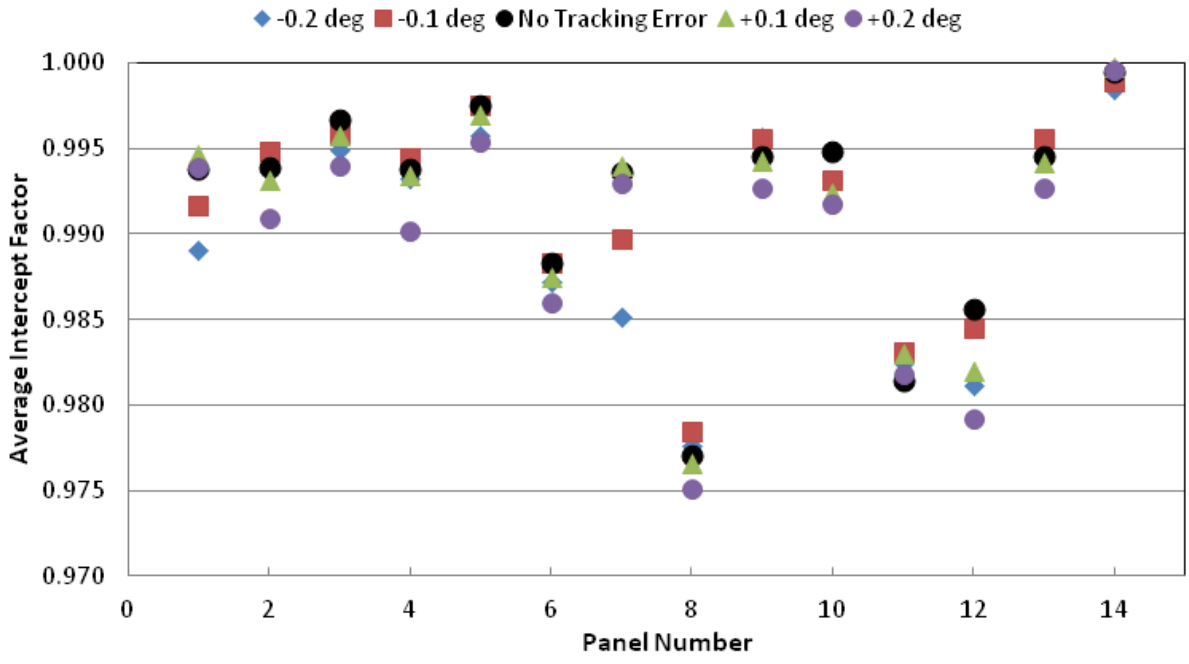

Figure 19. Intercept factor for tracking errors of -0.2° to +0.2°.

The tracking error sensitivity shown in Figure 19 indicates a very similar pattern to that of receiver misalignment. Most panels that show poor alignment sensitivity also show worse intercept factors with increased tracking error.

Overall Comments – VSHOT Testing

VSHOT testing and data processing clearly show that the Alcoa prototype has an intercept factor of 0.99. There are only small areas near the vertex and outer edges where improvements would increase optical performance. Ray tracing the 159 scans predicts an average RMS slope error of 2.70 mrad and a predicted average intercept factor of 0.99 (for an 80-mm diameter receiver). On average, only 3 panels show consistently poorer performance (relatively): Panels 8, 11 and 12. Additional VSHOT testing at NREL's SIMTA showed very similar results, validating the low slope errors and predicted intercept factor. There were a few areas on the single panel tested at SIMTA that showed some differences from previous test results, but these were within the acceptance envelope bounds maintaining high intercepts.

Optical Efficiency Testing

Background

The NREL Optical Efficiency Test Loop is used to determine the optical efficiency of parabolic trough solar collectors. Preliminary design and development of this facility began in the fall of 2007 and was completed in the summer of 2008. In January 2010, a prototype trough from Alcoa was installed. The Alcoa trough is nominally 14 m by 6 m in overall extent with an 83.68-m^2 aperture and uses three Schott PTR-80 receivers. The trough was tested for optical efficiency at normal incidence and incidence angles up to 50°.

The collector is mounted on an APS two-axis tracker at NREL's SIMTA (Figure 1). Figure 20 shows a simplified schematic of the closed-loop test system. Fluid from the storage tank is pumped through an electric heater and then up to the trough. The heater output can be modulated to maintain a constant inlet temperature to the trough. The pump motor is controlled by a variable-frequency drive, with the frequency modulated to maintain a constant flow rate through the system during data collection.

The receiver tube is connected to the system via hoses. The heated fluid exiting the receiver tube is directed through a three-way diverter valve. This valve adjusts the amount of fluid sent through a heat exchanger to be cooled by a vapor compression chiller to achieve a set mix-point temperature. The mix-point temperature is set a few degrees below the desired trough inlet temperature. By overcooling and reheating, the loop is able to achieve a more stable trough inlet temperature. The heat-transfer fluid used in this experiment was an approximately 43% (vol.) mixture of propylene glycol and deionized water. Figure 21 shows the complete piping and instrumentation diagram. A general plan for trough testing is included in Appendix 3.

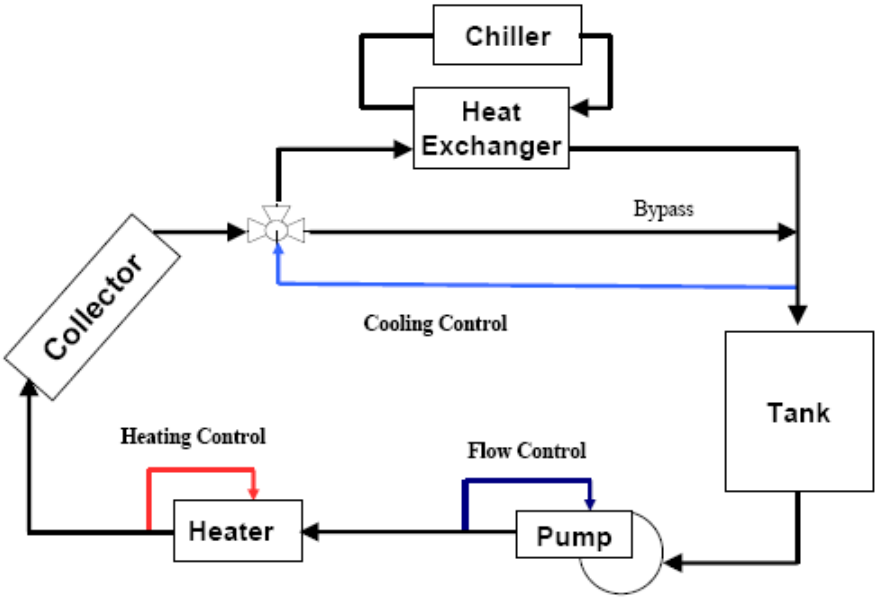

Figure 20. Schematic of the Optical Efficiency Test Loop.

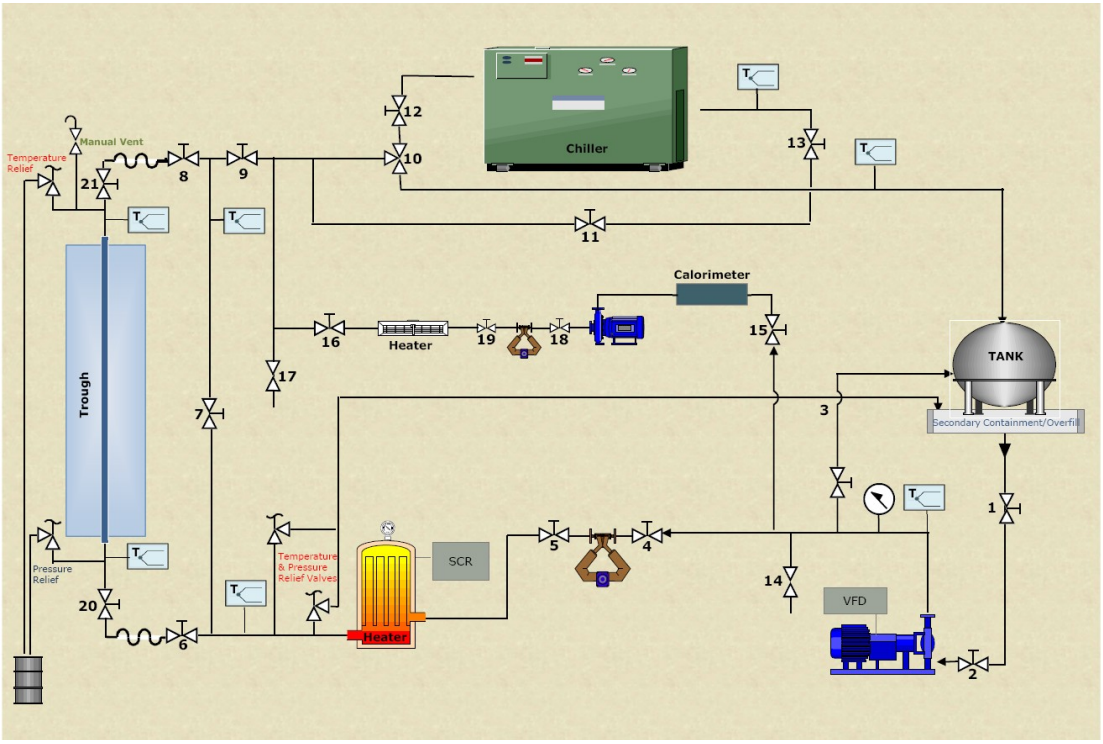

Figure 21. Piping and instrumentation diagram for the Optical Efficiency Test Loop.

Methodology

When the inlet collector temperature is kept within 15°C of the ambient air temperature— so that thermal losses to the environment are kept extremely low—the instantaneous optical efficiency ( ) can be calculated with Eq. (5) from the experimental data.

$$\eta_{opt} = \frac{\dot{m} c_p (T_{out} - T_{in})}{I_{DN} A_{aperture}} \quad (5)$$

The mass flow rate ( ) of the fluid is measured directly with a MicroMotion Coriolis-type mass flow meter. The temperatures at the trough inlet ( ) and outlet ( ) are measured with precision resistance temperature detectors (RTDs) that were calibrated at the Solar Research Radiation Laboratory (SRRL). Signal conditioning in the field is used to eliminate lead wire effects in these RTDs. The measurement of the direct-normal solar irradiance ( ) is obtained from a Kipp and Zonen CH1 pyrheliometer at SRRL[1], 20 m away. The specific heat of the heat-transfer fluid ( ) is determined using Engineering Equation Solver (EES) after measuring the volume concentration of glycol by a handheld refractometer. The procedure in EES was originally based on equations and data in the IIF handbook on secondary refrigerants.

[1] This pyrheliometer is frequently calibrated against a reference standard cavity radiometer.

For the propylene glycol-water mixture, EES uses the mass concentration of the mixture to determine the specific heat. The volume concentration is first determined with an Atago digital refractometer. Volume concentration is converted to mass concentration, and the built-in property functions in EES are used to determine the specific heat of the coolant. Volume concentration is measured each day during a test and a typical specific heat value is 3688 J/kg-K for a volume concentration of propylene glycol of 42.8%. To ensure that the fluid inlet temperature is close to ambient temperature and heat losses are negligible, the ambient air temperature is measured on site. Air temperature is taken with an RTD located within an aspirated probe containing two radiation shields.

Data Acquisition

A National Instruments PCI-MIO-16XE-50 data acquisition system with an SCXI 1102 module is used to acquire data from the measurement instruments. A data acquisition and control program written in LabVIEW 8.5 is used to organize and record data. Data are recorded every second as a 10-sample average. Figure 22 shows a screen shot of the virtual instrument.

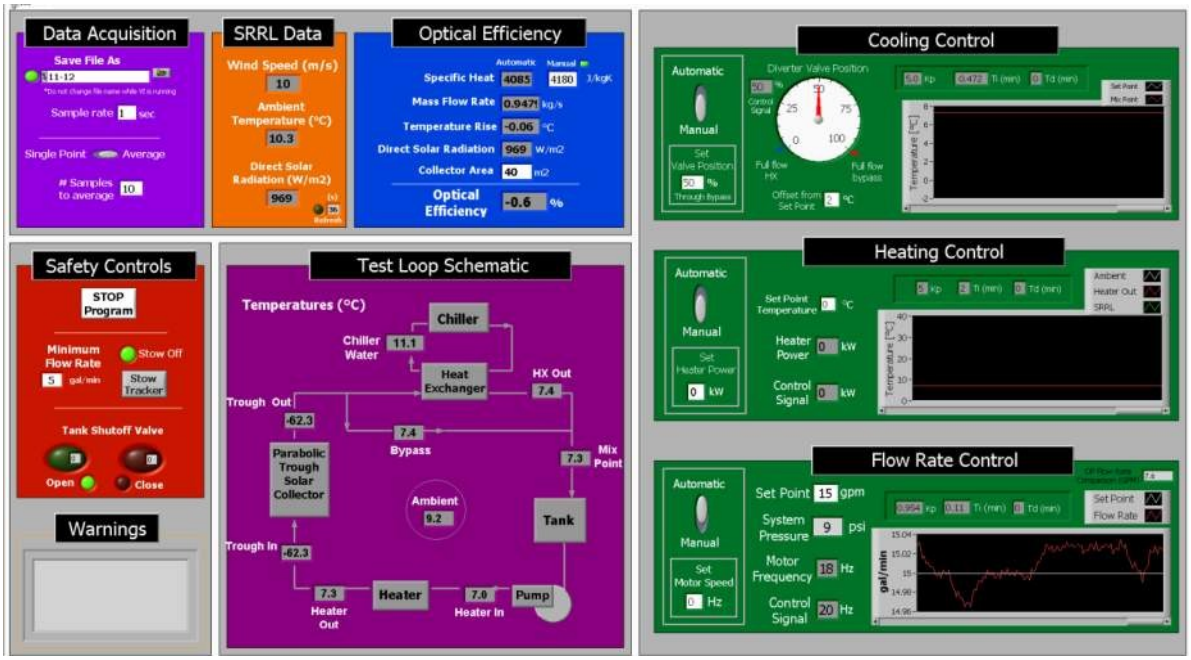

Figure 22. LabVIEW data acquisition and control program interface.

The optical efficiency test loop uses three feedback control loops to provide operator control and maintain steady-state conditions (shown on the right of Figure 22 in the three green panels). The cooling control modulates the position of a three-way valve to divert fluid through a plate-frame heat exchanger in the chiller coolant loop, or to bypass the heat exchanger and return to the storage tank.

The process variable for the cooling control is the fluid temperature at the inlet to the tank (labeled "mix point" in Figure 22). The set-point for this variable is controlled by the operator; however, it is usually set to 1°C below the trough inlet temperature. The cooling control works

in combination with the heating control to supply fluid to the trough inlet at a constant temperature. The heating control allows the user to provide a set-point for the trough inlet temperature. Because the cooling control is set below the trough inlet temperature, the fluid is overcooled and then reheated for increased precision.

The final control loop is the flow-rate control that maintains a constant flow rate as specified by the operator. The flow-rate control is necessary to accommodate changes in pressure drop through the system as the position of the three-way diverter valve is varied and fluid properties change with change in temperature. Each control can be adjusted manually or automatically. The manual mode allows the operator to input a set value for the three-way valve position, heater power, and motor frequency. During the shakedown period, the gains for the proportional, integral, and derivative components were tuned for fine control of flow rate, mix temperature, and supply temperature.

Results

The trough reflective surfaces and glass envelope of the receiver tubes were pressure-washed with deionized water after an application of a dilute solution of laboratory detergent. Coolant flow was started and allowed to stabilize. The temperature rise through the receiver tube was checked to be zero with receiver tube covers in place so that the tube was receiving no light at all. The covers were removed and the trough was then put on-sun.

The position of the receiver shadow was observed at the tube support bases and centered by making adjustments in the tracker control program, WinDial. The efficiency was observed while making these adjustments to ensure the trough was as close to being on its optical axis as possible. Final optical efficiency calculations were taken during periods of thermal stability of the test loop. As described in the test methods section of the appendix, periods of stable beam radiation and entering coolant temperatures were chosen as data subsets for averaging. This process was done manually by inspecting the data from the entire test and evaluating parameters such as standard deviation, which should be minimized in thermally stable regions, and looking for obvious transients that result in impossibly high or low efficiency. Data was averaged over the stable period, which had to be at least 10 minutes long, to deliver the optical efficiency value. The washing process and optical alignment check were done for each test day. Thermal equilibrium was often disturbed by clouds passing in front of the sun or windy conditions that would cause the tracker to move. Under those conditions, the efficiency values were not considered valid.

Optical Efficiency Performance

The optical efficiency was recorded throughout the day for each of the two tests on March 2 and 21, 2010. On these days, weather conditions were clear and calm, with direct-normal radiation values in the range of 850 to 1,000 W/m^2. Conditions on other days during this period were not favorable for optical efficiency testing, due to cloudiness and precipitation, high winds, or because work was being performed on the trough or test equipment. Flow rate through the receiver tube was 26 gpm, or 1.64 kg/s, which is ~0.02 kg/s per square meter of aperture area. Typical temperature rises under these conditions were about 10°C. The average optical efficiency measurements for these tests were 74.7% and 74.9%, respectively, showing excellent repeatability. Efficiency plots are shown in Figure 23 and Figure 24. Uncertainty of each measurement is shown in these figures in gray, measured data in blue.

Appendix 2 describes the uncertainty analysis and the general test conditions/requirements are summarized in Appendix 3.

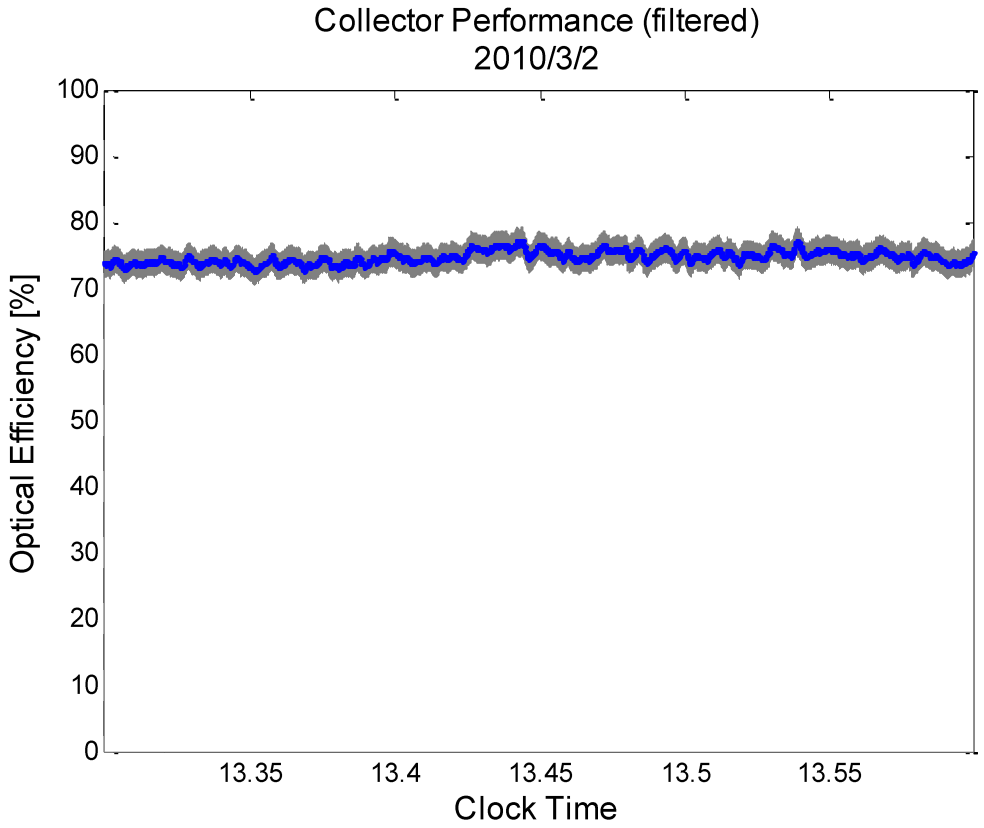

Figure 23. 74.7% result on March 2, 2010.

Figure 23 shows the calculated efficiency over the time period for the 74.7% result along with the estimated efficiency.

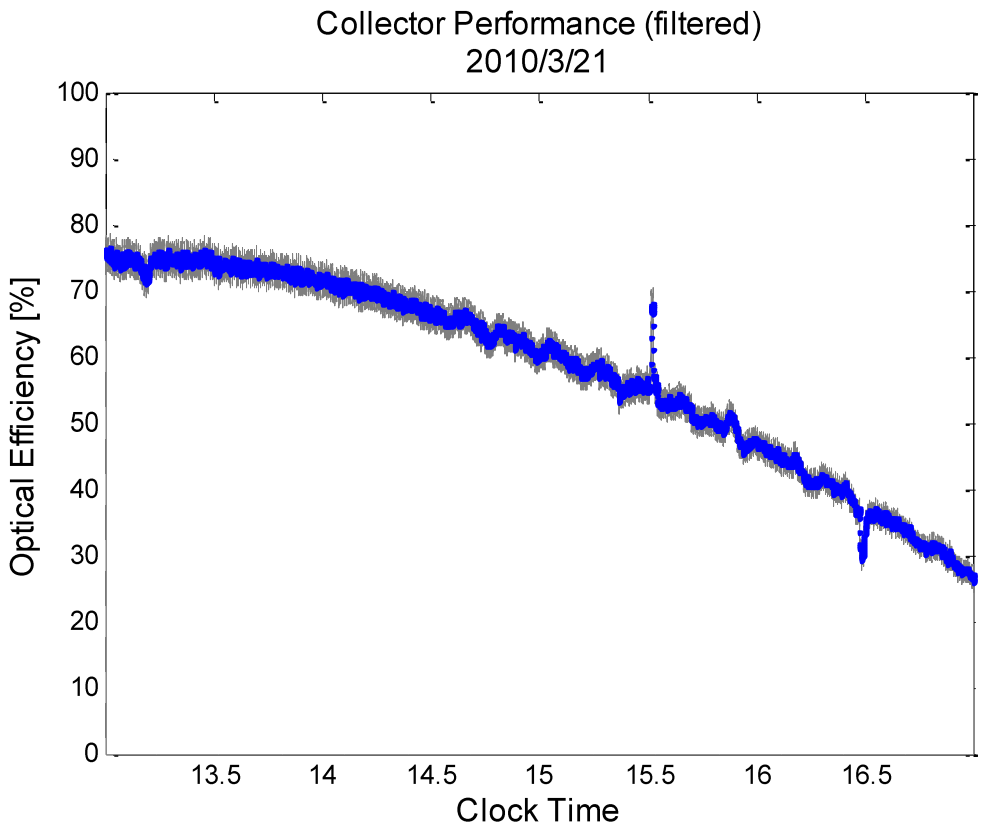

Figure 24. 74.9% result at solar noon (0° incidence angle) on March 21, 2010

Figure 24 includes incidence angle modifier results, discussed in the next section. For comparison to the test on March 2, the value just before solar noon is used. Note also that the data is plotted as a function of clock time. For this test on the equinox, the incidence angle changes by 15^{o} every hour with solar noon (0^{o} incidence at clock time 13:07). Data was collected all afternoon and converted from clock time to incidence angle for subsequent analysis.

Table 5. Summary of Nominal Trough Test Conditions for Data Collected.

Date and time	3-2-10 13:30 MST
Irradiance	1011 W/m^2
Incidence angle	0^o
Aperture	83.68 m^2
$T_{ambient}$	9^{o}C
Flow rate	1.6 kg/s
C_p	3681 J/kg-C
T_{in}	12^{o}C
T_{out}	23^{o}C
Efficiency	74.7% std. dev. 0.81%

Date and time	3-21-10 11:00 to 17:00 MDT
Irradiance	1001 to 805 W/m^2
Incidence angle	0^o to 50^o
Aperture	83.68 m^2
$T_{ambient}$	10^o to 12^o C
Flow rate	1.6 to 1.3 kg/s
C_p	3677 J/kg-C
T_{in}	12^{o}C
T_{out}	23^o to 17^o C
Efficiency	74.9% std. dev. 0.98% at solar noon

Table 6. Parameters Composing the Optical Efficiency of a Parabolic Trough. These parameters are from the Solar Advisor Model (SAM); values are adjusted to provide an estimate of the optical efficiency for the Alcoa collector as tested at the OETL.

Receiver optical parameters	**Schott PTR80**[1]
Bellows shading	0.963
Envelope transmittance	0.971
Absorber absorptance	0.960
Solar collector assembly factors	**Alcoa**
Tracking error and twist	0.999
Geometric accuracy	0.99
Mirror reflectance	0.88[2]
Mirror cleanliness field (average)	0.99[3]
Dust on envelope (average)	0.99
Total optical efficiency	**0.766**

Table 6 shows the estimated optical parameters for a Schott PTR80 and estimated parameters for the Alcoa collector. The combination of these optical losses yields a total optical efficiency of 76.6%. This value is almost 2% (absolute) higher than measured. It is possible that actual values of reflectivity, absorptance and transmittance were not the nominal values referenced.

[1] Values for envelope transmittance and absorber absorptance from [7]. Bellows shading from measurement of PTR80 at NREL

[2] Measured value for Alanod MIRO-SUN reflective material into 25 mrad aperture.

[3] Mirror cleanliness and envelope dust are assumed to be 0.99 after cleaning of the surfaces prior to testing.

Although arbitrary adjustment of these parameters cannot be justified without direct measurement, it would take only a small reduction in absorptance and transmittance to reduce the calculated product to the measured optical efficiency. Small adjustments in the cleanliness parameters could have the same impact. In addition, the bellows and welded sections between receiver tubes were not covered with an insulating shield. However, the small bare sections at the welds would probably result in a small additional heat gain compared with typical field installations.

Incidence Angle Modifier

Incidence angle modifier (IAM) tests were performed at angles up to 50°. During an IAM test, the trough is focused in elevation but the incident beam radiation enters the aperture at an acute angle to the receiver tube. When troughs are installed on single axis trackers, this is typically the way beam radiation enters the trough aperture. The IAM test was performed on the vernal equinox. On either equinox the sun's declination is essentially zero, which means that only minor elevation changes (or tracking updates) are needed to maintain focus. This allows the tracker to be put in a stationary position, with azimuth facing south and elevation fixed at the local latitude. It was only coincidental that testing was conducted on the equinox. Normally, the sun sensor on the tracker is adjusted to maintain a constant incidence angle.

Due to the dropping beam radiation in the afternoon, the receiver tube outlet temperatures were time shifted so that they matched the inlet temperatures, given the estimated time for the fluid to travel the length of the tube at the particular flow rate at that time. This prevented an upward bias in the efficiency calculation. The end effects of a single trough are considered in the test results and the reported IAM modifiers are appropriate for very long strings of troughs. Corrections to the results were made according to Gaul and Rabl [6] to account for end effects and shading by the radiation shields on the end-tube supports. The ratio of the two efficiencies at 0° and the particular incidence angle is the IAM for that angle.

Table 7. Incidence-Angle Modifier Test Results

Angle	0 deg.	Measured	Infinite tube	Cosine corrected	Relative to 0 deg.
0	74.93				1.00
5	74.93	74.12	74.99	75.28	1.00
10	74.93	71.815	73.75	74.89	1.00
15	74.93	70.07	73.08	75.66	1.01
20	74.93	66.95	70.99	75.55	1.01
25	74.93	62.94	67.95	74.97	1.00
30	74.93	59.2	65.18	75.26	1.00
35	74.93	54.47	61.32	74.86	1.00
40	74.93	49.56	57.25	74.73	1.00
45	74.93	43.83	52.2	73.82	0.99
50	74.93	36.99	45.73	71.14	0.95

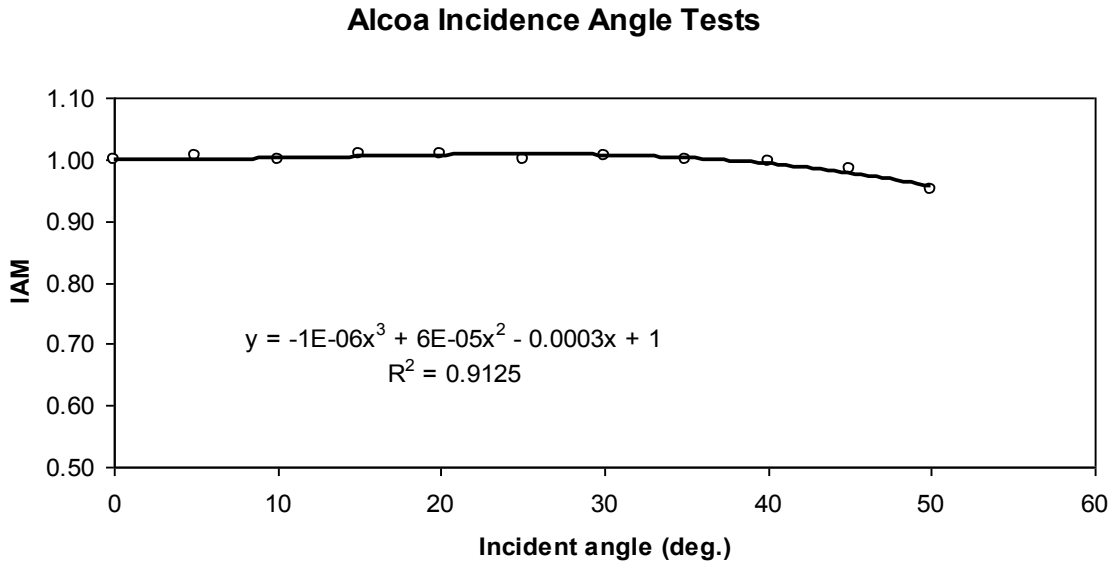

Figure 25. IAM results with curve fit.

Figure 25 shows the IAM results and a cubic curve fit. Note that the curve fit coefficients cannot be used directly for SAM modeling without additional processing that is beyond the scope of this report. These results are remarkably flat, perhaps due to the use of the larger diameter PTR-80 receiver. At non-zero incidence angles, rays will travel farther from reflector intersection to receiver and will spread farther from the ideal path (due to sunshape, slope, and specularity errors). With a larger receiver tube, there is potentially more receiver area to capture those slightly spread rays. This would be more likely with reflector surfaces that have relatively low slope errors, as is the case with the Alcoa collector.

Overall Thermal Efficiency

The overall thermal performance of a trough collector, when operating at temperatures above ambient, can be determined from its optical performance and the heat loss from its receivers. Testing at elevated

temperatures at or near those expected in field operation requires a test loop capable of delivering heated fluid to the collector at constant temperature. This capability exists at Sandia on their rotating platform [8]. Another approach is to independently test optical efficiency and receiver heat loss, and then calculate the thermal efficiency curve from these measured quantities. NREL's Receiver Heat Loss Test Facility has tested a number of evacuated receivers, including the Schott PTR80. Burkholder [9] describes this testing capability.

The overall efficiency is the difference between the optical efficiency and a heat loss term.

$$\eta = \eta_o - n_L \quad (1)$$

where η_0 = measured optical efficiency and

$$\eta_L = \frac{n \cdot q_L}{I_{DN} A_{Coll}} \quad (2)$$

The heat loss, q_L, is the total heat loss (W) from an individual receiver. Because there are three receivers in the tested collector module, n=3. Values for q_L are given as a function of absorber temperature in Table 8 for recent, unpublished as yet, tests of a single, improved Schott PTR80-4.7 receiver. Identical receivers were installed on the Alcoa collector for optical testing.

Table 8. Measured heat losses for a single PTR80 receiver tube

Absorber (°C)	Heat Loss (W)
113	62
209	194
254	305
297	464
306	507
355	754
398	1111
405	1130
445	1565

These heat losses are very low due to the evacuated receiver design, high absorptance, and low emissivity coating. The data in Table 8 are shown in Figure 26 (plotted per unit receiver length) along with a fit that includes linear and fourth order terms as a function of absorber tube temperature. This form was somewhat arbitrary and was used because radiative losses are a function of T^4. Other fits are possible, however this form shows excellent agreement with the data.

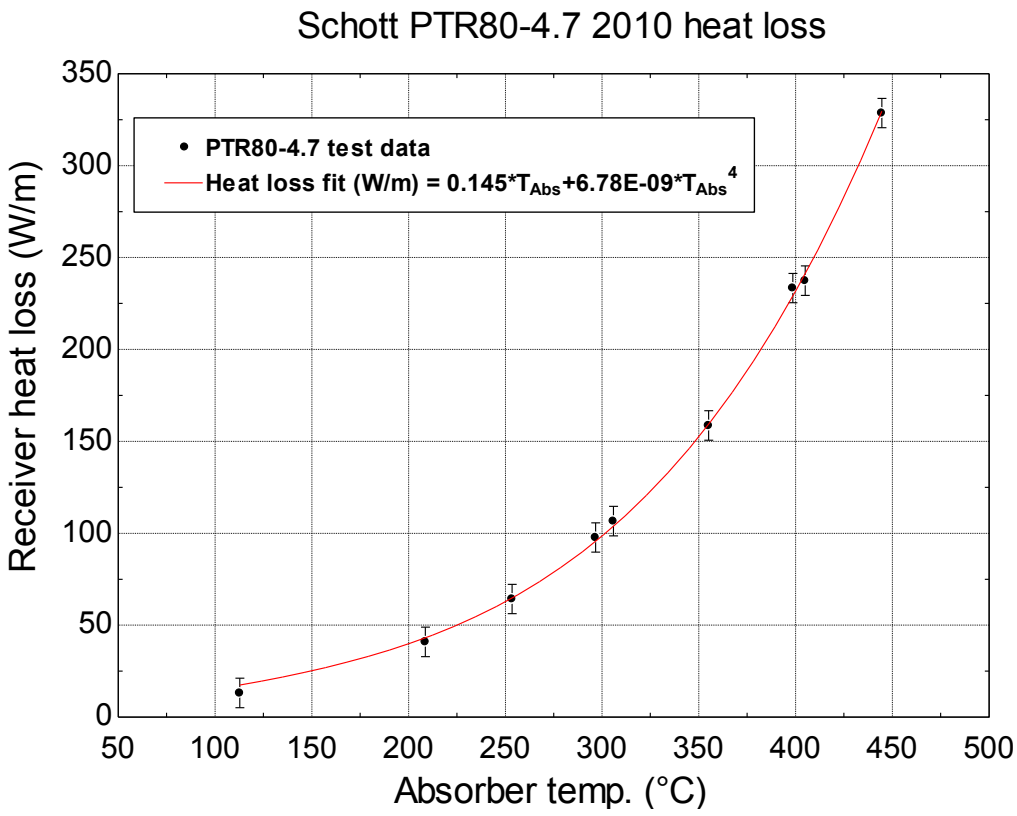

Figure 26. Recent heat loss test data for the Schott PTR80-4.7 receiver tube.

Typically the absorber temperature is not known in the field. Because fluid temperature is either known or can be reliably estimated, it is necessary to determine the difference between absorber temperature and fluid temperature for a range of operating conditions. A one-dimensional model [10] was used to generate the relationship between absorber tube temperature and fluid temperature. For a wide range of conditions when sunlight is concentrated onto the receiver, the absorber tube temperature is elevated by roughly 6°C above the fluid temperature. This difference is used in calculating the overall efficiency with heat loss test data that is a function of the fluid temperature as shown in Figure 27.

Another issue is the ambient conditions (air temperature, effective sky temperature, and wind speed). Because the heat losses are so low with evacuated tube receivers, these parameters have very little impact on the heat losses. In a report on testing the Schott PTR70 receiver [9] it was demonstrated that decreasing both the sky and ambient temperatures by 13°C results in an increased receiver heat loss of only 2 W/m. This increased loss results in a decrease in collector efficiency of 0.05%. Similar results were obtained for wind-induced losses. The conclusion is that heat loss is a very weak function of ambient conditions and those conditions can essentially be ignored in the calculations.

There is still an advantage in plotting an efficiency curve as a function of the difference between fluid and ambient temperature. That advantage is that the y-intercept is essentially equal to the optical efficiency. This has been the typical approach for solar collectors in general as described by the Hottel-Whillier-Bliss equation [5]. That equation is usually shown with the independent variable of □T/I, where □T is either the fluid inlet temperature minus ambient or the average fluid temperature minus ambient. The heat loss term is also usually shown with a second order dependency on $□T^2/I$. It is straightforward

to show that this characterization does not work well for the heat losses from evacuated tube receivers and for trough collectors in general. Based on these arguments, the overall efficiency is shown as a function of fluid temperature minus ambient temperature with the direct solar irradiance as a parameter (Figure 27). The ambient temperature was chosen as the measured laboratory air temperature during the receiver heat loss tests. A third order polynomial fit with the constant coefficient fixed to the optical efficiency for I=1000W/m^2 is displayed in addition. It would be possible to fit curves for other values of I and then fit those polynomial coefficients to obtain a single equation for efficiency. This step has not been taken.

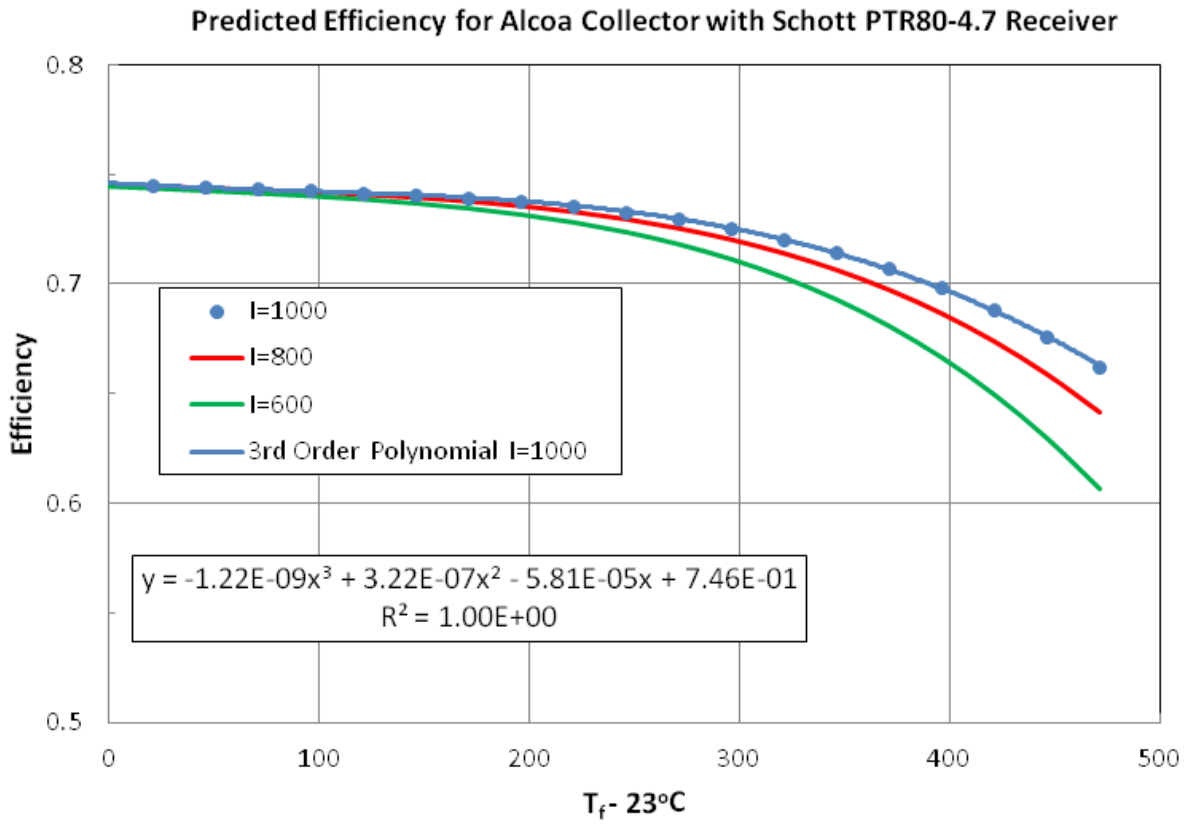

Figure 27. Overall thermal efficiency curve for the Alcoa collector using a Schott PTR80-4.7 receiver based on heat loss testing at 23°C ambient temperature.

Overall Comments – Optical Efficiency Testing

The measured optical efficiency of the Alcoa prototype collector is slightly less (2%) than in the ideal value listed in Table 6. This small discrepancy could be caused by small discrepancies in any of the optical loss parameters in the table. The incidence angle performance is also relatively flat. The small effects of incidence angle on performance are a result of very high intercept factors and the use of the 80-mm diameter Schott PTR-80 receiver tube. The optical efficiency testing and VSHOT results correlate well. This indicates the likelihood that this prototype and the one tested at Alcoa with VSHOT are nearly identical.

References

[1] Jones, S. Wendelin,T. Gruetzner, R. Houser, R. and Edgar, R. "VSHOT Measurement Uncertainty and Sensitivity Study," SAND-1627C, Albuquerque, NM, Sandia National Laboratories, 1997.

[2] Wendelin, T."SolTRACE: A New Optical Modeling Tool for Concentrating Solar Optics." International Solar Energy Conference, Kohala Coast, Hawaii, March 15-18 2003.

[3] Bendt, P., A. Rabl, H.W. Gaul, K.A. Reed, "Optical Analysis and Optimization of Line Focus Solar Concentrators," SERI/TR-34-092, Solar Energy Research Institute, Golden, CO, 1979.

[4] Neumann, A., A. Witzke, S. Jones, G. Schmitt, "Representative Terrestrial Solar Brightness Profiles," Transactions of the ASME, Vol. 124, pp 198-204, May 2002.

[5] Duffie, J. and Beckman, W. Solar Engineering of Thermal Processes. John Wiley & Sons, 3rd edition, 2003.

[6] Gaul, H. and Rabl, A., "Incidence-Angle Modifier and Average Optical Efficiency of Parabolic Trough Collectors," Journal of Solar Energy Engineering, 102, Feb. 1980, pp. 16–21.

[7] Kuckelkorn, T., Benz, N., Dreyer, S., Schulte-Fischedick, J., Moellenhoff, M., "Advances in Receiver Technology for Parabolic Trough Collectors – A step forward towards higher efficiency and longer lifetime," Proceedings of SolarPACES 2009, Berlin, Germany, 15-18 September, 2009.

[8] Moss, A. and Brosseau, D., "Final Test Results for the Schott HCE on a LS-2 Collector," SANDIA REPORT SAND2005-4034, July 2005

[9] Burkholder, F. and Kutscher, C., "Heat Loss Testing of Schott's 2008 PTR70 Parabolic Trough Receiver," NREL/TP-550-45633, May 2009.

[10] Forristall, R., "Heat Transfer Analysis and Modeling of a Parabolic Trough Solar Receiver Implemented in Engineering Equation Solver," NREL/TP-550-34169 October 2003

Appendix 1. VSHOT Data Tables, Slope Error, and Ray Trace Plots for Testing at Alcoa

The analysis in all subsequent tables assumes a focal length of 1.71 m and an aperture width of 6.0 m. Each of the plots is titled with the filename for the selected scan. The plotting program incorrectly outputs subscripts for certain characters. The initial plot in each sequence shows the VSHOT slope error for all scans for a given panel with a bounding curve of maximum allowable slope error for an 80 mm diameter receiver tube.

Also included in this plot are the edges of an 80 mm diameter receiver to indicate where direct shadowing of the receiver intersects the VSHOT data. In practice, the glass envelope around the receiver tube refracts light passing through it to an extent that no return rays will come back to the receiver tube. This increases the effective shadow to the overall diameter of the glass envelope. The initial plot is followed by a table that shows the averaged values of RMS error and intercept factor (for an 80 mm diameter receiver). This table is followed by two sets of plots, each one consisting of a ray-trace plot and a slope error plot for the selected scans within the panel. The selection is generally one near an edge and another somewhat random. A complete set of plots for each scan was not included to minimize the overall length of this report.

Results for Panel 1

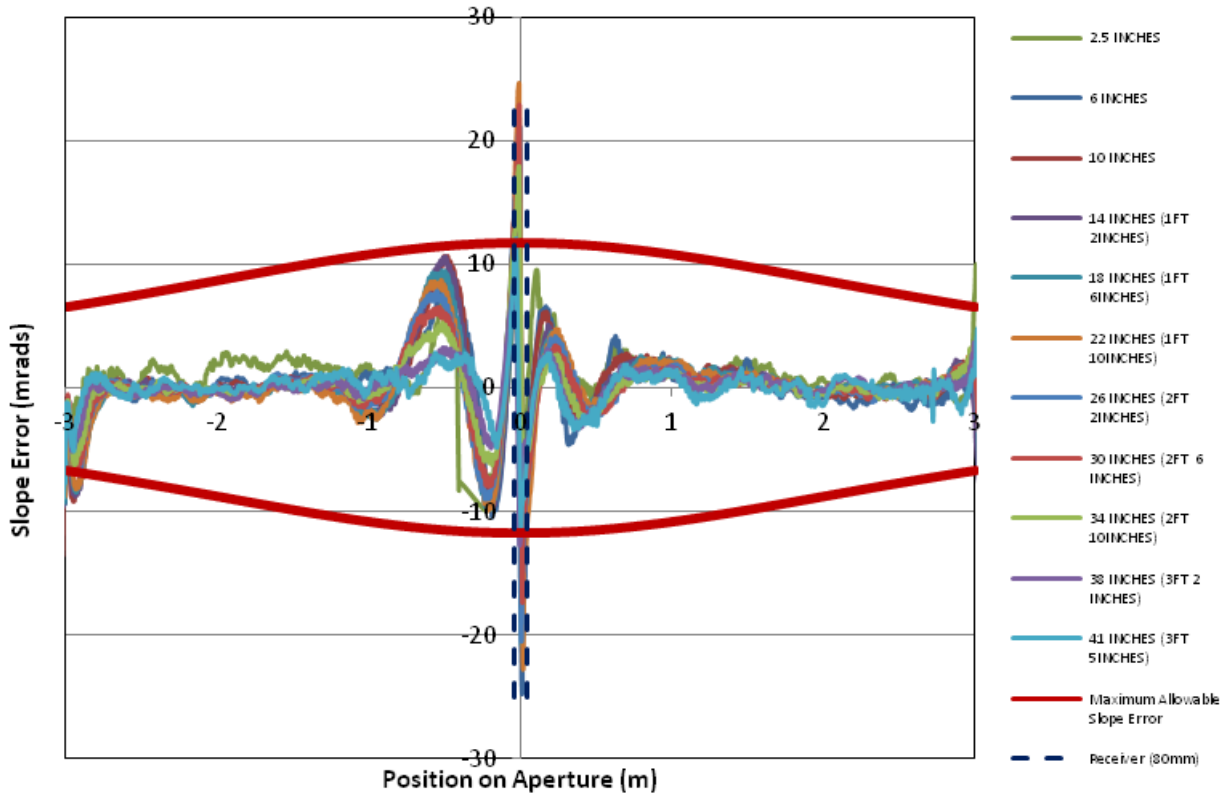

Figure 1. Slope errors along the aperture for each scan taken of Panel 1. The maximum allowable slope error over the aperture for an 80 mm receiver tube is plotted in red.

Table 1. Results for Panel 1 of the Alcoa collector.

File Name	RMS Slope Error Transverse (mrad)	Intercept Factor (straight rays)	Intercept Factor (DLR sun shape)
AA_p1_0_5inches_fixedEDIT.csv	2.06	0.998	0.998
AA_p1_6inches_2ofixedEDIT.csv	2.87	0.997	0.995
AA_p1_10inches_2fixedEDIT.csv	3.00	0.986	0.984
AA_p1_1ft_2inchefixedEDIT.csv	3.25	0.985	0.983
AA_p1_1ft_6inchefixedEDIT.csv	3.32	0.987	0.988
AA_p1_1ft_10inchfixedEDIT.csv	3.34	0.987	0.987
AA_p1_2ft_2inchefixedEDIT.csv	2.97	0.995	0.993
AA_p1_2ft_6inchefixedEDIT.csv	2.68	0.997	0.994
AA_p1_2ft_10inchfixedEDIT.csv	2.14	0.99-	0.996
AA_p1_3ft_2inchefixedEDIT.csv	1.60	1.00	1.00
AA_p1_3ft_5inchefixedEDIT.csv	1.53	1.00	1.00
Average	**2.61**	**0.994**	**0.993**

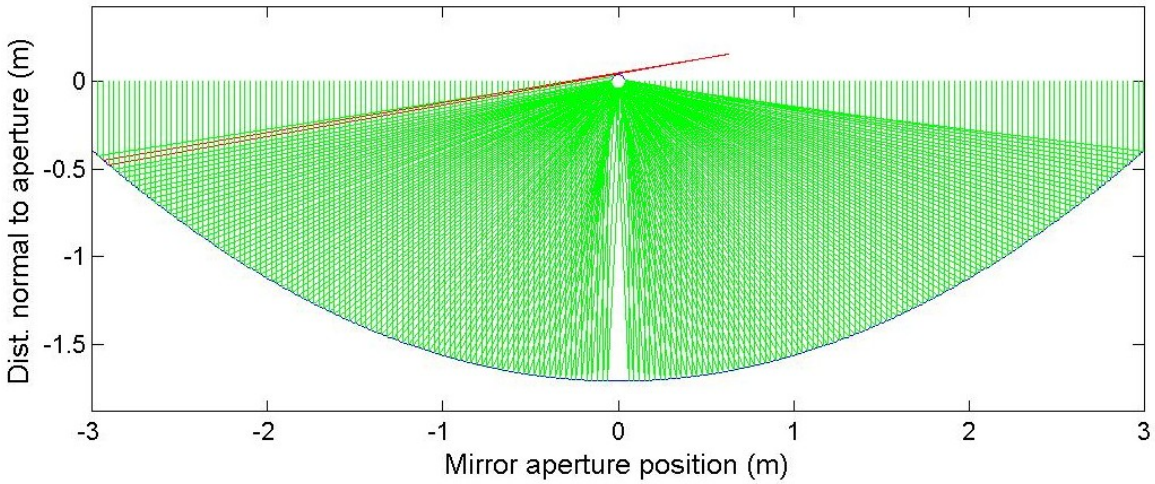

Figure 2. Ray trace results for scan AA_p1_1ft_2inchefixedEDIT.csv, RMS=3.25, Intercept=0.985.

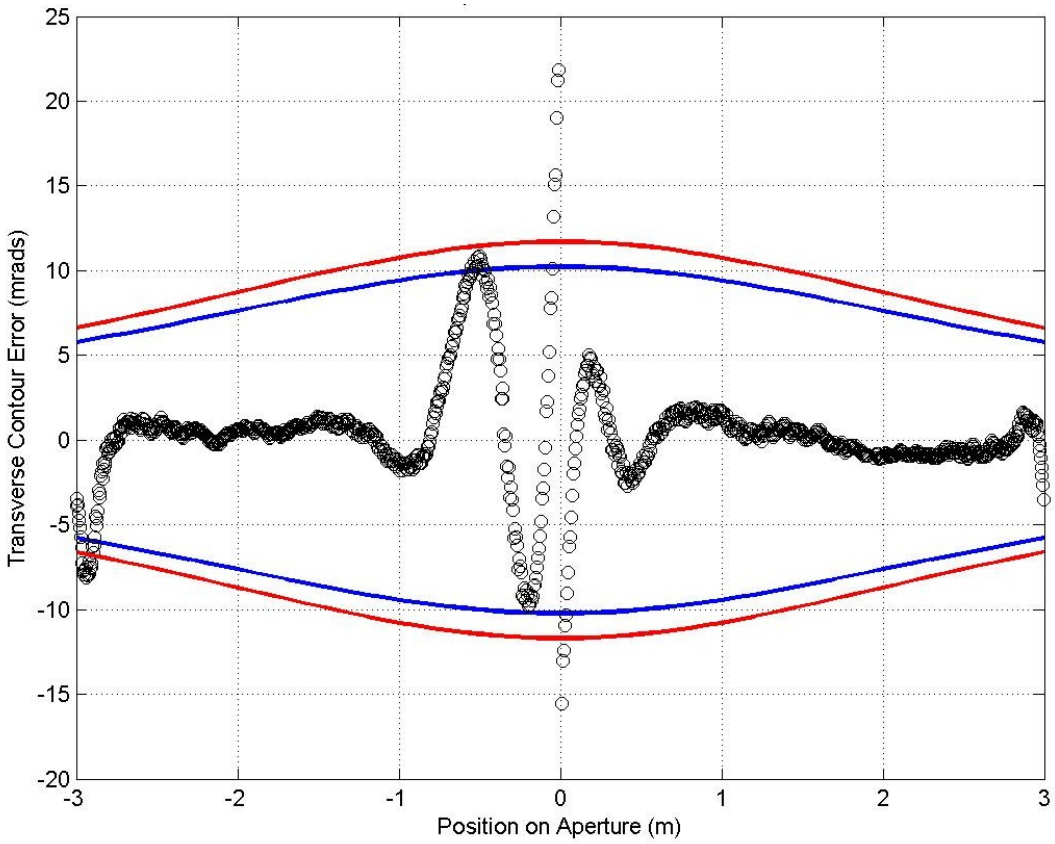

Figure 3. Slope errors along the aperture of scan AA_p1_1ft_2inchefixedEDIT.csv.

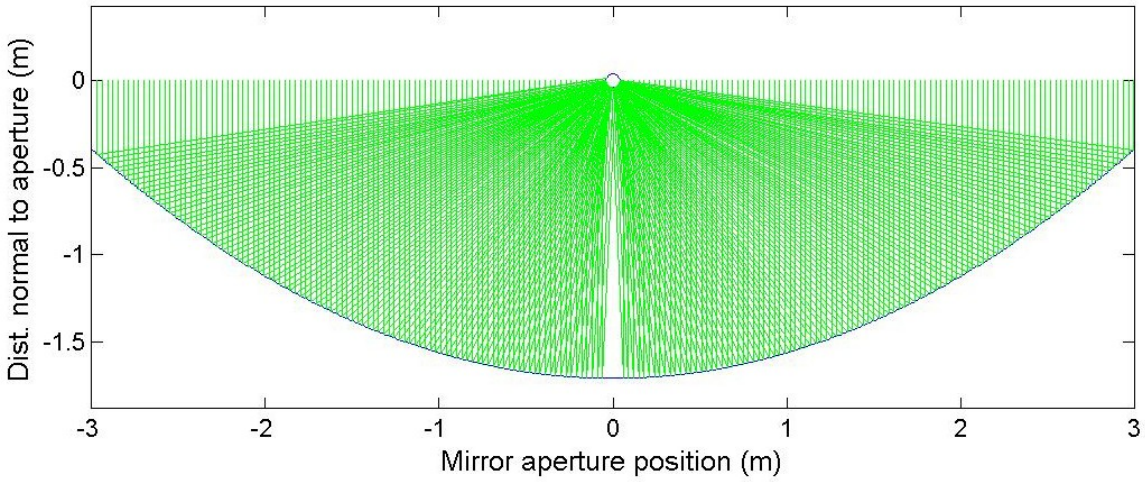

Figure 4. Ray trace results for scan AA_p1_3ft_5inchefixedEDIT.csv, RMS=1.53, Intercept=1.00.

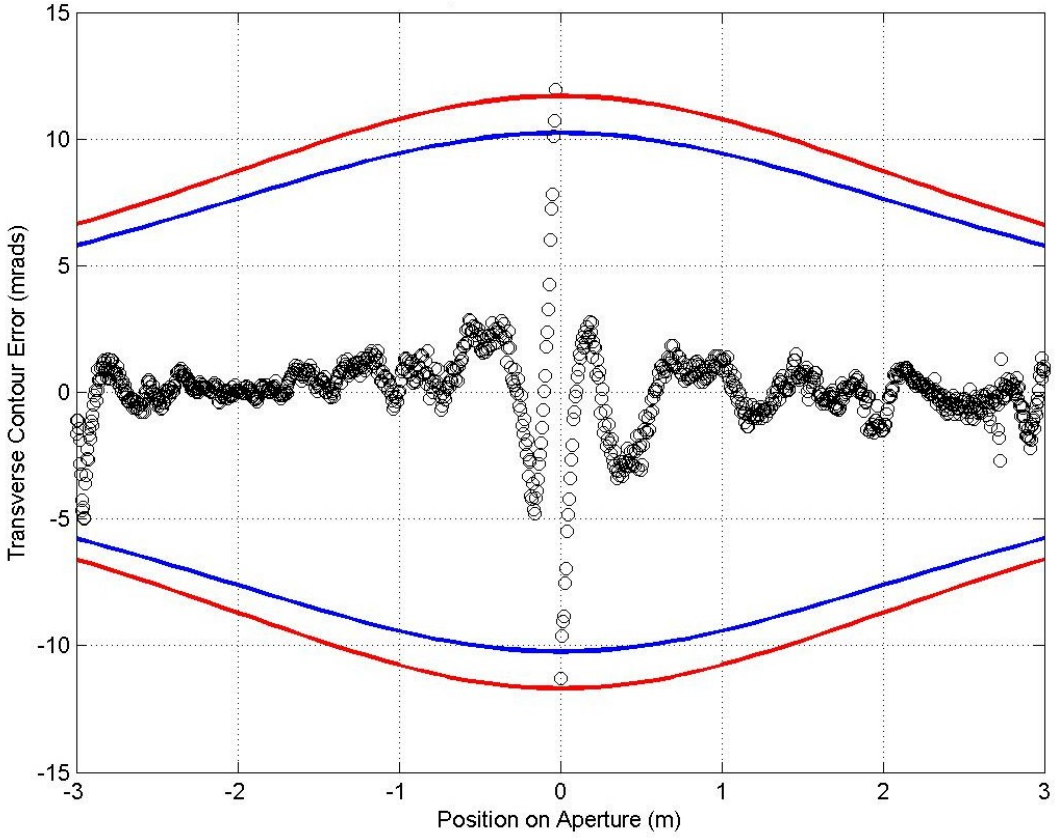

Figure 5. Slope errors along the aperture of scan AA_p1_3ft_5inchefixedEDIT.csv

Results for Panel 2

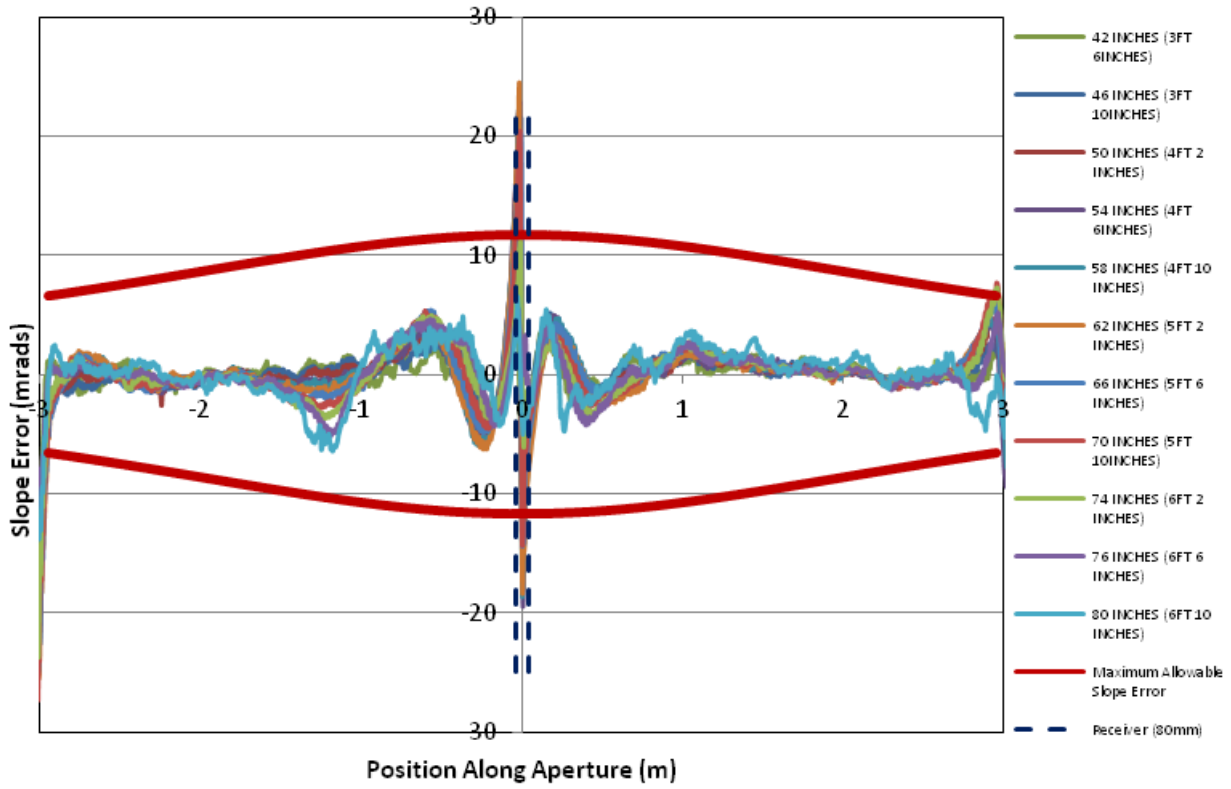

Figure 6. Slope errors along the aperture for each scan taken of Panel 2. The maximum allowable slope error over the aperture for an 80 mm receiver tube is plotted in red.

Table 2. Results for Panel 2 of the Alcoa collector.

File Name	RMS Slope Error Transverse (mrad)	Intercept Factor (straight rays)	Intercept Factor (DLR sun shape)
AA_p2_3ft_6nchesfixedEDIT.csv	1.38	0.998	0.998
AA_p2_3ft_10inchfixedEDIT.csv	2.21	0.995	0.995
AA_p2_4ft_2inchefixedEDIT.csv	2.39	0.994	0.993
AA_p2_4ft_6inchefixedEDIT.csv	2.58	0.994	0.993
AA_p2_4ft_10inchfixedEDIT.csv	2.64	0.993	0.992
AA_p2_5ft_2inchefixedEDIT.csv	2.85	0.992	0.989
AA_p2_5ft_6inchefixedEDIT.csv	2.76	0.994	0.991
AA_p2_5ft_10inchfixedEDIT.csv	2.70	0.989	0.987
AA_p2_6ft_2inchefixedEDIT.csv	2.14	0.991	0.990
AA_p2_6ft_6inchefixedEDIT.csv	1.88	0.997	0.997
AA_p2_6ft_8inchefixedEDIT.csv	2.20	0.997	0.997
Average	**2.34**	**0.994**	0.993

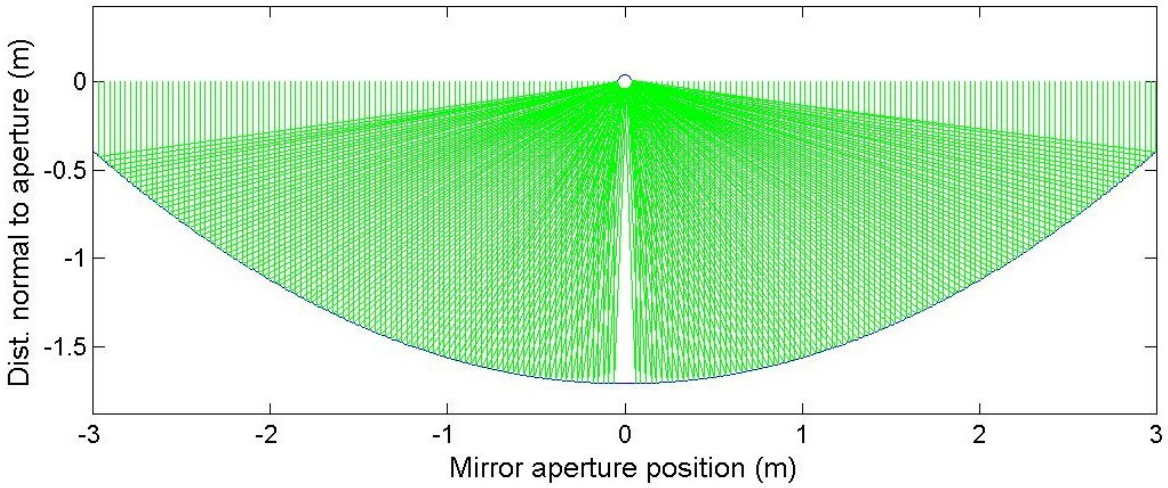

Figure 7. Ray trace results for scan AA_p2_3ft_6nchesfixedEDIT.csv, RMS=1.3769, Intercept=0.9985.

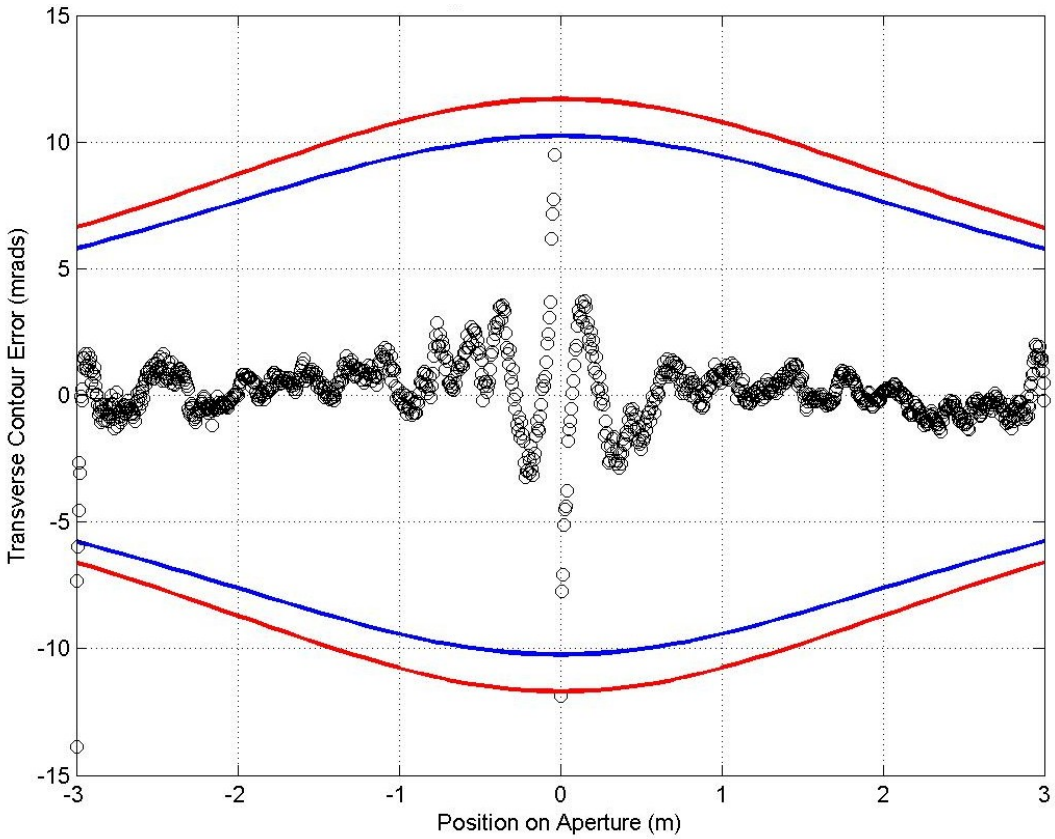

Figure 8. Slope errors along the aperture of scan AA_p2_3ft_6nchesfixedEDIT.csv.

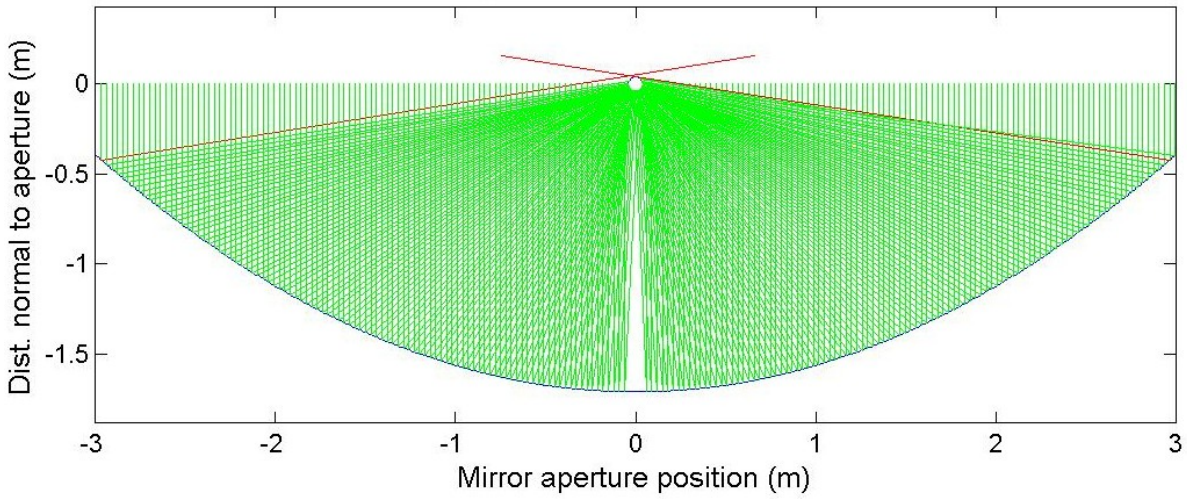

Figure 9. Ray trace results for scan AA_p2_5ft_10inchfixedEDIT.csv, RMS=2.70471, Intercept=0.989.

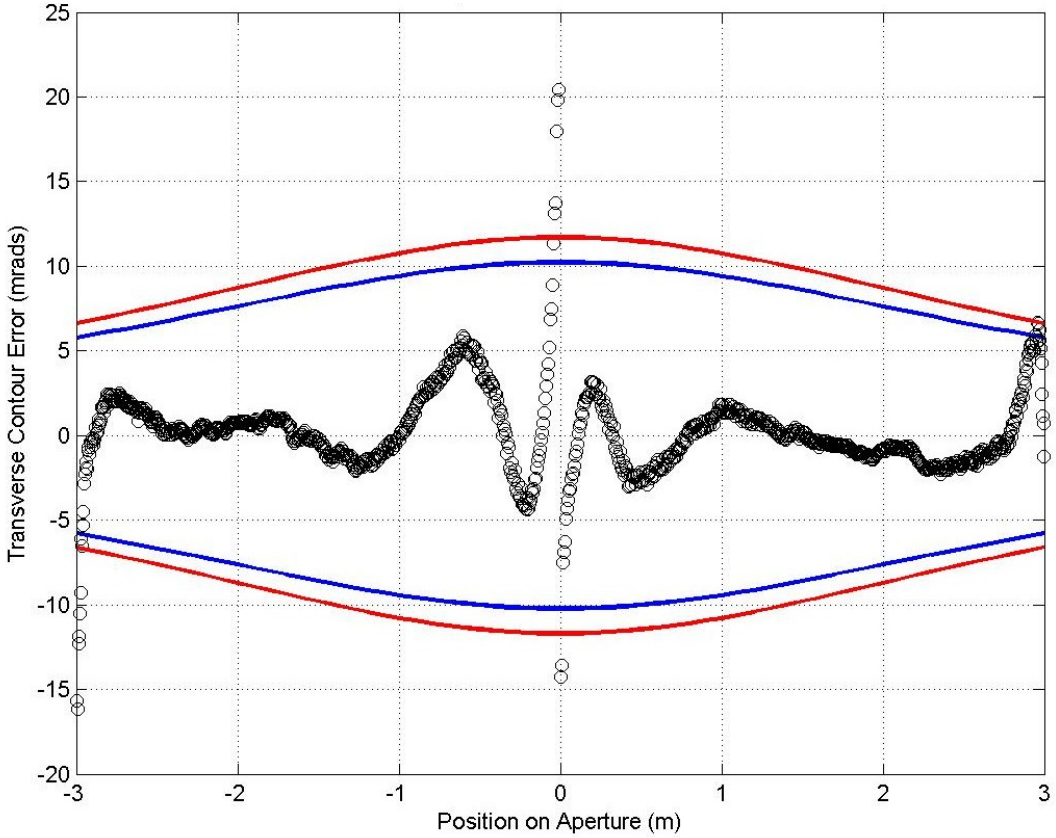

Figure 10. Slope errors along the aperture of scan AA_p2_5ft_10inchfixedEDIT.csv.

Results for Panel 3

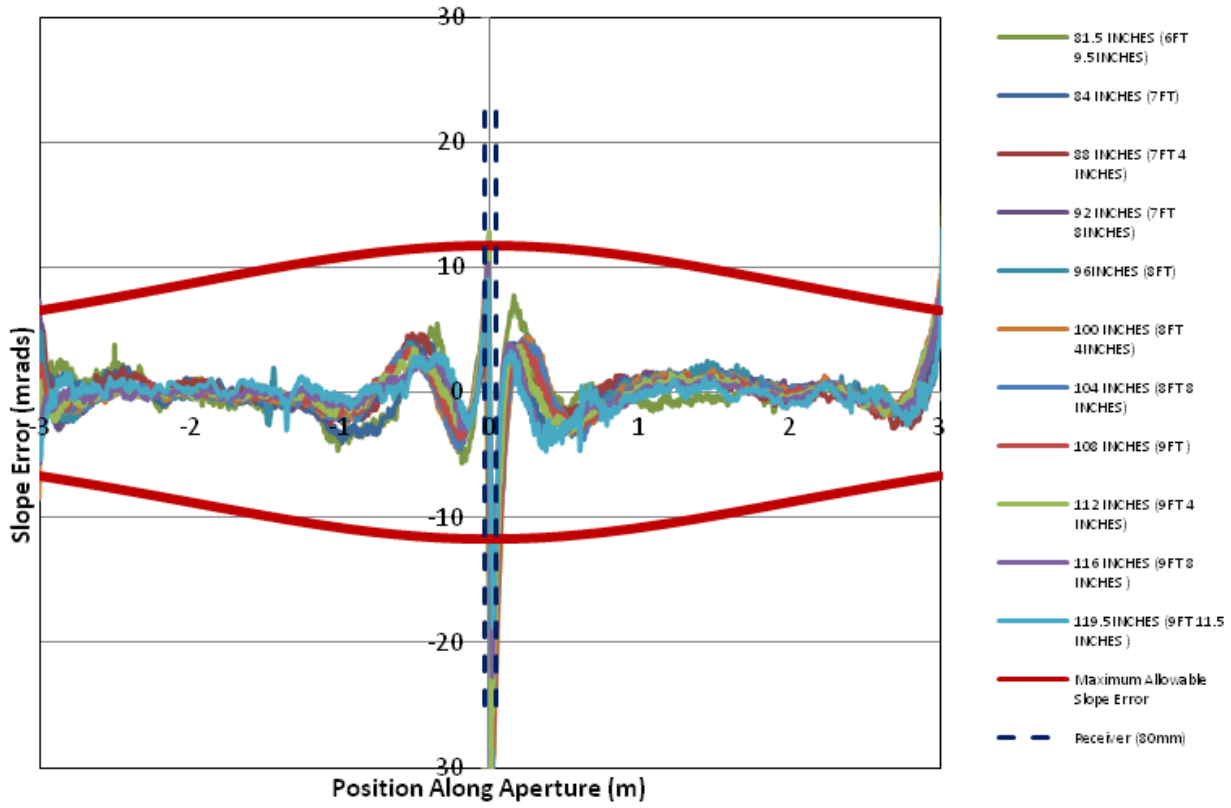

Figure 11. Slope errors along the aperture for each scan taken of Panel 3. The maximum allowable slope error over the aperture for an 80 mm receiver tube is plotted in red.

Table 3. Results for Panel 3 of the Alcoa collector.

File Name	RMS Slope Error Transverse (mrad)	Intercept Factor (straight rays)	Intercept Factor (DLR sun shape)
AA_p3_6ft_9_5incfixedEDIT.csv	2.35	1	0.999
AA_p3_7ft_2o_1DyfixedEDIT.csv	2.17	1.00	0.998
AA_p3_7ft_4inchefixedEDIT.csv	2.45	1.00	0.997
AA_p3_7ft_8inchefixedEDIT.csv	2.60	1.00	0.995
AA_p3_8ft_2o_1DyfixedEDIT.csv	2.64	0.995	0.994
AA_p3_8ft_4inchefixedEDIT.csv	3.08	0.991	0.991
AA_p3_8ft_8inchefixedEDIT.csv	3.08	0.996	0.995
AA_p3_9ft_2o_1DyfixedEDIT.csv	2.43	0.996	0.996
AA_p3_9ft_4inchefixedEDIT.csv	2.49	0.995	0.994
AA_p3_9ft_8inchefixedEDIT.csv	1.94	0.996	0.996
AA_p3_9ft_11_5infixedEDIT.csv	1.69	1.00	1.00
Average	2.45	1.00	1.00

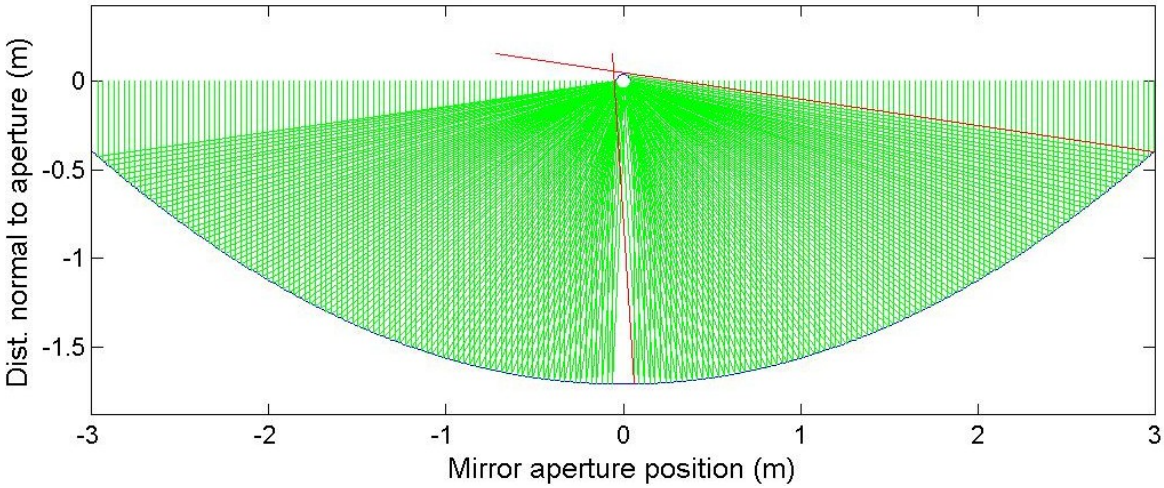

Figure 12. Ray trace results for scan AA_p3_8ft_4inchefixedEDIT.csv, RMS=3.08 Intercept=0.991.

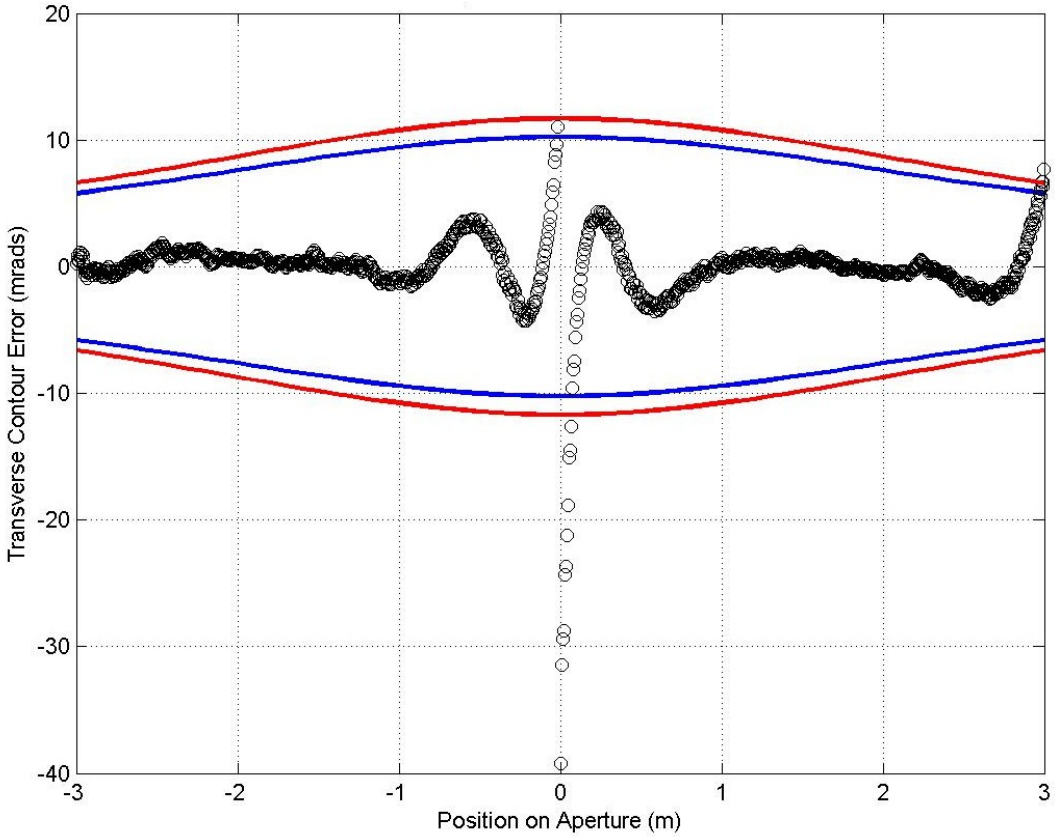

Figure 13. Slope errors along the aperture of scan AA_p3_8ft_4inchefixedEDIT.csv

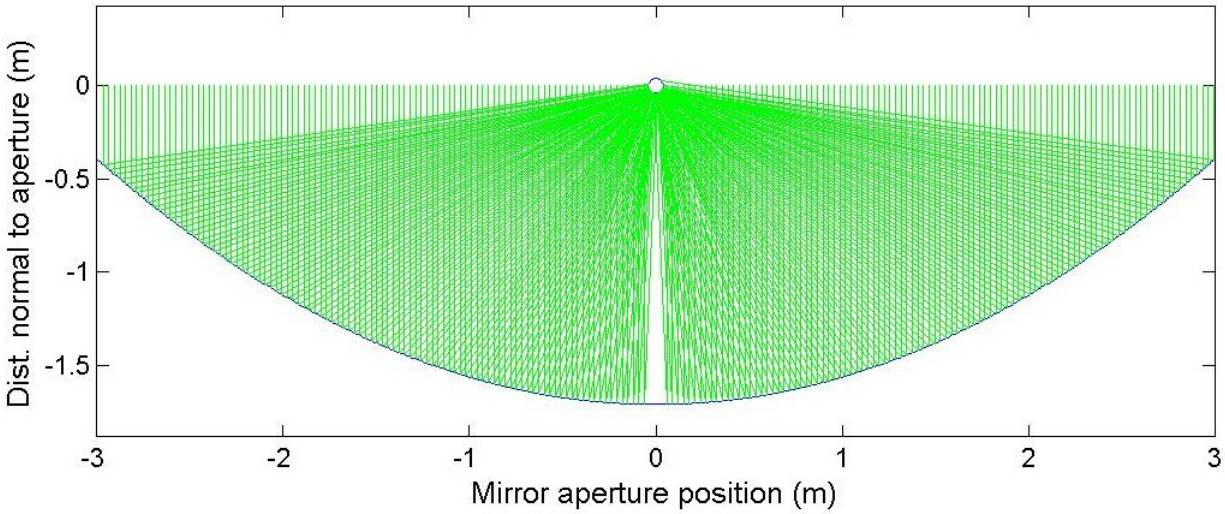

Figure 14. Ray trace results for scan AA_p3_9ft_11_5infixedEDIT.csv, RMS=1.69, Intercept=1.00.

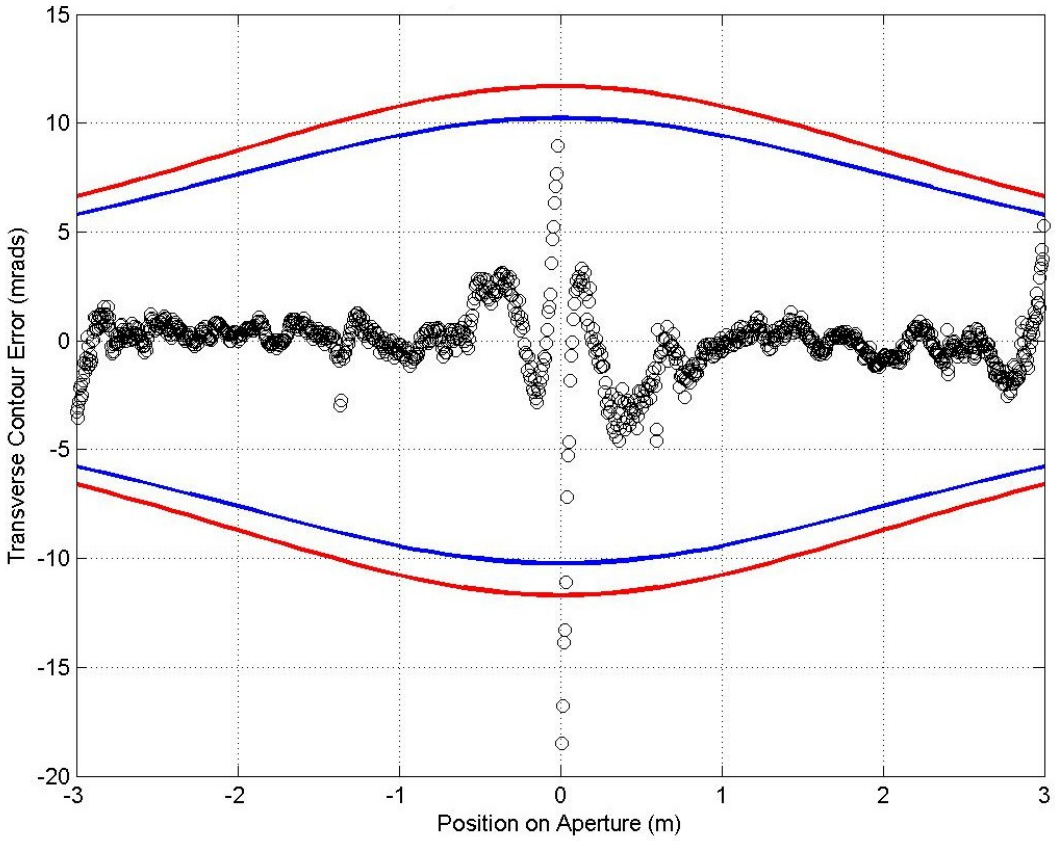

Figure 15. Slope errors along the aperture of scan AA_p3_9ft_11_5infixedEDIT.csv.

Results for Panel 4

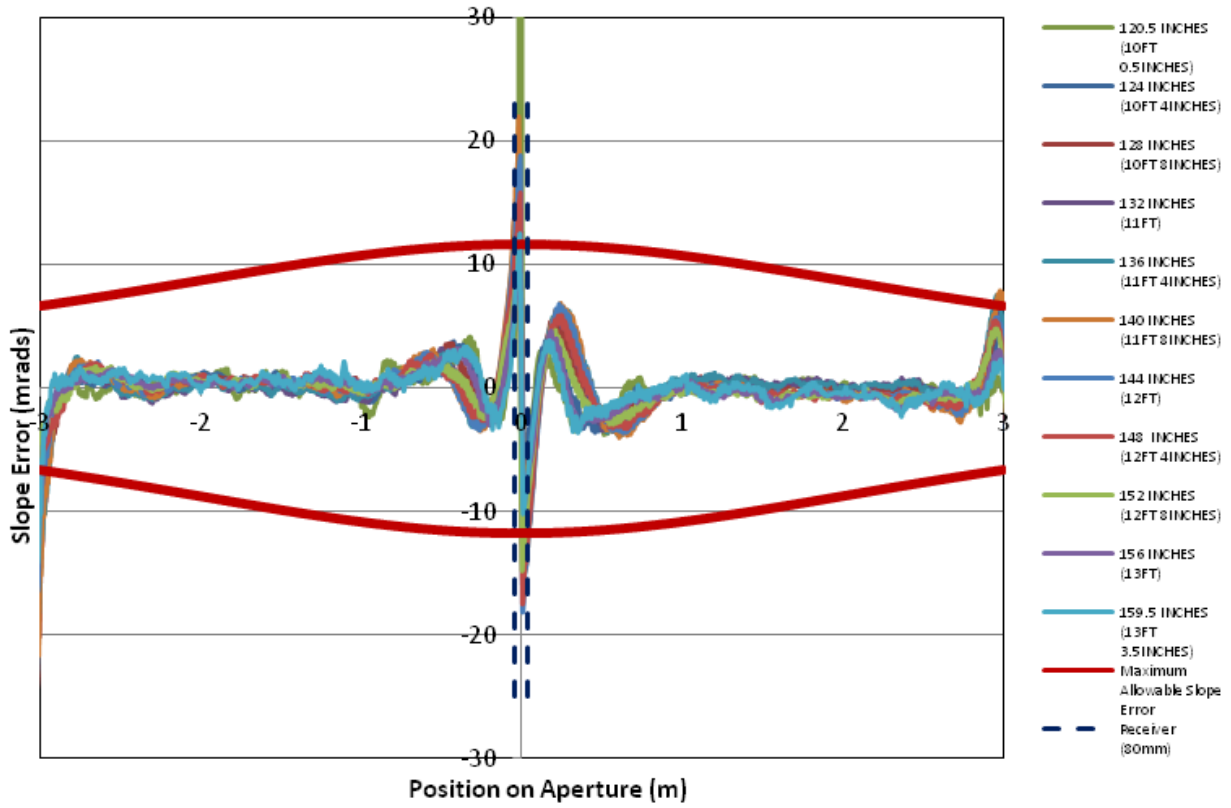

Figure 16. Slope errors along the aperture for each scan taken of Panel 4. The maximum allowable slope error over the aperture for an 80 mm receiver tube is plotted in red.

Table 4. Results for Panel 4 of the Alcoa collector.

File Name	RMS Slope Error Transverse (mrad)	Intercept Factor (straight rays)	Intercept Factor (DLR sun shape)
AA_p4_10ft_0_5infixedEDIT.csv	3.34	0.997	1.00
AA_p4_10ft_4inchfixedEDIT.csv	1.84	0.994	0.994
AA_p4_10ft_8inchfixedEDIT.csv	2.27	0.992	0.991
AA_p4_11ft_2o_1DfixedEDIT.csv	2.40	0.991	0.988
AA_p4_11ft_4inchfixedEDIT.csv	2.68	0.985	0.984
AA_p4_11ft_8inchfixedEDIT.csv	2.84	0.981	0.9814
AA_p4_12ft_2o_1DfixedEDIT.csv	2.68	0.996	0.993
AA_p4_12ft_4inchfixedEDIT.csv	2.40	1.00	0.997
AA_p4_12ft_8inchfixedEDIT.csv	1.85	1.00	1.00
AA_p4_13ft_2o_1DfixedEDIT.csv	1.61	0.990	0.998
AA_p4_13ft_3_5infixedEDIT.csv	1.65	0.998	0.998
Average	**2.32**	**0.994**	0.993

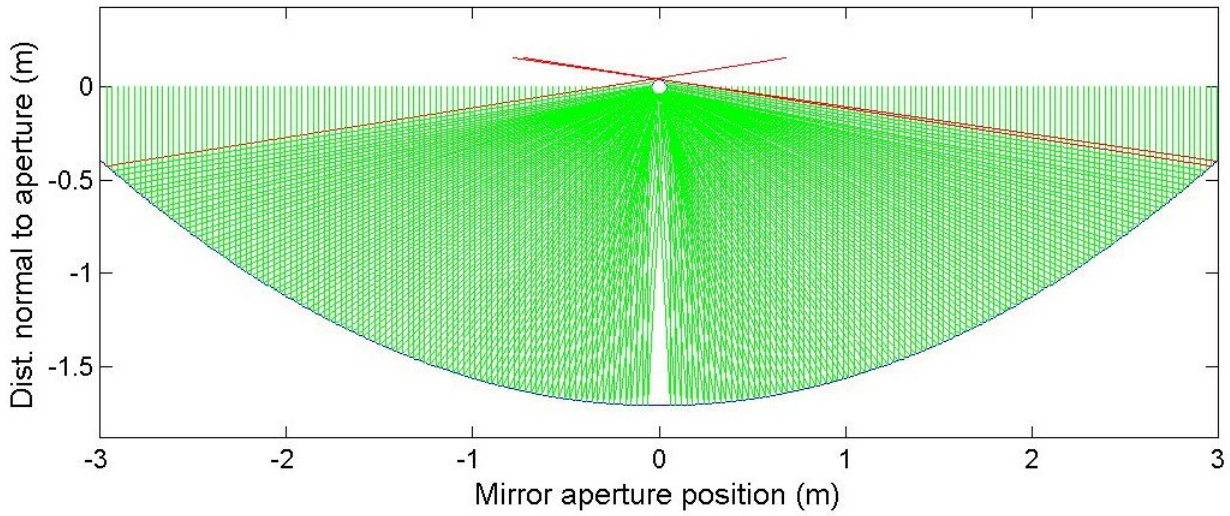

Figure 17. Ray trace results for scan AA_p4_11ft_8inchfixedEDIT.csv, RMS=2.84, Intercept=0.981.

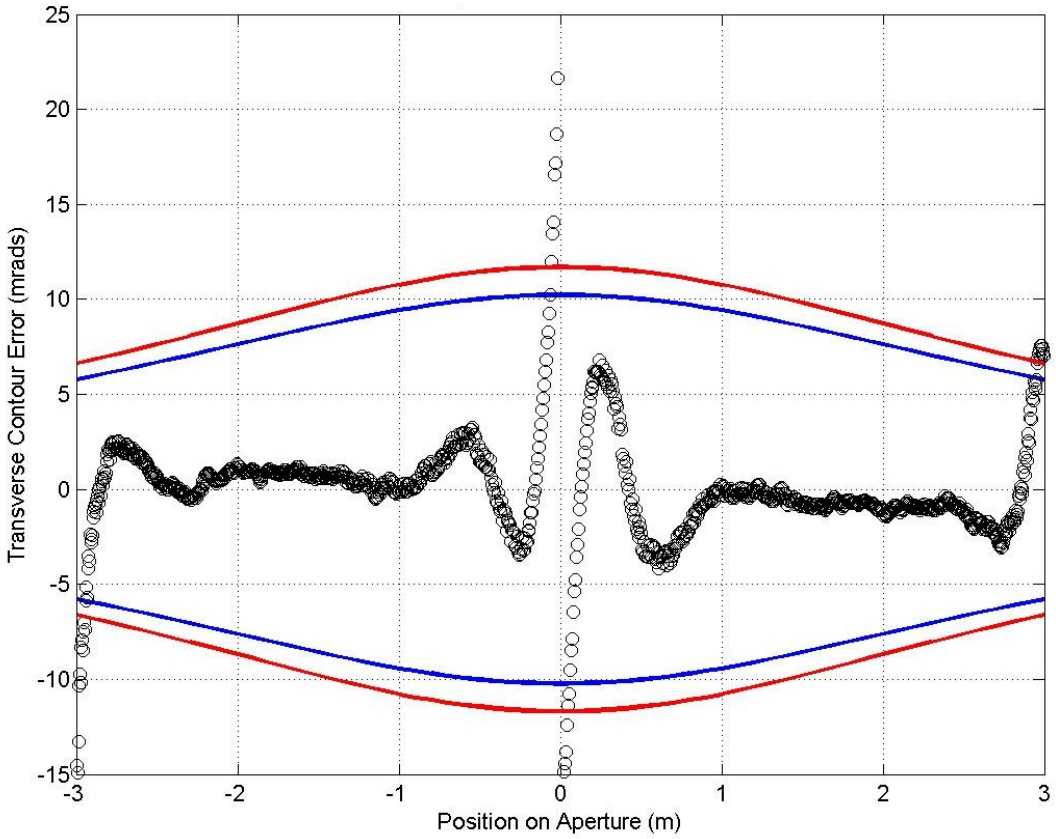

Figure 18. Slope errors along the aperture of scan AA_p4_11ft_8inchfixedEDIT.csv.

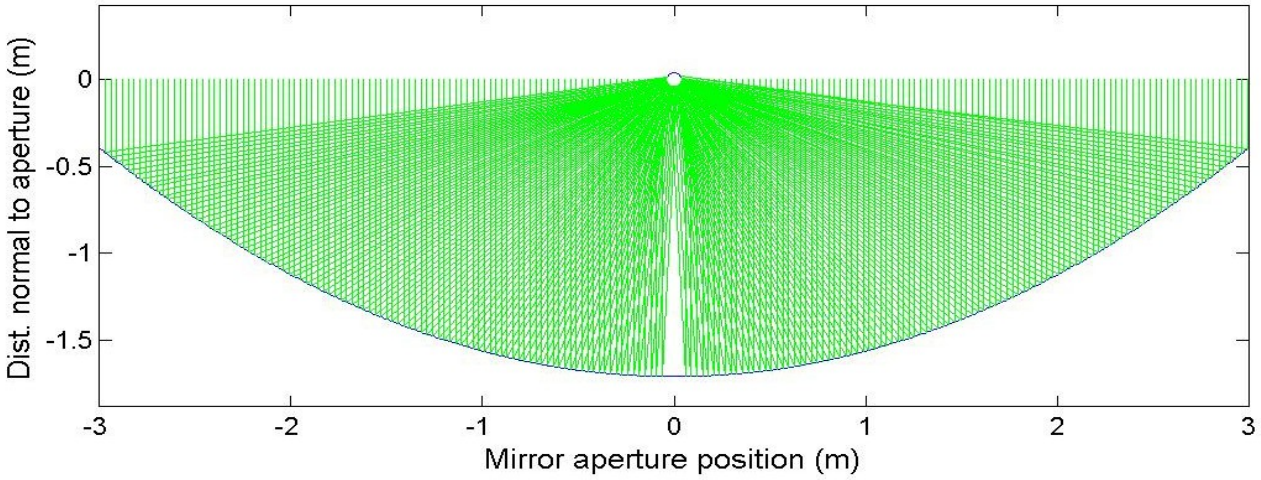

Figure 19. Ray trace results for scan AA_p4_12ft_8inchfixedEDIT.csv, RMS=1.85, Intercept=1.00.

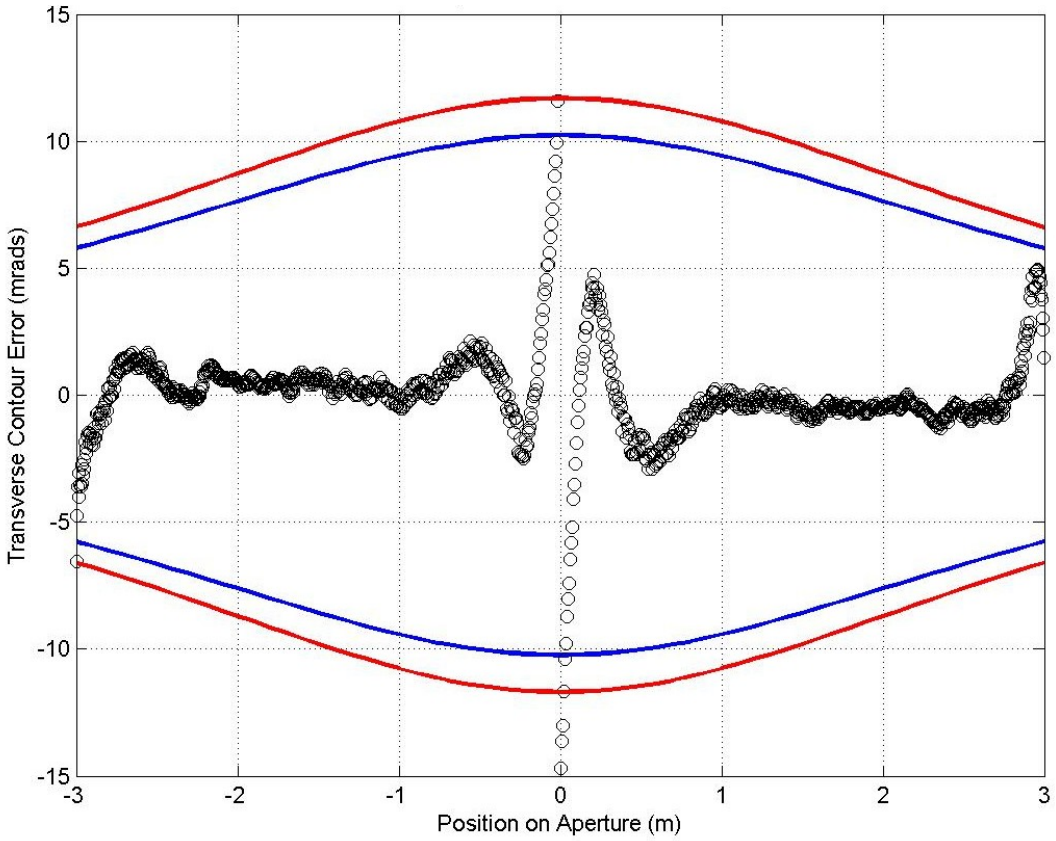

Figure 20. Slope errors along the aperture of scan AA_p4_12ft_8inchfixedEDIT.csv.

Results for Panel 5

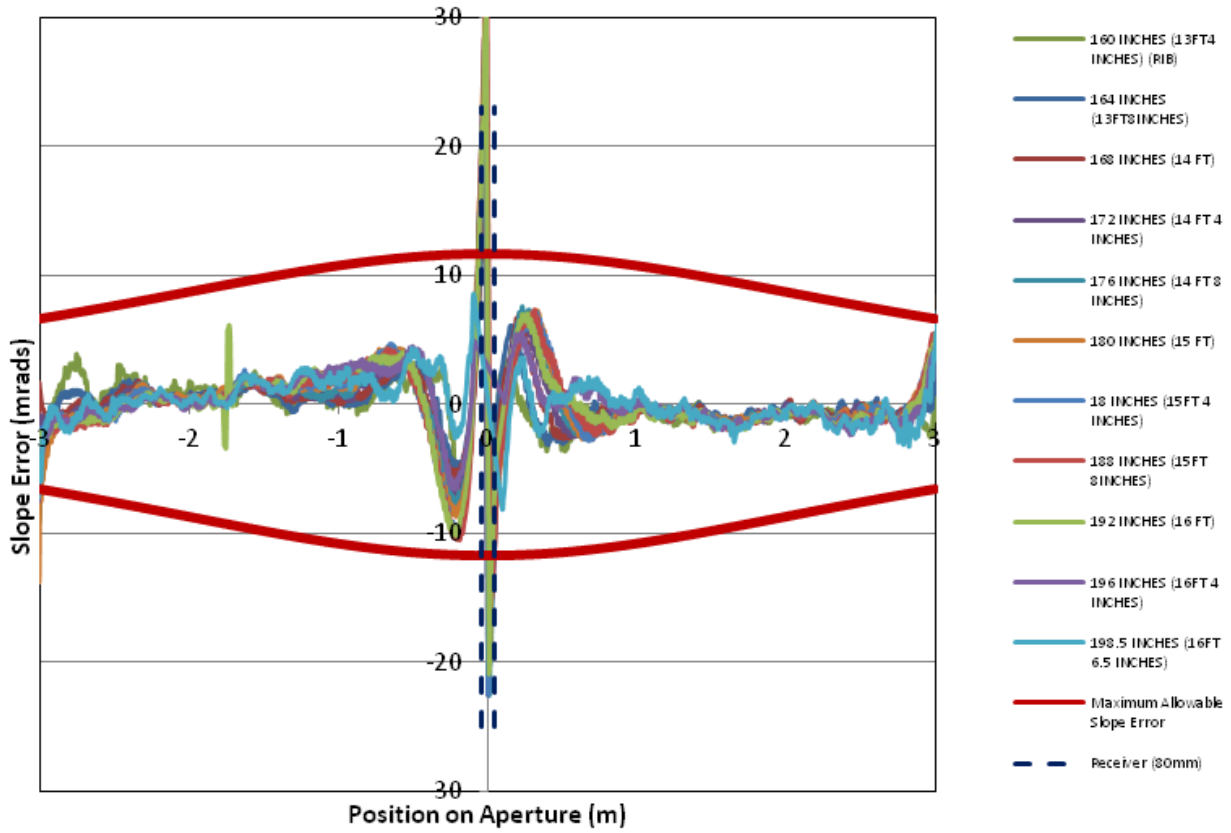

Figure 21. Slope errors along the aperture for each scan taken of Panel 5. The maximum allowable slope error over the aperture for an 80 mm receiver tube is plotted in red.

Table 5. Results for Panel 5 of the Alcoa collector.

File Name	RMS Slope Error Transverse (mrad)	Intercept Factor (straight rays)	Intercept Factor (DLR sun shape)
AA_p5_13ft_4inchfixedEDIT.csv	2.15	1.00	0.997
AA_p5_13ft_8inchfixedEDIT.csv	2.20	1.00	0.999
AA_p5_14ft_2o_1DfixedEDIT.csv	2.49	1.00	0.998
AA_p5_14ft_4inchfixedEDIT.csv	2.92	1.00	0.997
AA_p5_14ft_8inchfixedEDIT.csv	3.08	0.997	0.997
AA_p5_15ft_2o_1DfixedEDIT.csv	3.31	0.995	0.993
AA_p5_15ft_4inchfixedEDIT.csv	3.48	0.996	0.995
AA_p5_15ft_8inchfixedEDIT.csv	3.53	0.996	0.993
AA_p5_16ft_2o_1DfixedEDIT.csv	3.33	0.997	0.996
AA_p5_16ft_4inchfixedEDIT.csv	1.84	1.00	1.00
AA_p5_16ft_6_5infixedEDIT.csv	1.63	1.00	1.00
Average	2.72	0.998	0.997

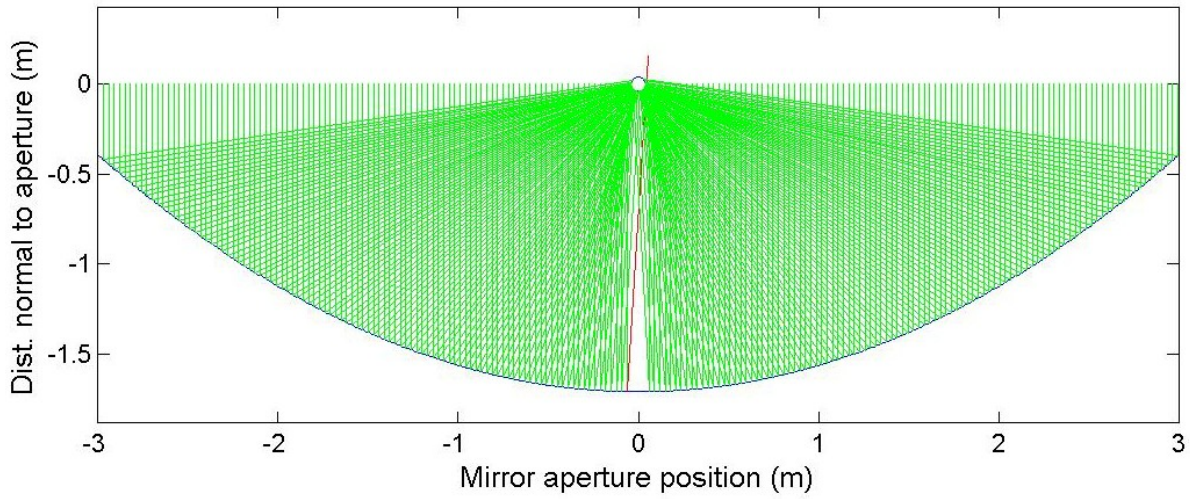

Figure 22. Ray trace results for scan AA_p5_15ft_2o_1DfixedEDIT.csv, RMS=3.31, Intercept=0.995.

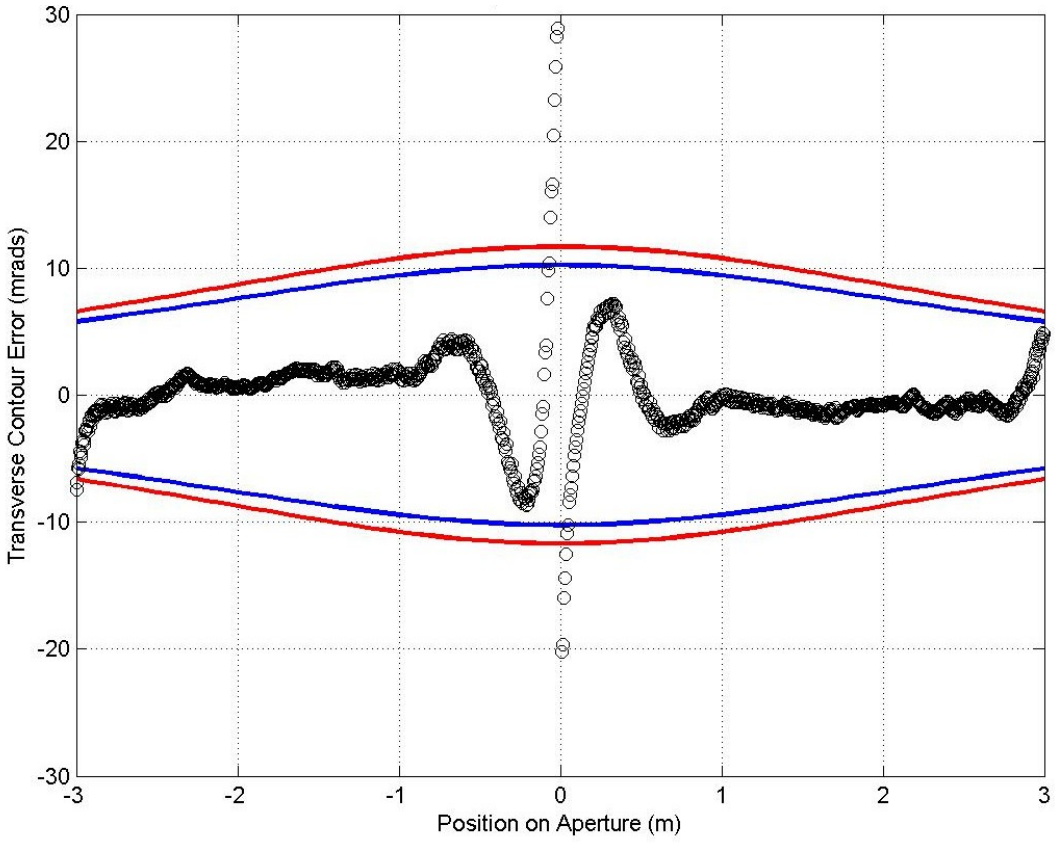

Figure 23. Slope errors along the aperture of scan AA_p5_15ft_2o_1DfixedEDIT.csv.

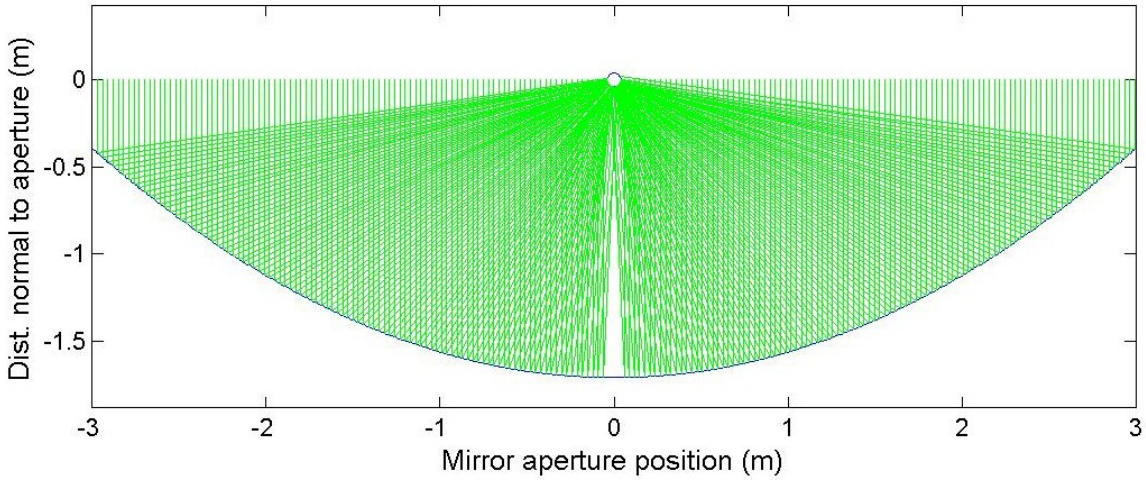

Figure 24. Ray trace results for scan AA_p5_16ft_6_5infixedEDIT.csv, RMS=1.62599, Intercept=1.00.

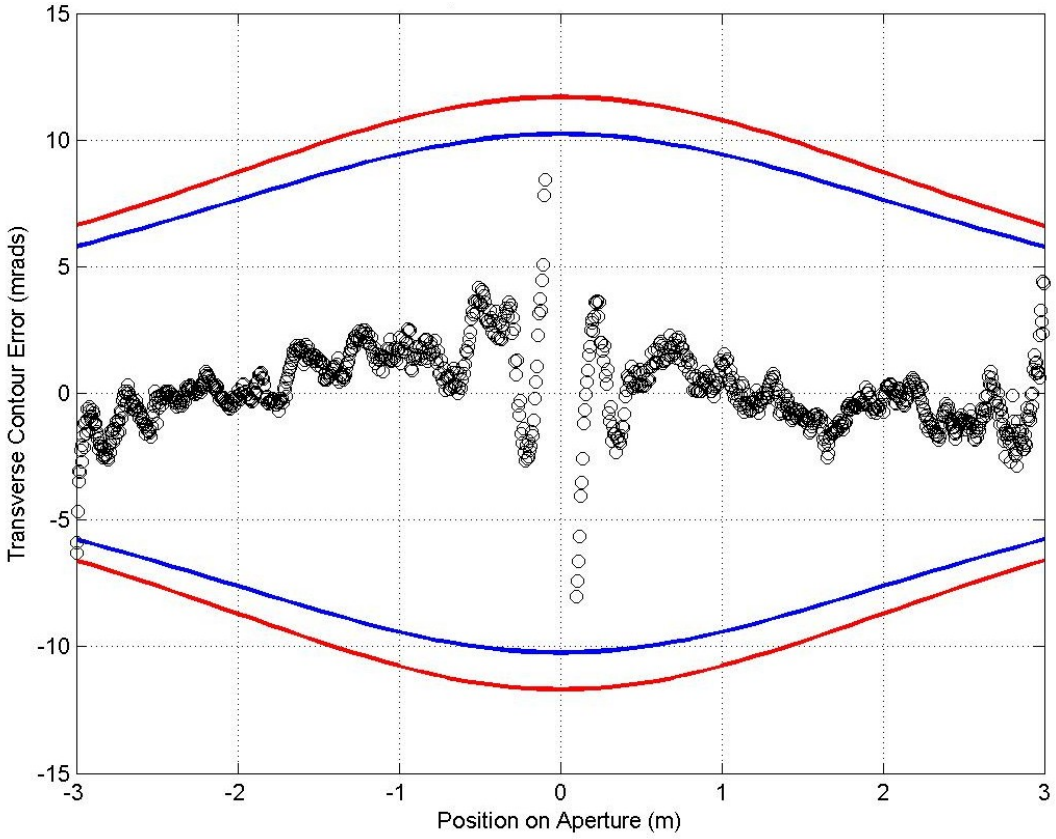

Figure 25. Slope errors along the aperture of scan AA_p5_16ft_6_5infixedEDIT.csv.

Results for Panel 6

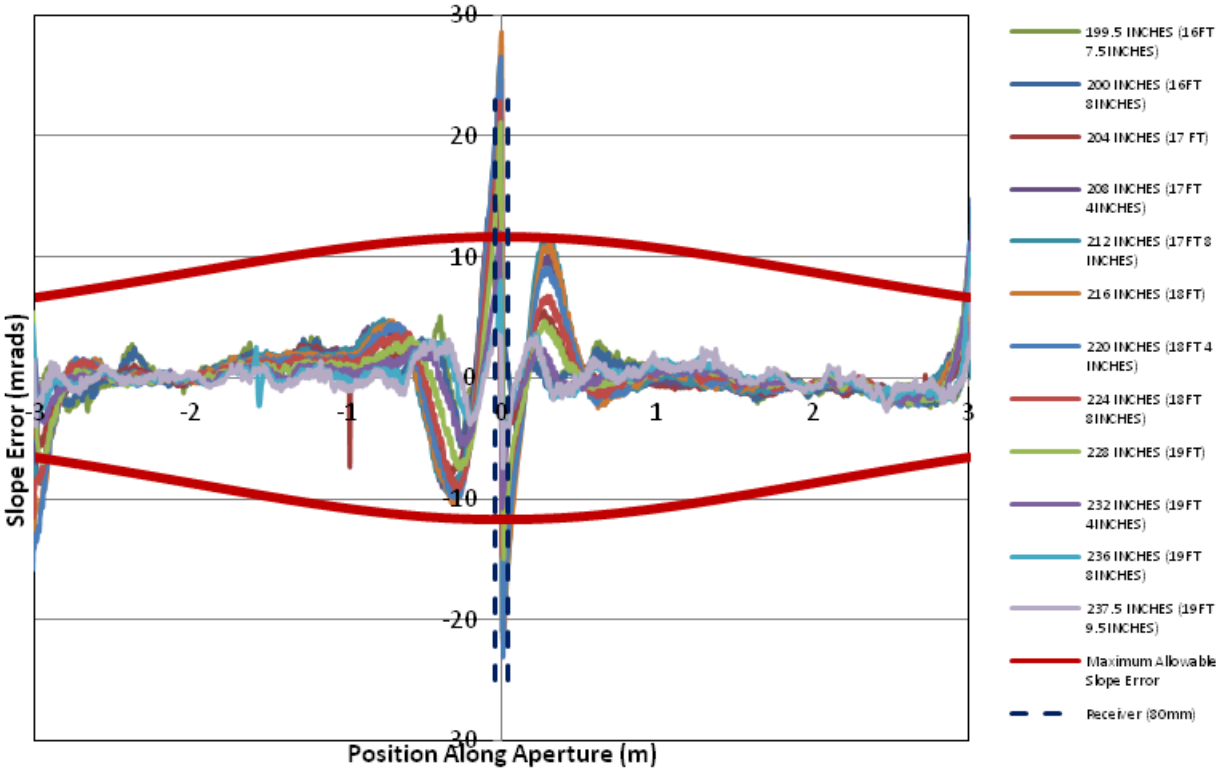

Figure 26. Slope errors along the aperture for each scan taken of Panel 6. The maximum allowable slope error over the aperture for an 80 mm receiver tube is plotted in red.

Table 6. Results for Panel 6 of the Alcoa collector.

File Name	RMS Slope Error Transverse (mrad)	Intercept Factor (straight rays)	Intercept Factor (DLR sun shape)
AA_p6_16ft_7_5infixedEDIT.csv	1.61	1.00	0.999
AA_p6_16ft_8inchfixedEDIT.csv	1.62	0.996	0.996
AA_p6_17ft_2o_1DfixedEDIT.csv	2.61	0.991	0.992
AA_p6_17ft_4inchfixedEDIT.csv	3.89	0.980	0.979
AA_p6_17ft_8inchfixedEDIT.csv	4.13	0.976	0.971
AA_p6_18ft_2o_1DfixedEDIT.csv	4.24	0.975	0.969
AA_p6_18ft_4inchfixedEDIT.csv	4.09	0.974	0.972
AA_p6_18ft_8inchfixedEDIT.csv	3.20	0.983	0.983
AA_p6_19ft_2o_1DfixedEDIT.csv	2.69	0.990	0.988
AA_p6_19ft_4inchfixedEDIT.csv	1.70	0.997	0.998
AA_p6_19ft_8inchfixedEDIT.csv	1.28	0.999	0.999
Average	1.17	1.00	1.00

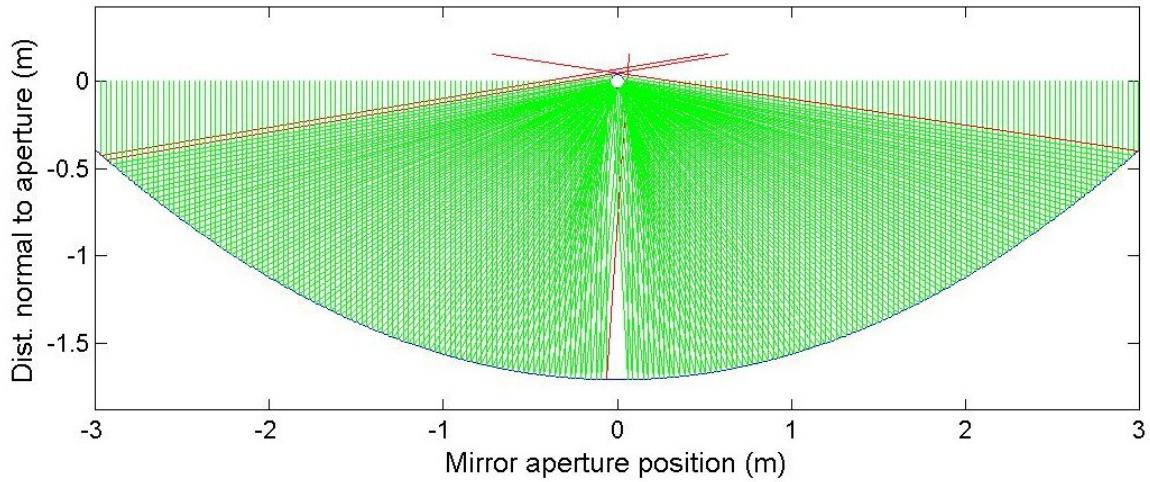

Figure 27. Ray trace results for scan AA_p6_18ft_4inchfixedEDIT.csv, RMS=4.09, Intercept=0.974.

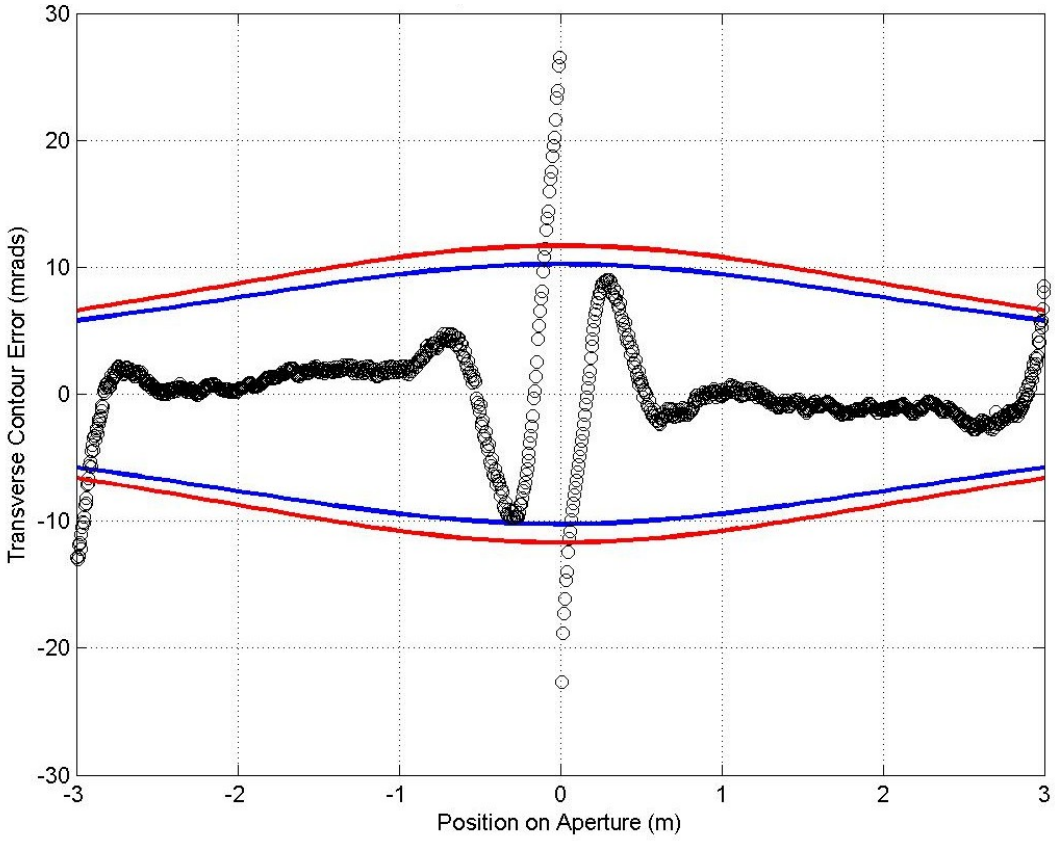

Figure 28. Slope errors along the aperture of scan AA_p6_18ft_4inchfixedEDIT.csv.

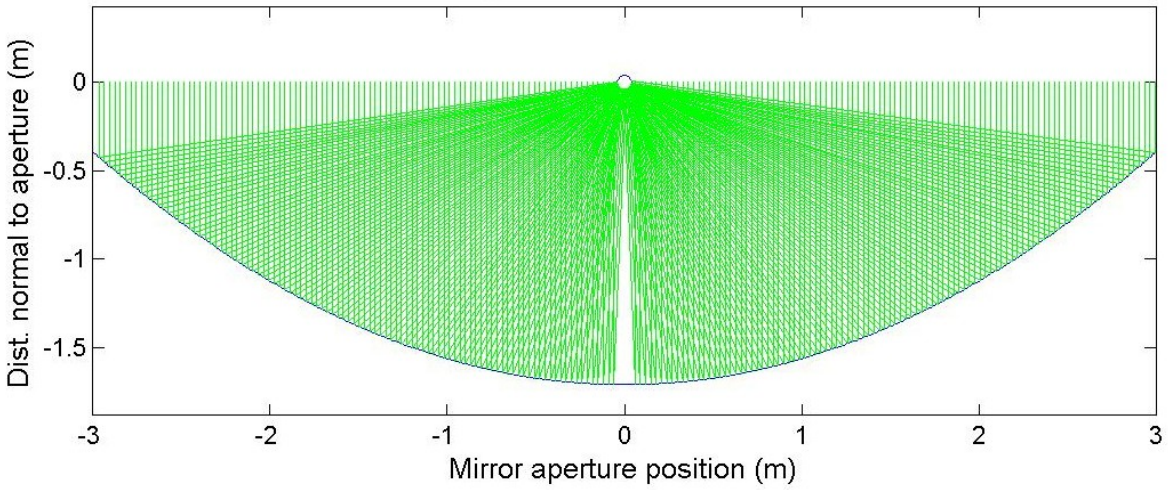

Figure 29. Ray trace results for scan AA_p6_19ft_9_5infixedEDIT.csv, RMS=1.17, Intercept=1.00.

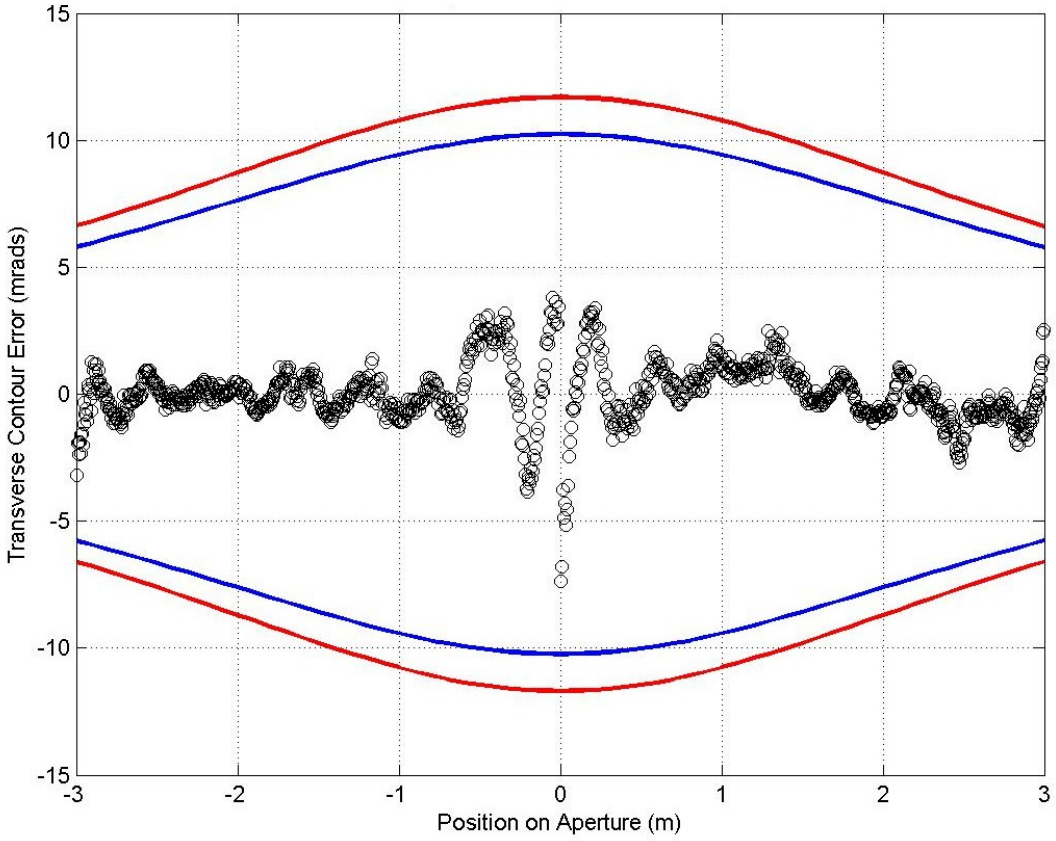

Figure 30. Slope errors along the aperture of scan AA_p6_19ft_9_5infixedEDIT.csv.

Results for Panel 7

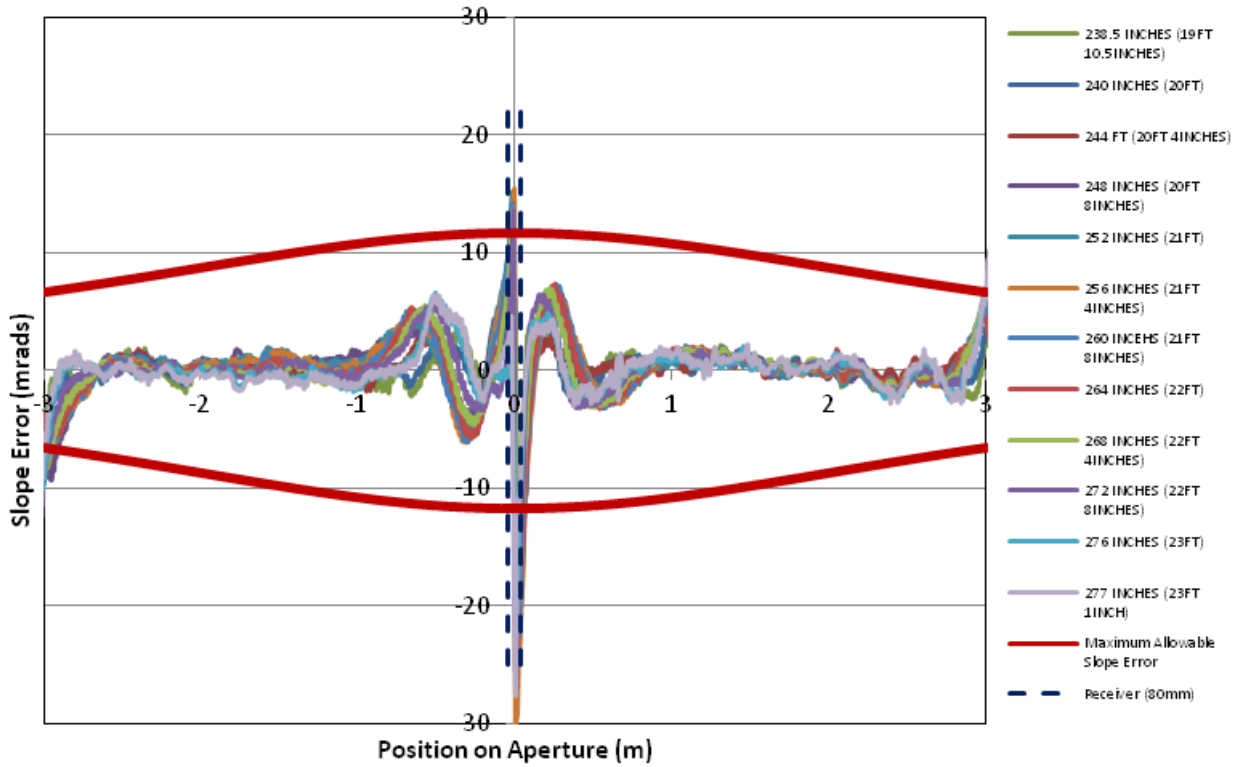

Figure 31. Slope errors along the aperture for each scan taken of Panel 7. The maximum allowable slope error over the aperture for an 80 mm receiver tube is plotted in red.

Table 7. Results for Panel 7 of the Alcoa collector.

File Name	RMS Slope Error Transverse (mrad)	Intercept Factor (straight rays)	Intercept Factor (DLR sun shape)
AA_p7_19ft_10_5ifixedEDIT.csv	1.53	1.00	1.00
AA_p7_20ft_2o_1DfixedEDIT.csv	1.77	0.998	0.998
AA_p7_20ft_4inchfixedEDIT.csv	2.33	0.989	0.990
AA_p7_20ft_8inchfixedEDIT.csv	2.93	0.984	0.983
AA_p7_21ft_2o_1DfixedEDIT.csv	3.01	0.993	0.990
AA_p7_21ft_4inchfixedEDIT.csv	3.41	0.989	0.988
AA_p7_21ft_8inchfixedEDIT.csv	3.05	0.994	0.989
AA_p7_22ft_2o_1DfixedEDIT.csv	2.83	0.998	0.995
AA_p7_22ft_4inchfixedEDIT.csv	2.61	0.990	0.989
AA_p7_22ft_8inchfixedEDIT.csv	2.62	0.994	0.994
AA_p7_23ft_2o_1DfixedEDIT.csv	2.02	0.997	0.996
Average	2.04	0.9987	0.997

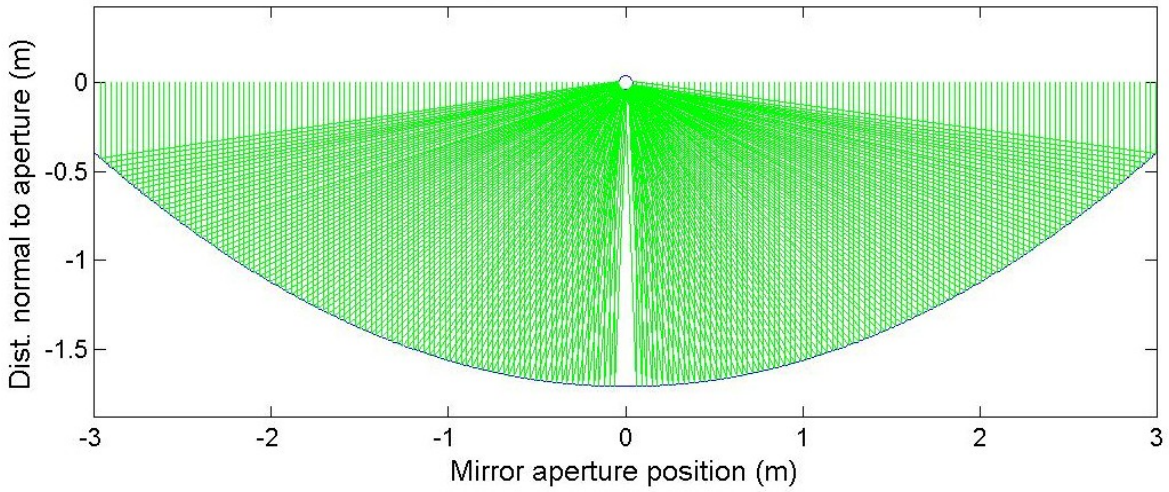

Figure 32. Ray trace results for scan AA_p7_19ft_10_5ifixedEDIT.csv, RMS=1.53, Intercept=1.00.

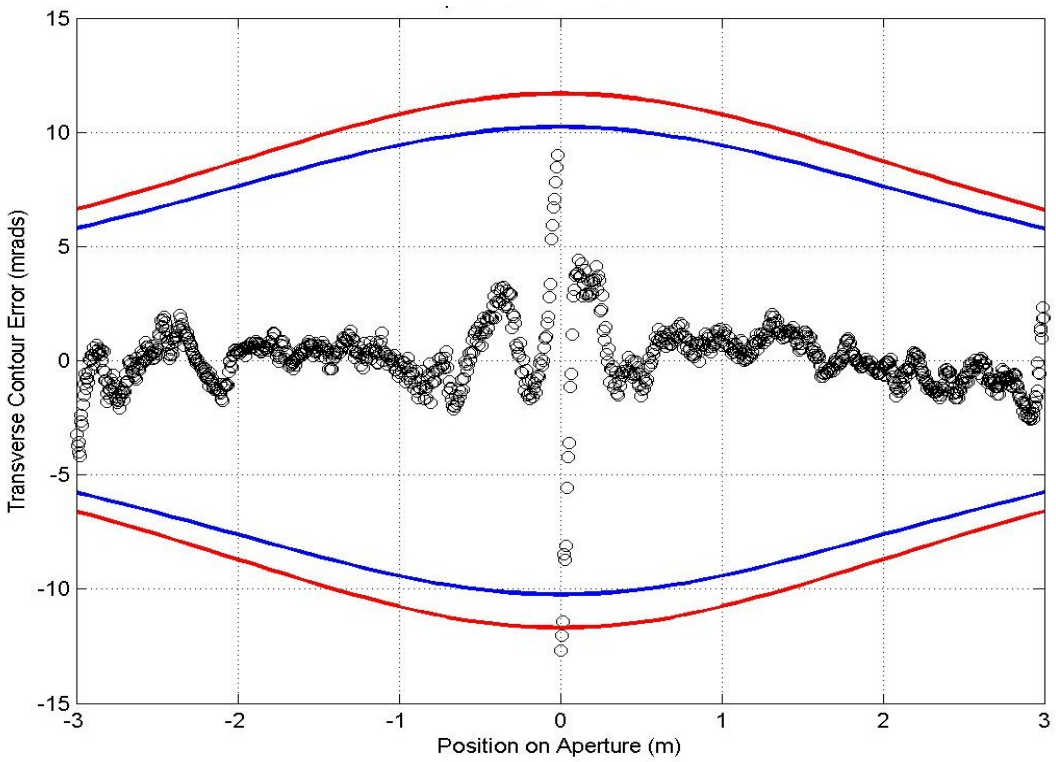

Figure 33. Slope errors along the aperture of scan AA_p7_19ft_10_5ifixedEDIT.csv.

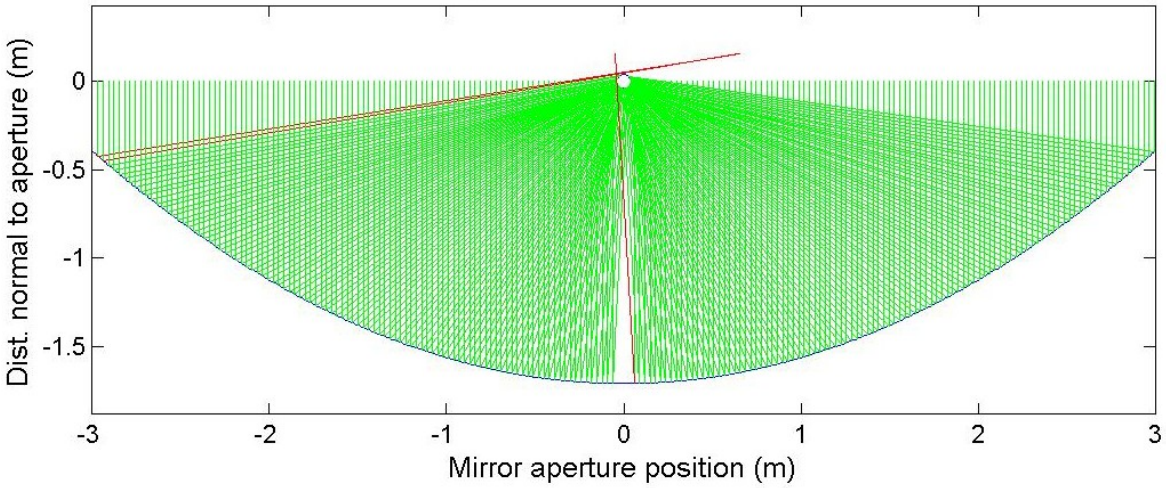

Figure 34. Ray trace results for scan AA_p7_20ft_8inchfixedEDIT.csv, RMS=2.93, Intercept=0.984.

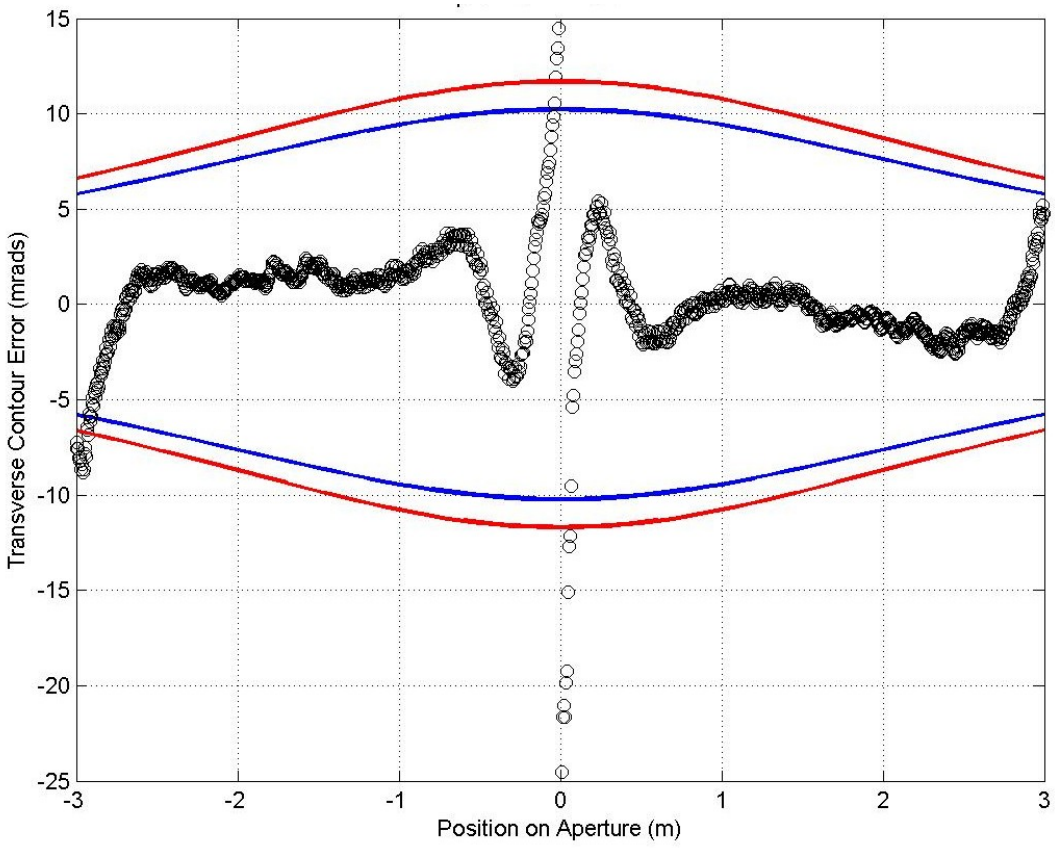

Figure 35. Slope errors along the aperture of scan AA_p7_20ft_8inchfixedEDIT.csv.

Results for Panel 8

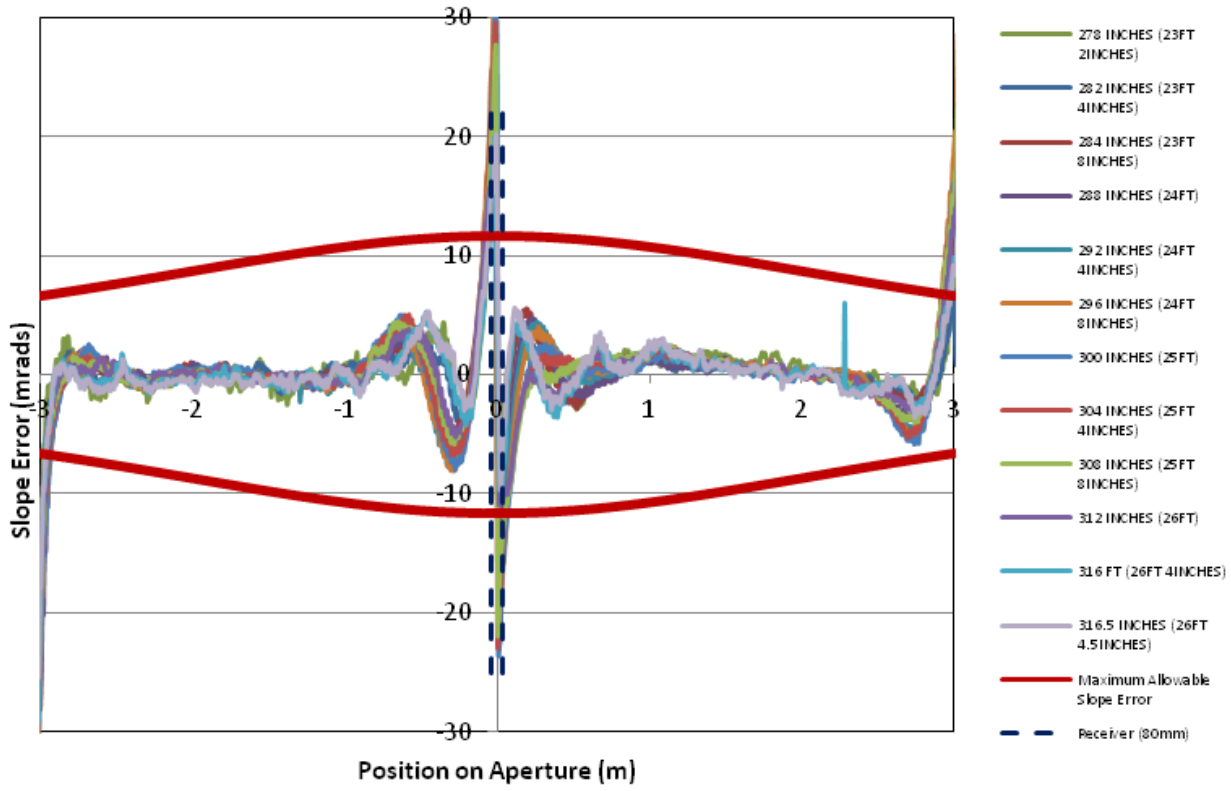

Figure 36. Slope errors along the aperture for each scan taken of Panel 8. The maximum allowable slope error over the aperture for an 80 mm receiver tube is plotted in red.

Table 8. Results for Panel 8 of the Alcoa collector.

File Name	RMS Slope Error Transverse (mrad)	Intercept Factor (straight rays)	Intercept Factor (DLR sun shape)
AA_p8_23ft_2inchfixedEDIT.csv	2.12	0.994	0.993
AA_p8_23ft_4inchfixedEDIT.csv	2.35	0.9884	0.988
AA_p8_23ft_8inchfixedEDIT.csv	3.02	0.977	0.977
AA_p8_24ft_2o_1DfixedEDIT.csv	3.87	0.9717	0.971
AA_p8_24ft_4inchfixedEDIT.csv	4.03	0.970	0.970
AA_p8_24ft_8inchfixedEDIT.csv	4.32	0.964	0.964
AA_p8_25ft_2o_1DfixedEDIT.csv	4.20	0.967	0.964
AA_p8_25ft_4inchfixedEDIT.csv	4.00	0.971	0.969
AA_p8_25ft_8inchfixedEDIT.csv	3.79	0.972	0.971
AA_p8_26ft_2o_1DfixedEDIT.csv	3.03	0.978	0.977
AA_p8_26ft_4_5infixedEDIT.csv	2.70	0.985	0.985
Average	2.61	0.987	0.985

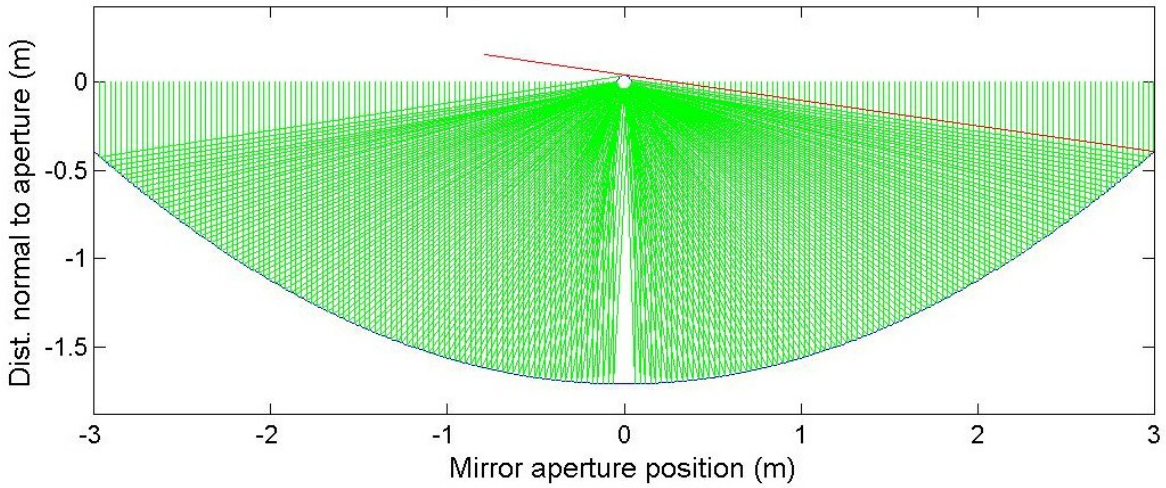

Figure 37. Ray trace results for scan AA_p8_23ft_2inchfixedEDIT.csv, RMS=2.12, Intercept=0.994.

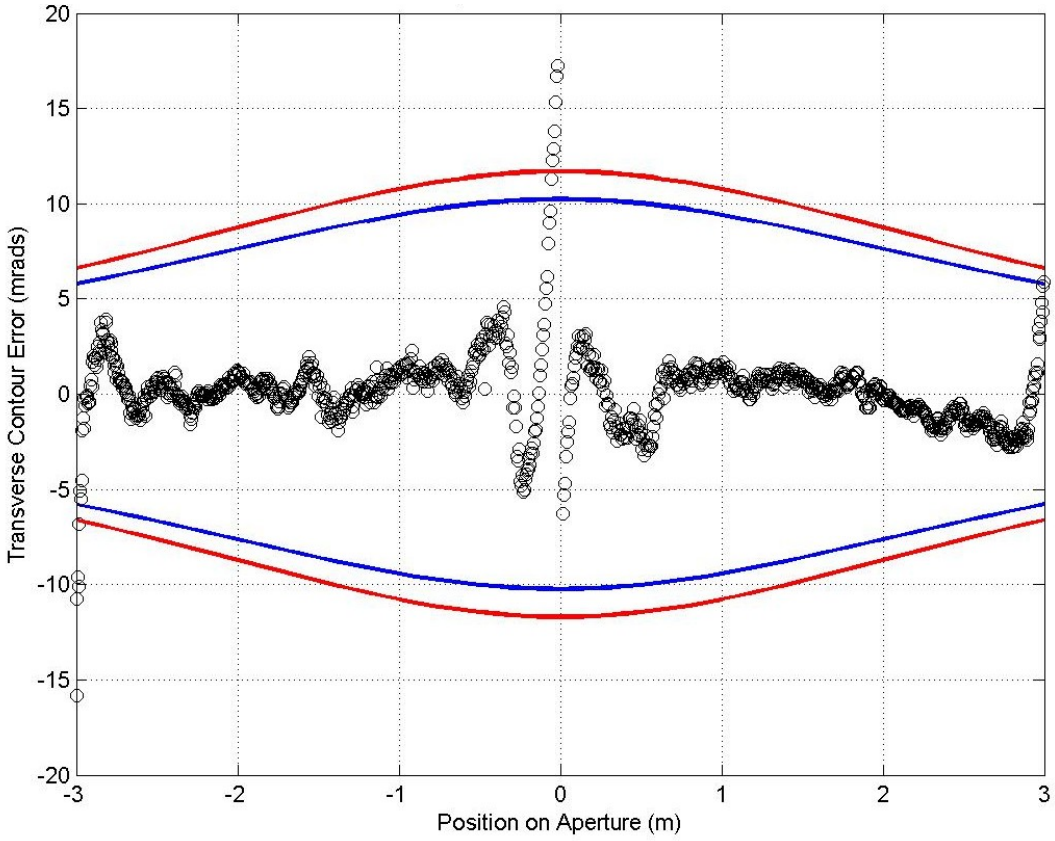

Figure 38. Slope errors along the aperture of scan AA_p8_23ft_2inchfixedEDIT.csv.

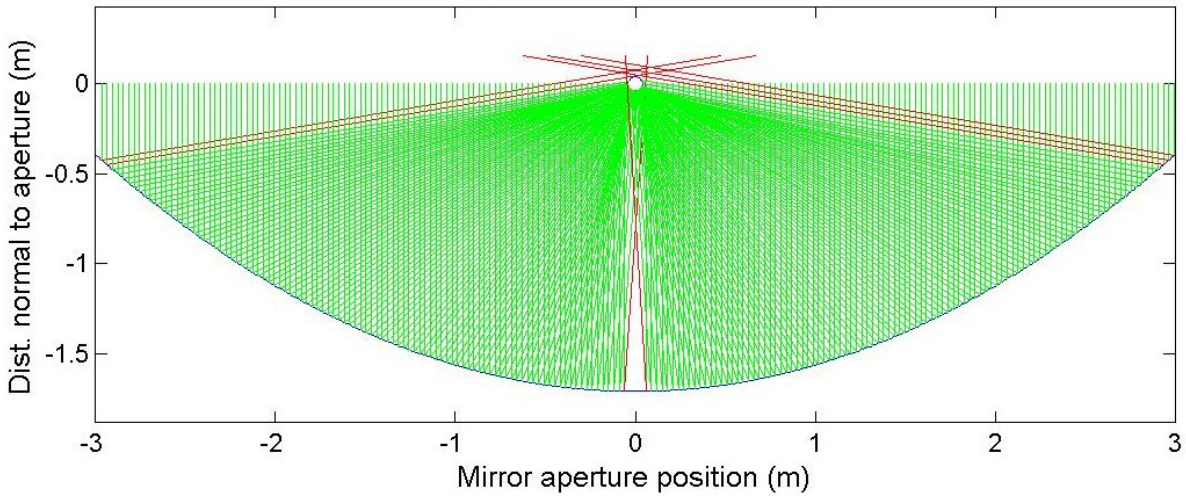

Figure 39. Ray trace results for scan AA_p8_24ft_8inchfixedEDIT.csv, RMS=4.32, Intercept=0.96.

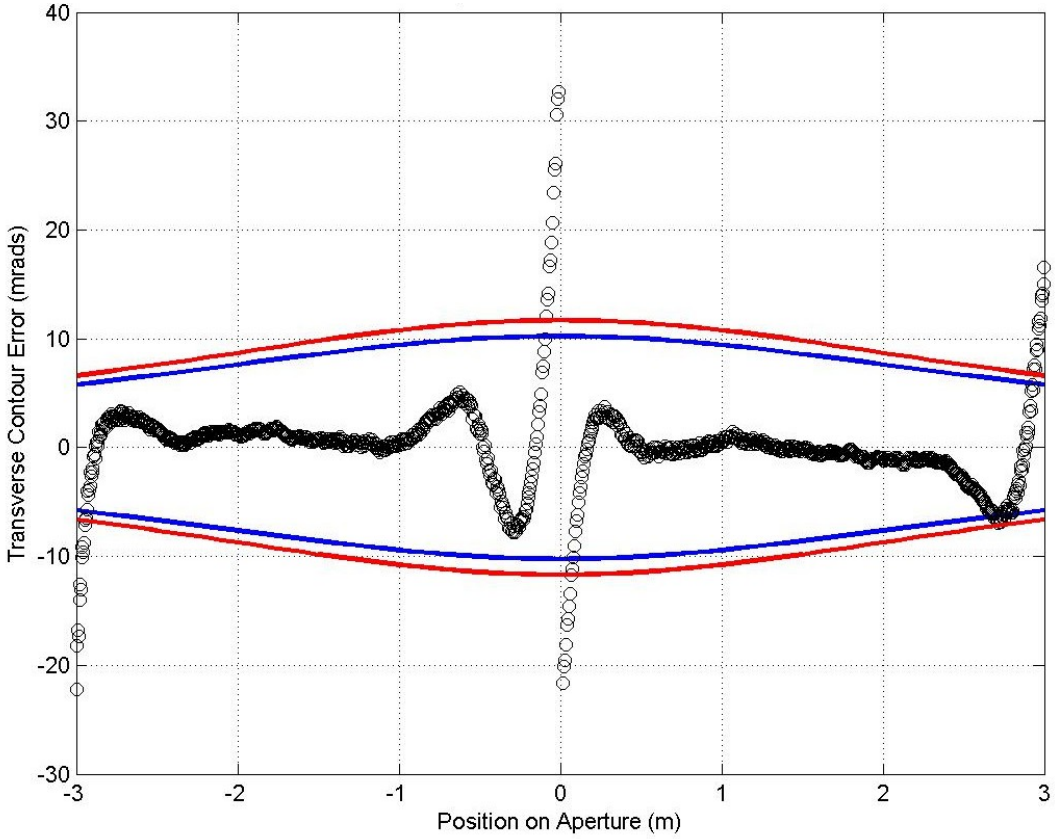

Figure 40. Slope errors along the aperture of scan AA_p8_24ft_8inchfixedEDIT.csv.

Results for Panel 9

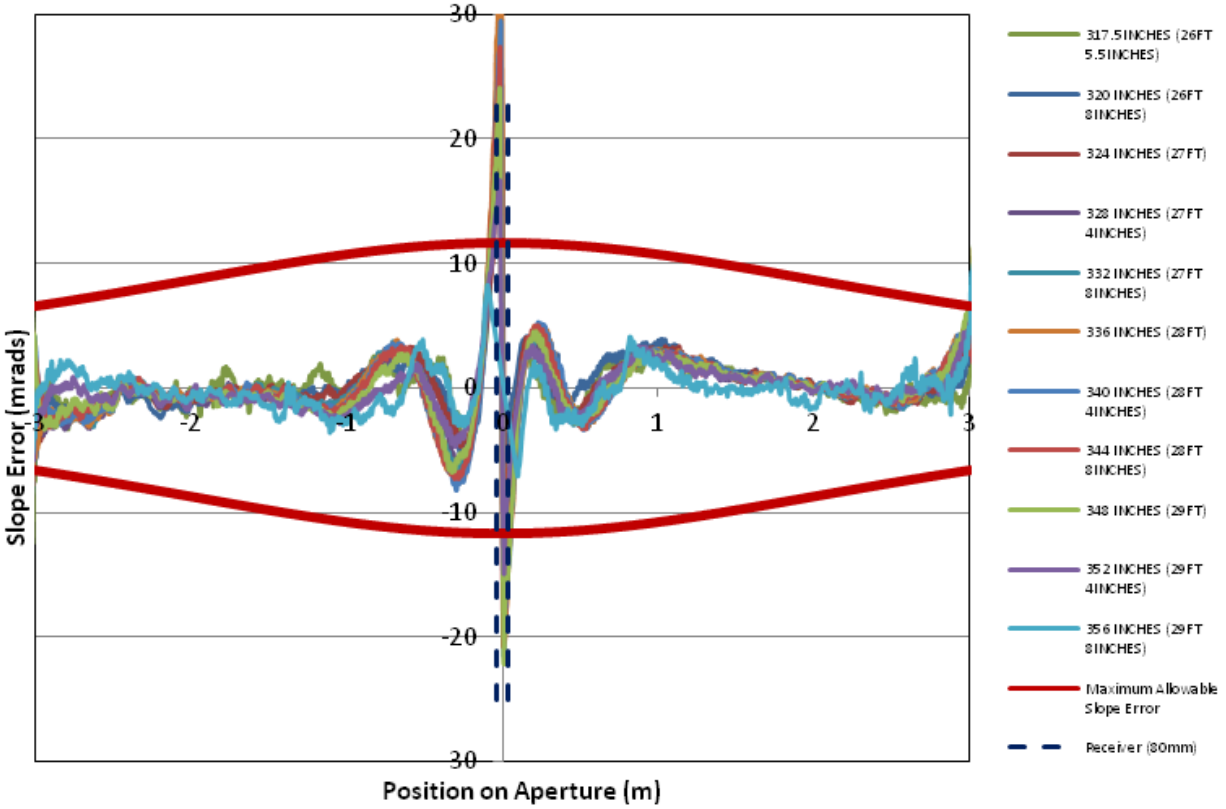

Figure 41. Slope errors along the aperture for each scan taken of Panel 9. The maximum allowable slope error over the aperture for an 80 mm receiver tube is plotted in red.

Table 9. Results for Panel 9 of the Alcoa collector.

File Name	RMS Slope Error Transverse (mrad)	Intercept Factor (straight rays)	Intercept Factor (DLR sun shape)
AA_p9_26ft_5_5infixedEDIT.csv	2.31	0.996	0.995
AA_p9_26ft_8inchfixedEDIT.csv	2.50	0.996	0.996
AA_p9_27ft_2o_1DfixedEDIT.csv	2.63	0.997	0.997
AA_p9_27ft_4inchfixedEDIT.csv	3.29	0.994	0.993
AA_p9_27ft_8inchfixedEDIT.csv	3.17	0.993	0.993
AA_p9_28ft_2o_1DfixedEDIT.csv	3.93	0.990	0.989
AA_p9_28ft_4inchfixedEDIT.csv	3.39	0.992	0.992
AA_p9_28ft_8inchfixedEDIT.csv	3.23	0.992	0.992
AA_p9_29ft_2o_1DfixedEDIT.csv	2.99	0.992	0.990
AA_p9_29ft_4inchfixedEDIT.csv	2.19	0.997	0.996
AA_p9_29ft_8inchfixedEDIT.csv	1.53	1.00	1.00
Average	**2.83**	**0.995**	0.994

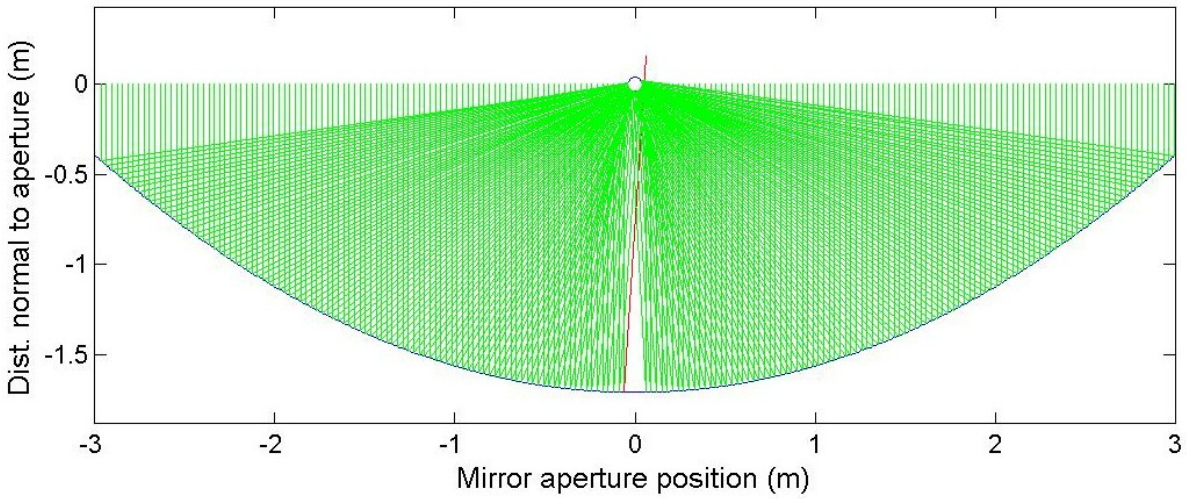

Figure 42. Ray trace results for scan AA_p9_28ft_4inchfixedEDIT.csv, RMS=3.39, Intercept=0.992.

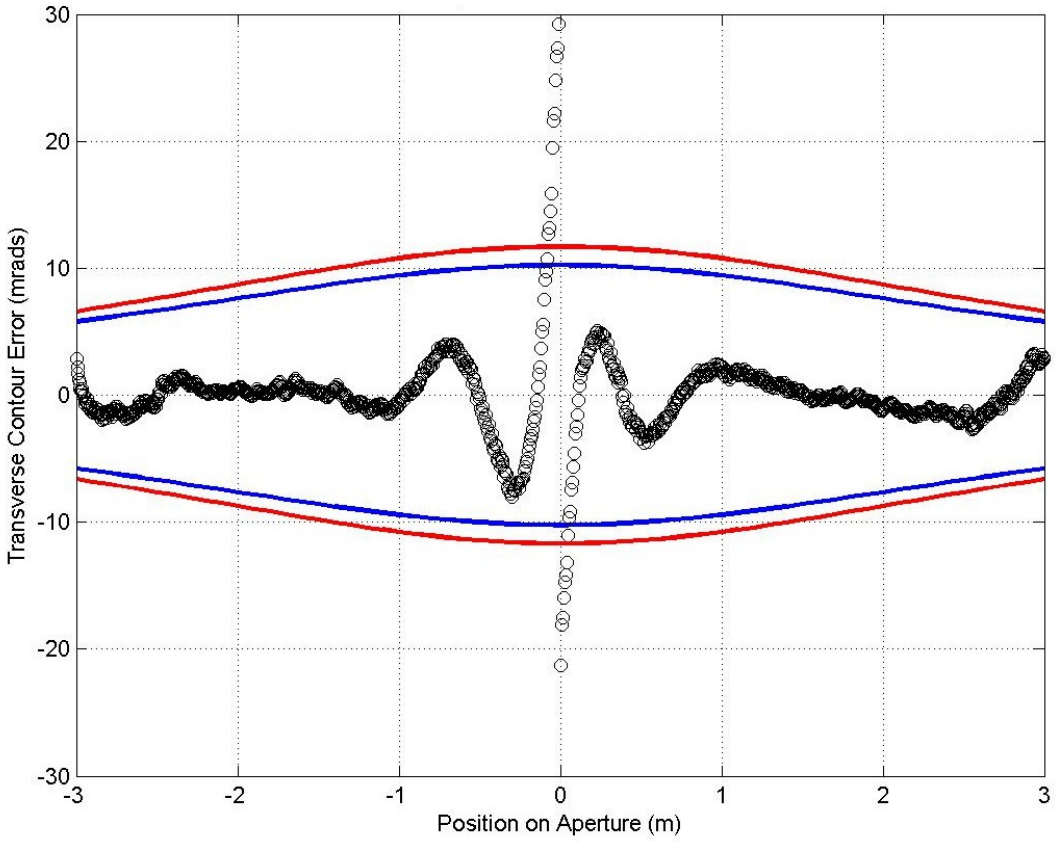

Figure 43. Slope errors along the aperture of scan AA_p9_28ft_4inchfixedEDIT.csv.

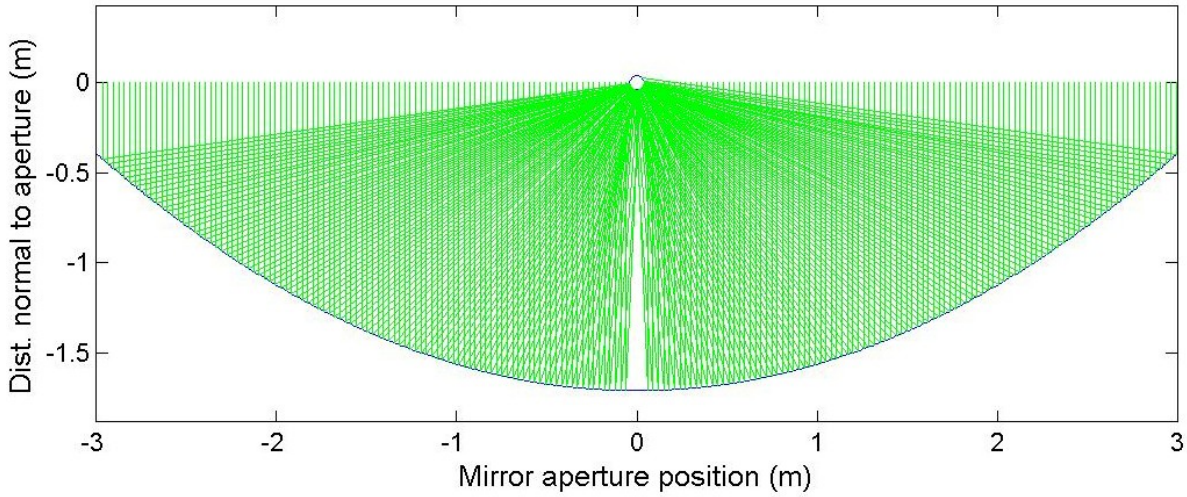

Figure 44. Ray trace results for scan AA_p9_29ft_8inchfixedEDIT.csv, RMS=1.53, Intercept=1.00.

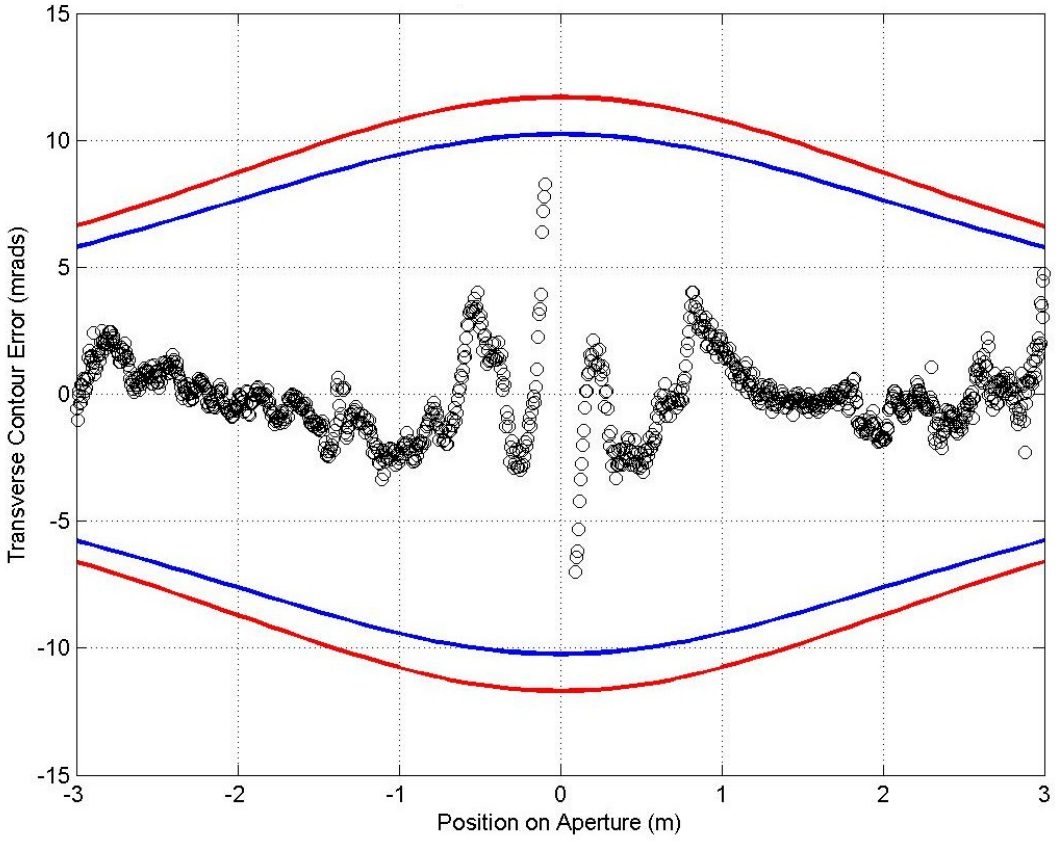

Figure 45. Slope errors along the aperture of scan AA_p9_29ft_8inchfixedEDIT.csv.

Results for Panel 10

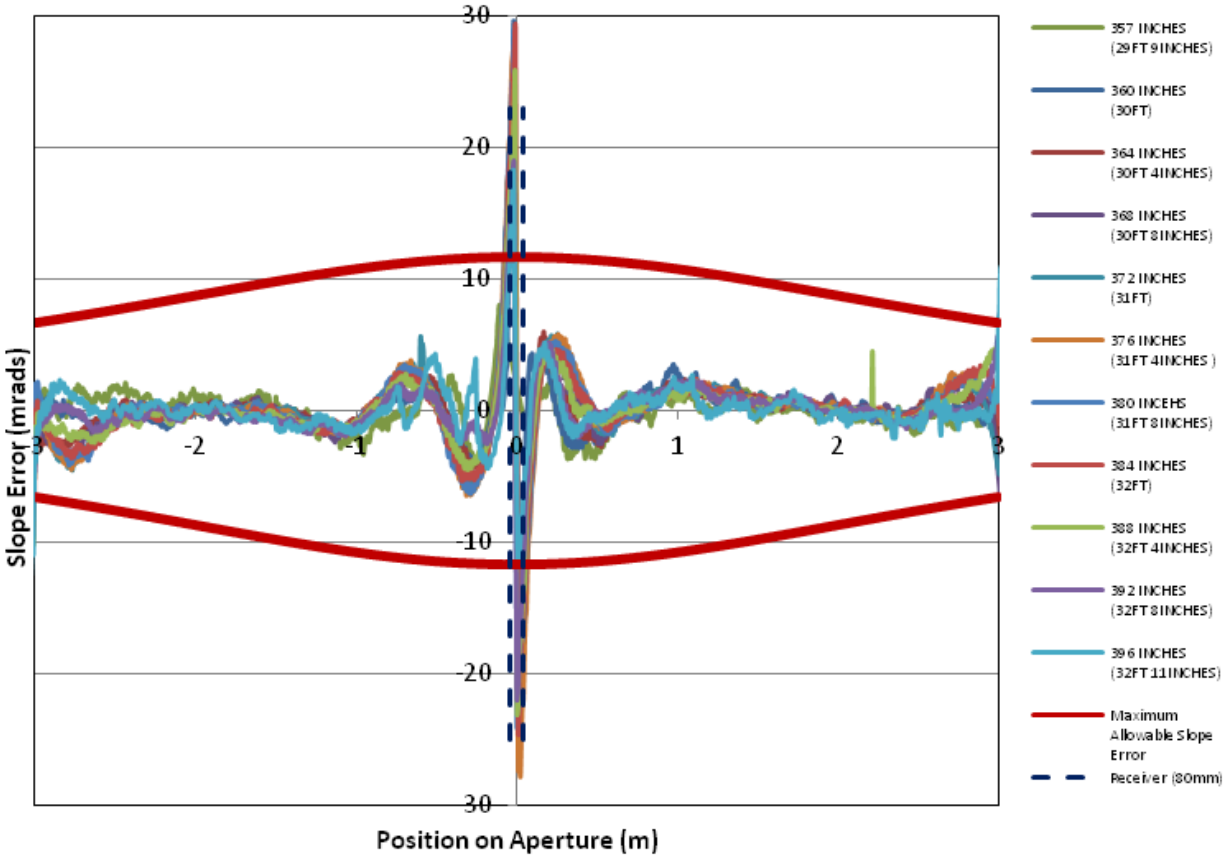

Figure 46. Slope errors along the aperture for each scan taken of Panel 10. The maximum allowable slope error over the aperture for an 80 mm receiver tube is plotted in red.

Table 10. Results for Panel 10 of the Alcoa collector.

File Name	RMS Slope Error Transverse (mrad)	Intercept Factor (straight rays)	Intercept Factor (DLR sun shape)
AA_p10_29ft_9incfixedEDIT.csv	1.34	1.00	1.00
AA_p10_30ft_2o_1fixedEDIT.csv	2.31	1.00	0.999
AA_p10_30ft_4incfixedEDIT.csv	2.67	1.00	0.995
AA_p10_30ft_8incfixedEDIT.csv	2.90	0.993	0.993
AA_p10_31ft_2o_1fixedEDIT.csv	3.01	0.991	0.991
AA_p10_31ft_4incfixedEDIT.csv	3.49	0.990	0.990
AA_p10_31ft_8incfixedEDIT.csv	3.30	0.991	0.991
AA_p10_32ft_2o_1fixedEDIT.csv	3.18	0.992	0.992
AA_p10_32ft_4incfixedEDIT.csv	2.84	0.994	0.994
AA_p10_32ft_8incfixedEDIT.csv	2.32	0.998	0.997
AA_p10_32ft_11infixedEDIT.csv	1.84	1.00	0.999
Average	**2.65**	**0.995**	0.995

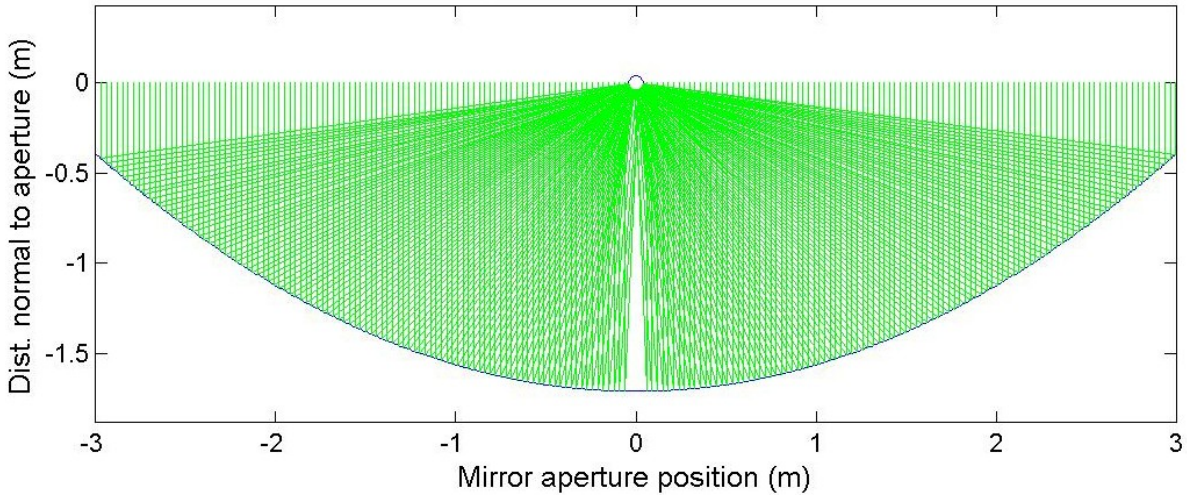

Figure 47. Ray trace results for scan AA_p10_29ft_9incfixedEDIT.csv, RMS=1.34, Intercept=1.00. Red rays in the plots indicate rays that miss the receiver decreasing the intercept factor for that scan.

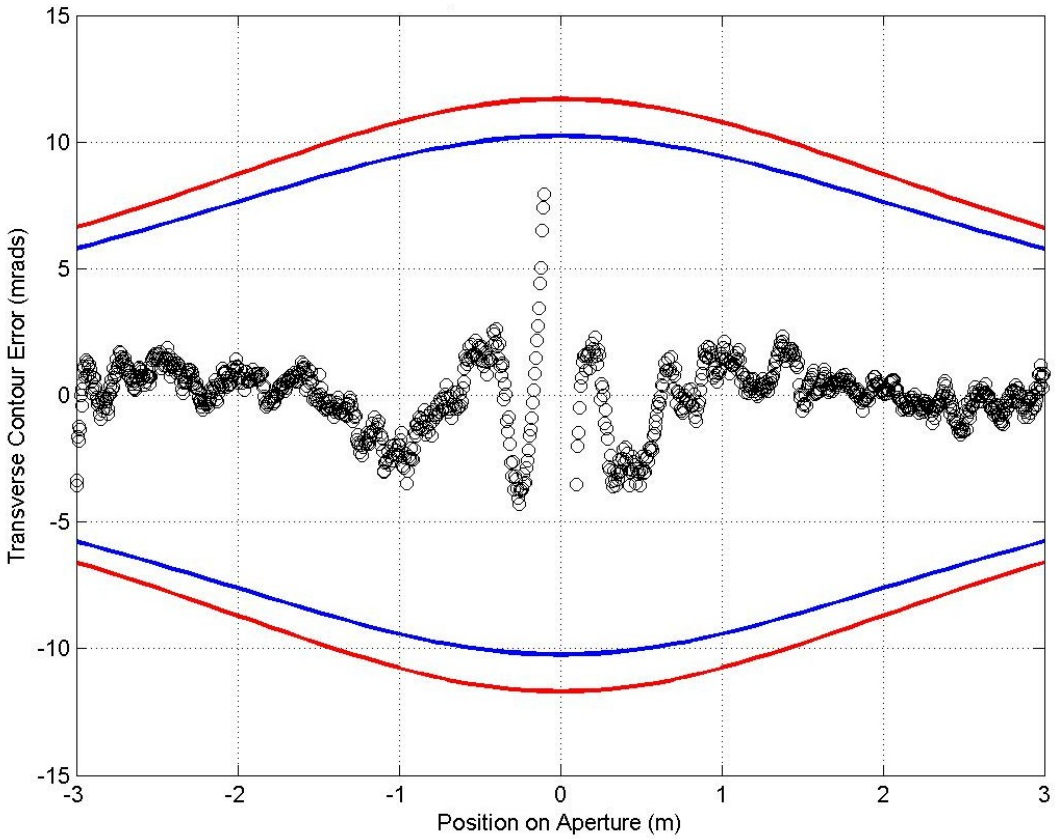

Figure 48. Slope errors along the aperture of scan AA_p10_29ft_9incfixedEDIT.csv.

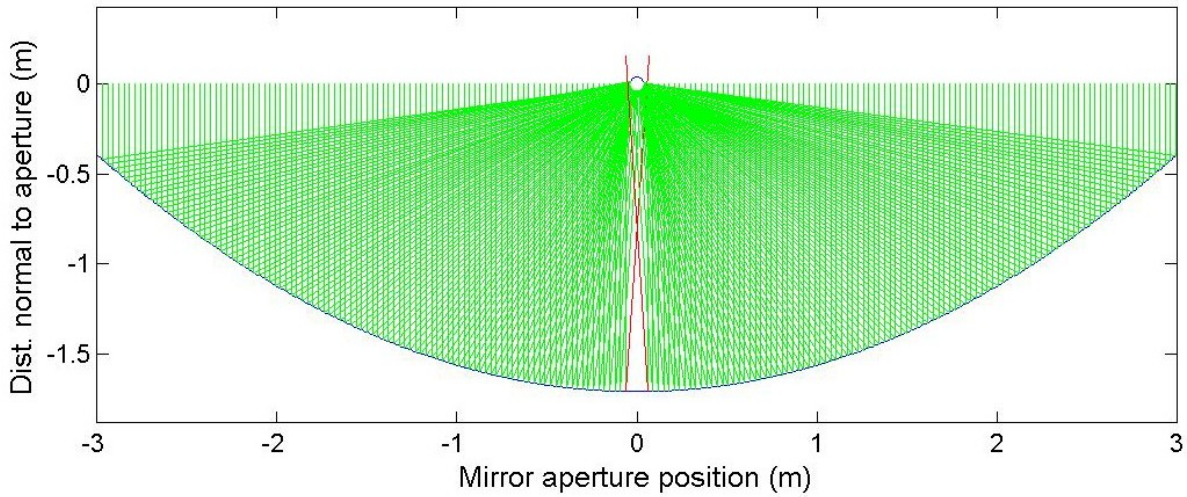

Figure 49. Ray trace results for scan AA_p10_30ft_4incfixedEDIT.csv, RMS=3.48483, Intercept=0.990.

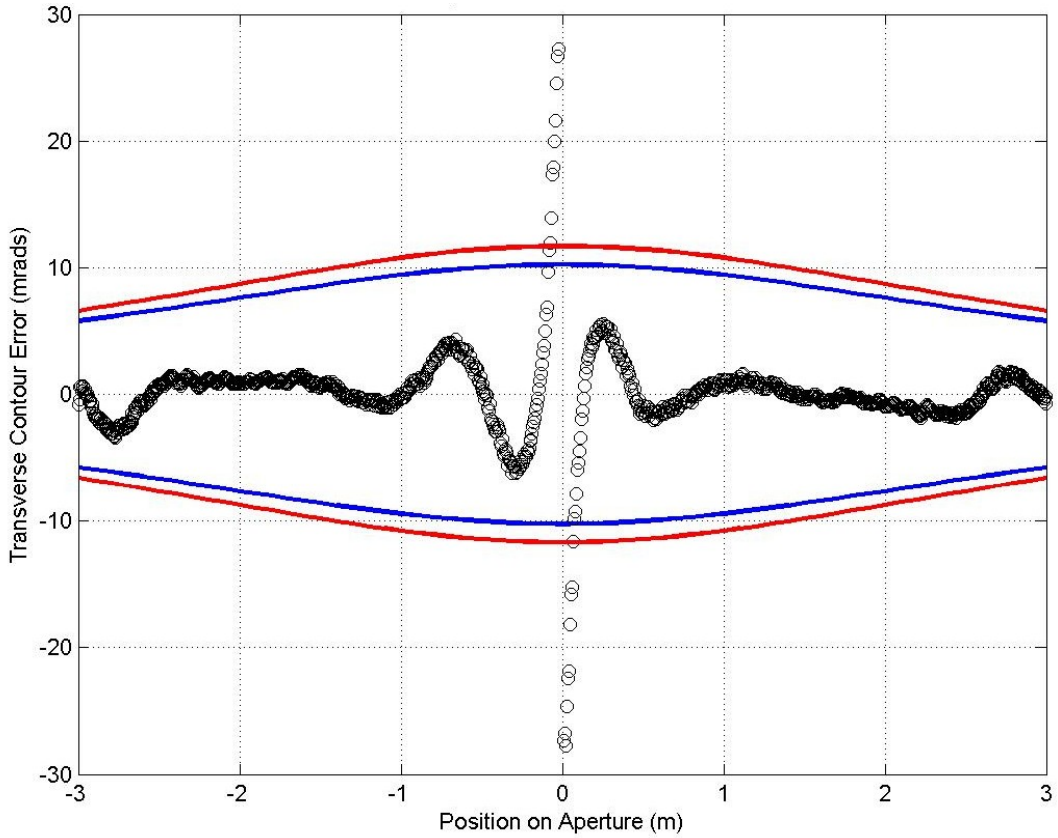

Figure 50. Slope errors along the aperture of scan AA_p10_30ft_4incfixedEDIT.csv.

Results for Panel 11

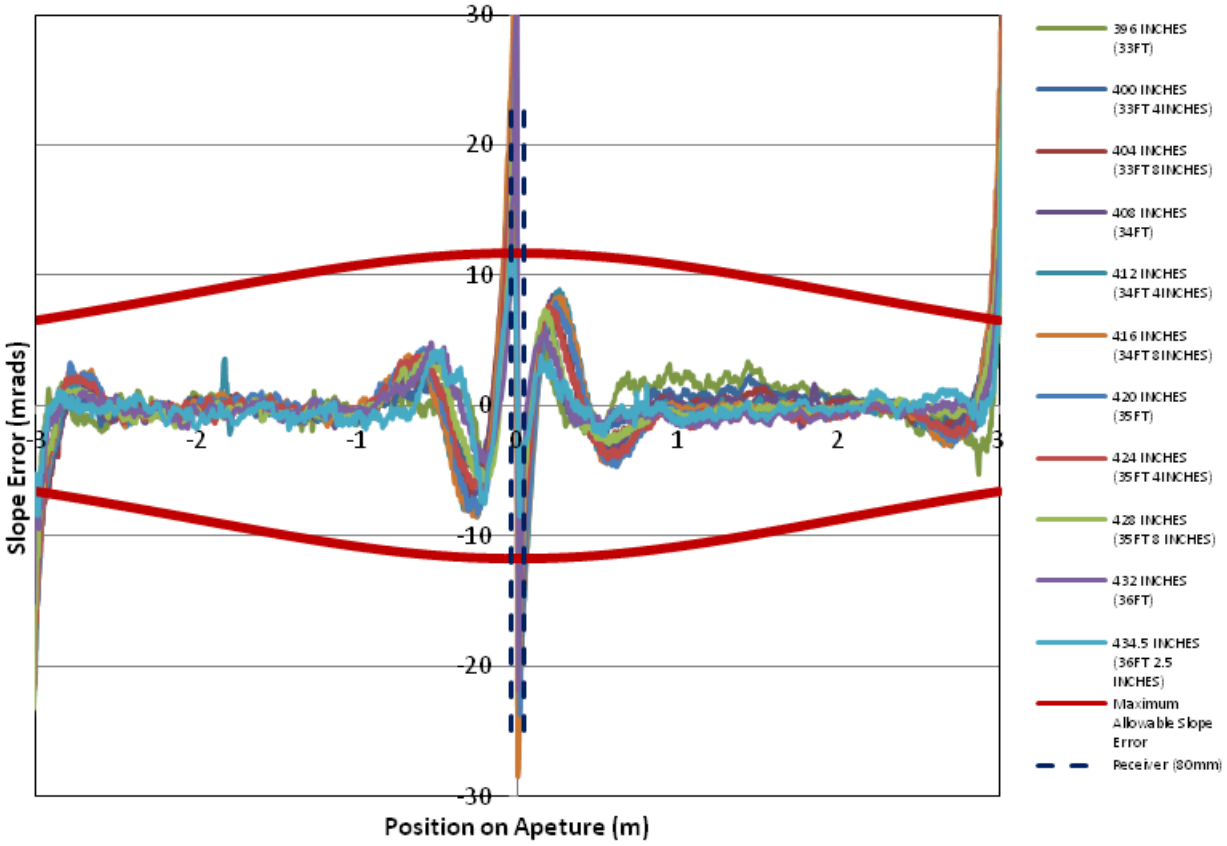

Figure 51. Slope errors along the aperture for each scan taken of Panel 11. The maximum allowable slope error over the aperture for an 80 mm receiver tube is plotted in red.

Table 11. Results for Panel 11 of the Alcoa collector.

File Name	RMS Slope Error Transverse (mrad)	Intercept Factor (straight rays)	Intercept Factor (DLR sun shape)
AA_p11_33ft_2o_1fixedEDIT.csv	2.21	0.995	0.994
AA_p11_33ft_4incfixedEDIT.csv	2.85	0.983	0.983
AA_p11_33ft_8incfixedEDIT.csv	3.53	0.976	0.975
AA_p11_34ft_2o_1fixedEDIT.csv	3.81	0.973	0.972
AA_p11_34ft_4incfixedEDIT.csv	3.99	0.974	0.972
AA_p11_34ft_8incfixedEDIT.csv	4.54	0.970	0.971
AA_p11_35ft_2o_1fixedEDIT.csv	3.82	0.977	0.976
AA_p11_35ft_4incfixedEDIT.csv	3.59	0.979	0.978
AA_p11_35ft_8incfixedEDIT.csv	3.18	0.984	0.984
AA_p11_36ft_2o_1fixedEDIT.csv	2.81	0.989	0.989
AA_p11_36ft_2_5ifixedEDIT.csv	1.82	0.995	0.995
Average	3.29	0.981	0.981

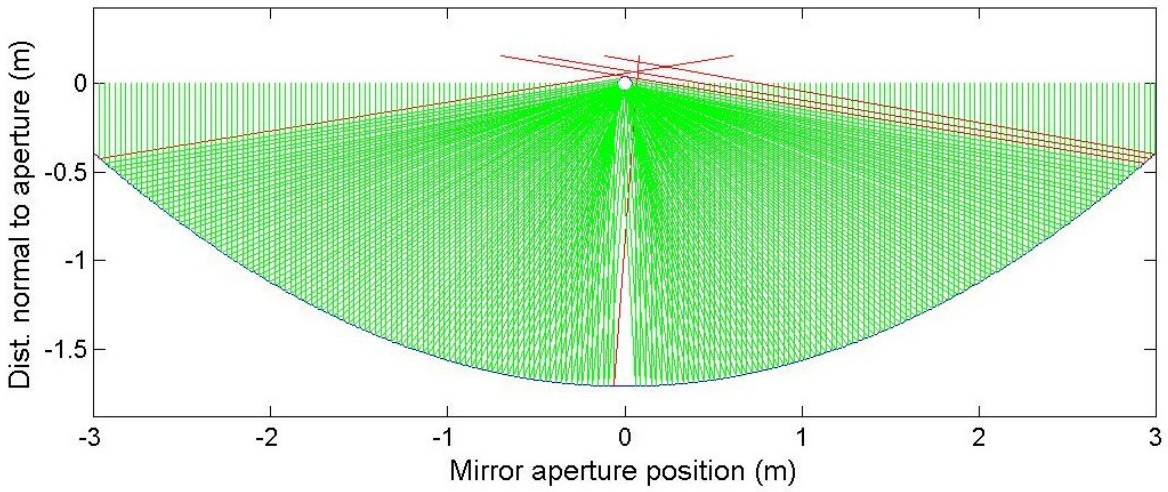

Figure 52. Ray trace results for scan AA_p11_34ft_8incfixedEDIT.csv, RMS=4.54, Intercept=0.970.

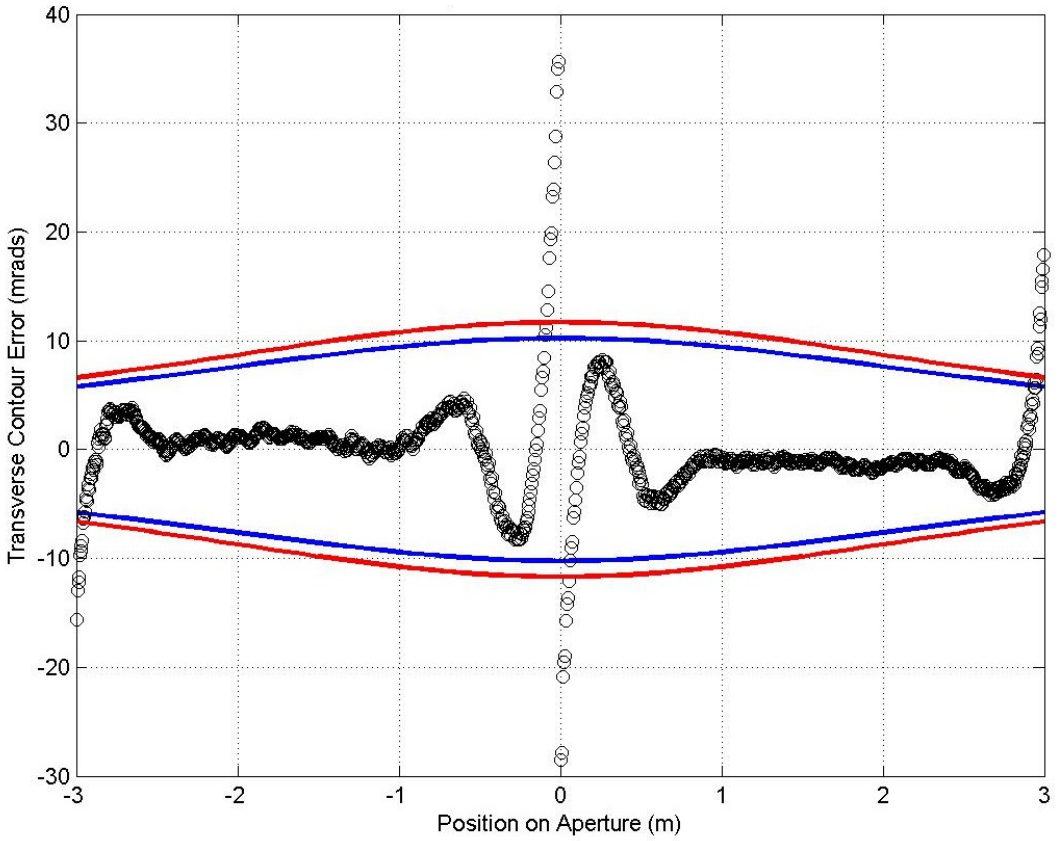

Figure 53. Slope errors along the aperture of scan AA_p11_34ft_8incfixedEDIT.csv.

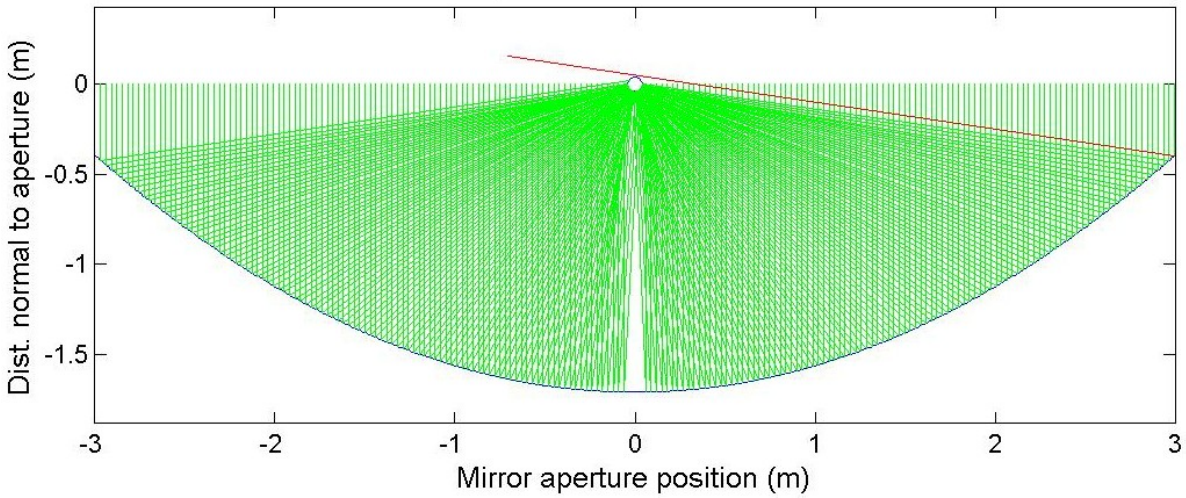

Figure 54. Ray trace results for scan AA_p11_36ft_2_5ifixedEDIT.csv, RMS=1.82, Intercept=0.995.

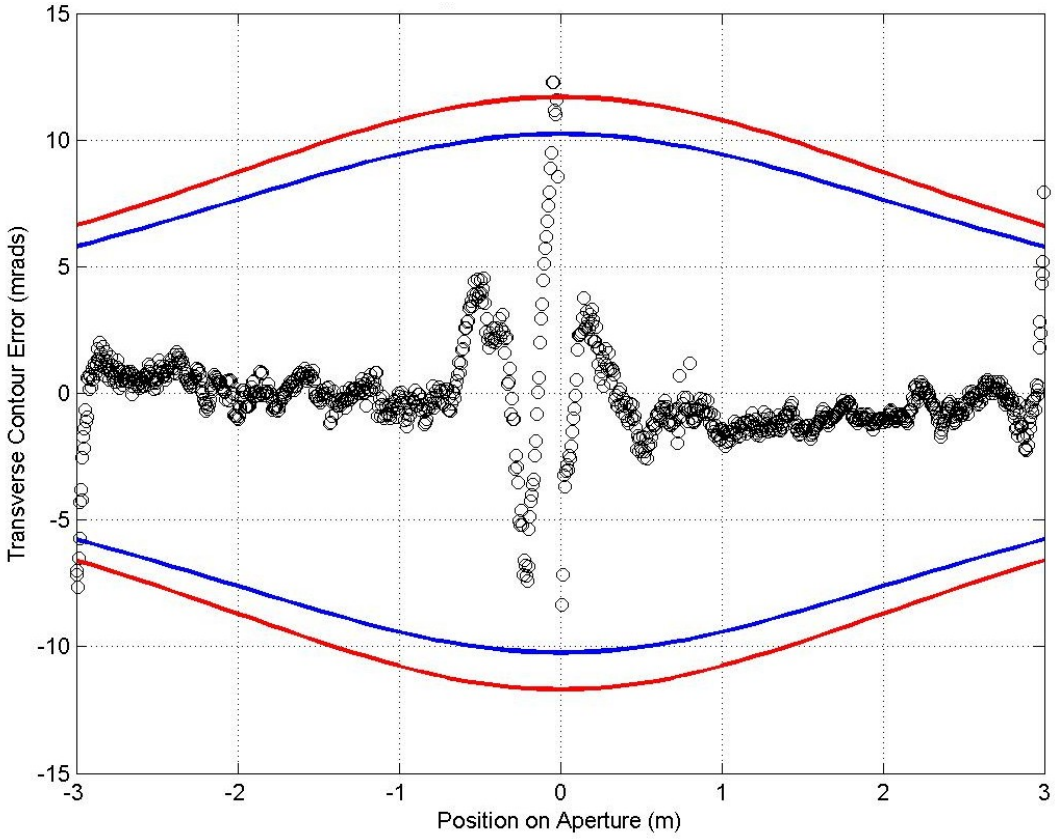

Figure 55. Slope errors along the aperture of scan AA_p11_36ft_2_5ifixedEDIT.csv

Results for Panel 12

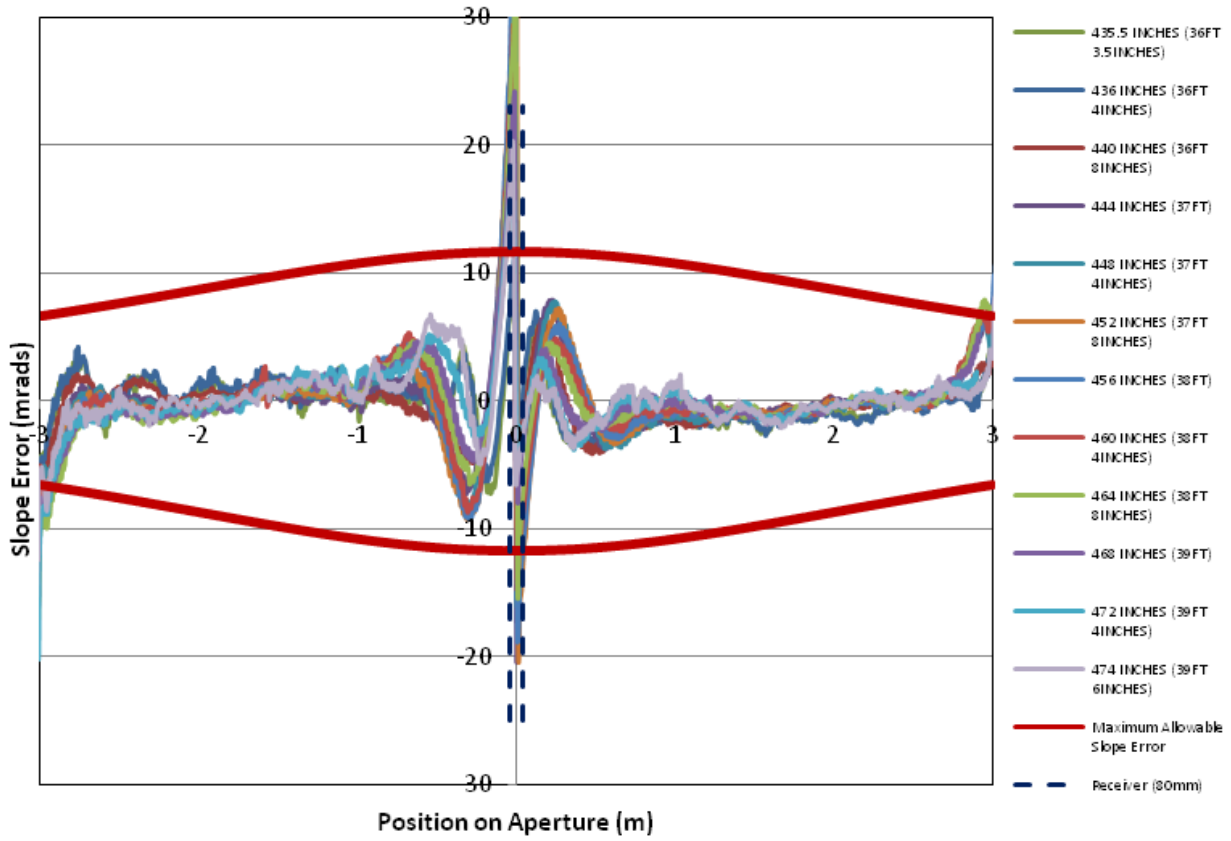

Figure 56. Slope errors along the aperture for each scan taken of Panel 1. The maximum allowable slope error over the aperture for an 80 mm receiver tube is plotted in red.

Table 12. Results for Panel 12 of the Alcoa collector.

File Name	RMS Slope Error Transverse (mrad)	Intercept Factor (straight rays)	Intercept Factor (DLR sun shape)
AA_p12_36ft_3_5ifixedEDIT.csv	1.86	1.00	1.00
AA_p12_36ft_4incfixedEDIT.csv	1.94	1.00	0.999
AA_p12_36ft_8incfixedEDIT.csv	2.40	0.996	0.994
AA_p12_37ft_2o_1fixedEDIT.csv	3.56	0.984	0.980
AA_p12_37ft_4incfixedEDIT.csv	3.80	0.991	0.983
AA_p12_37ft_8incfixedEDIT.csv	4.23	0.980	0.974
AA_p12_38ft_2o_1fixedEDIT.csv	4.13	0.975	0.971
AA_p12_38ft_4incfixedEDIT.csv	3.46	0.980	0.975
AA_p12_38ft_8incfixedEDIT.csv	3.70	0.965	0.966
AA_p12_39ft_2o_1fixedEDIT.csv	2.99	0.980	0.978
AA_p12_39ft_4incfixedEDIT.csv	2.46	0.985	0.984
Average	2.43	0.992	0.991

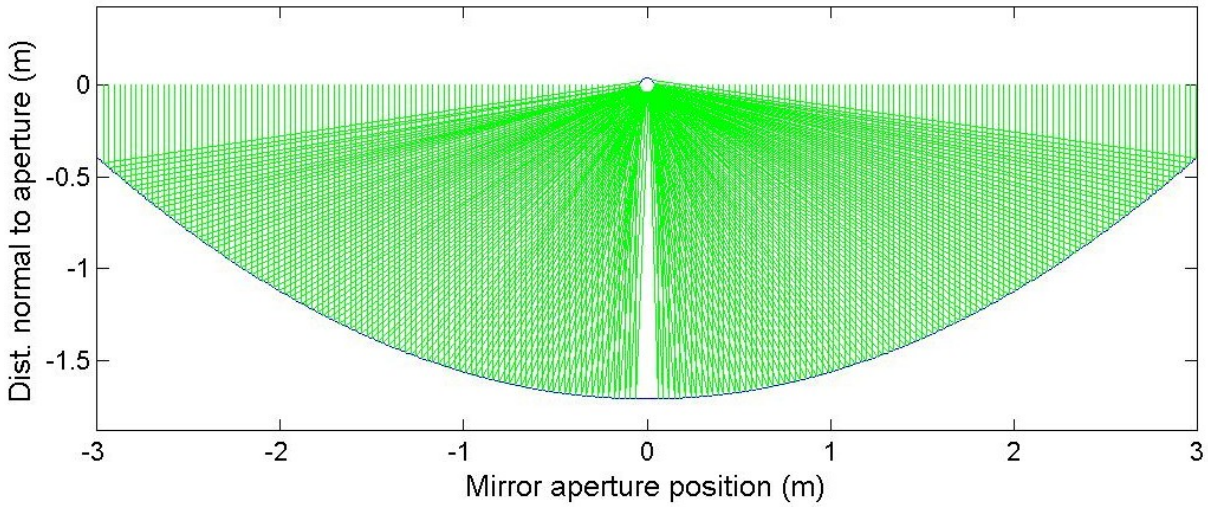

Figure 57. Ray trace results for scan AA_p12_36ft_3_5ifixedEDIT.csv, RMS=1.86, Intercept=1.00.

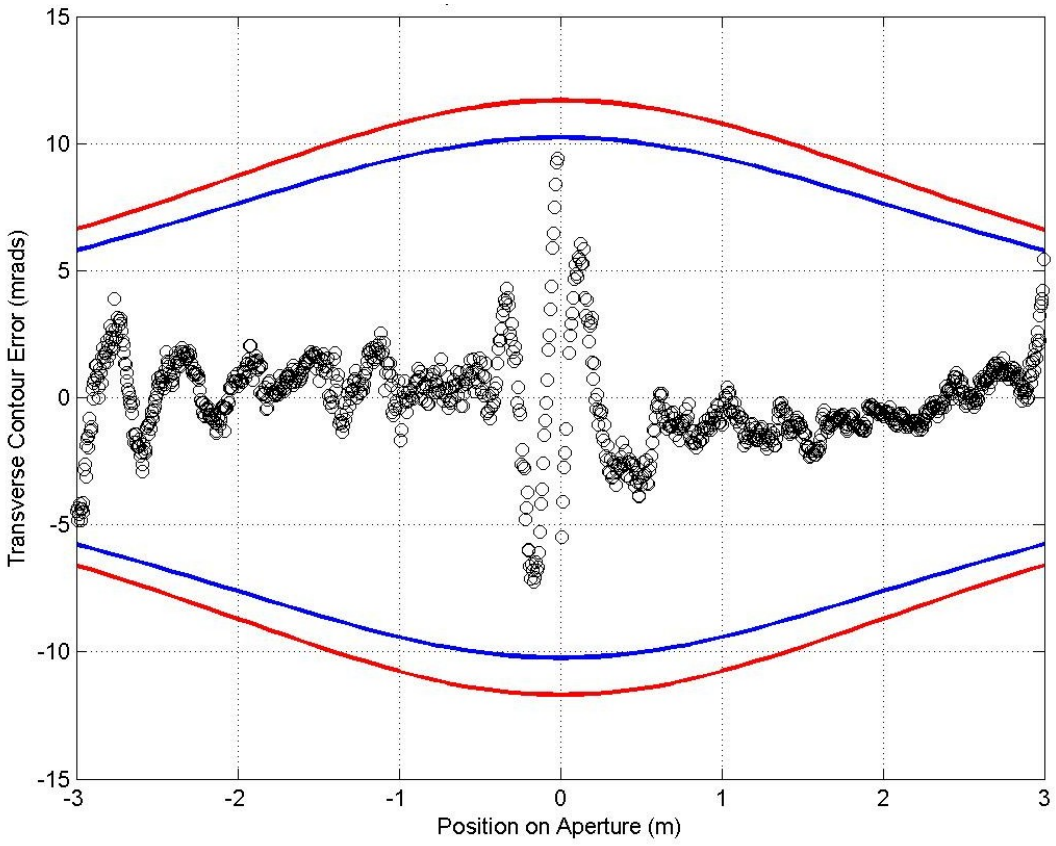

Figure 58. Slope errors along the aperture of scan AA_p12_36ft_3_5ifixedEDIT.csv.

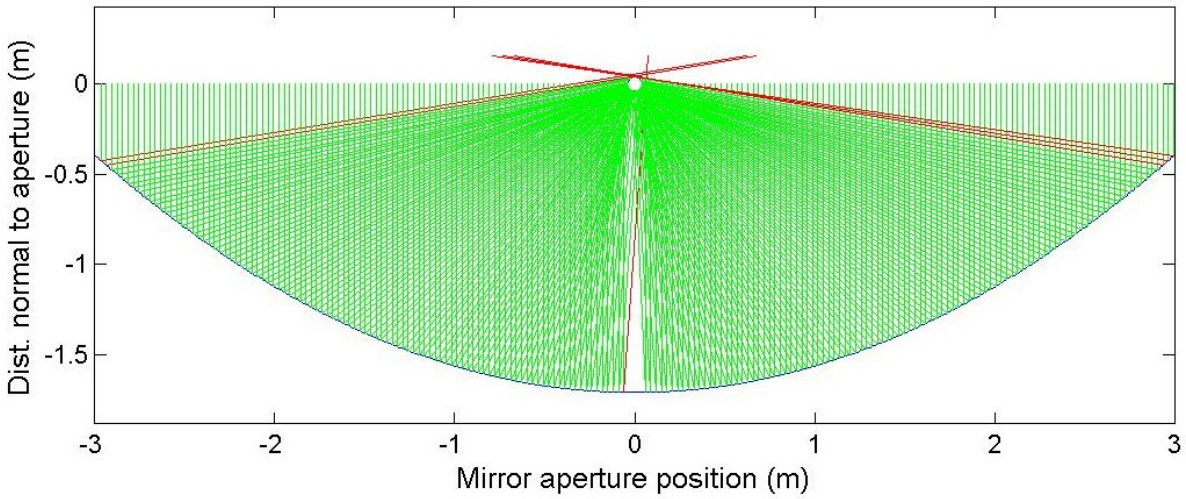

Figure 59. Ray trace results for scan AA_p12_38ft_8incfixedEDIT.csv, RMS=3.70, Intercept=0.965.

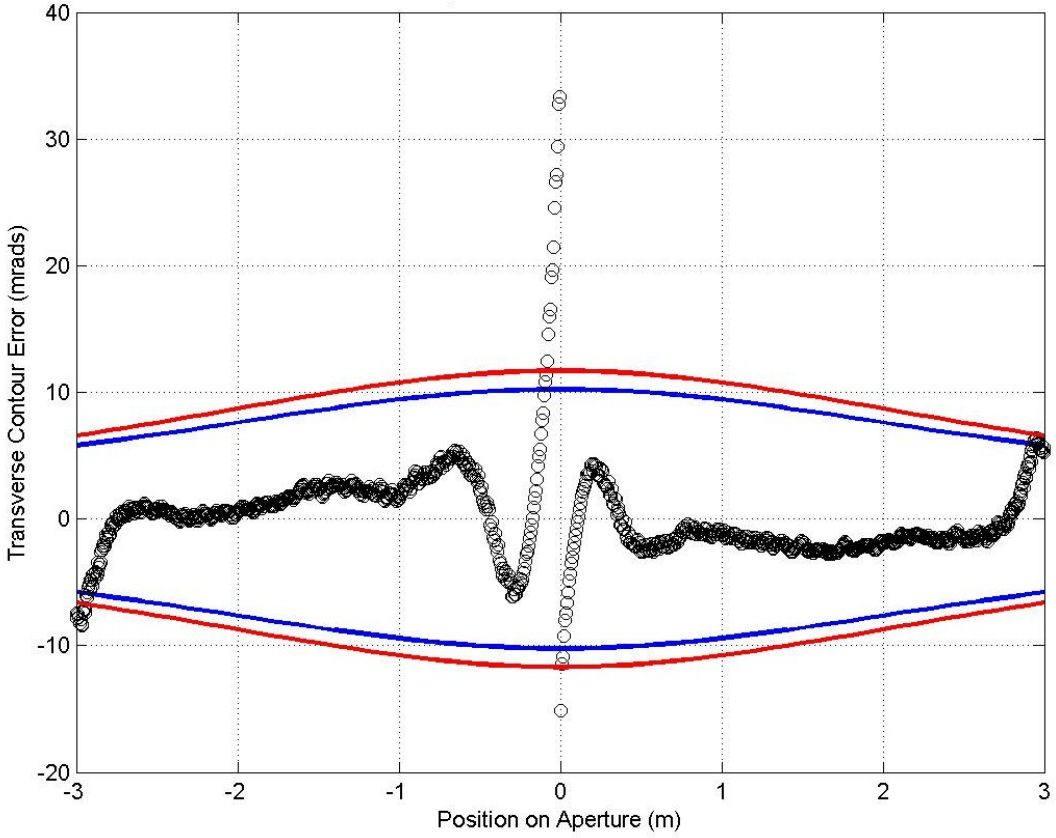

Figure 60. Slope errors along the aperture of scan AA_p12_38ft_8incfixedEDIT.csv.

Results for Panel 13

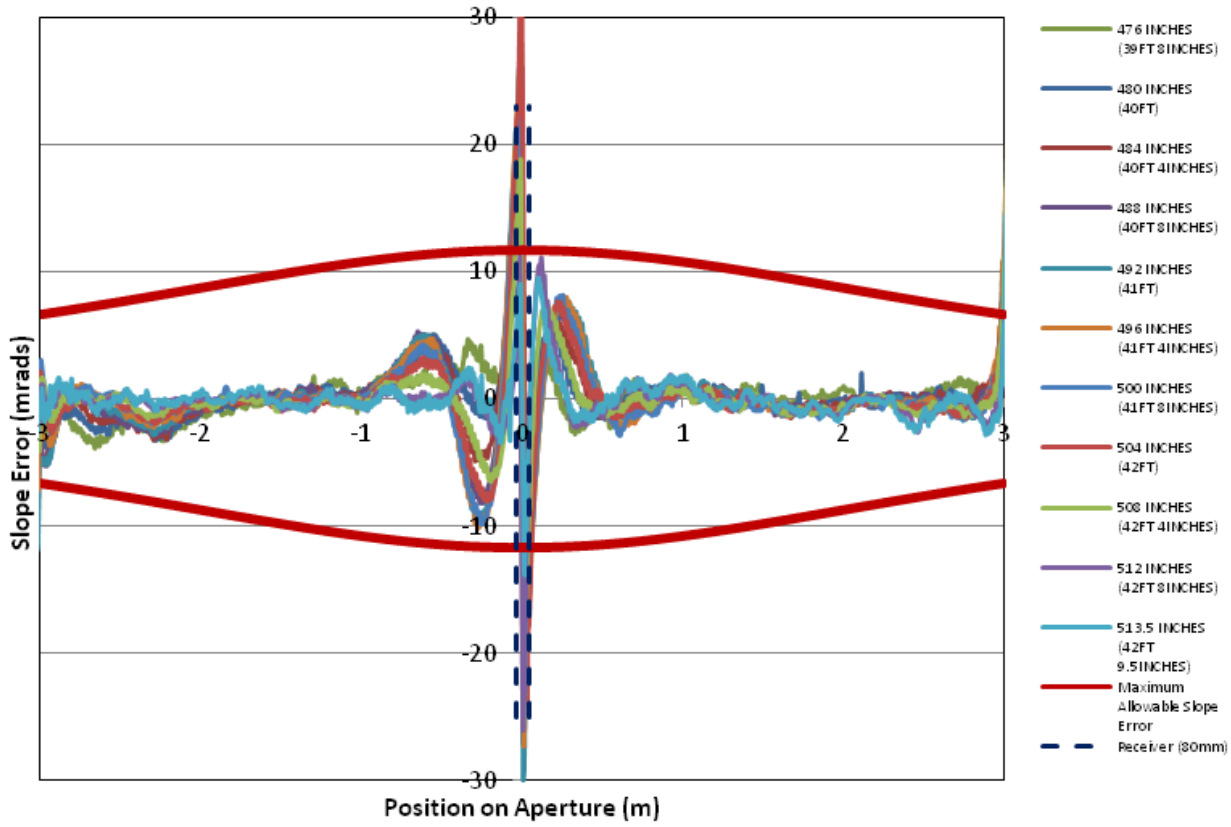

Figure 61. Slope errors along the aperture for each scan taken of Panel 1. The maximum allowable slope error over the aperture for an 80 mm receiver tube is plotted in red.

Table 13. Results for Panel 13 of the Alcoa collector.

File Name	RMS Slope Error Transverse (mrad)	Intercept Factor (straight rays)	Intercept Factor (DLR sun shape)
AA_p13_39ft_8incfixedEDIT.csv	1.79	0.997	0.998
AA_p13_40ft_2o_1fixedEDIT.csv	1.99	1.00	1.00
AA_p13_40ft_4incfixedEDIT.csv	2.91	0.995	0.994
AA_p13_40ft_8incfixedEDIT.csv	3.38	0.992	0.992
AA_p13_41ft_2o_1fixedEDIT.csv	3.84	0.988	0.984
AA_p13_41ft_4incfixedEDIT.csv	3.60	0.988	0.988
AA_p13_41ft_8incfixedEDIT.csv	3.33	0.991	0.990
AA_p13_42ft_2o_1fixedEDIT.csv	3.27	0.991	0.991
AA_p13_42ft_4incfixedEDIT.csv	2.43	0.998	0.998
AA_p13_42ft_8incfixedEDIT.csv	2.05	1.00	0.999
AA_p13_42ft_9_5ifixedEDIT.csv	1.48	1.00	1.00
Average	**2.73**	**0.995**	0.994

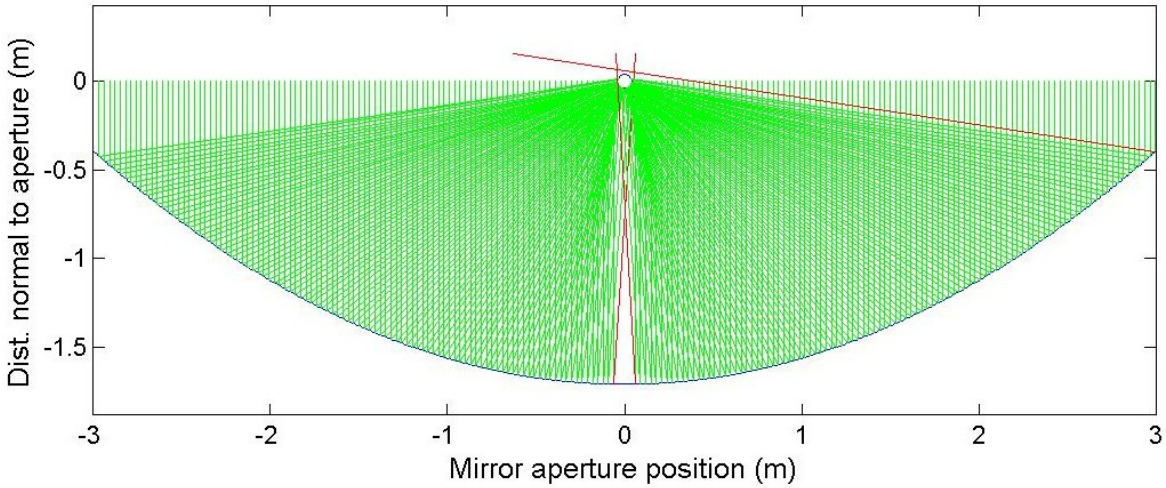

Figure 62. Ray trace results for scan AA_p13_41ft_4incfixedEDIT.csv, RMS=3.59699, Intercept=0.988.

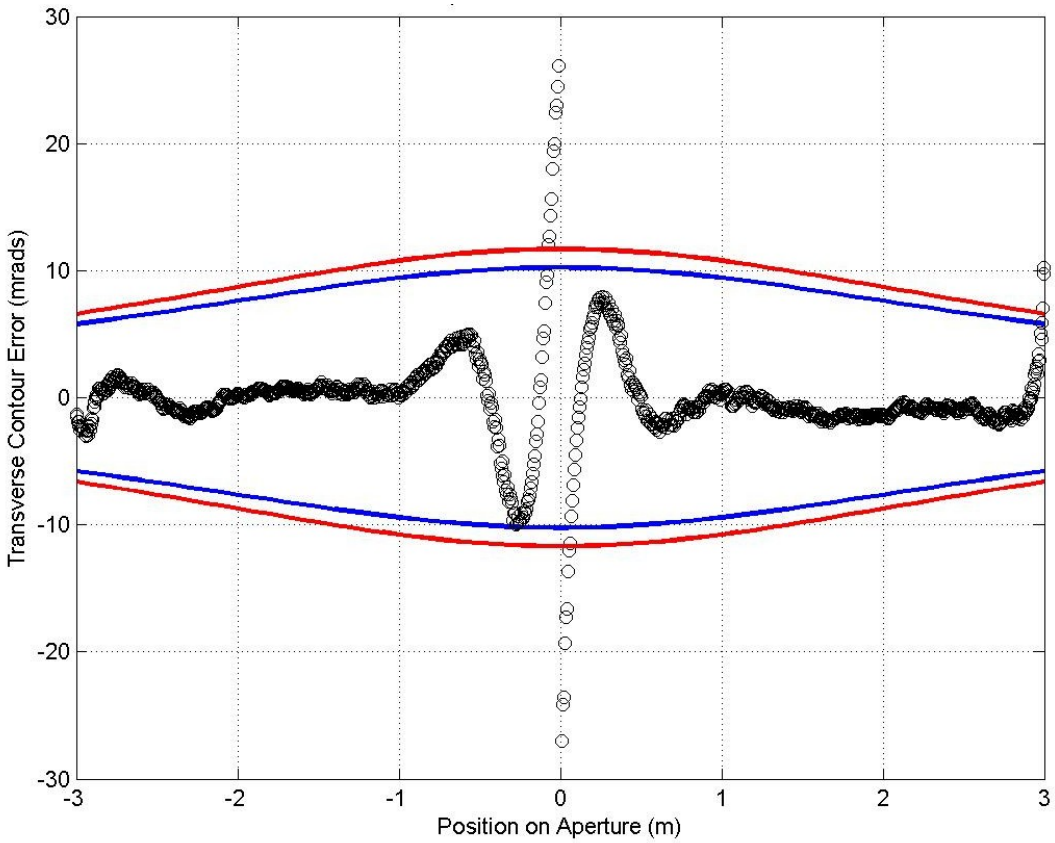

Figure 63. Slope errors along the aperture of scan AA_p13_41ft_4incfixedEDIT.csv.

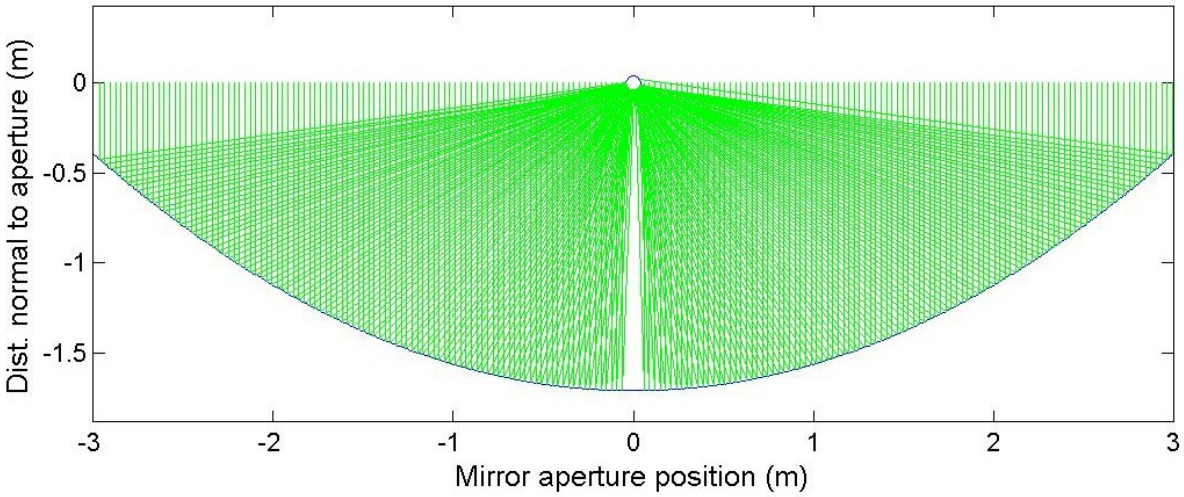

Figure 64. Ray trace results for scan AA_p13_42ft_9_5ifixedEDIT.csv, RMS=1.47934, Intercept=1.00.

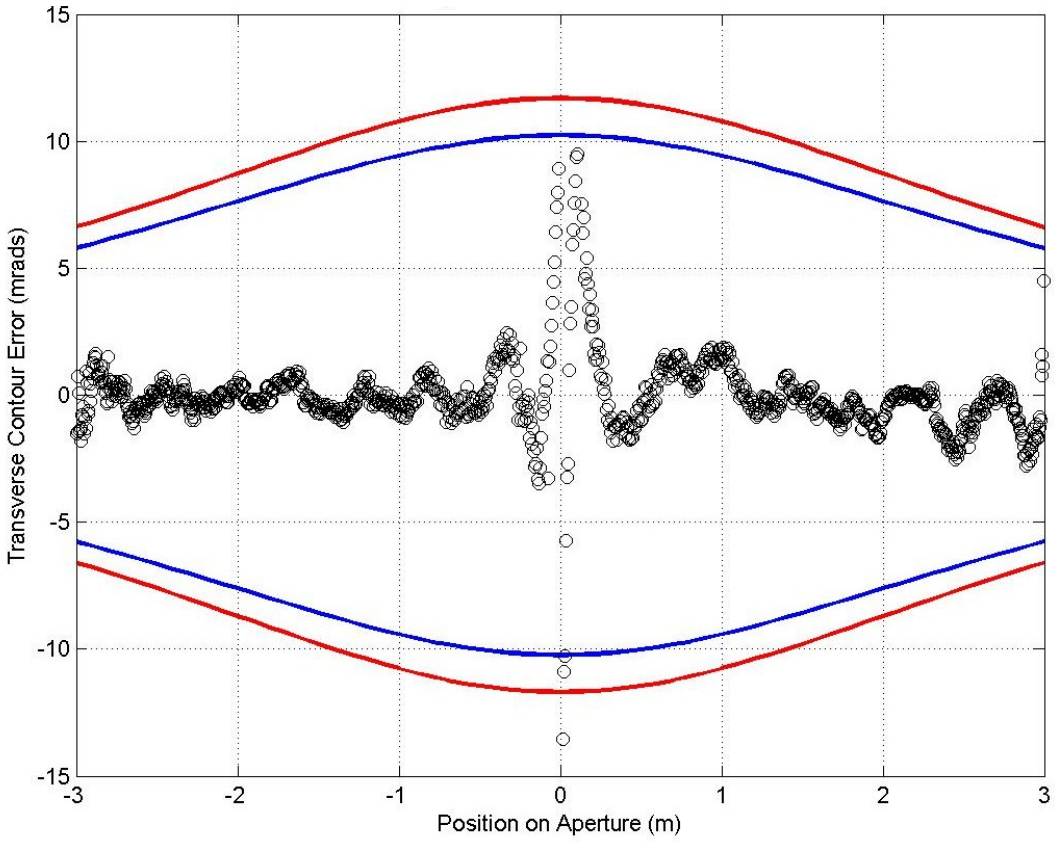

Figure 65. Slope errors along the aperture of scan AA_p13_42ft_9_5ifixedEDIT.csv.

Results for Panel 14

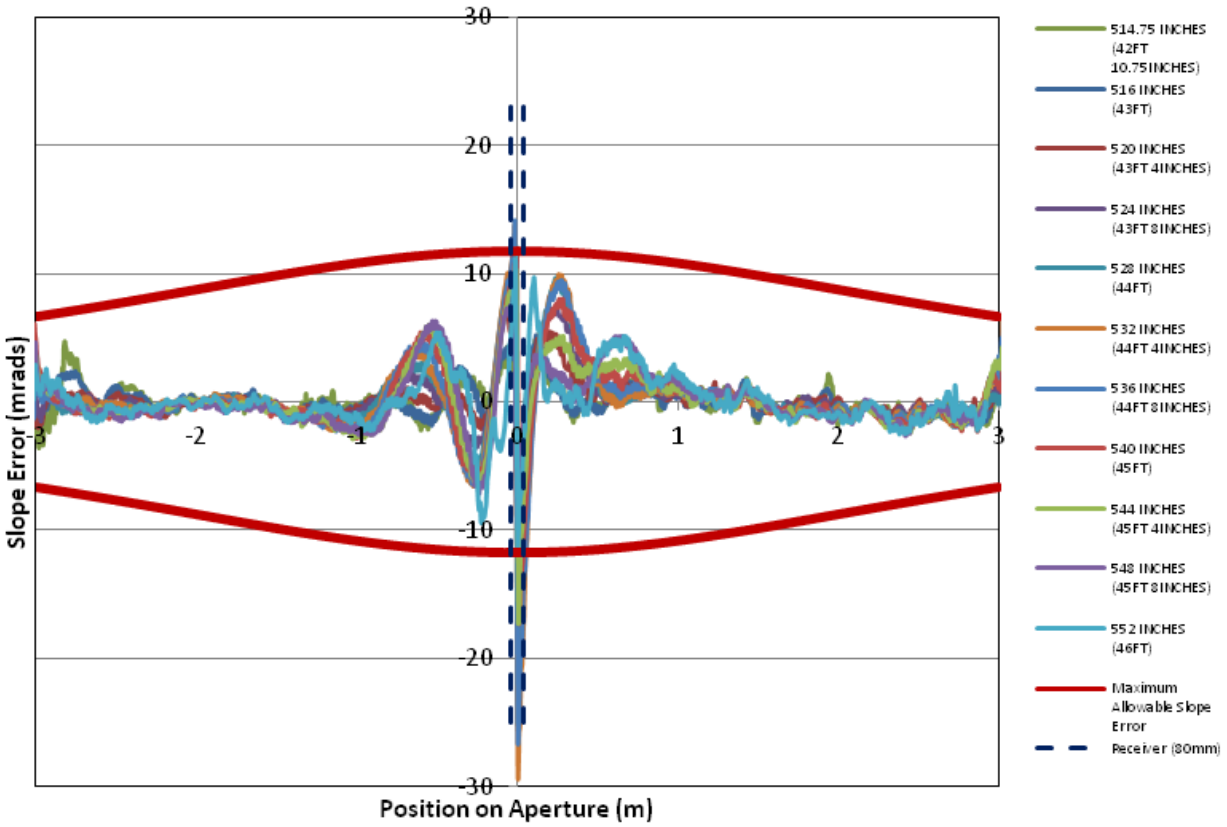

Figure 66. Slope errors along the aperture for each scan taken of Panel 1. The maximum allowable slope error over the aperture for an 80 mm receiver tube is plotted in red.

Table 14. Results for Panel 14 of the Alcoa collector.			
File Name	RMS Slope Error Transverse (mrad)	Intercept Factor (straight rays)	Intercept Factor (DLR sun shape)
AA_p14_42ft_10_7fixedEDIT.csv	1.28	1.00	1.00
AA_p14_43ft_2o_1fixedEDIT.csv	1.22	1.00	1.00
AA_p14_43ft_4incfixedEDIT.csv	1.61	1.00	1.00
AA_p14_43ft_8incfixedEDIT.csv	2.36	1.00	0.999
AA_p14_44ft_2o_1fixedEDIT.csv	2.78	0.999	0.998
AA_p14_44ft_4incfixedEDIT.csv	3.10	0.998	0.997
AA_p14_44ft_8incfixedEDIT.csv	3.01	0.998	0.998
AA_p14_45ft_2o_1fixedEDIT.csv	2.62	1.00	1.00
AA_p14_45ft_4incfixedEDIT.csv	2.37	1.00	1.00
AA_p14_45ft_8incfixedEDIT.csv	2.13	1.00	1.00
AA_p14_46ft_2o_1fixedEDIT.csv	2.11	1.00	1.00
AA_p14_46ft_0_5ifixedEDIT.csv	1.98	1.00	1.00
Average	**2.21**	**1.00**	0.999

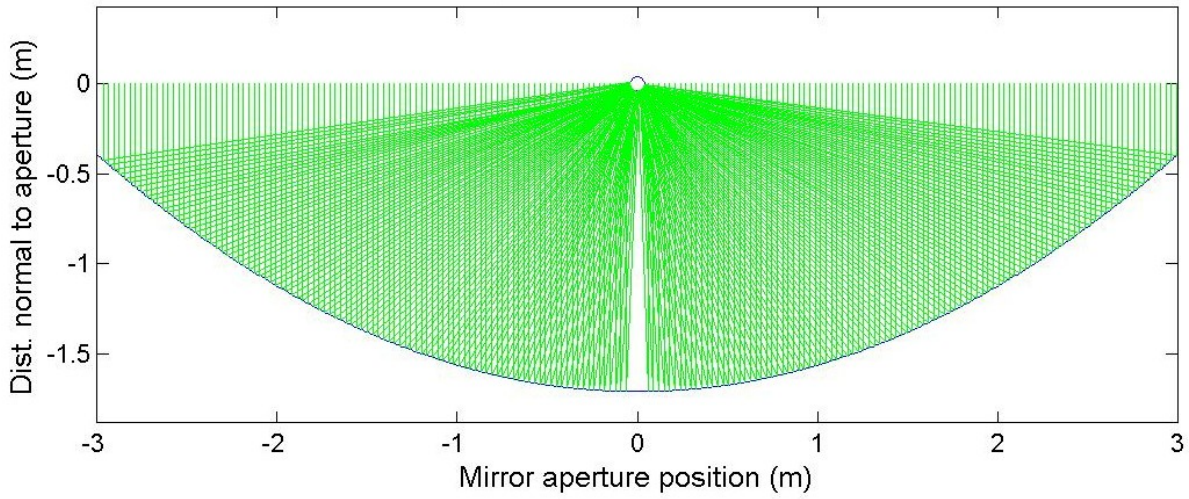

Figure 67. Ray trace results for scan AA_p14_42ft_10_7fixedEDIT.csv, RMS=1.28, Intercept=1.00.

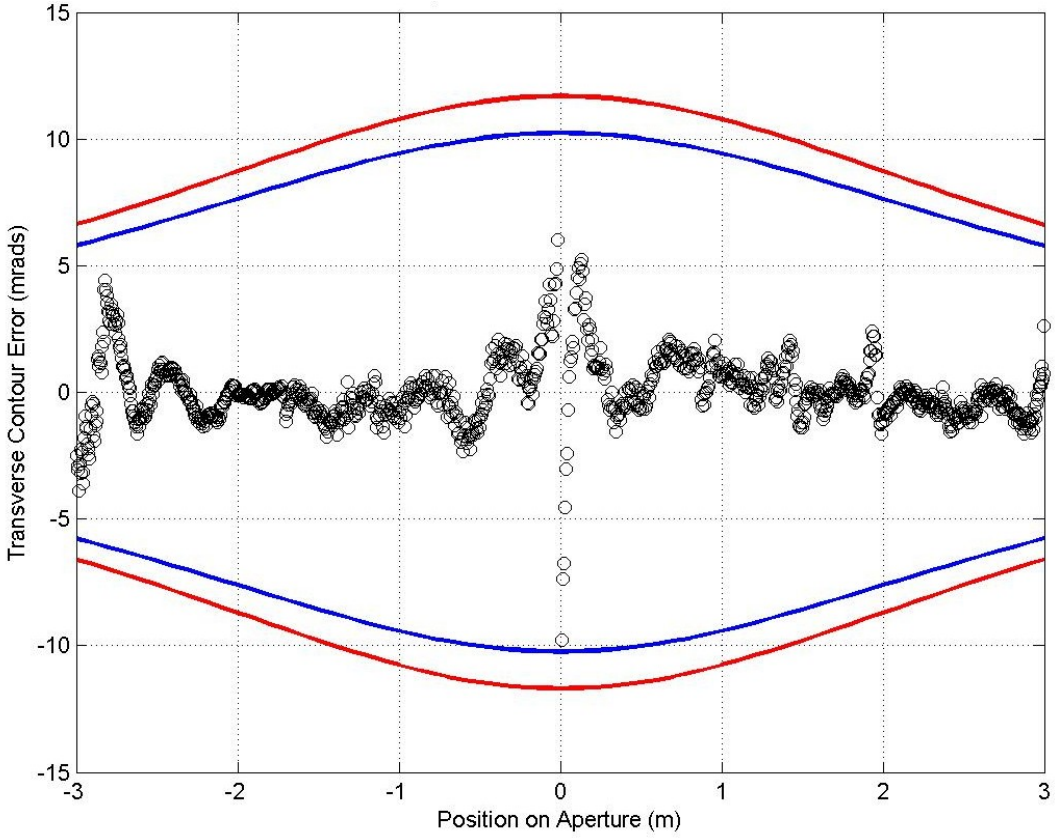

Figure 68. Slope errors along the aperture of scan AA_p14_42ft_10_7fixedEDIT.csv.

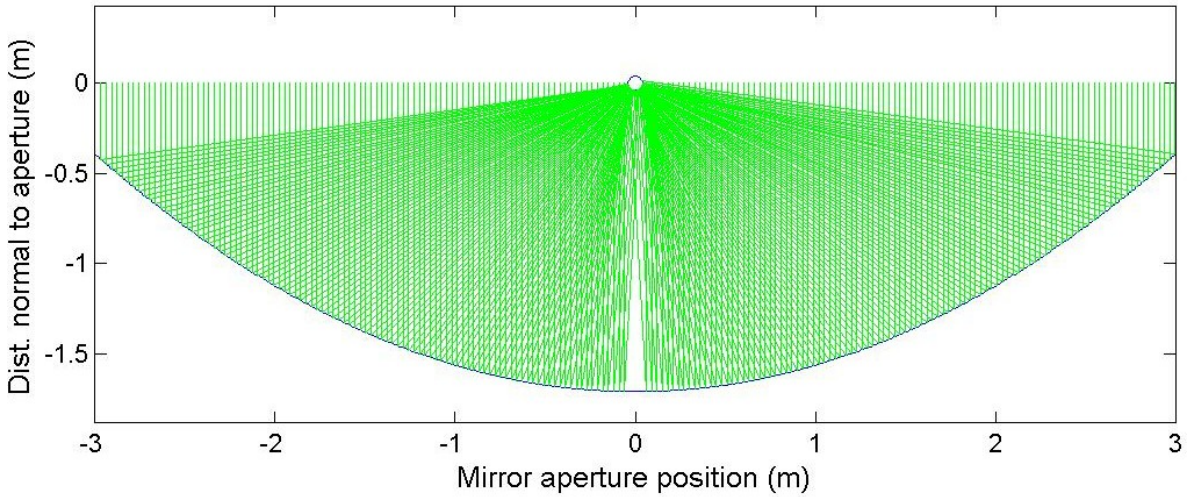

Figure 69. Ray trace results for scan AA_p14_44ft_4incfixedEDIT.csv, RMS=3.10, Intercept=0.998.

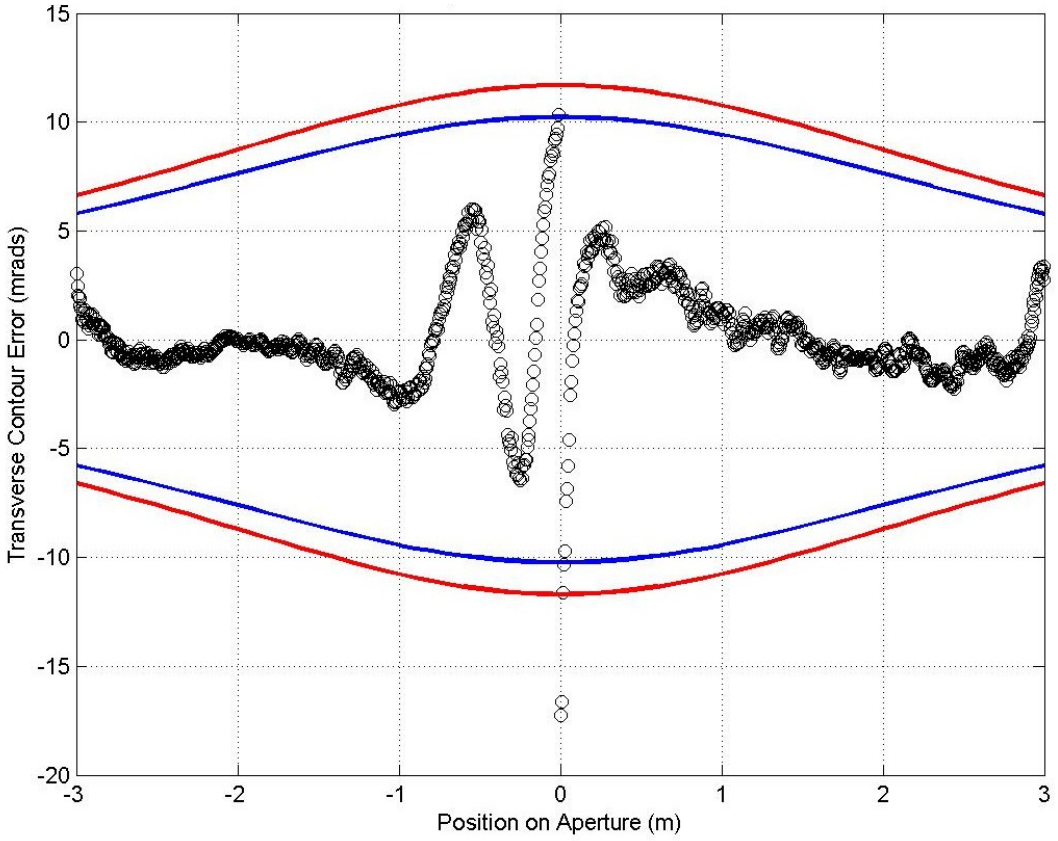

Figure 70. Slope errors along the aperture of scan AA_p14_44ft_4incfixedEDIT.csv

Appendix 2. Optical Efficiency Test Loop Uncertainty Analysis

The uncertainty in the optical efficiency measurement depends on each of the measured variables in Eq. (1). Total uncertainty, U, was computed from Eq. (1). For large (n>20) samples, *k=2* may be used[1].

$$U^2 = \sum_i (Type\ B)^2 + \sum_i (k \cdot Type\ A)^2 \quad (1)$$

Type A uncertainty represents precision, or random, error specified either by the manufacturer or during calibration. Type B uncertainty represents known bias, or systematic errors, which cannot be eliminated from the experiment. The propagation of error formula (Eq. 4) is used to determine each component of uncertainty.

$$U^2 = \sum_i \left(\partial_{x_i} R \cdot e_{x_i}\right)^2 \quad (2)$$

The resultant, R, is the optical efficiency, which depends on each variable, . The sensitivity function, , is the partial derivative of the optical efficiency with respect to that variable, , and is the estimated uncertainty in the measurement of . The heat losses are not exactly zero, but cannot be determined exactly during the test; therefore, the modeled heat losses for the test setup are included as a bias uncertainty. The uncertainty in the optical efficiency measurement is then determined with Eq. (3):

$$(\Delta\eta_o)^2 = \left(\frac{\partial\eta_o}{\partial\dot{m}}\right)^2 \cdot \Delta\dot{m}^2 + \left(\frac{\partial\eta_o}{\partial c_p}\right)^2 \cdot \Delta c_p{}^2 + \left(\frac{\partial\eta_o}{\partial T_{in}}\right)^2 \Delta T_{in}{}^2 + \left(\frac{\partial\eta_o}{\partial T_{out}}\right)^2 \Delta T_{out}{}^2 +$$

$$\left(\frac{\partial\eta_o}{\partial I_{DN}}\right)^2 \Delta I_{DN}{}^2 + \left(\frac{\partial\eta_o}{\partial A_{Coll}}\right)^2 \Delta A_{Coll}{}^2 \quad (3)$$

The estimated uncertainty for each variable takes into account the uncertainty in both the measurement instrument and the data acquisition system[2]. The uncertainties for each instrument are shown in Table 1. The total uncertainty due to both type A and type B sources for a 95% confidence interval at optimum conditions is 1.7%.

[1] Myers, D., Reda, I., Wilcox, S., and Lester, A. *An Update on Reducing the Uncertainty in Solar Radiometric Measurements.* National Renewable Energy Laboratory, NREL/PR-560-38202, (2005).

[2] Uncertainty in the data acquisition system was calculated using National Instruments' online accuracy calculator: http://www.ni.com/advisor/accuracy/default.htm

Table 1. Estimated Type A and B Uncertainty for Each Variable at Optimum Operating Conditions

Variable	Measurement	Type A ±Precision		Type B ±Bias	
T_{in}	Inlet temperature (°C)	0.05	0.2%	-	-
T_{out}	Exit temperature (°C)	0.05	0.2%	0.02	0.07%
	Mass flow rate (kg/s)	0.0022	0.13%	0.001	0.06%
C_p	Specific heat (kJ/kg-K)	7	0.19%	15	0.41%
I_{DN}	Direct normal irradiance (W/m^2)*	4.3	0.43%	6.1	0.61%
A_{Coll}	Collector area (m^2)	0.1	0.12%	-	-
$\Delta\eta_o$	Optical efficiency uncertainty	0.65%		0.59%	

The type B uncertainties were minimized during the experimental design and construction. The bias uncertainty in the temperature difference was minimized by zeroing the temperature difference between the inlet and outlet RTDs during conditions of no irradiance. The remaining bias uncertainty in the outlet temperature is due to potential heat losses and heating of the exposed ends of the receiver tube. The flow meter was also zeroed during no-flow conditions to minimize bias error. The remaining uncertainty is due to potential leakage through the valve bypassing the collector. Bias error in the specific-heat measurement is due to the accumulation of solid particles in the heat-transfer fluid that could change its fluid properties. The uncertainty in the direct-normal irradiance measurement was determined by comparison with a reference cavity radiometer on location at SRRL for zenith angles between 15° and 85°.

The optimum operating conditions are those for which the overall uncertainty is minimized. Maximum direct-normal solar radiation and maximum temperature difference across the trough provide the minimum uncertainty. Figure 1 shows the increase in uncertainty for reduced solar resource. A maximum of 2.4% uncertainty is introduced for irradiance levels of 500 W/m^2; therefore, testing is limited to clear-sky condition with a high solar resource.

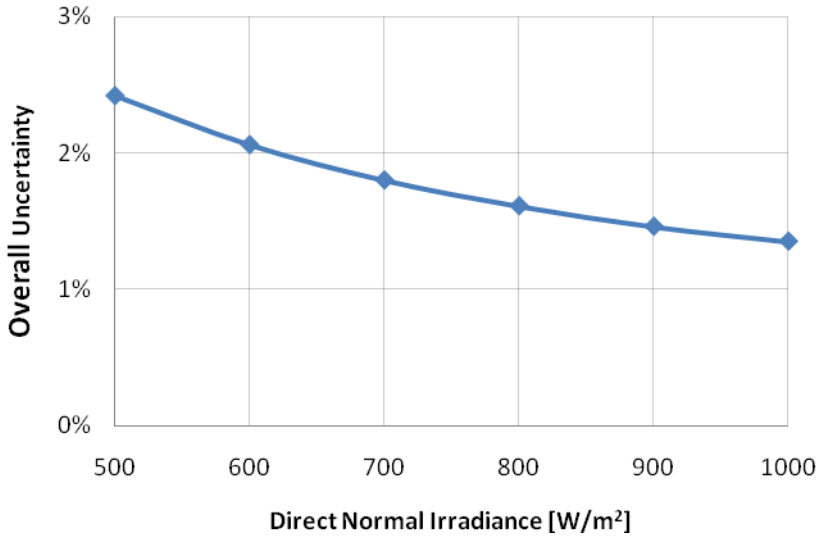

Figure 1. Dependence of uncertainty on direct-normal solar irradiance.

Appendix 3. Optical Efficiency Test Loop General Test Plan

Test Scheduling

All reasonable efforts will be made to prevent scheduling conflicts between trough suppliers. Discussions will take place so that trough suppliers' needs and wants are accommodated to the greatest extent possible. If a resolution is not possible, final scheduling decisions will rest with NREL, with consideration given to greatest perceived technical and market benefits.

Test Setup

Months ahead of the installation date, the trough supplier will coordinate with NREL personnel on trough mounting and installation. NREL will be responsible for verifying adequacy of mounting hardware and safety of installation. NREL will modify existing mounting hardware or fabricate new hardware to place the bearings at the position appropriate for the particular trough. The trough supplier will fabricate mounting hardware to attach to their trough to mate to the bearings.

The trough supplier will provide and install tube supports. The tube supports will be modified to eliminate axial receiver tube offsets, if necessary, so that the tube is centered with the trough.

NREL or the trough supplier will weld receiver tubes to make a receiver-tube assembly, to be decided on a case-by-case basis. NREL and the trough supplier will coordinate on receiver installation.

The trough supplier will align the receiver with the trough focal line. The trough supplier will provide a method of checking trough alignment with respect to the tracker torque tube.

Test Conditions

The receiver tube will be actively cooled whenever it is unshaded to prevent tube warping. At the beginning of a test, a check will be made for zero temperature rise through the tube when off-sun and shaded.

At the beginning of the test, the reflective surfaces and the glass envelope of the receiver tube will be cleaned using a pressure washer, deionized water, and detergent recommended by the trough supplier, as long as the detergent is acceptable to Environmental, Safety, and Health (ES&H).

The minimum direct-normal irradiance (DNI) will be 632 W/m^2, as measured at the SRRL. Maximum DNI variance will be ±32 W/m^2 in a 10-minute period.

Wind speed will be less than 20 mph as measured at the control building.

Mass flow rate of coolant on a per-unit-aperture basis will be 0.02 kg/s-m^2. Additional tests at different mass flow rates may be performed as the trough supplier desires and the schedule allows.

The inlet temperature of the coolant will be manually set to the prevailing ambient temperature as measured with the aspirated RTD probe above the control building.

At least two different days at 0 degree incidence angle with identical optical efficiency results will be required.

Incidence angle modifier tests will be run at up to 50°.

Accurate tracking in open- and closed-loop modes will be verified.

Post-Processing

Transients in DNI, inlet temperature, and flow rate introduce errors in the optical efficiency result. All data will be processed to eliminate the effect of transients.

Test Conclusion

At the end of the test period, the trough supplier and NREL will coordinate on receiver tube and trough removal. Depending on trough size, it may be possible to store the trough onsite for a limited amount of time. The trough supplier will be responsible for removing the trough from NREL property in a timely manner.